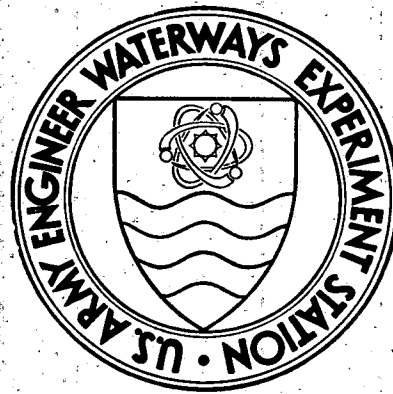


05
1975
84-75

DL-1516



TECHNICAL REPORT E-75-2

PROJECT R. D. BAILEY EXPERIMENTAL EXCAVATION PROGRAM

William R. Bechtell



950 0007

June 1975

U. S. Army Engineer Waterways Experiment Station
Explosive Excavation Research Laboratory
Livermore, California

Approved for public release; distribution unlimited

MASTER

DISTRIBUTION OF THIS DOCUMENT UNLIMITED

Destroy this report when no longer needed.
Do not return it to the originator.

The findings in this report are not to be construed as an
official Department of the Army position unless so
designated by other authorized documents.

Printed in USA. Available from Defense Documentation Center,
Cameron Station, Alexandria, Virginia 22314 or
National Technical Information Service,
U. S. Department of Commerce
Springfield, Virginia 22161

DISCLAIMER

This report was prepared as an account of work sponsored by an agency of the United States Government. Neither the United States Government nor any agency Thereof, nor any of their employees, makes any warranty, express or implied, or assumes any legal liability or responsibility for the accuracy, completeness, or usefulness of any information, apparatus, product, or process disclosed, or represents that its use would not infringe privately owned rights. Reference herein to any specific commercial product, process, or service by trade name, trademark, manufacturer, or otherwise does not necessarily constitute or imply its endorsement, recommendation, or favoring by the United States Government or any agency thereof. The views and opinions of authors expressed herein do not necessarily state or reflect those of the United States Government or any agency thereof.

DISCLAIMER

Portions of this document may be illegible in electronic image products. Images are produced from the best available original document.

UNCLASSIFIED

SECURITY CLASSIFICATION OF THIS PAGE (When Data Entered)

REPORT DOCUMENTATION PAGE		READ INSTRUCTIONS BEFORE COMPLETING FORM
1. REPORT NUMBER TR E-75-2	2. GOVT ACCESSION NO.	3. RECIPIENT'S CATALOG NUMBER
4. TITLE (and Subtitle) PROJECT R. D. BAILEY EXPERIMENTAL EXCAVATION PROGRAM		5. TYPE OF REPORT & PERIOD COVERED Final
		6. PERFORMING ORG. REPORT NUMBER
7. AUTHOR(s) William R. Bechtell		8. CONTRACT OR GRANT NUMBER(s)
9. PERFORMING ORGANIZATION NAME AND ADDRESS U. S. Army Engineer Waterways Experiment Sta. Explosive Excavation Research Laboratory Livermore, California 94550		10. PROGRAM ELEMENT, PROJECT, TASK AREA & WORK UNIT NUMBERS Materials, rock, experi- mental excavation projects, 31153
11. CONTROLLING OFFICE NAME AND ADDRESS		12. REPORT DATE June 1975
		13. NUMBER OF PAGES 148
14. MONITORING AGENCY NAME & ADDRESS (if different from Controlling Office)		15. SECURITY CLASS. (of this report) Unclassified
		15a. DECLASSIFICATION/DOWNGRADING SCHEDULE
16. DISTRIBUTION STATEMENT (of this Report) Approved for public release; distribution unlimited		
17. DISTRIBUTION STATEMENT (of the abstract entered in Block 20, if different from Report)		
18. SUPPLEMENTARY NOTES		
19. KEY WORDS (Continue on reverse side if necessary and identify by block number) Value Engineering Contract Specifications Engineering Design Rock Excavation Construction Rock Blasting Test Fills		
20. ABSTRACT (Continue on reverse side if necessary and identify by block number) This technical report presents the results of the R. D. BAILEY Lake Project experimental excavation program. The experimental program was conducted at the site for the spillway of the R. D. BAILEY Lake Project, near Justice, West Virginia, from February to August 1973. The primary objective of the experimental excavation program was to investigate the feasibility of using bulk explosives in blastholes larger than normally used in structural excavations, in conjunction with controlled blasting techniques, to reduce the cost of drilling and blasting. (continued on reverse)		

DD FORM 1 JAN 73 1473 EDITION OF 1 NOV 65 IS OBSOLETE

UNCLASSIFIED
SECURITY CLASSIFICATION OF THIS PAGE (When Data Entered)

DISTRIBUTION OF THIS DOCUMENT UNLIMITED

[Handwritten signature]

UNCLASSIFIED

SECURITY CLASSIFICATION OF THIS PAGE(When Data Entered)

Item 20, continued

Other objectives were to obtain basic scientific data on blasting techniques and effects, and to provide the Huntington District and prospective bidders information on appropriate excavation techniques for the spillway at R. D. BAILEY Lake.

The experimental excavation included a comparison of the results obtained by blasting with ANFO and aluminized slurry in holes varying from 3 to 12-1/4 in. in diameter in shale and sandstone. During the course of the experiment, data were collected concerning fragmentation, ground shock, blast-induced fracturing, seismic motions, and airblast overpressures. This information has been analyzed in order to arrive at a better understanding of basic blasting mechanisms and side effects. The results of the experimental excavation were made available to contractors interested in bidding on the project to help them prepare estimates of the cost of spillway excavation. By reducing the uncertainties about the nature of the rock and its excavation characteristics, substantial savings were realized in the cost of the spillway excavation.

UNCLASSIFIED

SECURITY CLASSIFICATION OF THIS PAGE(When Data Entered)

TECHNICAL REPORT E-75-2

PROJECT R. D. BAILEY EXPERIMENTAL EXCAVATION PROGRAM

William R. Bechtell
Principal Author and Technical Editor

Contributing Authors:

Michael Hoefft
Stephen Kelley
Colin McAneny
Thomas Tami
Hudson Washburn
Mathew Zahn

NOTICE
This report was prepared as an account of work sponsored by the United States Government. Neither the United States nor the United States Energy Research and Development Administration, nor any of their employees, nor any of their contractors, subcontractors, or their employees, makes any warranty, express or implied, or assumes any legal liability or responsibility for the accuracy, completeness or usefulness of any information, apparatus, product or process disclosed, or represents that its use would not infringe privately owned rights.

U. S. ARMY ENGINEER WATERWAYS EXPERIMENT STATION
EXPLOSIVE EXCAVATION RESEARCH LABORATORY
Livermore, California

MS. date: March 1975

This document is
PUBLICLY RELEASABLE

Larry E Williams

Authorizing Official

Date: 08/10/2007

DISTRIBUTION OF THIS DOCUMENT UNLIMITED

leg

Foreword

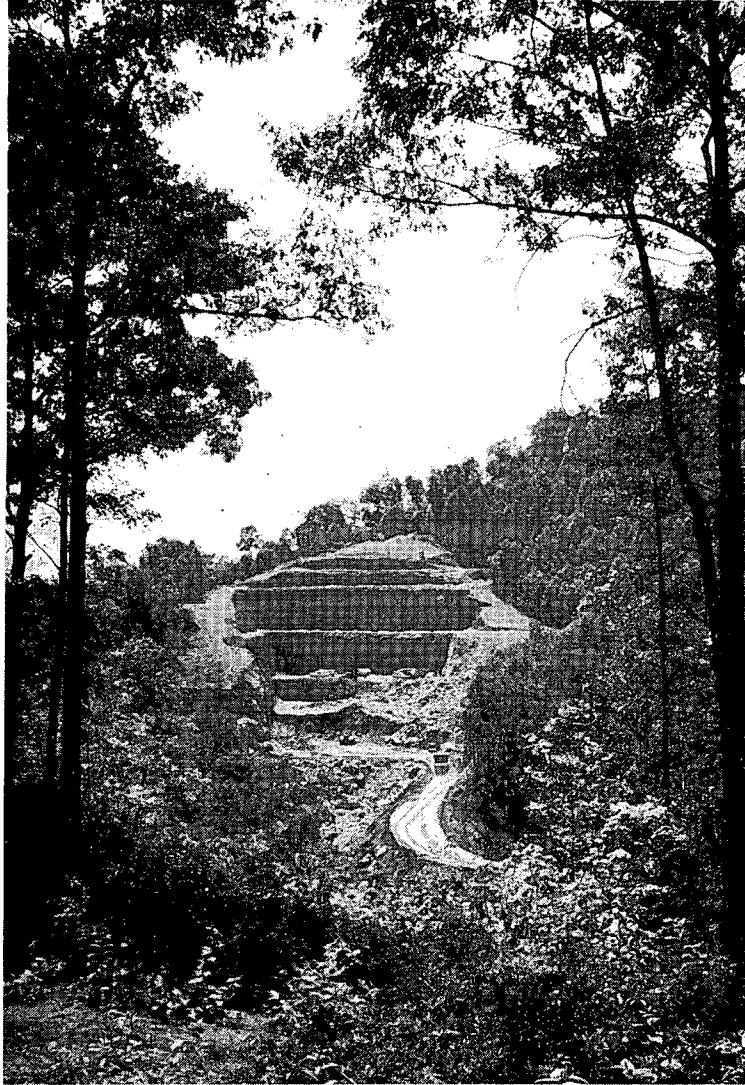
The Explosive Excavation Research Laboratory (EERL), in order to fulfill part of its mission, "manages, conducts and coordinates military and civil excavation research with both chemical and nuclear explosives and provides related consultation capability to the Corps of Engineers and other Government agencies." The experimental excavation program accomplished by EERL and the Huntington District at the site of the R. D. BAILEY Lake Project served a research function and provided information on appropriate excavation techniques for the spillway at R. D. BAILEY Lake. Most of this report is concerned with technical programs associated with the research function of the experimental excavation program, but the impact of the program on the R. D. BAILEY Lake Project is also discussed. The technical knowledge gained on blast effects and the cost savings realized on the dam project as a result of the experimental excavation emphasize the value of this type of program.

Abstract

This technical report presents the results of the R. D. BAILEY Lake Project experimental excavation program. The experimental program was conducted at the site for the spillway of the R. D. BAILEY Lake Project, near Justice, West Virginia, from February to August 1973.

The primary objective of the experimental excavation program was to investigate the feasibility of using bulk explosives in blastholes larger than normally used in structural excavations, in conjunction with controlled blasting techniques, to reduce the cost of drilling and blasting. Other objectives were to obtain basic scientific data on blasting techniques and effects, and to provide the Huntington District and prospective bidders information on appropriate excavation techniques for the spillway at R. D. BAILEY Lake.

The experimental excavation included a comparison of the results obtained by blasting with ANFO and aluminized slurry in holes varying from 3 to 12-1/4 in. in diameter in shale and sandstone. During the course of the experiment, data were collected concerning fragmentation, ground shock, blast-induced fracturing, seismic motions, and airblast overpressures. This information has been analyzed in order to arrive at a better understanding of basic blasting mechanisms and side effects. The results of the experimental excavation were made available to contractors interested in bidding on the project to help them prepare estimates of the cost of spillway excavation. By reducing the uncertainties about the nature of the rock and its excavation characteristics, substantial savings were realized in the cost of the spillway excavation.



Frontispiece: Overall view of experimental excavation,
R. D. BAILEY Lake Project.

5 July 1973

Contents

FOREWORD	ii
ABSTRACT	iii
CONVERSION FACTORS	ix
ACKNOWLEDGMENTS	x
CHAPTER 1. INTRODUCTION	1
CHAPTER 2. SITE DESCRIPTION	4
Location	4
Regional Geology	4
Site Geology	4
CHAPTER 3. DESCRIPTION OF TEST BLASTS	10
General	10
PB-1 Test Blast	13
PB-2 Test Blast	13
PB-3 Test Blast	13
PB-4 Test Blast	15
PB-4A through PB-4E Test Blasts	17
PB-5 Test Blast	17
PB-6A Test Blast	17
PB-6B Test Blast	19
PB-6C Test Blast	20
PB-7 Test Blast	20
PB-8 Test Blast	20
Summary	25
CHAPTER 4. FRAGMENTATION PROGRAM	33
Background	33
Field Procedure	34
Analyses	34
Discussion and Conclusions	38
CHAPTER 5. SUBSURFACE SHOCK AND BLAST-INDUCED FRACTURING PROGRAM	40
Background	40
Objectives and Approach	41
Equipment	42
Procedure	42
Data	44
Analyses	44
Conclusions	48
CHAPTER 6. SEISMIC MOTION PROGRAM	56
Background	56
Objectives and Approach	56
Equipment	57
Procedure	57
Data	57
Analyses	59
Conclusions	63
CHAPTER 7. AIRBLAST OVERPRESSURE PROGRAM	63
Introduction	63
Background	64
Objectives and Approach	65
Equipment	65
Data	66
Analyses	69
Conclusions	75

CHAPTER 8. TEST FILLS	75
Introduction	75
Equipment	75
Procedure	76
Results and Conclusions	78
CHAPTER 9. RECOMMENDATIONS FOR IMPROVED BLAST DESIGN	79
General	79
Blast Design Techniques	80
Blast Design Considerations	81
Critique of Test Blasts	91
CHAPTER 10. COST ANALYSES	97
CHAPTER 11. SUMMARY AND CONCLUSIONS	100
APPENDIX A. GRADATION CURVES	103
APPENDIX B. SUBSURFACE PARTICLE VELOCITY RECORDS	112
APPENDIX C. SEISMIC DATA	123
APPENDIX D. AIRBLAST DATA	127
REFERENCES	132

FIGURES

1	Site location map	5
2	Generalized geologic column	6
3	Rock units in pilot excavation	7
4	Weathered sheet joint in fissile clayey shale, PB-3	8
5	Sheet joint in Upper Gilbert sandstone, PB-6B	9
6	Appearance of back west wall, pilot excavation, lifts PB-3 and PB-4 above coals	10
7	Centerline profile of pilot excavation (looking north)	11
8	Cross section of pilot excavation (looking west)	11
9	Declaration of performance, composition and safety for Dow MS 80-25 slurry blasting agent	12
10	PB-1 blast design	14
11	Excavating from PB-1 blast	15
12	Ripping PB-2	15
13	Trimming PB-2	15
14	PB-3 blast design	16
15	PB-3 trimming/presplit, rear wall	17
16	Excavating PB-3 blasted rock	17
17	PB-4 blast design	18
18	Ripping PB-4	19
19	PB-4 preshot	19
20	PB-4 postshot surface	19
21	PB-4 after excavation of fractured rock	19
22	Blast designs for PB-4A through PB-4E	20
23	Blasted rock from PB-4A	21
24	Blasted rock from PB-4B	21
25	Blasted rock from PB-4C	21
26	Blasted rock from PB-4D	21
27	PB-4E preshot	21
28	PB-5 blast design	22
29	Blasted rock from PB-5	23
30	PB-6A blast design	24
31	PB-6A preshot	25
32	Blasted rock from PB-6A	25
33	PB-6B blast design	26
34	PB-6B preshot	27
35	PB-6B during excavation	27
36	PB-6C blast design	28

FIGURES (continued)

37	PB-6C preshot	28
38	PB-6C during excavation	28
39	PB-7 blast design	29
40	PB-7 preshot (from left rear)	30
41	PB-7 preshot (left wall)	30
42	PB-7 during excavation	30
43	PB-8 blast design	31
44	PB-8 preshot (from right front)	32
45	PB-8 postshot surface (from right front)	32
46	PB-8 during excavation (from left rear)	32
47	Left wall of PB-8 after excavation	32
48	Right wall of PB-8 after excavation	32
49	Measurement of rock fragments	34
50	Gradation curve for PB-8	35
51	Gradation curves for weathered shale	35
52	Gradation curves for 3-in.-diameter blastholes in hard shale and sandstone	36
53	Gradation curves for Upper Gilbert sandstone	37
54	Gradation curves for PB-7	37
55	Zingg shape indices for rock from PB-4A	38
56	Average Zingg shape indices for all test blasts	39
57	Typical mounting bracket indicating gage and canister placement	43
58	Permeability test packer assembly	44
59	Velocity gage configuration for PB-1	45
60	Velocity gage configuration for PB-3	46
61	Velocity gage configuration for PB-4	47
62	Velocity gage configuration for PB-6A	48
63	Velocity gage configuration for PB-6B	49
64	Velocity gage configuration for PB-7	50
65	Velocity gage configuration for PB-8	51
66	Plot of effects of presence of buffer zone on peak particle velocities	54
67	Peak particle velocity vs distance for both horizontal and vertical gage orientations, PB-7	55
68	Rear of PB-7 showing approximate location of velocity gage holes, 18 and 25 ft from main charge	55
69	Seismic station locations	57
70	Location of Seismic Stations SS3A and SS3C at intake structure foundation	62
71	PPV's with high probability of not being exceeded at various distances from various weights of explosive	63
72	Typical airblast overpressure vs time record	64
73	Airblast gage	65
74	Plan view of airblast gage locations	66
75	Topographic profiles through airblast gage locations	67
76	Overpressure at Gage E-2 from Test Blast PB-3	69
77	Overpressure at Gage E-2 from Test Blast PB-1	70
78	Overpressure at Gage E-2 from 200 ft of detonating cord lying perpendicular to spillway centerline	70
79	Overpressure at Gage E-2 from typical single charge	71
80	Overpressure at Gage E-2 from Test Blast PB-6A	71
81	Impulse at 1000 ft east vs largest simultaneous weight of explosive	73
82	Double-drum tamping roller	76
83	Buffalo-Bomag 10-ton vibratory roller	76
84	Two typical test fills	77
85	Dumping and spreading test fill material	77
86	Digging test pit	78
87	Typical geometrical relationships and notations for blastholes and presplit planes	86

FIGURES (continued)

88	Nomograph for computing relative energy density	87
89	Critical distance as a function of relative energy density and charge diameter for weathered shale	88
90	Critical distance as a function of relative energy density and charge diameter for Upper Gilbert sandstone	89
91	Scaled depth of burial vs blasthole depth for stemming depths of 4 and 6 ft	90
92	Recommended stemming depths for ANFO and Dow MS 80-25 slurry in weathered shale and Upper Gilbert sandstone for various blasthole diameters	92
93	Change in detonation velocity of ANFO as a function of blasthole diameter	92
94	Improved design for PB-8 test blast - slurry	95
95	Improved design for PB-8 test blast - ANFO	96
96	Unit cost for drilling and blasting vs bench height for various blast hole diameters - ANFO	99
97	Unit cost for drilling and blasting vs bench height for various blasthole diameters - slurry	100

TABLES

1	R. D. BAILEY experimental excavation test blast summary	33
2	Summary of peak particle velocity measurements	52
3	Summary of permeability test data	53
4	Variation of peak particle velocities with depth	55
5	Summary of peak particle velocity (PPV) measurements	58
6	Parameters obtained from regression analyses of PPV as a function of charge weight and distance	59
7	Parameters obtained from regression analyses of maximum PPV, regardless of component, as a function of charge weight and distance for sandstone and shale	60
8	Comparison of PPV's at Seismic Stations SS3A and SS3C from the PB-6C blast	62
9	Airblast gage locations	67
10	Summary of peak positive overpressure measurement and time of arrival	68
11	Peak overpressure and impulse data	73
12	Airblast suppression factors	74
13	Comparison of predicted and measured peak airblast overpressures at Gage E-2	75
14	Test fill data	76
15	Summary of test fill settlement data	77
16	Physical properties of explosives	89
17	Estimated reduction in project cost attributable to test excavation	98

Conversion Factors

British units of measurement used in this report can be converted to metric units as follows:

Multiply	By	To Obtain
inches	2.54	centimeters
feet	0.3048	meters
cubic feet	0.02832	cubic meters
cubic yard	0.764555	cubic meters
pounds	0.4535924	kilograms
pounds per cubic foot	16.02	kilograms per cubic meter
Fahrenheit degrees	5/9	Celsius or Kelvin degrees ^a

^aTo obtain Celsius (C) temperature readings from Fahrenheit (F) readings, use the following formula: $C = (5/9)(F - 32)$. To obtain Kelvin (K) readings, use: $K = (5/9)(F - 32) + 273.15$.

The contents of this report are not to be used for advertising, publication, or promotional purposes. Citation of trade names is intended to describe the experimental setup, and does not constitute an official endorsement or approval of the use of such commercial products.

Acknowledgments

The success of the R. D. BAILEY Lake Project Experimental Excavation Program was the result of the efforts of many personnel from EERL and the Huntington District. Walter Day (Assistant Director, EERL) coordinated with the District to establish the direction of the test program. Richard Fraser, test manager, and John Shaler, project engineer, were responsible for the fielding of the experimental excavation program. The test fill program was conducted by the Geology, Soils and Materials Branch of the Huntington District. Gaylord Robinette, resident engineer for the R. D. BAILEY Lake Project, and his assistant, Niel Schilling, were instrumental in coordinating the efforts of the contractor, Huntington District, and EERL.

Specific chapters of this report were authored by the following: Colin McAneny, Chapter 2, SP5 Stephen Kelley, Chapter 5, Thomas Tami, Chapter 6, SP4 Hudson Washburn and SP4 Michael Hoeft, Chapter 7. William Bechtell authored the remaining chapters and edited all chapters with respect to technical content and format of presentation. Lyman Watson and James Tarver of the Waterways Experiment Station Instrumentation Services Division were responsible for setting up and operating the data recording systems.

Robert Holmes and Bruce Redpath provided valuable technical and editorial comments on the report. Mrs. Helen Sarles also deserves special thanks for her tireless effort in typing the manuscript.

COL Ernest D. Peixotto and COL G. H. Hilt were Directors of the Waterways Experiment Station during the course of the experimental excavation program and the preparation of this report. COL Kenneth E. McIntyre was District Engineer, Huntington District, and LTC Robert R. Mills, Jr., was Director of EERL.

TECHNICAL REPORT E-75-2

PROJECT R. D. BAILEY

EXPERIMENTAL EXCAVATION PROGRAM

Chapter 1. Introduction

This report describes the procedures and results of an experimental excavation program at the R. D. BAILEY Lake Project.

The program was conducted by the U. S. Army Corps of Engineers Explosive Excavation Laboratory (EERL) and the Huntington Engineer District between February and August, 1973. The site of the experiment was the R. D. BAILEY Lake Project, near Justice, West Virginia. Material excavated from the spillway will be used to construct the rock-fill dam embankment.

One of the primary objectives of the experimental program was to investigate the feasibility of using large charges of bulk explosives, up to 12-1/4 in. in diameter and 50 ft deep, to reduce the cost of drilling and blasting in the spillway. Although blastholes this large are common in open-pit mining applications, they are seldom used in structural excavations because of the potential danger of damage to rock outside the limits of excavation. Methods of reducing this potential overbreak were studied during the program.

The R. D. BAILEY Lake Project presented a number of interesting blasting problems:

1. The rock excavated from the spillway will be used in the dam embankment,

and therefore must meet specific gradation requirements.

2. The maximum depth of the spillway cut will be about 360 ft. Controlled blasting techniques, such as presplitting, must be used to protect the spillway walls from damage due to production blasts. The integrity of the nearby right dam abutment must also be preserved.

3. A 300-ft-high water intake structure will be under construction about 2000 ft from the spillway excavation. The maximum weight of explosive that can be detonated simultaneously must be limited to assure that the structure will not be damaged by blast-induced ground motions.

4. The town of Justice is approximately 1 mi from the spillway site. Blasts must be designed to preclude subjecting the town to damaging blast effects, such as ground motion and airblast.

In order to address these problems, a pilot excavation consisting of 14 test blasts was made in the rock at the upstream end of the spillway. Controlled blasting experiments were conducted in conjunction with most of the blasts. The production blastholes varied from 3 to 12-1/4 in. in diameter. Burdens, spacings, lift heights, delays, and explosive types were varied to begin the process of determining the most economical blasting techniques that satisfied the design criteria.

The following four technical programs were conducted during the course of the pilot excavation to study specific aspects of blast phenomena:

1. Fragmentation
2. Subsurface shock and blast-induced fracturing
3. Ground motions
4. Airblast overpressures

In addition to these programs, most of the blasts were photographed with high-speed movie cameras, and test fills were constructed from samples of the excavated material.

Several types of cameras were used to document the experimental excavation program. These included high-speed movie cameras, standard 16-mm movie cameras, 35-mm cameras, and a videotape machine. A 1/2-hr documentary color movie has been made of the entire experimental excavation program. This movie is titled "Thunder Along the Guyandot," and is available at the Waterways Experiment Station Public Affairs Office.

Two Hycam cameras, a 400-ft model and a 100-ft model, were used for high-speed photography. These cameras were operated at a maximum speed of 500 and 250 frames/sec, respectively. The 400-ft Hycam was located at the control trailer for all shots, looking directly into the excavation. The other was located in a portable wooden bunker, which was moved around the perimeter of the excavation in order to get a good view of each shot. A small Urban 16-mm "gun" camera, operating at 50 frames/sec, was used as a backup camera in this bunker, or used in place of the Hycam when there was a high probability of damage from

flyrock. These cameras were remotely triggered. Motion pictures were also taken from the control trailer with a Canon Scoopic 16-mm movie camera operated at 48 frames/sec, and a 34-mm Topcon camera with a motor drive was used to take still pictures at a rate of approximately one picture every 0.4 sec. Color film was used in all cameras.

A videotape machine, a Sony "Videocorder," was used on an experimental basis during the first several months of the experimental excavation program. This machine was quite useful for "instant replays" of a blast while waiting for the regular movie film to be processed.

The high-speed motion pictures were viewed on a Kodak Film Analyzer, which can be operated on a frame-by-frame basis. The movies were viewed with the intent of identifying the detonation sequence of charges, or groups of charges, and detection of any premature venting, either through stemming failure or other zones of weakness.

The high-speed motion pictures were generally not too useful for determining the detonation sequence of production charges. The production charges for most of the test blasts were all initiated with instantaneous detonating cord on the surface, and the delays were built into detonators down in the hole. The first indicator seen in the movies that a charge had detonated was upward movement of the stemming. Variations in stemming depths or compaction might make stemming motion an unreliable indicator of detonation time. In PB-1 (pilot blast), however, where each "vee" delay of charges was detonated by delayed trunk lines of detonating cord, the detonation

sequence as the detonating cord trunk lines were initiated from the front to the rear of the pattern was very apparent.

The high-speed movies were more useful for identifying the origin of fly-rock and premature venting. For example, it was apparent in the PB-7 movies that much flyrock originated in the weak, weathered rock at the toe of the sloping front face. In the PB-8 movies a "fire-ball" of burning gases was visible at the location of a sheet joint in the front face of that blast.

The proposed experimental excavation program was transmitted to the Huntington District on 10 November 1972 in the Technical Concept and support criteria for the experimental excavation program at R. D. BAILEY Lake.¹ This was followed in February 1973 by an Operations Plan.² The support work for the experimental excavation was advertised, and the low bidder was Dow Chemical Company. Construction began in mid-February 1973. EERL mobilized the following staff, to field the experimental excavation program, which was completed in August 1973:

Director, EERL:	LTC R. R. Mills, Jr.
Project Coordinator:	W. C. Day
Technical Deputy:	W. R. Bechtell J. E. Lattery (Asst.)
Test Manager:	R. L. Fraser MAJ G. M. Miller (Asst.)
Project Engineer:	J. E. Shaler R. J. Gerbino (Asst.) K. A. Crichton (Asst.) W. R. McLoud (Asst.)
Technical Program Officers:	
Airblast overpressures:	H. A. Washburn M. J. Hoeft
Subsurface shock:	S. C. Kelley
Fragmentation:	M. Zahn
Seismic motions:	T. M. Tami
Geologist:	C. C. McAneny
Photographer:	M. Zahn

During the course of the experimental excavation, EERL reviewed and offered comments on the plans and specifications prepared by Huntington District for the spillway excavation. After completing the series of test blasts, a Data Report was published and made available to all holders of plans and specifications for the dam contract.³ The purpose of the data report was to provide bidders with information about the experience gained during the experimental excavation to assist them in formulating their bids. This information significantly reduced the uncertainty in geology and blasting normally associated with bidding on rock excavation projects.

Another product of the experimental program was a set of blasting guidelines developed by EERL for use by the resident engineer on the R. D. BAILEY Project.⁴ These guidelines were designed to aid the resident engineer in evaluating blasting procedures proposed by the contractor for spillway excavation.

This report is organized into 11 chapters. Chapter 2 describes the site of the experiment, including a discussion of the geology, and Chapter 3 describes each of the test blasts. Chapters 4 through 7 present data from the various technical programs. Test fills are discussed in Chapter 8. Chapter 9 makes recommendations on how to improve test blast designs. The results of analyses made of drilling and blasting costs are presented in Chapter 10, and Chapter 11 contains a summary and conclusions. Data too bulky or not appropriate for the main body of the report are included in Appendix A through Appendix D.

Chapter 2. Site Description

LOCATION

The R. D. BAILEY Lake Project is located on the Guyandot River in Mingo and Wyoming Counties, West Virginia. The site is about 100 mi southeast of Huntington and 1 mi northeast of the town of Justice (see Fig. 1).

REGIONAL GEOLOGY

The following discussion of geology is based primarily on Design Memorandum 7B, prepared by Huntington District.⁵

The project site is located in the maturely dissected Kanawha section of the Appalachian Plateau physiographic province. The generally flat-lying sedimentary rocks have been eroded to produce mature topography. Stream gradients and hill slopes are steep, and flat land is found only in small discontinuous flood plains in the bottoms of river valleys.

The bedrock in the upper Guyandot River basin is composed of nearly flat-lying sandstones and shales with some coals and underclays. A generalized stratigraphic column for the dam and reservoir area is shown in Fig. 2. The spillway is in the Kanawha formation of the Pottsville group, from the Eagle sandstone member down to and including the Glenalum Tunnel shale member.

The geologic structure in the area is homoclinal, with beds dipping generally northwestward at approximately 1 deg. No folding was observed near the site and outcrops in the Guyandot valley walls showed nearly level beds dipping gently

downstream. No major faulting has been mapped in the reservoir area, and rocks exposed in the pilot excavation showed no evidence of faulting or shearing movements.

The formations of the Pottsville group contain numerous beds of bituminous coal. The thicker ones are commercially mined in southern West Virginia and adjacent states. The Little Eagle and the Lower War Eagle coal beds were penetrated by the pilot excavation, but neither is of sufficient thickness at this location to be economically mineable.

The rocks of the region show typical coal measures. Limited horizontal continuity of beds, rising and falling contacts, and rapid alternation of beds with very different mechanical properties are not uncommon.

SITE GEOLOGY

Rock Units

A description of the rock types in which the pilot excavation was performed is given in Fig. 3. The excavation was conducted in 5 lifts and 15 pilot blasts (PB) as discussed in Chapter 3. Figure 3 also shows the rock units associated with each pilot blast. The excavation was predominantly shale down through lift PB-4, and the lift comprising shots PB-5, 6, 7, and 8 was composed of sandstone, except for part of its base.

The Little Eagle coal, located slightly above the top of lift PB-1, was severely-to-moderately weathered near the ground surface. The 4-ft bed of sandstone at elevation 1328, which contains carbonaceous laminations, was also severely-to-moderately

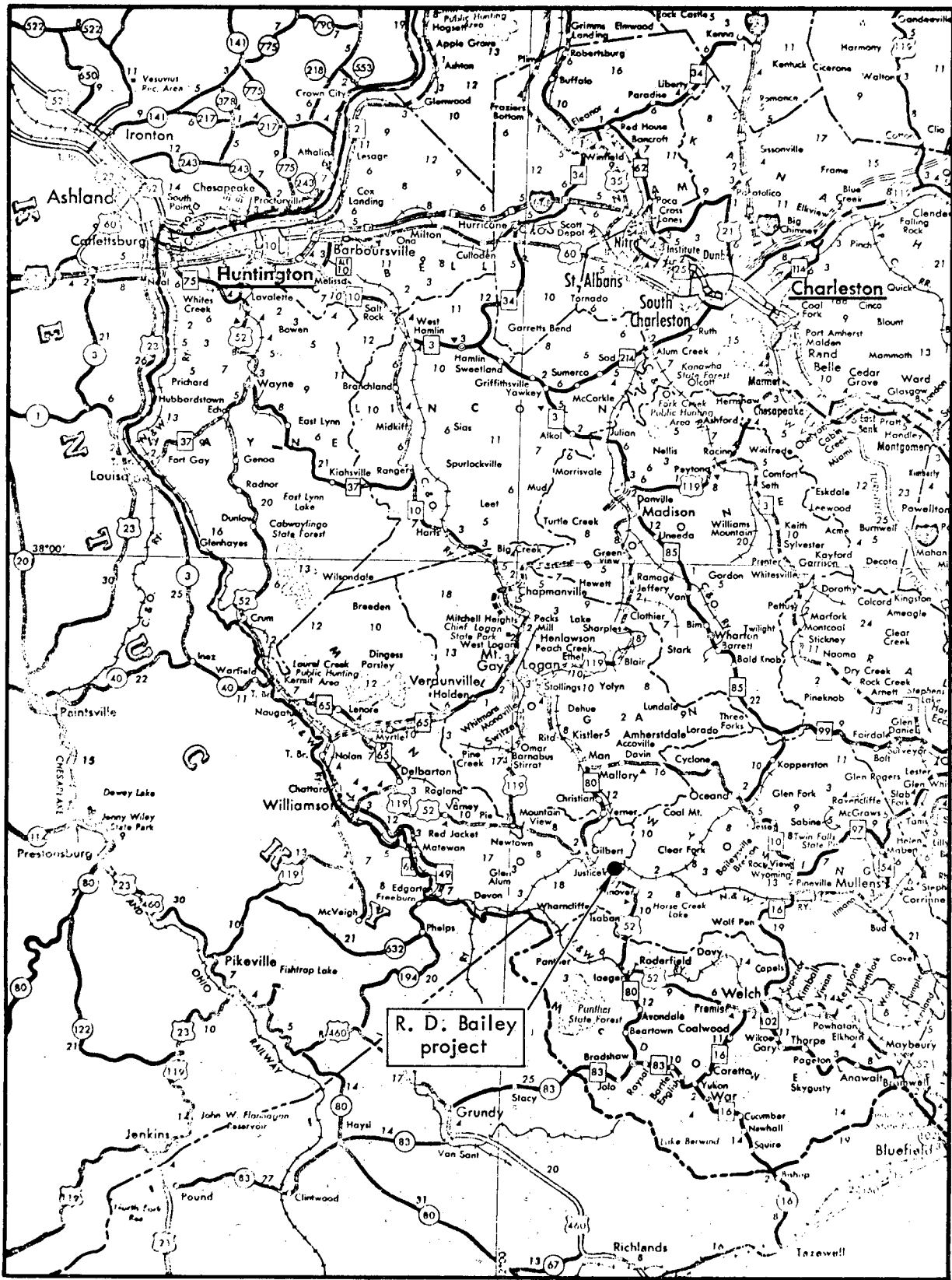


Fig. 1. Site location map.

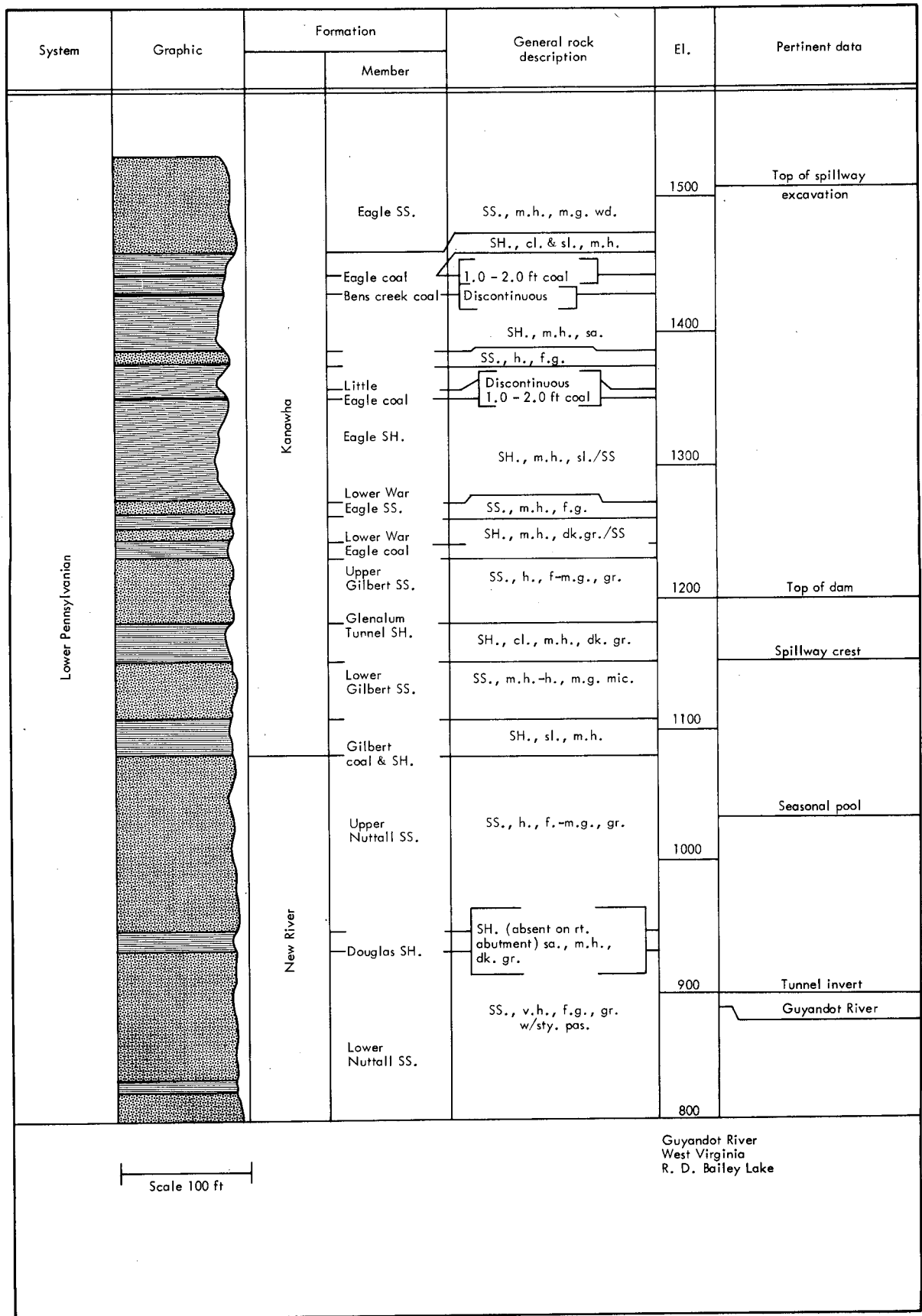


Fig. 2. Generalized geologic column.⁵

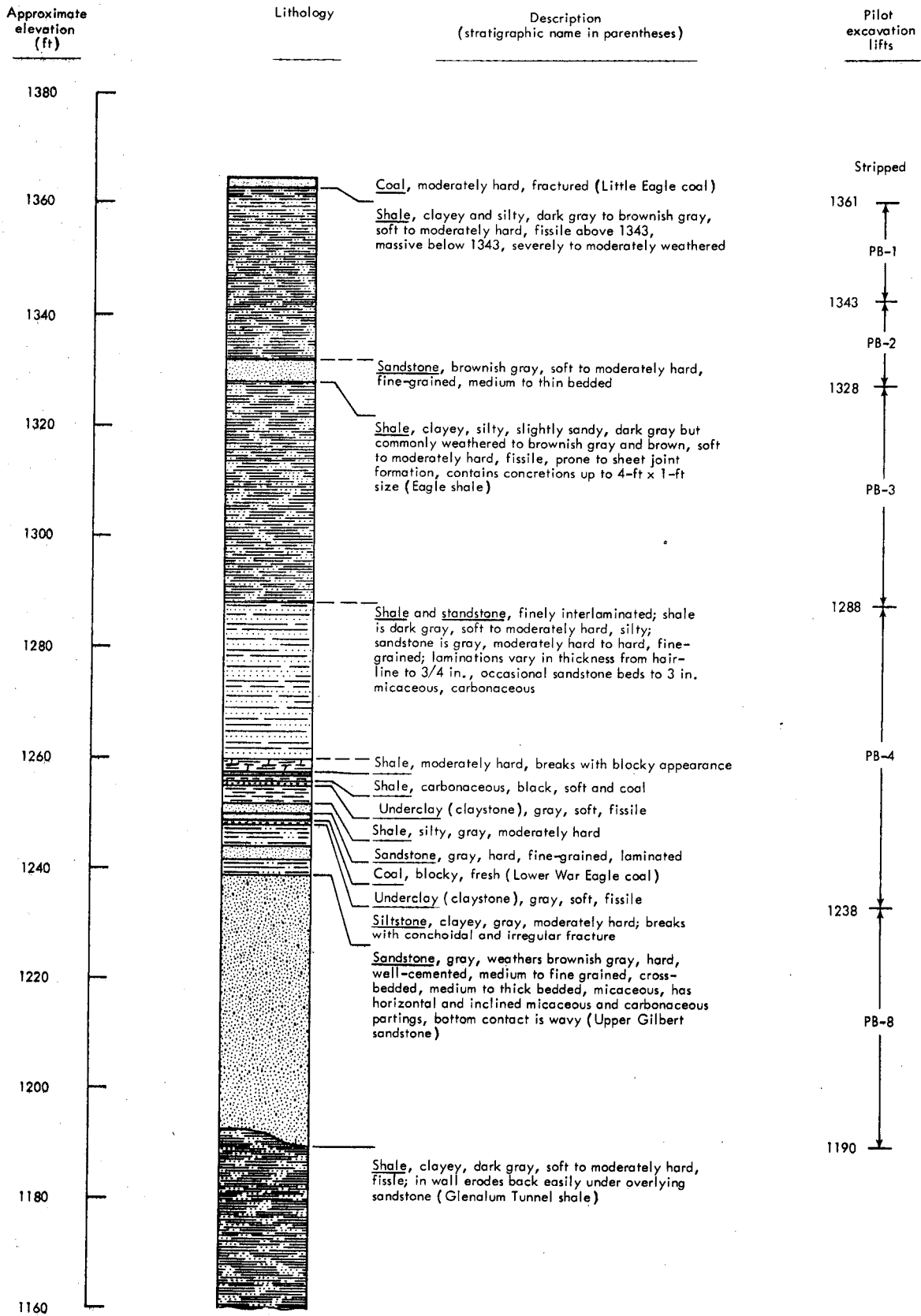


Fig. 3. Rock units in pilot excavation.

weathered. In the rhythmically inter-laminated shale and sandstone between elevations 1288 and 1260, the individual laminations showed lateral variations in thickness. Blasted surfaces in this unit had a characteristic rough appearance due to differences in hardness of the laminations. Two coal layers were found between elevations 1260 and 1240. The upper one was 6 in. thick or less and discontinuous. The lower coal bed, the Lower War Eagle coal, was about 1 ft thick and persistent. The siltstone beneath the two coals contained a bed of massive, hard, fine-grained sandstone near its base. This entire siltstone unit was found to be tough, and would definitely require blasting to excavate.

The Upper Gilbert sandstone, though generally medium-to-thick bedded, was locally thin-bedded in places. This unit was generally found to be fresh, but near the ground surface and along joints and partings it was weathered, stained, and softened.

Structural Geology

The strike of the bedding at the pilot excavation site was parallel to the back (west) wall, N17°W, with a dip to the west-southwest of about 22 ft in 1000 ft.

Jointing was the structural feature of most interest at the pilot excavation. A pattern of joints termed "sheet joints" was extensively developed. These sheet joints had a great influence on the mechanical character of the rocks, the distribution of weathering, and the groundwater flow. Rather than a single joint occurring separately, several closely spaced joints commonly occurred together, producing the appearance of vertical

"sheets" of rock. The spacing between the individual joints was a fraction of an inch in the shales and approximately 1 to 4 in. in the sandstones. Sheet jointing was more common in fissile shale than in nonfissile shale, and occurred at high angles. In some places, notably in the Eagle shale near the northwest corner of the pilot excavation, the joints showed a spheroidal pattern.

The Eagle shale member above the Lower War Eagle coal showed extensive sheet jointing in the pilot excavation. This jointing was most pronounced near the surface and decreased with depth. A sheet joint in the Eagle shale (lift PB-3) is shown in Fig. 4.



Fig. 4. Weathered sheet joint in fissile clayey shale, PB-3 (metal rule in lower left is 2 in. square).



Fig. 5. Sheet joint in Upper Gilbert sandstone (to right of center), PB-6B.

Sheet jointing diminished markedly below the two coals in PB-4. It was present in the Upper Gilbert sandstone, but at much wider spacing than in the shale above. Figure 5 shows sheet joint development in the Upper Gilbert sandstone. In the sandstone, as in the shale, rock near the sheet joints was usually highly weathered.

The two principal joint orientations observed at the project site were N50°E with a dip 75 to 90° to the northwest, N40°W with a dip 75 to 90° to the southwest. The set with strike of N50°E was best developed. The joints in this set were spaced at intervals of 6 to 30 ft in the Upper Gilbert sandstone, whereas joints in the set with strike of N40°W were spaced at about 40 ft. The spacing between sheet joints in the Eagle shale was much closer, roughly 5 to 10 ft.

Wedge-shaped blocks of rock fell out of the wall at locations where sheet joints intersected near the walls of the pilot excavation. This phenomenon was observed particularly in the south wall of PB-4 in the laminated shale and sandstone above the coals.

An oblique discontinuity, probably of sedimentary origin, was noted in the beds of hard siltstone in PB-4 beneath the Lower War Eagle coal. The discontinuity dipped at an angle of about 25° to the southwest, and was continuous through a horizontal interval of 32 ft and a vertical interval of 15 ft; it did not continue into the overlying Lower War Eagle coal.

Weathering

All the rock units in the pilot excavation, down through the Upper Gilbert sandstone, showed weathering. In the surface material there was a pervasive alteration to brown clayey material, leading ultimately to a clayey and colluvial soil rich in silt, sand, and weathered rock fragments. At depth, the weathering was generally controlled by sheet jointing.

Brownish weathered material existed in the vicinity of sheet joints in the shales above elevation 1288. About 90% of the Eagle shale in the south face of PB-3 and about 50% in the north face were stained brown. Weathering discoloration also followed along bedding planes and along a few fractures oblique to the bedding.

Sheet jointing and its accompanying weathering continued into the laminated shale and sandstone in the upper part of PB-4, but less pervasively than in the shale above. Sheet joints and weathering diminished abruptly at the upper coal layer; the weathering was directly related to the groundwater flow pattern. The appearance of the weathering pattern, as seen in the rear wall of the pilot excavation, is shown in Fig. 6.

Weathered joints were present but more widely spaced in the hard siltstone and in the Upper Gilbert sandstone below

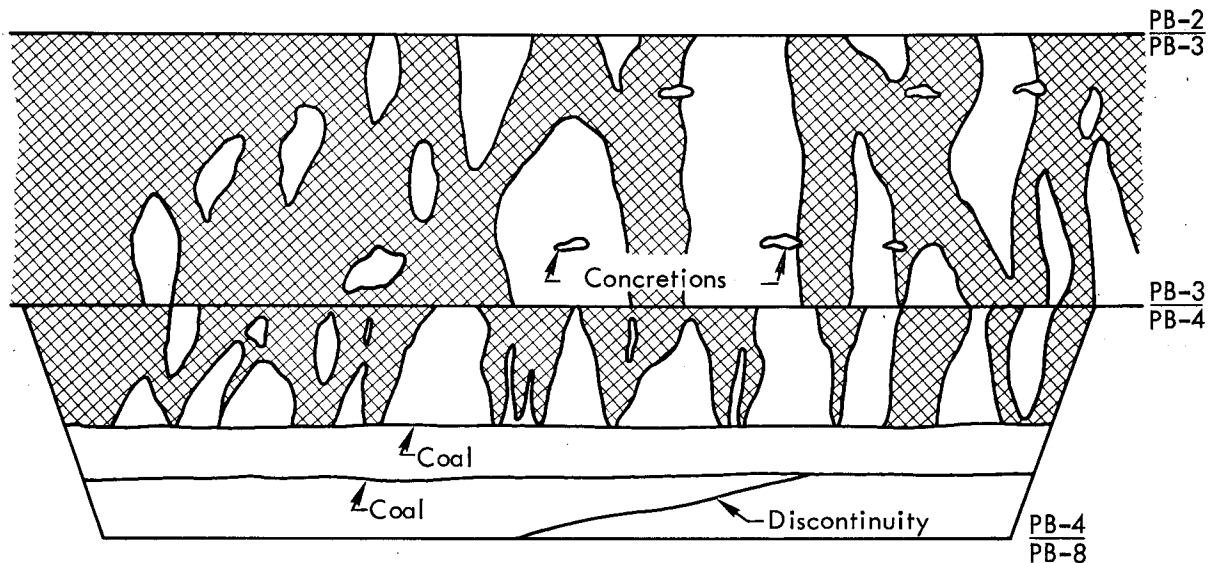


Fig. 6. Appearance of back (west) wall, pilot excavation, lifts PB-3 and PB-4 above coals – crosshatched areas are brown-stained (from weathering along sheet joints; white areas, unweathered gray rock. (From a sketch by R. J. Lutton, WES Soils and Pavements Laboratory.)

the coals. Weathering in the sandstone extended out from the joints along bedding planes and micaceous partings. The rock was effectively softened and weakened in the weathered joint zones, as it was near the ground surface.

Groundwater Hydrology

The two coal beds exposed in the walls of PB-4 were notably wet, particularly the upper one. The coals appeared to

weep and in places there were small springs at the level of the upper coal. Groundwater evidently percolates downward through the sheet joints in the Eagle shale until it reaches the upper coal and finds a permeable bed underlain by the relatively impermeable underclay. The water then flows laterally in the coal till it finds a breach in the underclay or until it exits at the ground surface as a spring.

Chapter 3. Description of Test Blasts

GENERAL

The principal feature of the program was a pilot excavation located in the upstream end of the spillway. The excavation was conducted in five lifts, resulting in a cut 300 ft long with a maximum depth of 175 ft. There were nine principal pilot blasts: PB-1 through PB-5, PB-6A,

PB-6B, PB-7, and PB-8. Figures 7 and 8 show the PB's, a centerline profile, and a cross section of the pilot excavation. Approximately 152,000 yd³ of rock were removed from the cut.

The material consisted of two major rock types, shale and sandstone, as discussed in detail in the preceding chapter. Test blasts were conducted in

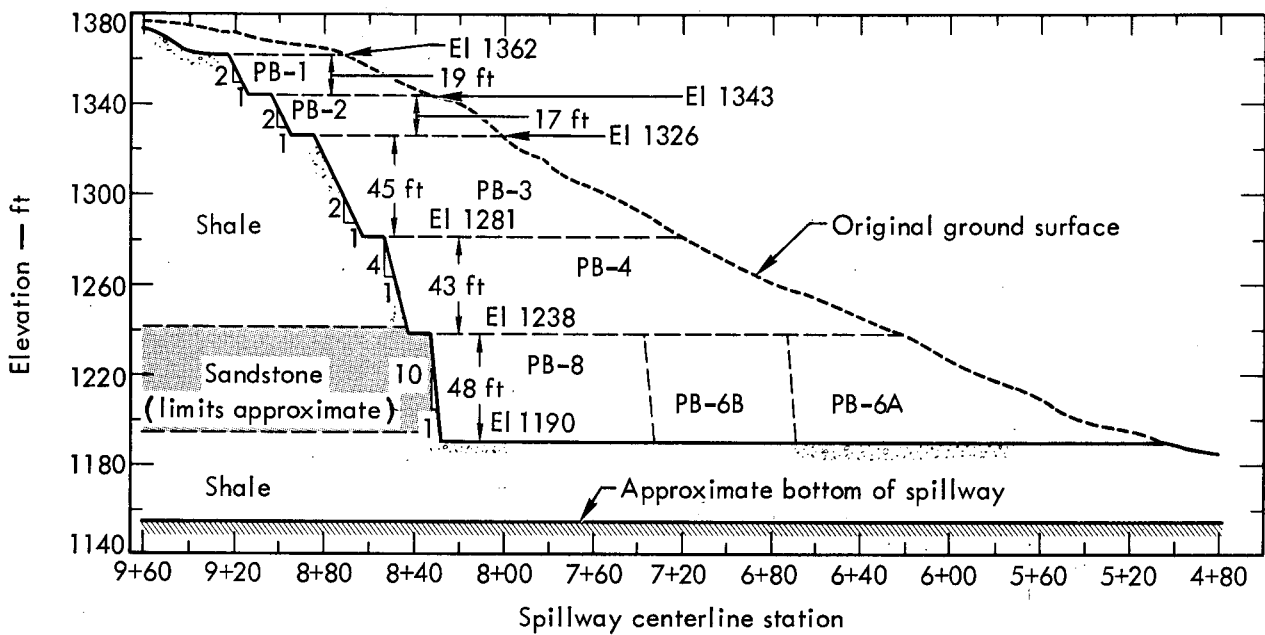


Fig. 7. Centerline profile of pilot excavation (looking north).

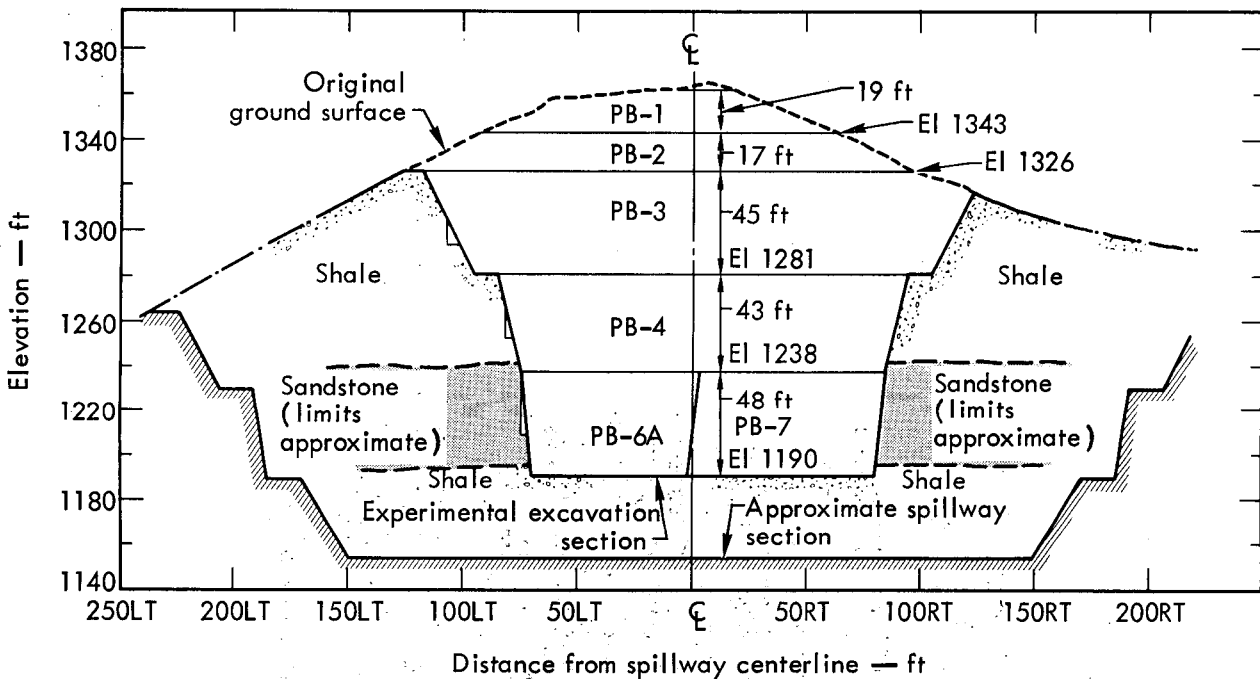


Fig. 8. Cross section of pilot excavation (looking west).

the shale using blastholes with diameters of 3, 6-3/4, and 9 in. Test blasts in the sandstone were performed with 3-, 6-1/4-, 9-, and 12-1/4-in.-diameter blastholes.

Two types of explosives were used and compared in the test blasts, ANFO and aluminized ammonium nitrate slurry. A declaration of composition and performance for the slurry is presented in

Manufacturers Declaration -2-

Manufacturers Declaration of Performance Composition and Safety for Slurry Blasting Agent MS 80-25 Manufactured by Dow Chemical U. S. A.

A. Performance

1. Confined detonation velocity: 4,783 ft/Sec., 15° C.
(See Attachment I for procedure)
2. Detonation pressure: 31.97 kilobars; 13° C.
(See Attachment II for procedure)
3. Density: 1.10 gm/cm³; 13° C.
(See Attachment III for procedure)
4. % Aluminum Content: 22.5
5. Total energy: 1332 ±50 cal/gm; 13° C.
(See Attachment II for procedure)

B. Composition

- | | | |
|---|-------------------|-------|
| 1. Oxidizers: | Ammonium nitrate | 49.1% |
| | Sodium nitrate | 9.0% |
| 2. Liquid vehicle: | Water | 14.0% |
| | Formamide | 4.0% |
| | Ethylene glycol | 2.0% |
| 3. Aluminum | | 22.5% |
| 4. Gelling agent and stabilizer: | Modified guar gum | 1.12% |
| 5. Miscellaneous ingredients: (includes inorganic pH control and organic preservatives) | | 2.65% |

Safety

1. Rifle bullet sensitivity: 3 3/8" dia. x 3" deep, 15° C.
(200 Swift) 4" dia. x 2" deep, 15° C.
result: no reaction
(See Attachment IV for procedure)

2. No. 9 test cap sensitivity: no reaction
(see Attachment V for procedure)
3. Flame sensitivity test: no reaction (See Attachment VI)
4. DOT class: Nitro-Carbo-Nitrate: Oxidizing Material
5. Compatibility:

- a. Storage and test containers and instrumentation
Incompatible with copper and copper alloys, zinc and zinc alloys; severe corrosion of these metals will take place.
Generally compatible with mild steel for periods up to 30 days, however, a layer of rust will form at the slurry/steel interface.
Compatible for extended periods of time in plastic (ie. polyethylene, saran, PVC, lucite, etc.), aluminum, stainless steel, nickel and tin; also epoxy resins and paints without pigments which could react.
- b. Compatibility with common explosive for priming purposes.
Do not prime with dynamites or other compounds with low heat and or low detonation pressures. Compatible primers include 50/50 Pentolite; RDX; Compositions B, C-4, H-6 and others with equivalent or higher detonation heats and pressures.

R. B. Moen
R. B. Moen
Business Development Engineer

Subscribed and sworn to before me 6th day of March, 1973.

Marianne R. Kyzar
Notary Public

Notary Public, Dallas County, Texas
My Commission Expires July 1, 1978.



Fig. 9. Declaration of performance, composition and safety for Dow MS 80-25 slurry blasting agent.

Fig. 9. Several controlled blasting techniques were tested in conjunction with each blast, and details of the test blast designs are presented in the following paragraphs.

After commencing work in the weathered shale, it was decided that much of the shale should be ripped. Ripping tests were conducted down to a depth at which ripping was no longer practical.

Samples of both blasted rock and ripped material removed from the pilot excavation were used to construct test fills. Various lift thicknesses and several types of compaction equipment were tested. Details of the test fill program are presented in Chapter 8.

PB-1 TEST BLAST

PB-1 was the first experimental blast and was located near the crest of a ridge crossing the spillway centerline. Approximately 8 ft of overburden was stripped from the area before rock was encountered hard enough that it could not be scraped with the blade of a D-8 bulldozer. Although the material could not be moved with a dozer blade, it would have been possible to rip it.

As shown in Fig. 10, the blast design was a vee-cut delay sequence. The blast holes were 3 in. in diameter and contained a total of 1150 lb of ANFO. The average loading density was 2.71 lb of ANFO per foot of drill hole.

There was very little flyrock associated with the blast, and the ground surface above the blast appeared relatively intact, although it was lifted about 3 ft above the preshot elevation. Fracturing in the surface rock tended to follow the joint pattern.

The blasted rock was readily excavated with the front-end loader, and blocks about 5 ft in diameter crumbled upon handling during excavation. Figure 11 shows the front-end loader excavating the the blasted rock from PB-1.

The presplit line was undiscernible in the severely weathered material, but in the moderately weathered region it was well-defined. There was some overbreak in the top 2 to 3 ft of the presplit line, and tension cracks were noted as far as 5 ft beyond the presplit line.

PB-2 TEST BLAST

All of the material in PB-2 was ripped by a D-8 tractor with the exception of a 10- to 15-ft section adjacent to the rear wall. The PB-2 material appeared to be similar to that observed in PB-1, and it was ripped with little difficulty (see Fig. 12).

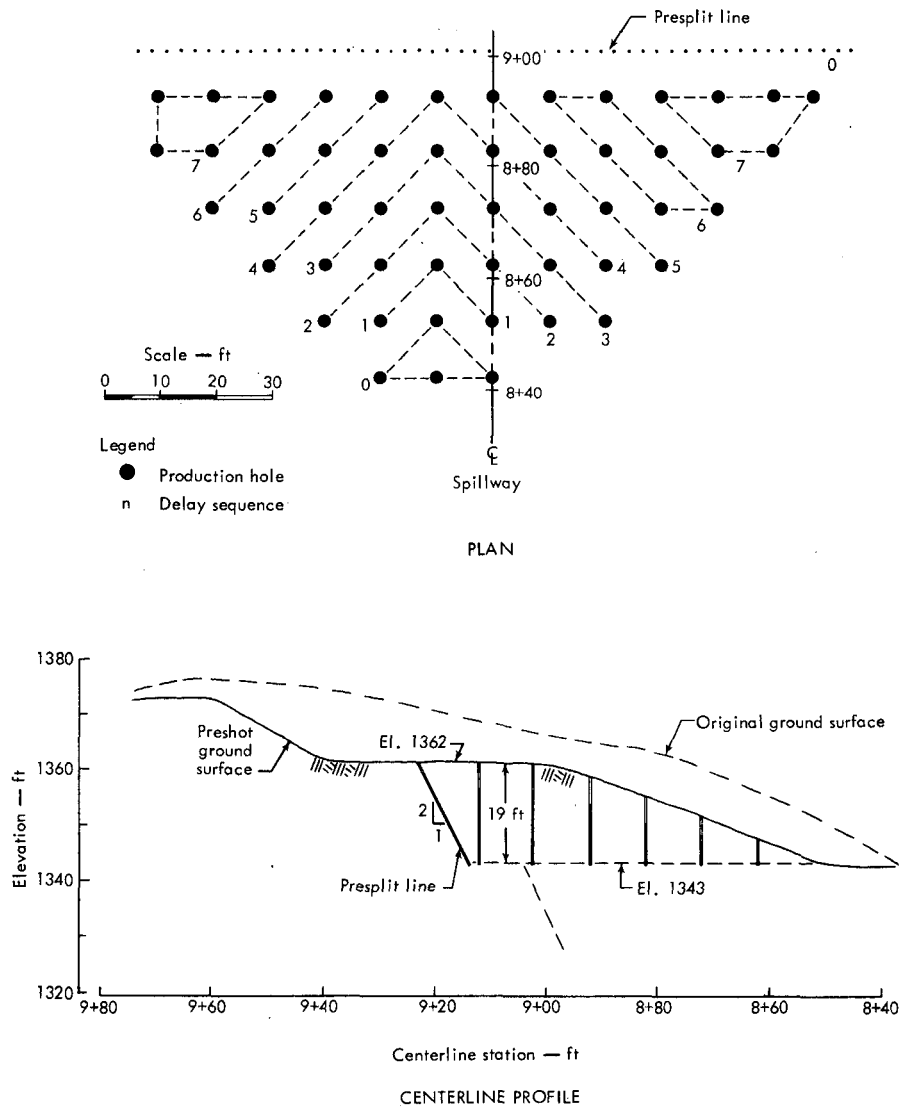
The rear wall was formed into a smooth face with a trimming blast identical to the presplitting array on PB-1, except that most of the material in front of the face had been previously removed. Very little overbreak occurred behind the trimming line (see Fig. 13). The trimming procedure was advantageous from a construction standpoint because ripping and drilling could proceed concurrently.

PB-3 TEST BLAST

Approximately two thirds of the PB-3 material was ripped (down to elevation 1296), and most of the remainder was blasted. All of the weathered rock was similar to that encountered in PB-1 and PB-2, but some zones of less weathered

shale were encountered. The blast design is shown in Fig. 14. The PB-3 charges were designed to break to the top surface of the bench rather than to the vertical face. Therefore, the charges were detonated simultaneously.

The rear and left (looking downstream) walls of PB-3 were formed by a combination trimming/presplitting shot (see Fig. 15). The top 30 ft of PB-3 had been ripped and excavated to within 10 to 15 ft of the final walls. Consequently, the top



Additional information:

Production holes

Diameter = 3 in.
 Pattern = 10 x 10 ft sq.
 Delays = "V" cut, 25 msec intervals
 Explosive = ANFO
 Boosters = HDP-1, 2 per hole
 Burden = 7 ft
 Spacing = 14 ft
 Stemming = 5 ft
 Subdrill = 1 ft

Presplit holes

Diameter = 3 in.
 Spacing = 30 in.
 Stemming = 4 ft
 Explosive = Trinitex, 70%, 1/4 lb/ft

Fig. 10. PB-1 blast design.

30 ft of PB-3 were trimmed, and the bottom 15 ft were presplit; there was no discernable difference in the results of the two techniques.



Fig. 11. Excavating from PB-1 blast.



Fig. 12. Ripping PB-2.



Fig. 13. Trimming PB-2.

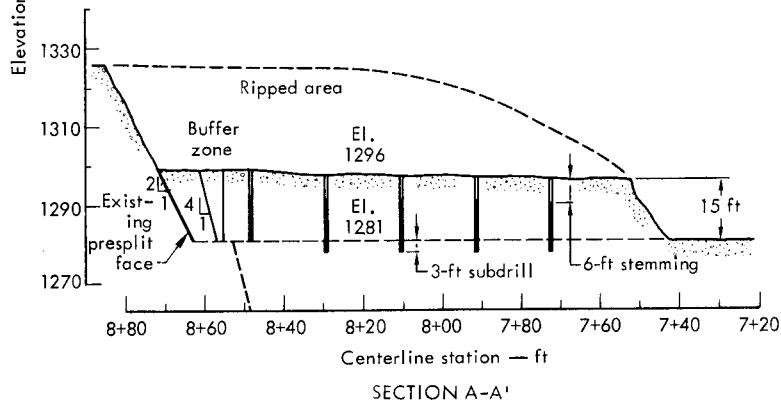
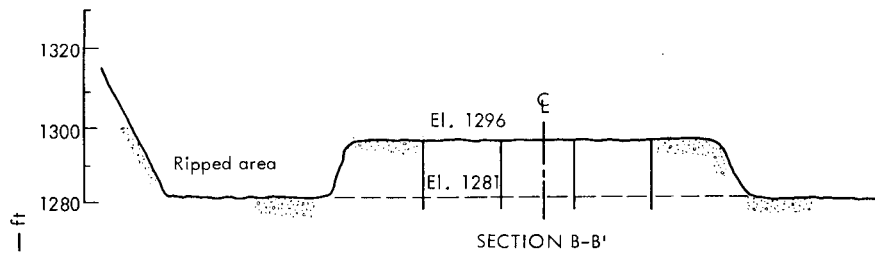
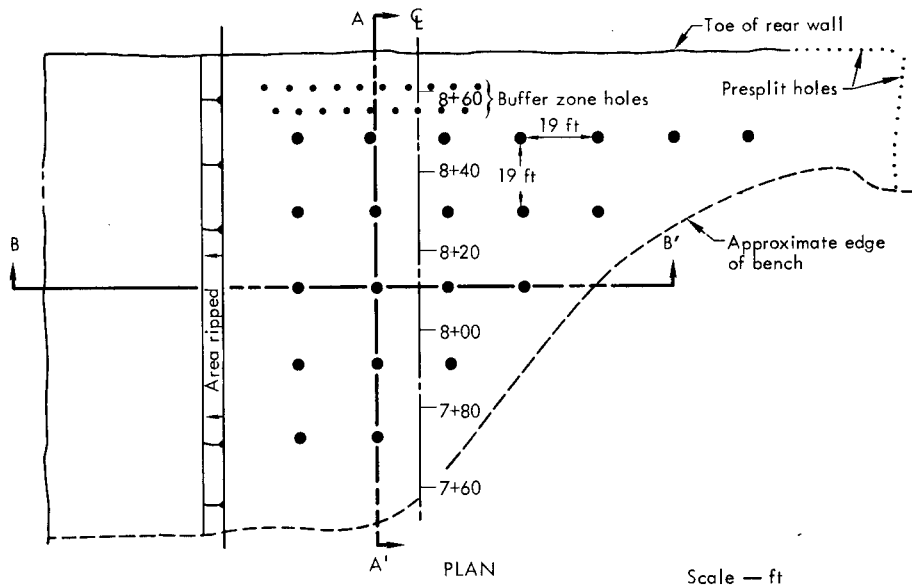
A total of 3300 lb of ANFO was used in the production charges of the PB-3 blast, and the average loading density for the 6-3/4-in.-diameter blasthole was 13.65 lb/ft of hole. Flyrock was thrown to a height of about 150 ft over a 150-ft radius, but no appreciable quantity of rock was lost. Yellow-brown smoke visible after the shot suggested partial deflagration or improper oxygen balance of the explosive even though the blastholes were dry prior to loading. All of the blasted rock was sufficiently fractured to be excavated with the front-end loader (Fig. 16).

PB-4 TEST BLAST

Ripping operations were continued on the right-hand side of the PB-4 area until it was no longer practical to do so at elevation 1265, where a hard, gray shale was encountered in the rear of the cut.

The presplit blast for PB-4 was fired several days prior to the production charges. Most of the presplit holes along the left side contained 18 to 20 ft of water, and the production charge holes also contained up to 18 ft of water. The production charge holes were bailed out and lined with a plastic sleeve prior to loading with ANFO. Figure 17 shows the blast design for PB-4. Figure 18 shows ripping operations, and Figs. 19 and 20 show pre-shot and postshot views of PB-4.

The rock in the PB-4 lift included two coal layers 6 to 12 in. thick, approximately in the middle of the lift. These were the principal sources of water inflow. Sandstone and shale were encountered below the coal that were harder than the shale overlying the coal. After



Additional information:

Production holes
 Diameter = 6-3/4 in.
 Pattern = 19 x 19 ft sq.
 Delays = All production charges fired simultaneously
 Explosive = ANFO
 Boosters = 2 x 8-in. sticks 85% dynamite; 3 per hole
 Burden = NA
 Spacing = NA
 Stemming = 6 ft
 Subdrill = 3 ft

Presplit holes
 Diameter = 3 in.
 Spacing = 30 in.
 Stemming = 4 ft
 Explosive = Trintex, 70%, 1/4

Buffer zone holes
 Diameter = 3 in.
 Pattern = 2 rows, staggered
 Spacing = 6 ft
 Explosive = Trintex, 70%, 1/4 lb/ft
 Stemming = 4 ft

Fig. 14. PB-3 blast design.



Fig. 15. PB-3 trimming/presplit, rear wall.

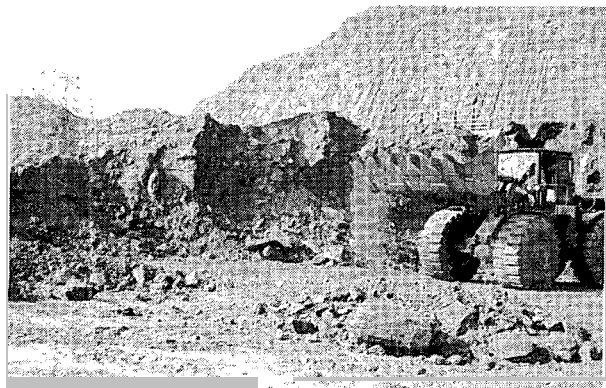


Fig. 16. Excavating PB-3 blasted rock.

excavating as much of the blasted rock as possible, the bottom of PB-4 was still 6 to 12 ft above the planned grade (see Fig. 21).

PB-4A THROUGH PB-4E TEST BLASTS

Although the rock in the bottom of PB-4 had been previously blasted with ANFO in 9-in.-diameter holes in a 24-ft square pattern, the only discernible blast-induced fracturing was found in the immediate vicinity of some of the blast-holes. The rock could not have been removed without supplementary blasting. Blasts PB-4A through PB-4E were five blasts intended to lower the floor of the PB-4 area down to elevation 1238. The

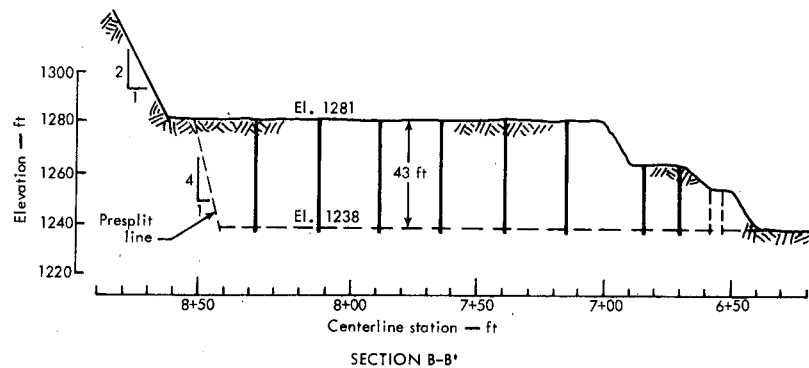
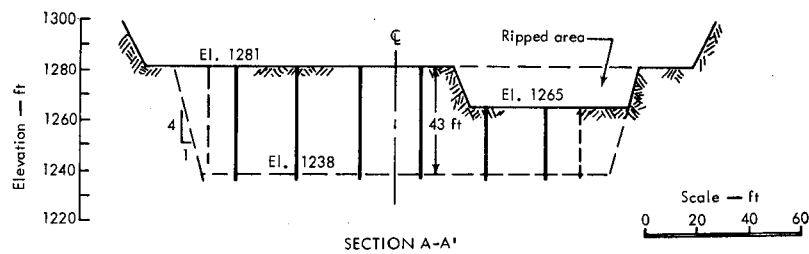
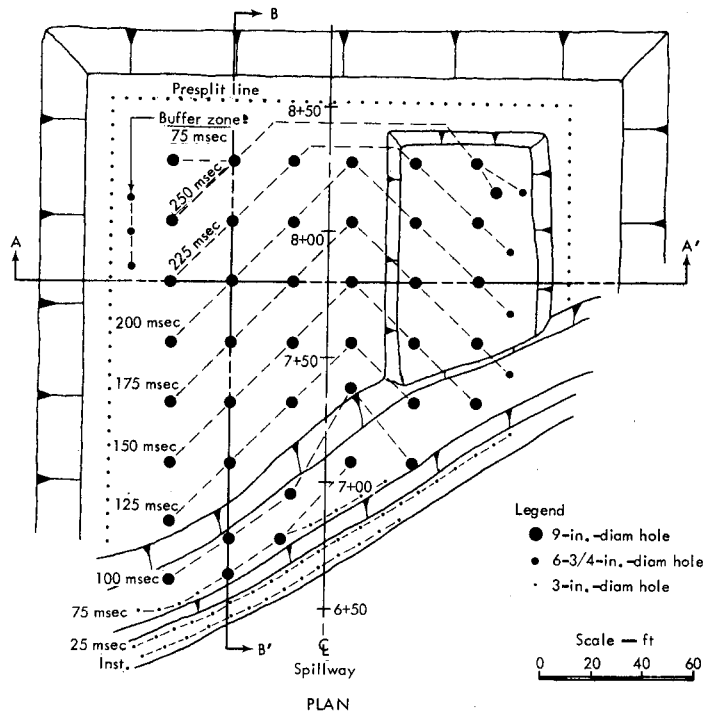
blasts consisted of various patterns of 3-in.-diameter holes (see (Fig. 22). PB-4E was in sandstone, while the other shots contained both sandstone and hard shale. PB-4A, 4B, and 4D all broke to elevation 1238, (Figs. 23 through 26), but PB-4C left a triangular-shaped shelf approximately 4 ft high in the right rear corner of the cut. This shelf was bounded on the top by a shale-sandstone contact and on the side by a joint. The shelf was redrilled and designated PB-4E (see Fig. 27); almost all of the holes contained water at the time they were loaded with slurry explosive. The shot successfully removed the shelf, however. The explosive quantities used for each shot were PB-4A, 803 lb ANFO; PB-4B, 3128 lb ANFO; PB-4C, 1683 lb ANFO; PB-4D, 1581 lb ANFO; and PB-4E, 550 lb slurry.

PB-5 TEST BLAST

The rock adjacent to the PB-5 area had previously been blasted with 6-in.-diameter charges during construction of the haul road. This blasting had severely fractured the PB-5 rock and caused difficulty in drilling and loading the shot. Some holes were blocked and could not be loaded at all, and some of the explosive was lost in fractures intercepted by the drill-holes. The total weight of ANFO used was 1188 lb. The blast design for PB-5 is shown in Fig. 28. Much of the sandstone was weathered, and broke into thin slabs when blasted (see Fig. 29).

PB-6A TEST BLAST

The purpose of the PB-6A test blast was to test 6-1/4-in. blastholes loaded with



Additional information:

Production holes

Diameter = 9 in.
 Pattern = 24 ft sq.
 Delays = "V" cut, intervals shown on plan
 Explosive = ANFO
 Boosters = HDP-1, 4 per hole
 Burden = 17 ft
 Spacing = 34 ft
 Stemming = 14 ft
 Subdrill = 3 ft

Presplit holes

Diameter = 3 in.
 Spacing = 30 in.
 Stemming = 4 ft
 Explosive = Trimtex, 70%, 1/4 lb/ft

Buffer zone holes

Diameter = 6-3/4 in.
 Spacing = 20 ft
 Explosive = ANFO, 4 50-lb decked charges
 Boosters = HDP-1, 2 per deck
 Stemming = 12 ft top, 4 ft between decks

Fig. 17. PB-4 blast design.

ANFO in the Upper Gilbert sandstone (see Fig. 30). The presplit was fired several days before the production charges. Most of the production charge holes in the



Fig. 18. Ripping PB-4.

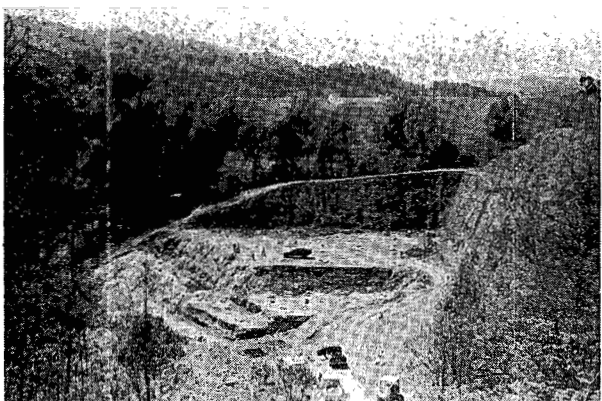


Fig. 19. PB-4 preshot.



Fig. 20. PB-4 postshot surface.

interior of the pattern were already drilled to the bottom of the sandstone at the time of the presplit blast. Many of these holes were blocked at about elevation 1196 because of mass shifting of rock from the presplit blast. PB-6A was loaded down only to elevation 1196, therefore, and the remainder of the lift was redrilled and blasted along with PB-6B.

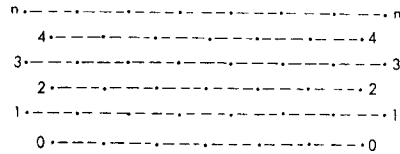
The loading density for ANFO in these holes was estimated to be 12.60 lb/ft with a total weight of 15,350 lb of explosive. Figures 31 and 32 show preshot and post-shot views of the PB-6A area.

PB-6B TEST BLAST

The PB-6B blast was intended to test Dow MS 80-25 slurry in 6-1/4-in.-diameter blastholes in the Upper Gilbert sandstone. The blast design for PB-6B is shown in Fig. 33. The bottom of the PB-6A area was redrilled and blasted along with PB-6B (Fig. 34). Some difficulty was encountered in loading the slurry into the 6-1/4-in.-diameter holes. The slurry was packaged in two sizes of plastic sausages, 4 in. in diameter and 8 in. in diameter. The 4-in. sausages loaded easily, but the



Fig. 21. PB-4 after excavation of fractured rock.



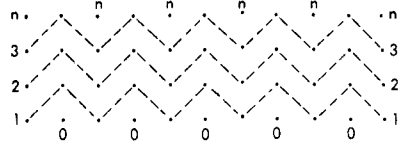
Legend
 • Production hole
 n Delay sequence

Scale — ft
 0 10 20 30

Plan (typical)

Additional information:
 Hole diameter = 3 in.
 Number of holes = 50
 Number of rows = 8
 Average hole depth = 6 ft
 Pattern = 10 x 5 ft staggered
 Explosive = ANFO
 Boosters = HDP-1, 1 per hole
 Stemming = 2 ft

PB-4A



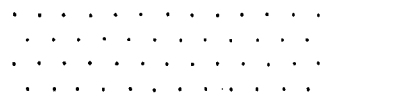
Legend
 • Production hole
 n Delay sequence

Scale — ft
 0 10 20 30

Plan (typical)

Additional information:
 Hole diameter = 3 in.
 Number of holes = 247
 Number of rows = 8
 Average hole depth = 9 ft
 Pattern = 7 x 7 ft sq
 Explosive = ANFO
 Boosters = 1-lb cast
 Stemming = 4 ft

PB-4B



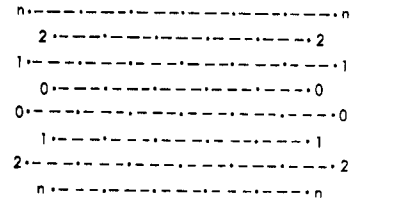
Legend
 • Production hole

Scale — ft
 0 10 20 30

Plan (typical)

Additional information:
 Hole diameter = 3 in.
 Number of holes = 176
 Number of rows = 4
 Average hole depth = 12 ft
 Pattern = 5 x 5 ft staggered
 Delays = none
 Explosive = ANFO
 Boosters = 1-lb cast
 Stemming = 4 ft

PB-4C



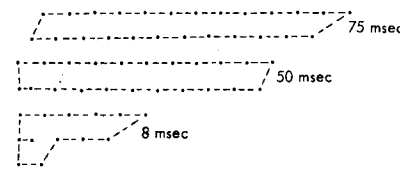
Legend
 • Production hole
 n Delay sequence

Scale — ft
 0 10 20 30

Plan (typical)

Additional information:
 Hole diameter = 3 in.
 Number of holes = 169
 Number of rows = 16
 Average hole depth = 6 ft
 Pattern = 10 x 5 ft staggered
 Delays = 25 msec
 Explosive = ANFO
 Boosters = HDP-1
 Stemming = 2 ft

PB-4D



Legend
 • Production hole

Scale — ft
 0 10 20 30

Plan

Additional information:
 Hole diameter = 3 in.
 Number of holes = 60
 Number of rows = 7
 Average hole depth = 6 ft
 Pattern = 5 x 5 ft staggered
 Delays = as shown
 Explosives = DOW MS-80-25
 Al-AN slurry
 Boosters = 1/2 lb cast, 2 per hole
 Stemming = 3 ft

PB-4E

Fig. 22. Blast designs for PB-4A through PB-4E.

slurry in the 8 in. sausages had to be cut up and dropped down the hole. The slurry tended to bridge in the hole before



Fig. 23. Blasted rock from PB-4A (1-ft² grids).



Fig. 24. Blasted rock from PB-4B.

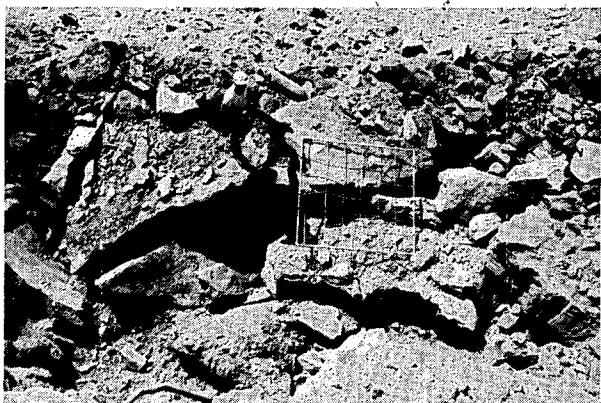


Fig. 25. Blasted rock from PB-4C (1-ft² grids).

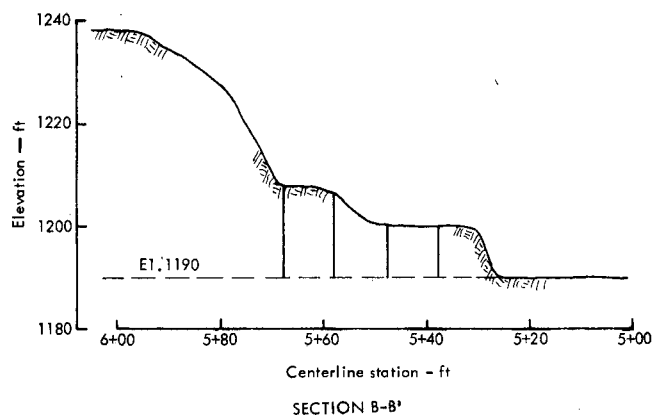
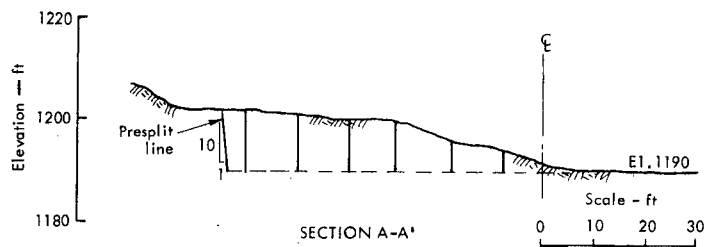
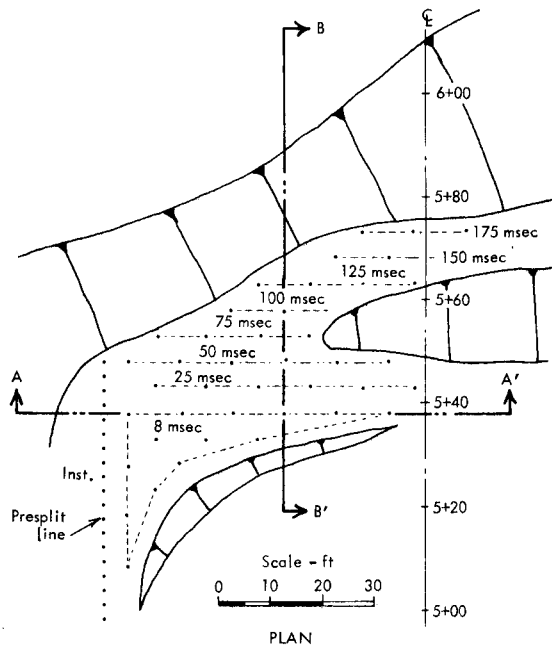
reaching the bottom and in several cases the blockages could not be dislodged. Blockages occurred in the two blast holes nearest the vertical face (i.e., those charges on the 25-msec delay). The lack of sufficient explosive in these first two holes possibly resulted in over-confinement of charges in the following delays. Consequently, the rock was fractured sufficiently only to excavate down to about one half of the total lift height (Fig. 35). The total weight of slurry used was 8600 lb, and the average loading density (not including holes that were known to be blocked) was about 12 lb/ft of hole.



Fig. 26. Blasted rock from PB-4D (1-ft² grids).



Fig. 27. PB-4E preshot.



Additional information:

Production holes	Presplit holes
Diameter = 3 in.	Diameter = 3 in.
Pattern = 5x10 ft staggered	Spacing = 30 in.
Delays = row by row, as shown	Stemming = 4 ft
Explosive = ANFO	Explosive = Trinitex, 70% 1/4 lb/ft
Boosters = 1-lb cast	
Burden = 5 ft	
Spacing = 10 ft	
Stemming = 4 ft	
Subdrill = 0 ft	

Fig. 28. PB-5 blast design.



Fig. 29. Blasted rock from PB-5 (1-ft² grids).

PB-6C TEST BLAST

This blast was in rock remaining from the PB-6B blast. The charges were located between the PB-6B charge locations to facilitate drilling and to place the explosive in the less fractured rock (Fig. 36). Two holes in the right-front area were deleted because the rock was too fractured to drill. The total weight of slurry used in this shot was 1960 lb, and the loading density was 14.4 lb/ft of hole. Figure 37 shows the PB-6C preshot condition, and Fig. 38 shows the blasted rock during excavation.

PB-7 TEST BLAST

The PB-7 blast (Fig. 39) was designed to test Dow MS 80-25 slurry in 9-in.-diameter blastholes, based on experience

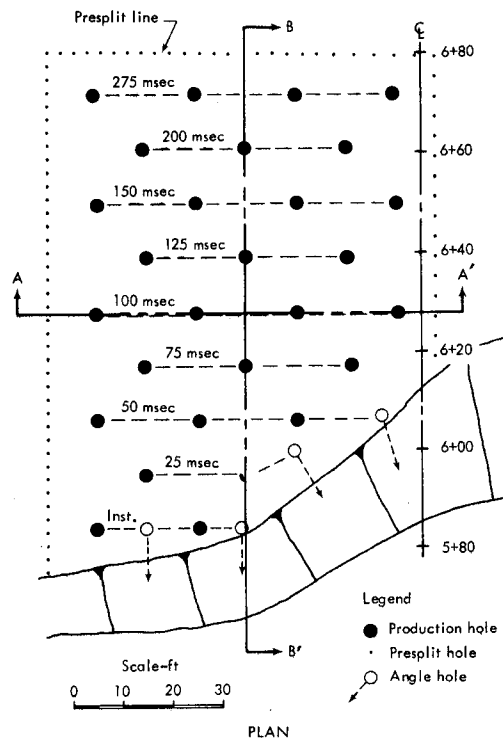
gained in PB-6B. The slurry was packaged in 8-in.-diameter sausages. Each sausage was cut in half and dropped down the 9-in.-diameter holes, occasionally bridging on the way to the bottom and requiring a poke from a loading pole.

Because the left-rear hole in PB-7 was monitored by a radial array of subsurface velocity transducers, this charge was fired with a zero delay so that velocity measurements could be recorded without interference from other charges. In a normal delay sequence this particular hole would have been fired with delay number 5. The total weight of slurry used in PB-7 was 19,950 lb, and the average loading density was 31.7 lb/ft of hole. Figures 40 and 41 show preshot views of PB-7.

During excavation of PB-7 some large blocks were encountered in the area of the spillway centerline, between the first row of blastholes and the vertical free surface. Inside this area the rock was well-fractured (Fig. 42).

PB-8 TEST BLAST

PB-8, the largest blast in the series, tested 12-1/4-in.-diameter blastholes loaded with Dow MS 80-25 slurry and delayed in a vee pattern (Fig. 43). The original plan for drilling the production holes for PB-8 was to drill 9-in.-diameter holes to full depth and then to ream them out to 12-in.-diameter, using foam to carry out the cuttings. This procedure was followed until the reamer bearings failed after drilling approximately 130 linear ft. The decision was made to drill the remaining holes with a full-face, 12-1/4-in. bit. An air compressor was connected



Additional information:

Production holes
 Diameter = 6-1/4 in.
 Pattern = 11 x 20 ft staggered rows
 Delays = Row by row, as shown
 Explosive = ANFO
 Boosters = HDP-1's, cluster of 3 per hole
 Burden = 11 ft
 Spacing = 20 ft
 Stemming = 7 ft
 Subdrill = 0 ft

Presplit holes
 Diameter = 3 in.
 Spacing = 30 in.
 Stemming = 4 ft
 Explosive = Trinitex, 70%
 1/4 lb/ft

Legend

- Production hole
- Presplit hole
- Angle hole

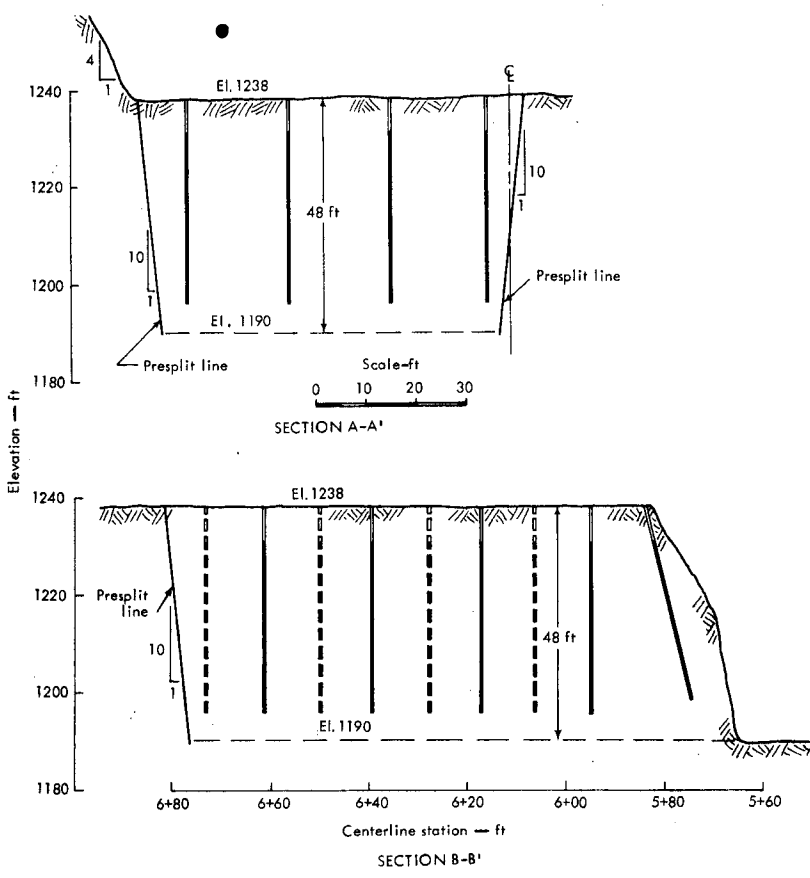


Fig. 30. PB-6A blast design.

in tandem with the compressor on the drill, and the cuttings were blown out with air. The blastholes were loaded with slurry packaged in 8-in. sausages. It was not necessary to cut the slurry as was done for the smaller diameter holes. Figures 44 and 45 show preshot and postshot views of PB-8, and Fig. 46 shows excavation of the blasted rock.



Fig. 31. PB-6A preshot.



Fig. 32. Blasted rock from PB-6A.

A 10-ft bench was to be left along the rear of the cut at the original ground surface of PB-8, but the bench was destroyed by the blast. Although the rock was well-fractured up to the left and right presplit walls (see Figs. 47 and 48), some supplemental blasting was required along the rear wall. In the left-rear corner, a segment of rock bounded by two joint surfaces (Fig. 47) was removed by drilling and shooting one horizontal 6-in.-diameter hole about 10 ft deep.

The presplit walls along the sides of the excavation were, in places, offset along horizontal planes of weakness (see Fig. 48). The overlying rock mass was generally displaced into the cut with a maximum offset of about 3 in.

The total weight of explosive used in PB-8 was 32,100 lb, and the average loading density was 64.6 lb/ft of hole. Figure 43 shows the blast design for PB-8. Most of the blasted rock pulled away from the presplit walls and was deposited in the middle of the excavation; however, some large flyrock was thrown about 300 ft downhill and damaged trees in that area.

SUMMARY

A summary of information on the test blasts is presented in Table 1.

Additional information:

Rear production holes

Diameter = 6-1/4 in.
 Pattern = 15 x 30 ft (nominal) staggered rows
 Delays = Row by row, as shown
 Explosive = Dow MS-80-25, AI-AN slurry
 Boosters = HDP-1's, 3 per hole; top, middle and bottom of charge
 Burden = 15 ft
 Spacing = 30 ft
 Stemming = 10 ft
 Subdrill = 0 ft

Forward production holes

Diameter = 6-3/4 in.
 Pattern = 15 x 15 ft sq
 Delays = Simultaneous (9 delay)
 Explosive = Dow MS-80-25
 Boosters = 1-lb cast in bottom, 1/2-lb cast in middle and top
 Stemming = Varies, approx. 1/2 hole depth

Presplit holes

Diameter = 3 in.
 Spacing = 30 and 60 in. (left wall)
 Stemming = 6 ft
 Explosive = Trinitex, 70%, 1/4 lb/ft

Legend
 ● 6-1/4-in.-diam holes
 ○ 6-3/4-in.-diam holes
 · 3-in.-diam holes
 Note: All 6-3/4-in.-diam holes and presplit lines detonated instantaneously

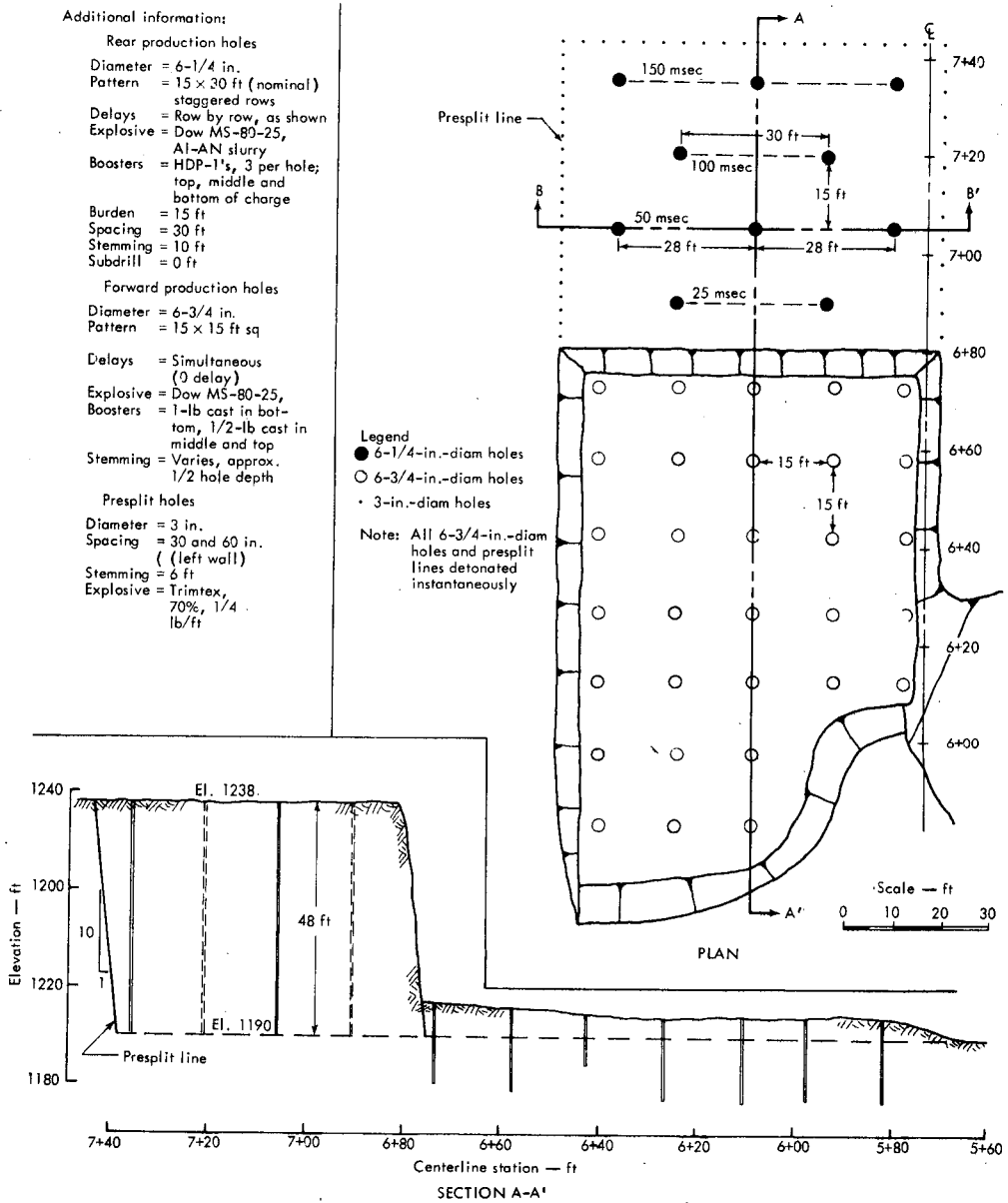


Fig. 33. PB-6B blast design.

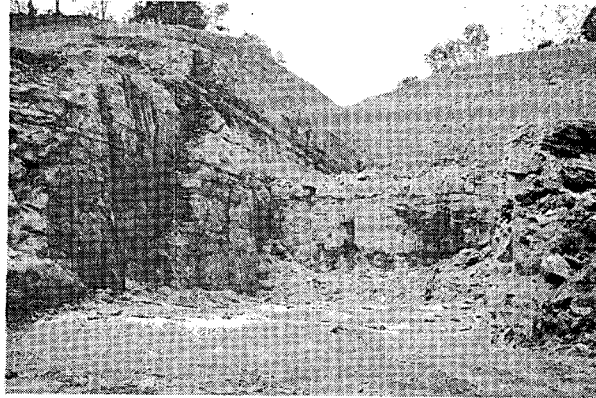


Fig. 34. PB-6B preshot.

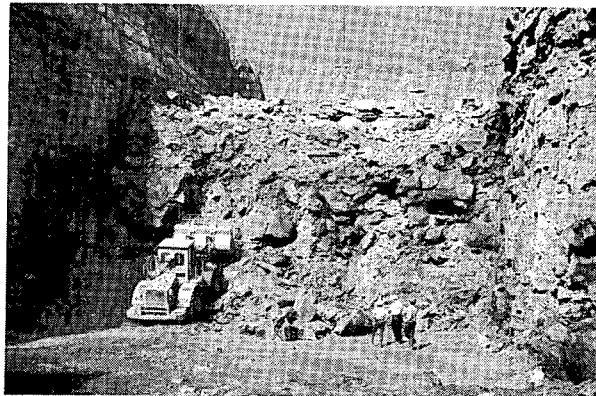
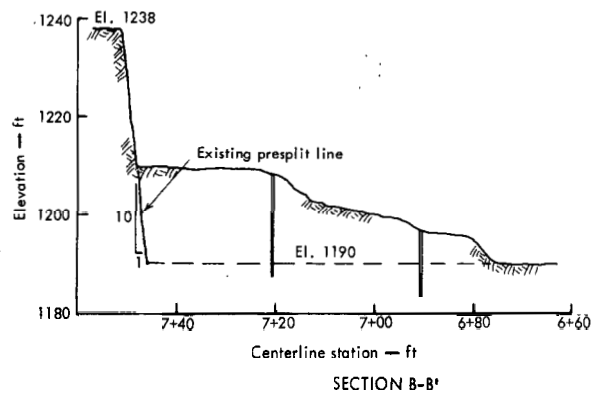
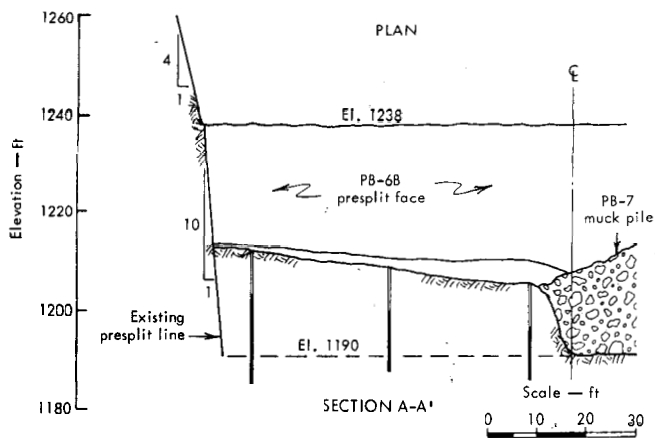
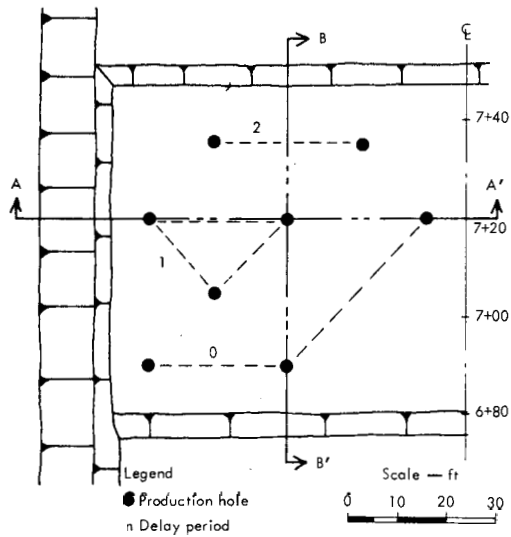


Fig. 35. PB-6B during excavation.



Additional informations:

- Production holes
- Diameter = 6-3/4 in.
- Pattern = 15 x 30 ft (nominal) staggered rows
- Delays = as shown (25-msec periods)
- Explosive = Dow MS-80-25, Al-AN slurry
- Boosters = HDP-1's, 2 per hole, top and bottom
- Stemming = 9 ft
- Subdrill = varies

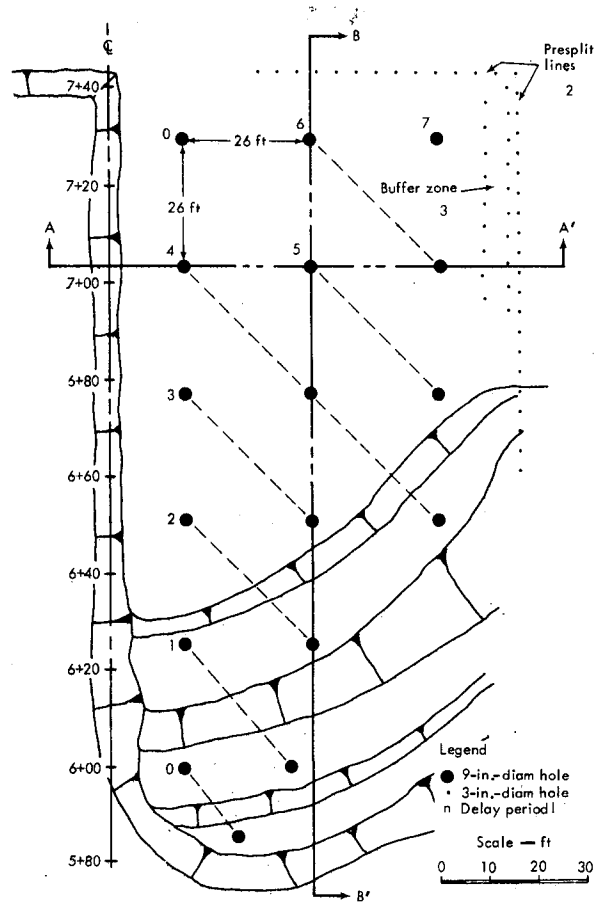
Fig. 36. PB-6C blast design.



Fig. 37. PB-6C preshot.



Fig. 38. PB-6C during excavation.



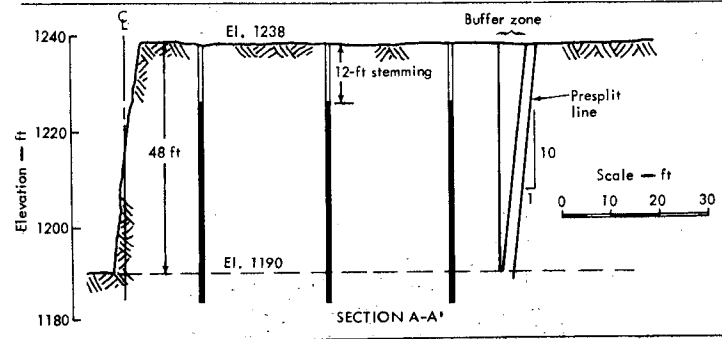
Additional information:

Production holes
 Diameter = 9 in.
 Pattern = 26 ft sq.
 Delays = Diagonal, 25-msec periods, as shown
 Explosive = Dow MS-80-25 AI-AN slurry
 Boosters = HDP-1's, cluster of 4, top and bottom of charge
 Burden = 18 ft
 Spacing = 36 ft
 Stemming = 12 ft
 Subdrill = 7 ft

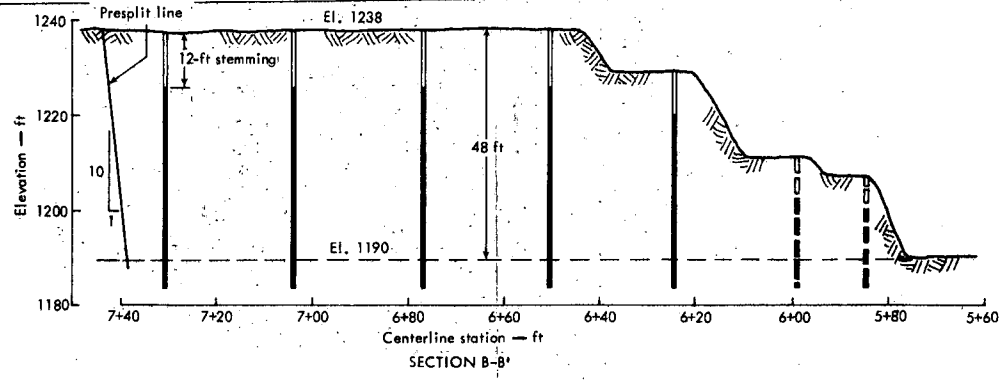
Presplit holes
 Diameter = 3 in.
 Spacing = 42 in.
 Stemming = 4 ft
 Explosive = Trinitex, 70%, 1/4 lb/ft

Buffer zone holes
 Diameter = 3 in.
 Pattern = 2 rows, staggered
 Spacing = 5 ft
 Explosive = Trinitex, 70%, 1/4 lb/ft
 Stemming = 4 ft

PLAN



SECTION A-A'



SECTION B-B'

Fig. 39. PB-7 blast design.

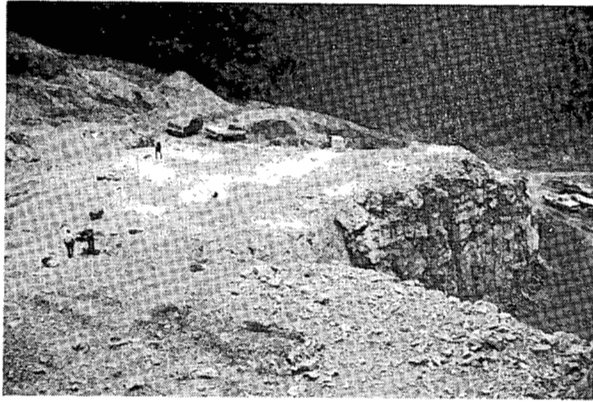


Fig. 40. PB-7 preshot (from left rear).

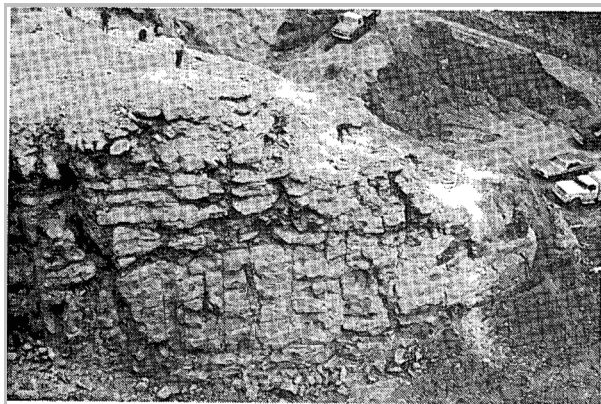
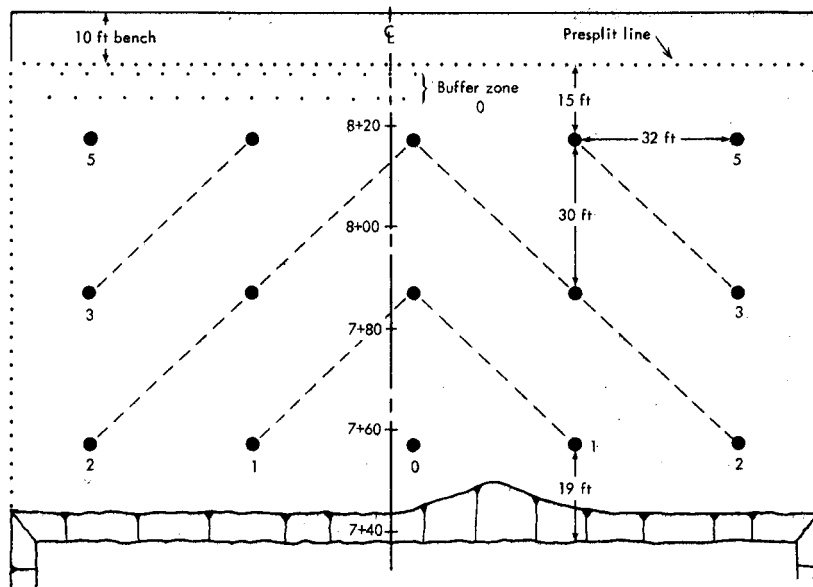


Fig. 41. PB-7 preshot (left wall).



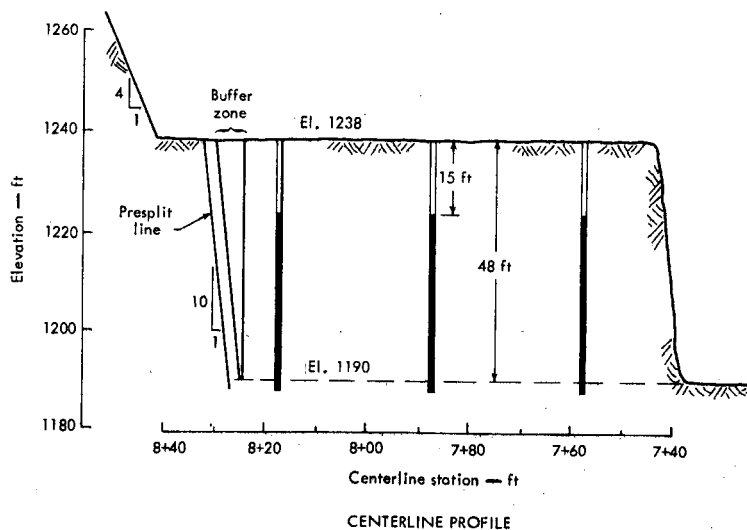
Fig. 42. PB-7 during excavation.



Legend
 ● 12-1/4-in. diam hole
 ○ 3-in.-diam buffer zone and presplit hole
 n Delay sequence (25-msec periods)

Scale — ft
 0 10 20 30

PLAN



CENTERLINE PROFILE

Additional information:

Production holes

Diameter = 12-1/4 in.
 Pattern = 30 x 32 ft
 Delays = "V" cut, 25-msec periods shown on plan
 Explosive = Dow MS-80-25
 Al-AN slurry
 Boosters = HDP-1's, cluster of 4 top and bottom of charge
 Burden = 22 ft
 Spacing = 44 ft
 Stemming = 15 ft
 Subdrill = 2 ft

Buffer zone holes

Diameter = 3 in.
 Pattern = 2 rows, staggered
 Spacing = 5 ft
 Stemming = 6 ft
 Explosive = Trimtex, 70%
 1/4 lb/ft

Presplit holes

Diameter = 3 in.
 Spacing = 3, 5 and 4 ft
 Stemming = 6 ft
 Explosive = Trimtex, 70%, 1/4 lb/ft

Fig. 43. PB-8 blast design.

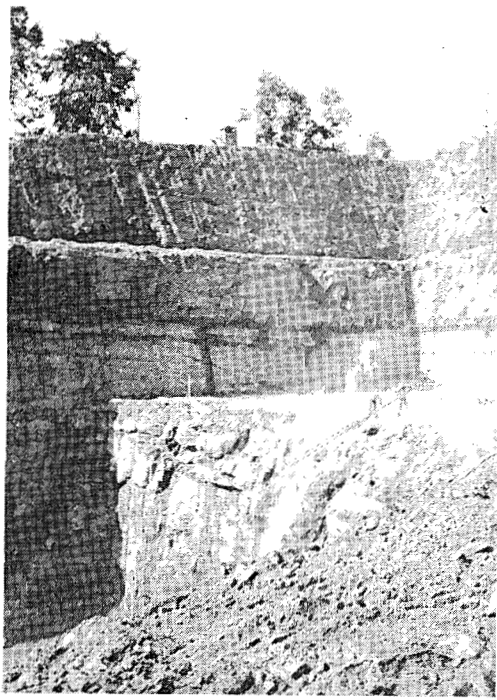


Fig. 44. PB-8 preshot (from right front).



Fig. 46. PB-8 during excavation (from left rear).



Fig. 45. PB-8 postshot surface (from right front).

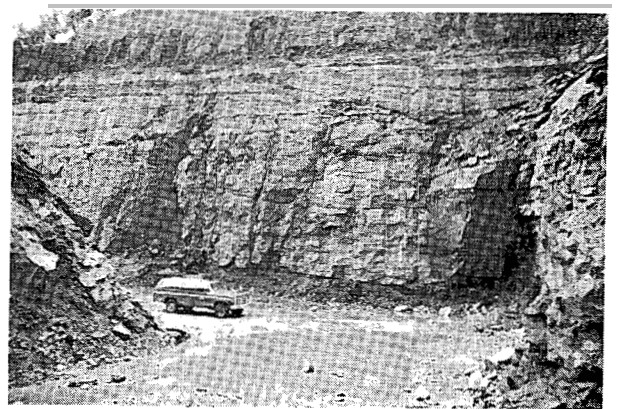


Fig. 47. Left wall of PB-8 after excavation.



Fig. 48. Right wall of PB-8 after excavation.

Table 1. R. D. BAILEY experimental excavation test blast summary.

Test blast	Date	Material type	Explosive type	Blasthole diameter (in.)	Average depth (ft)	Effective burden (ft)	Effective spacing (ft)
PB-1	6 Apr	Weathered shale	ANFO	3	17	7	14
PB-3	7 May	Weathered shale	ANFO	6-3/4	15	19	19
PB-4	19 May	Weathered shale shale, coal, and sandstone	ANFO	9	43	17	34
PB-4A	7 Jun	Sandstone and shale	ANFO	3	6	5	10
PB-4B	7 Jun	Sandstone and shale	ANFO	3	9	5	10
PB-4C	7 Jun	Sandstone and shale	ANFO	3	9	5	5
PB-4D	9 Jun	Sandstone and shale	ANFO	3	6	5	10
PB-5	9 Jun	Weathered sandstone	ANFO	3	15	5	10
PB-6A	18 Jun	Sandstone	ANFO	6-1/4	45	11	20
PB-4E	22 Jun	Sandstone	MS-80-25 slurry	3	6	5	5
PB-6B	23 Jun	Sandstone	MS-80-25 slurry	6-1/4	49	15	30
PB-7	30 Jun	Sandstone	MS-80-25 slurry	9	55	18	36
PB-6C	5 Jul	Sandstone	MS-80-25 slurry	6-3/4	27	15	30
PB-8	12 Jul	Sandstone	MS-80-25 slurry	12-1/4	50	22	44

Chapter 4. Fragmentation Program

BACKGROUND

The fragmentation measurements were intended primarily for comparing the efficiency of various blast designs according to the degree of fragmentation of the blasted rock. The objectives of the fragmentation program were to make quantitative determinations of both the particle size distributions (gradations) and the shapes of the rock fragments. Because the rock excavated from the spillway will be placed in 1- and 2-ft lifts in the dam embankment, much interest focused on the percentage of the rock that could be placed in the embankment without secondary blasting or crushing.

There are several means of estimating the gradation of blasted rock. One is a subjective estimate based on personal observation and experience. The percentage of large blocks often tends to be overestimated, however, because the

large blocks readily attract the eye and tend to remain on the surface of the muck pile if they originated in the collar region.

Grid photography has been used in the past to develop gradation curves, but the results have not correlated well with standard screen analyses.

The most accurate way of determining the gradation of a muck pile, if the sample analyzed is representative, is a screen analysis. This procedure was used on the test-pit material taken from the test fills (see Chapter 8).

A technique called point counting was used to obtain gradation curves for the rock produced by the experimental blasts. The details of this method are discussed later; essentially it involves measuring manually the size of a sufficient number of randomly selected rocks. The method generates gradation curves that correlate well with screen analyses. The principal advantages of point counting over screening

are (1) point counting is less expensive, and (2) it is faster. The technique of point counting was originated by Wolman in 1954 for sampling coarse river-bed materials.⁶ It was modified later by Anderson for determining the size distribution of crater fallback and ejecta.⁷ Further theoretical justification for the method has been offered by McAneny.⁸

FIELD PROCEDURE

It is extremely important that the rocks selected for measurement be representative of the blast product as a whole; this is also true in the selection of a sample for screening. A random sample of rocks is chosen by laying a cloth measuring tape over the surface of the rock and measuring the particular rocks lying directly beneath selected distance marks along the tape, say every 5 ft. The length, breadth, and thickness of each rock particle is measured and recorded (see Fig. 49). Because rocks on the top of a muck pile might not be representative of those at depth, additional point counts are done on the rocks dumped in the spoil area.

ANALYSES

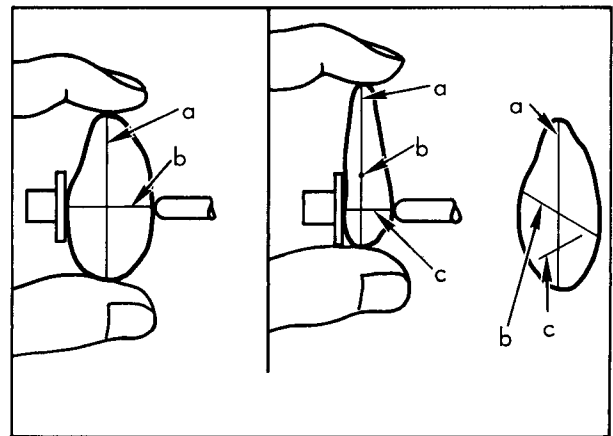
Two types of analyses were made of the fragmentation data from each test blast. One was a comparison of the gradation curves, and the other was a comparison of the shapes of the fragments. These analyses are discussed in detail in the following paragraphs.

Gradation

Gradation curves were developed for the rock produced by each test blast.

The breadths, as shown in Fig. 49, were used for this analysis because they have been shown to correlate well with screen analyses.^{7,10} The data were also analyzed to determine the 95% confidence intervals for the gradation curves.¹¹ An example of the calculations required to establish this confidence interval is presented in Appendix A. Figure 50 shows the gradation curve for PB-8 and the 95% confidence band. The statistical significance of the band is a 95% probability that the actual gradation curve for PB-8 rock will fall somewhere within the band indicated in Fig. 50. Gradation curves for the entire series of test blasts are presented in Appendix A.

Some general observations may be made by comparing the different gradation curves for the rock produced by various blasts. It may be seen in Fig. 51 that the



a = length
b = breadth
c = thickness

Fig. 49. Measurement of rock fragments (reproduction of W. C. Krumbein figure on p. 66 of Vol. II of *Journal of Sedimentary Petrology*, published by the Society of Economic Paleontologists and Mineralogists; used by permission).

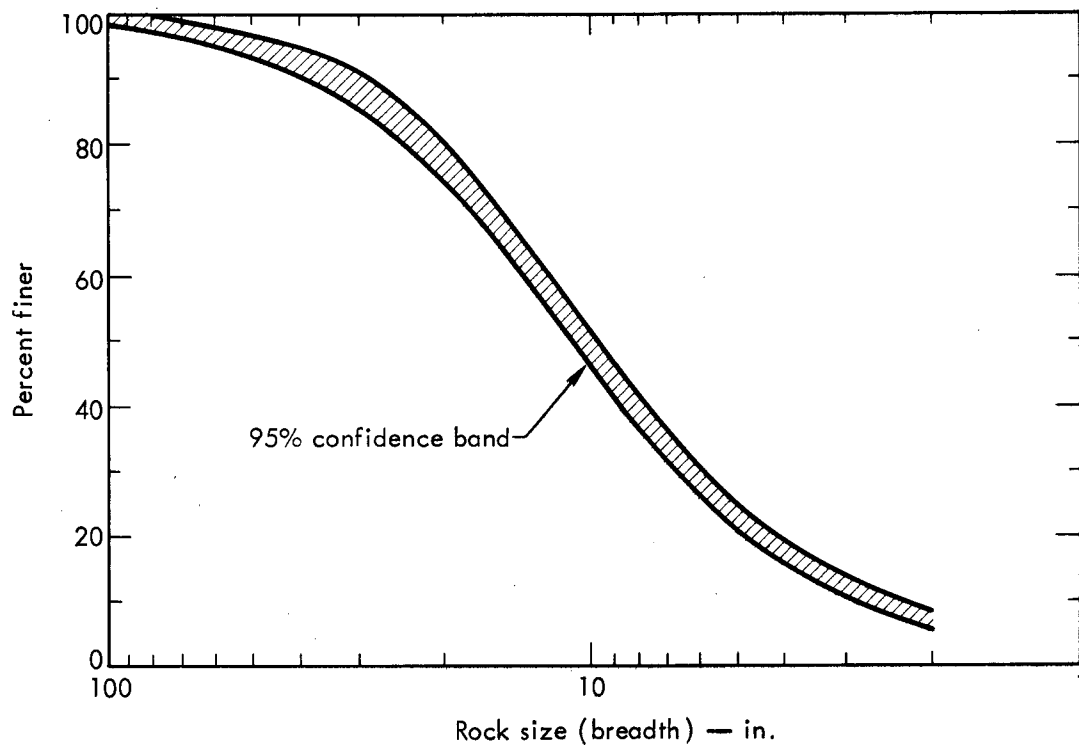


Fig. 50. Gradation curve for PB-8 (based on point count of 879 particles).

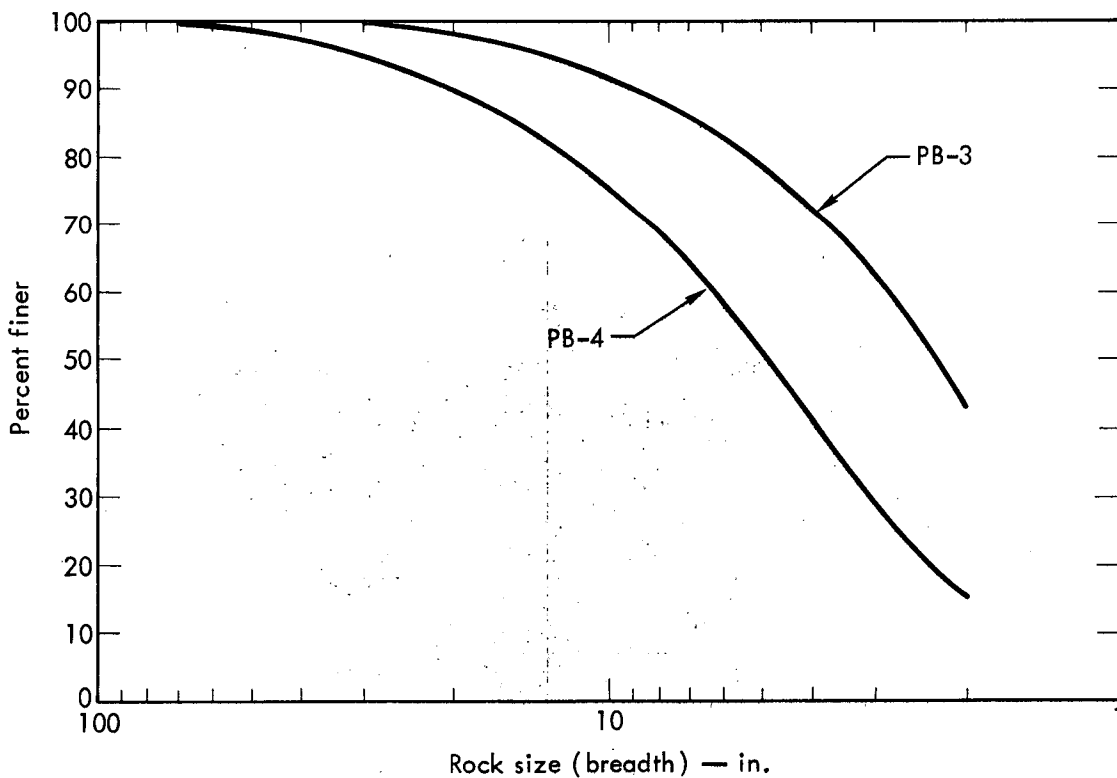


Fig. 51. Gradation curves for weathered shale.

PB-3 material was considerably finer than that produced by PB-4. This could have been because the PB-3 rock was weathered more than the PB-4 rock, and because the blastholes in PB-3 were shallower and smaller in diameter. (Refer to Chapter 3 for specific blast designs.)

Blasts PB-4A through PB-4E were located in the bottom 6 to 12 ft of those portions of PB-4 in which the rock was not fractured to the depth intended in the PB-4 design. All of the patterns in PB-4A through PB-4E consisted of 3-in.-diameter blastholes fired with a variety of delay schemes. The rock was hard shale and sandstone. As may be seen in Fig. 52, the gradation curves for all of the blasts, except PB-4C, are within 10% of each other at the coarse end. The

reason for the poorer fragmentation in PB-4C may have been the fact that delays were not used.

Figure 53 shows gradation curves for four blasts in sandstone. Blasthole diameters varied from 3 in. in PB-5 to 12-1/4 in. in PB-8. The general trend is that coarser rock fragments are produced by the larger diameter blastholes.

Gradation curves can also be plotted for the thickness and length dimensions. If one is trying to determine what percentage of a blast product can be placed directly in a specified lift thickness, a gradation curve based on fragment thickness rather than breadth may be more useful. Figure 54 shows three gradation curves based on each fragment dimension for the rock blasted in PB-7.

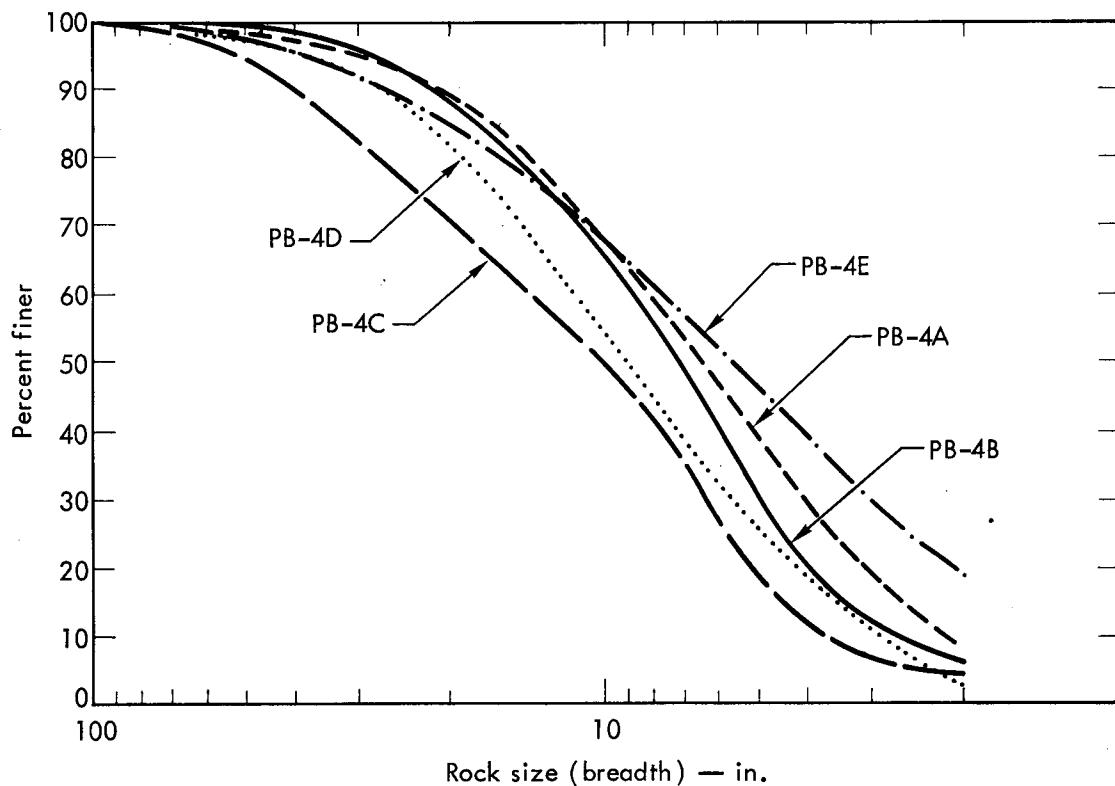


Fig. 52. Gradation curves for 3-in.-diameter blastholes in hard shale and sandstone.

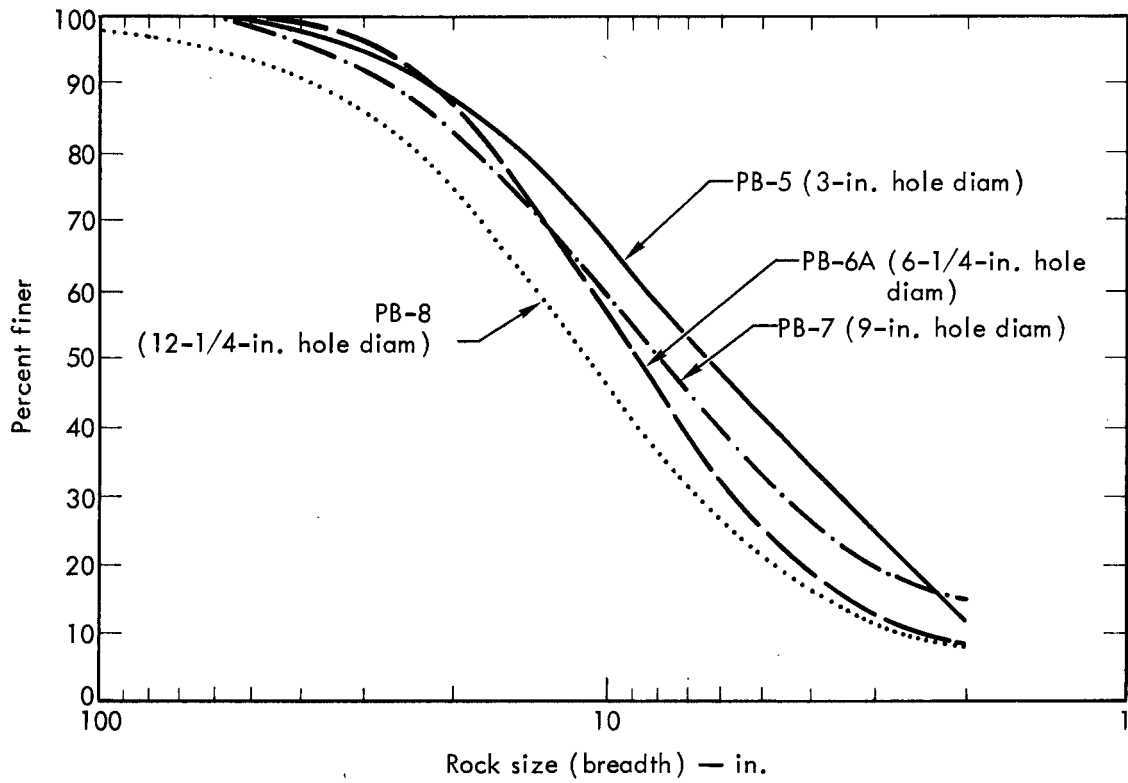


Fig. 53. Gradation curves for Upper Gilbert sandstone.

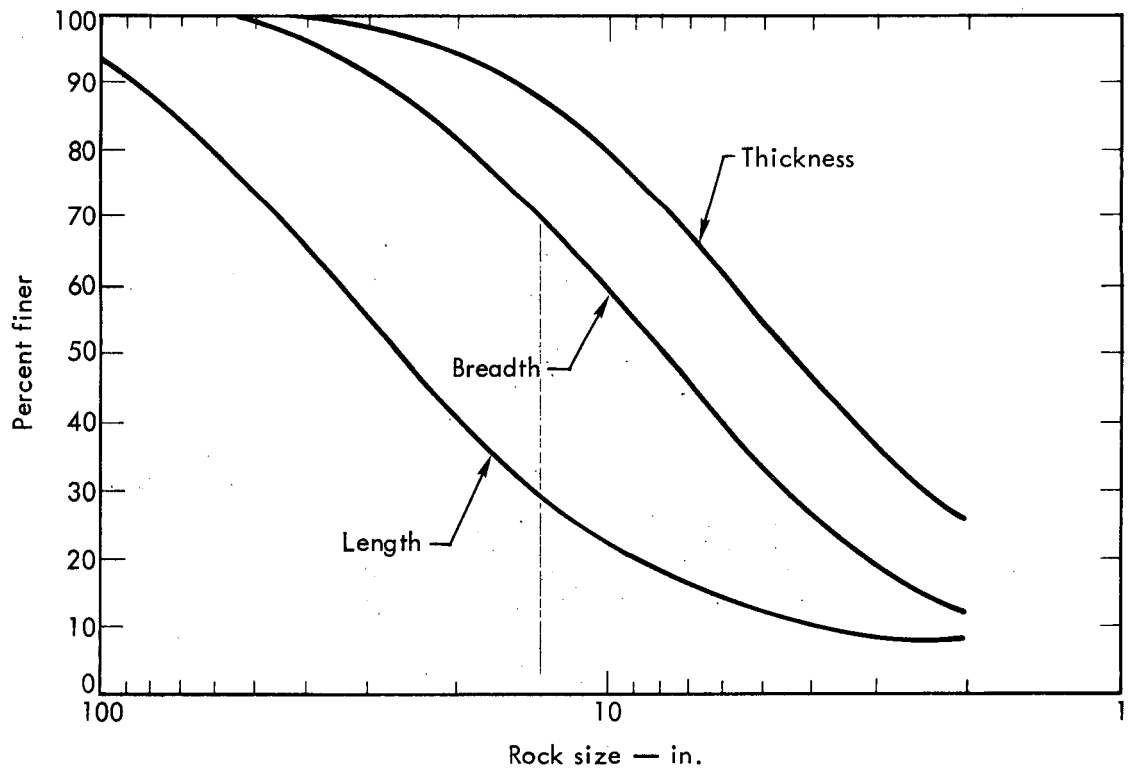


Fig. 54. Gradation curves for PB-7 (based on point count of 391 particles).

Fragment Shapes

Another type of analysis was performed on the point count data to quantify the shape of the blasted rock. When observing a pile of blasted rock it is often obviously "blocky" or "slabby." Blocky material is preferred for dam embankments because it compacts better and because there is less chance of voids occurring in the embankment due to bridging. The shapes of rock fragments produced by the test blasts were quantified and plotted according to the Zingg Classification System.⁹ The Zingg shape index is determined by plotting ratios of the rock dimensions, as shown for PB-4A fragments in Fig. 55. It may be observed

from this plot that the average rock shape falls within the "bladed" sector; this is also true for the rock from most of the other blasts as shown in Fig. 56.

DISCUSSION AND CONCLUSIONS

The point counting technique is very expedient and useful for establishing gradation curves, but the method does have some shortcomings. It does not provide a reliable estimate of the number of fines in a given rock sample, and a certain amount of judgment is required on the part of the person performing the count. For example, consider the case where the measuring point falls upon a

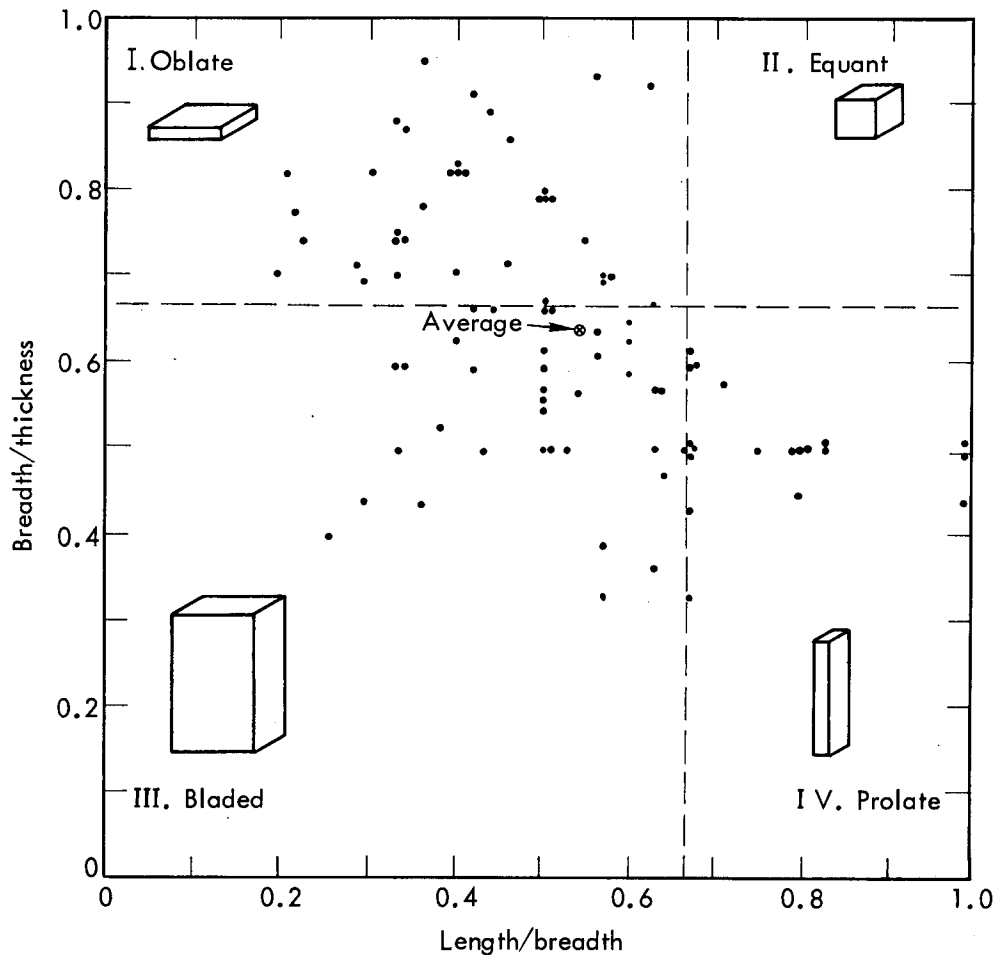


Fig. 55. Zingg shape indices for rock from PB-4A.

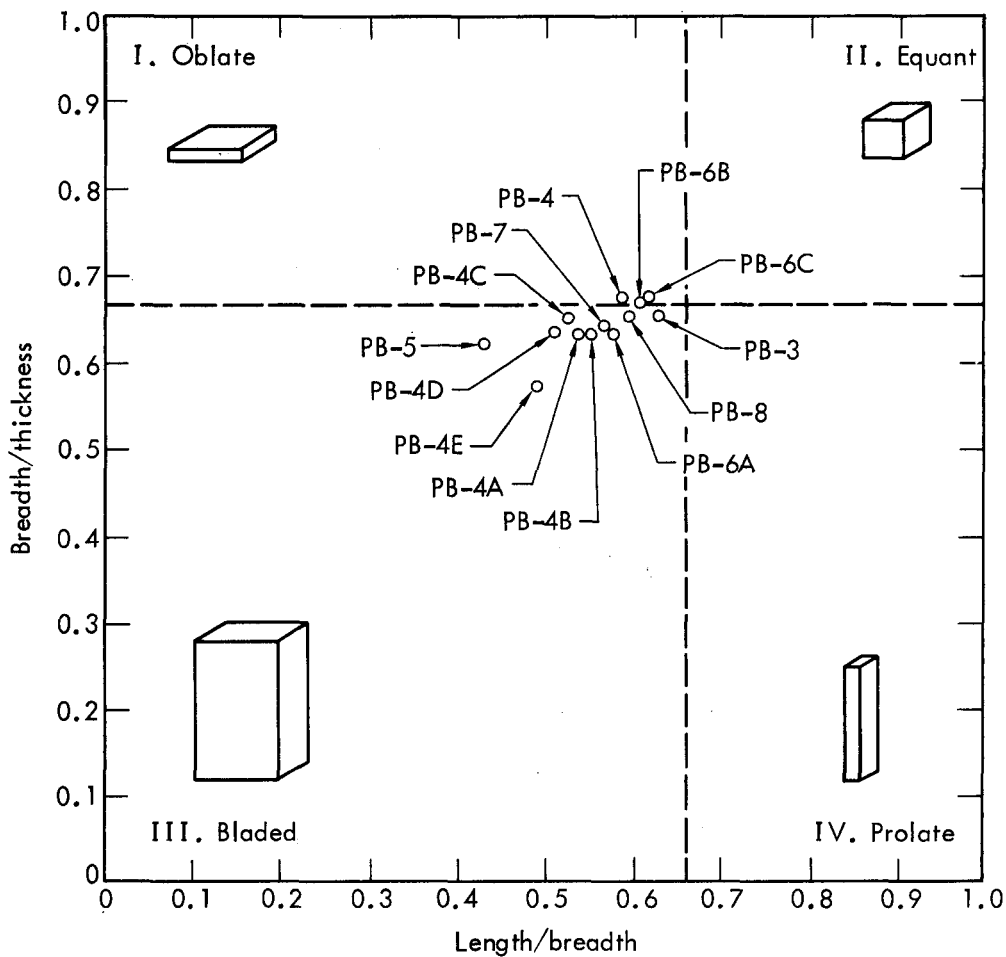


Fig. 56. Average Zingg shape indices for all test blasts.

large rock covered with a layer of fine material. Should the large rock be counted, or should the fines be counted? The point counts performed at R. D. BAILEY were intended to provide accurate data on the distribution of the larger size rocks, realizing that the gradation curve may not be reliable at the finer end. Most of the point counts were performed by the same person, so that even though some judgment was required, it was consistent throughout the course of the experiments.

Although several techniques for estimating the percentage of rock that could be placed in a fill to meet specific dimensional criteria have been described

in this chapter, caution should be exercised when the attempt is made to perform this type of survey. The major portion of the fragmentation data was gathered in the blast area and in the spoil area prior to spreading. The amount of mechanical breakage experienced by the rock will depend on the rock type, the type of loading and hauling equipment, and, if the rock is to be placed in a fill, the type of spreading and compacting equipment. The person estimating the percentage of acceptable rock should be familiar with the manner in which the specifications or other criteria are going to be interpreted. Part of the fragmentation data was made available to potential bidders on

the dam project.³ During the course of the R. D. BAILEY spillway excavation, it would be desirable to keep a record of the contractor's blasting patterns and the amount of secondary blasting or crushing required. This record could then be compared to the results of the fragmentation data collected during this experimental excavation.

The following are the conclusions drawn from the fragmentation data obtained at R. D. BAILEY:

1. As expected, the weathered shale found in PB-3 and PB-4 breaks into smaller sizes more readily when blasted than the hard shale and Upper Gilbert sandstone. This weathered shale also breaks down more than the sandstone when handled by heavy equipment.

2. The five blasts in hard shale and sandstone, PB-4A through PB-4E, all produced roughly similar fragmentation except for PB-4C, where no delays were used in the blast pattern. The rock from PB-4C was considerably coarser than that produced by the other patterns, confirming the effectiveness of millisecond delays for improving the fragmentation of blasted rock.

3. Rock fragments from the blasts in the Upper Gilbert sandstone and the

weathered shale tended to become coarser with increases in charge separation distances associated with larger blasthole diameters. It may be possible to alter this trend by the use of decking charges and satellite holes (see Chapter 9).

4. The best blasting technique to use is ultimately a matter of economics, depending on such items as equipment availability and the size specifications (if any) that must be met by the blasted rock. Several blasting techniques to consider are:

a. Use of closely spaced, small-diameter blastholes in shallow benches to get good fragmentation.

b. Use of widely spaced, large-diameter blastholes in high benches with decking charges and/or smaller satellite blastholes to get good fragmentation.

c. Use of widely spaced, large-diameter blastholes in high benches with secondary blasting or crushing to compensate for coarser fragmentation.

5. The majority of the rock fragments produced by the experimental blasts had a bladed shape. The bladed and slabby nature of the blasted rock is to be expected for sedimentary rocks containing relatively thin beds.

Chapter 5. Subsurface Shock and Blast-Induced Fracturing Program

BACKGROUND

The objectives of the subsurface shock and blast-induced fracturing technical program were (1) to evaluate the effectiveness of various presplit planes and buffer zones in creating and maintaining a finished stable boundary for a structural

excavation and (2) to develop data on minimum safe separation distances between production charges and finished surfaces.

Presplitting has gained wide acceptance throughout the construction industry as an excellent way to form the walls of a structural excavation. A presplit plane is quite effective in reducing or

eliminating overbreak from production blasting.

For the last several years EERL has been investigating the feasibility of using relatively large charges for structural excavation in order to reduce drilling and blasting costs. It is anticipated that a presplit surface may need protection from the stresses and explosion gases generated by these large charges. One approach is to place a conservative lower limit on the separation distance that must be maintained between large-diameter production charges and the presplit plane. Smaller diameter blastholes can be used to break up the intervening rock. Another approach, still experimental, involves the creation of a "buffer zone." This is a zone of relatively crushed or fractured rock between the presplit plane and the main charges that attenuates stress and provides an escape vent for the gases produced by the blast. It is hypothesized that the shock wave would be attenuated by the buffer zone because of its decreased density and shear strength relative to the intact rock, thus limiting the fracturing beyond that zone. In this way, the presplit plane is protected from damage by high stresses.

Techniques for creating a buffer zone with small diameter blastholes are still under investigation. Several methods tested at R. D. BAILEY are discussed later in this chapter. Previous work in this area has included model studies¹² and prototype field experiments.^{13,14}

OBJECTIVES AND APPROACH

The principal objectives of the close-in particle velocity measurement program

were (1) to evaluate the effectiveness of various presplit and buffer panels in protecting rock behind the presplit face from damage due to the charges, and (2) to determine minimum safe separation distances between production charges and finished surface. Secondary objectives were to correlate the degree of rock fracturing with peak particle velocity, to measure the in situ particle velocity response characteristics of the rock being blasted, and to study the variation of particle velocity with depth below the ground surface.

These things were accomplished through two separate but related measurement programs. First, horizontal and vertical particle velocities generated by the test blasts were measured behind the buffer zones and compared to those observed in identical configurations without buffer zones. The purpose of these measurements was to investigate possible attenuation of particle velocity by the buffer zones. Second, permeability tests were attempted in boreholes located near velocity gage holes both before and after the blasting for each lift. These latter tests were designed to measure qualitatively the amount of blast-induced fracturing by detecting change in the permeability of the rock surrounding the test hole. It was hoped that permeability changes could be correlated with the particle velocities measured nearby.

Particle velocity was chosen as the parameter to be measured, rather than stress or strain, because of the relative ease with which it could be measured. Particle velocity can also be related mathematically to either stress or strain.¹⁵

EQUIPMENT

Particle Velocity Measurement Equipment

The particle velocity measurements were accomplished with piezoelectric crystal transducers grouted into drill holes. Signals were carried through approximately 2000 ft of cable to the Control Point trailer, which housed the power supplies and recording systems.

Three transducer models, all products of Bell and Howell, were used during the project: Models 4-155-0107, 4-155-0001, and 4-155-0111. The gages were self-integrating accelerometers and their characteristics were generally similar. Approximately two thirds of the gages were rated by the manufacturer as having a 1-Hz to 2-KHz frequency range (although in practice the lower limit appeared to be about 10 Hz); the remainder had a lower limit of 30 Hz. Some of the gages could record velocities up to 200 in./sec.

An IRIG time signal generator and a zero-time unit were used to provide a time scale on the records. The IRIG generator produced a digital code that gave a continuous signal containing information on the time given - in days, hours, minutes, and seconds. The zero-time unit sensed a break in a circuit placed in a blasthole and produced pulses that marked detonation times. The record of detonation times allowed computation of propagation velocities, and helped to identify the origins of the pulses seen in the records.

Mounting brackets and canisters for the gages, shown in Fig. 57, were designed by EERL. The assemblies were grouted into 4-in.-diameter boreholes.

Two types of grout were used. One was a nonshrink, quick-setting, nonmetallic grout that the manufacturer claimed to be capable of achieving an initial set in 4 to 5 hr and of developing a compressive strength of over 8000 psi after a period of 24 hr. The other was also a nonshrink, nonmetallic grout but it was slower setting and achieved a compressive strength of 8000 psi after about 3 days.

Permeability Measuring Equipment

Permeability measurements were attempted with the use of a double packer assembly consisting of two inflatable packers held 4 ft apart by a section of galvanized pipe. The unit was made for a 3-in.-diameter borehole. The pipe was perforated so that the space between the packers could be filled with water through removable sections of water pipe. The packers were inflated with air from a hand pump. Figure 58 is a diagram of the packer assembly; note that the water pressure between the packers is due only to gravity acting on the column of water in the pipe.

PROCEDURE

Instrument holes for the velocity transducers and holes for permeability testing were generally 5 ft apart at the same distance from the blasthole of interest. It was originally planned that permeability measurements would be made before and after each blast, and that the permeability would be determined as a function of depth in 4-ft increments.

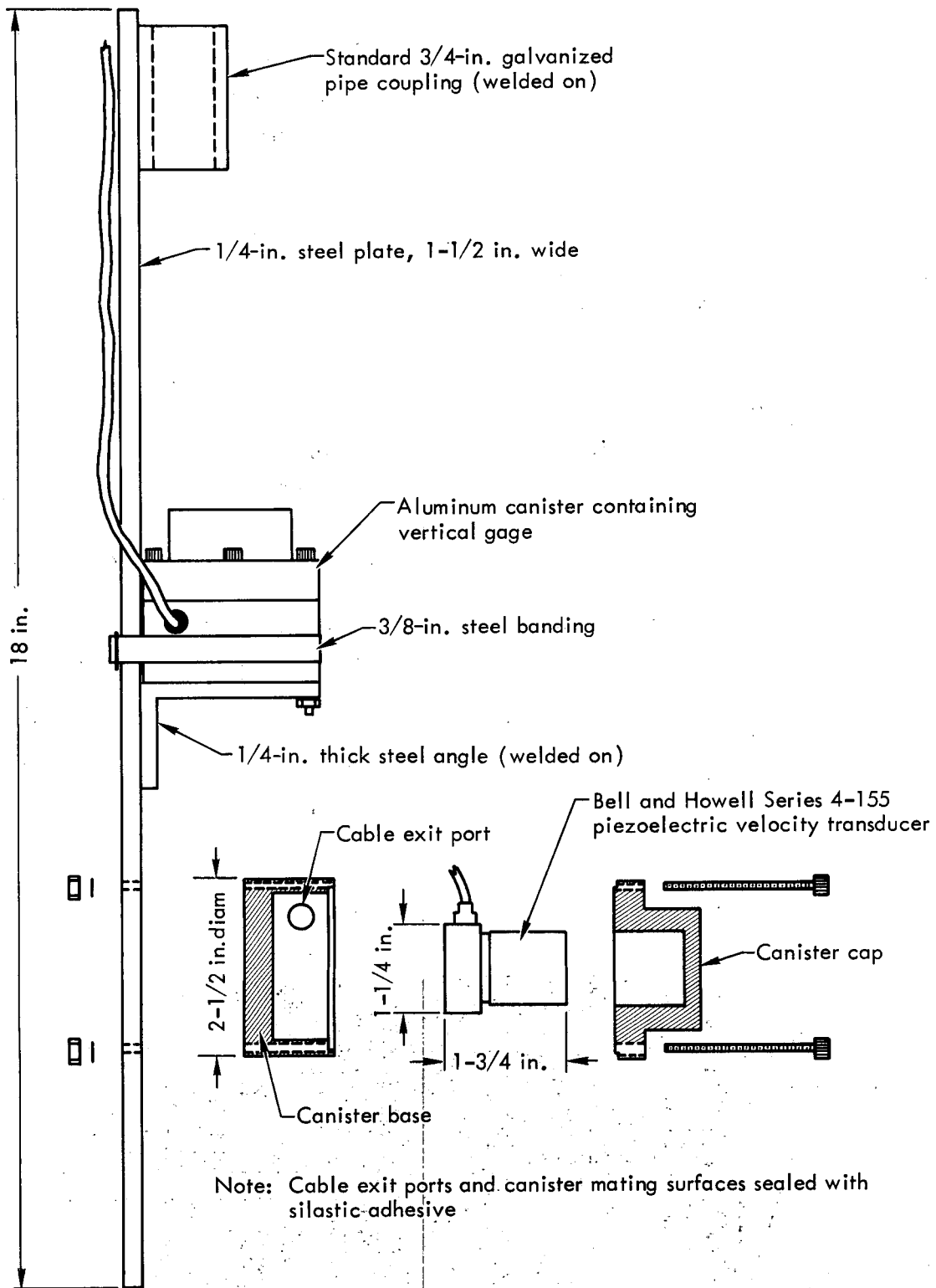


Fig. 57. Typical mounting bracket indicating gage and canister placement.

DATA

Forty-four records of particle velocity data were accumulated during the test program. Most of the desired permeability data, however, was not collected because of numerous operational problems with the packer apparatus. After a successful operation at the PB-1 site, the permeability test failed to produce any additional significant data.

Particle Velocity Data

Figures 59 through 65 show cross sections of the gage installation for each

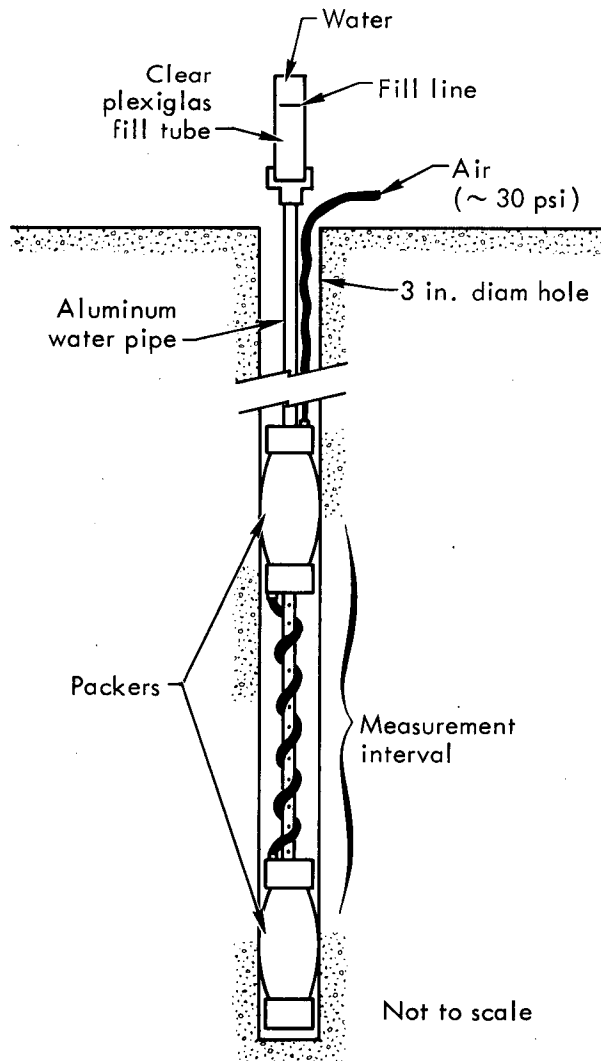


Fig. 58. Permeability test packer assembly.

of the blasts that were instrumented. Information on the gage depth, the distance to the charges of interest, and the type and quantity of explosive is shown in the figures. The particle velocity signal traces were analyzed to obtain the rise time to peak amplitude and the peak acceleration. The rise time to peak amplitude, defined as the time interval from the initial time of pulse arrival to the time of peak amplitude, was measured directly from the traces. The peak acceleration was computed from the maximum slope of the pulse.

The identification code of the gages is as follows: the first number represents the burial depth of the gage in feet while the following letter denotes the orientation of the gage (H for horizontal and V for vertical); a B following the H or V indicates that the gage was located behind a buffer zone. Finally, the last number tells the distance in feet from the gages to the nearest production charge.

Table 2 presents a summary of the peak particle velocity data obtained during the production blasts; the recorded traces are reproduced in Appendix B.

Permeability Data

Table 3 presents the permeability test data obtained. The difficulties are described in those cases where problems occurred.

ANALYSES

Several types of analyses were made on the velocity data from the test blasts. These analyses are discussed in the following paragraphs.

Effect of Buffer Zone on Shock Wave Propagation

Buffer zones have not yet been clearly shown to be a useful controlled blasting technique. In the past, observations of the attenuation of particle velocities by buffer zones interposed between the gages and production blasts have been inconclusive. Apparently, the effect of a buffer zone on particle velocity has been too small to observe above the scatter caused by inhomogeneities in the rock and other uncontrollable factors. Out of eight comparisons of nonbuffered-to-buffered peak particle velocities at R. D. BAILEY only three exhibited an effect that might

be attributed to attenuation by a buffer zone. It is likely that these three cases are favorable instances of data scatter.

Figure 66 is a presentation of the data obtained from this particular investigation in which the ratios of "buffered" velocities to "nonbuffered" velocities are plotted for otherwise identical charge-gage configurations. The locations of the points indicate ratios of buffered to nonbuffered particle velocities either greater than one or less than one. Ratios that are less than one indicate attenuation of the particle velocities by the buffer panels. No definite trend is apparent, however.

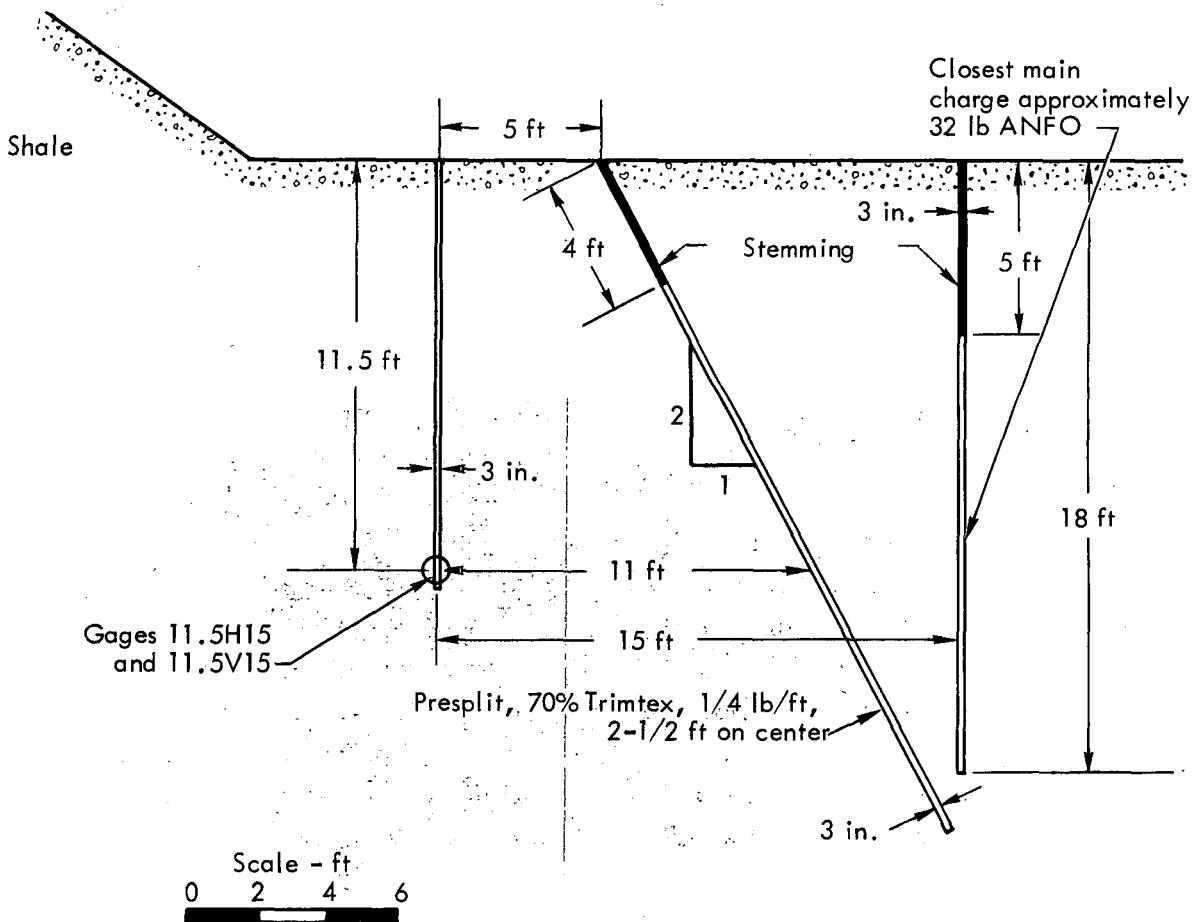


Fig. 59. Velocity gage configuration for PB-1.

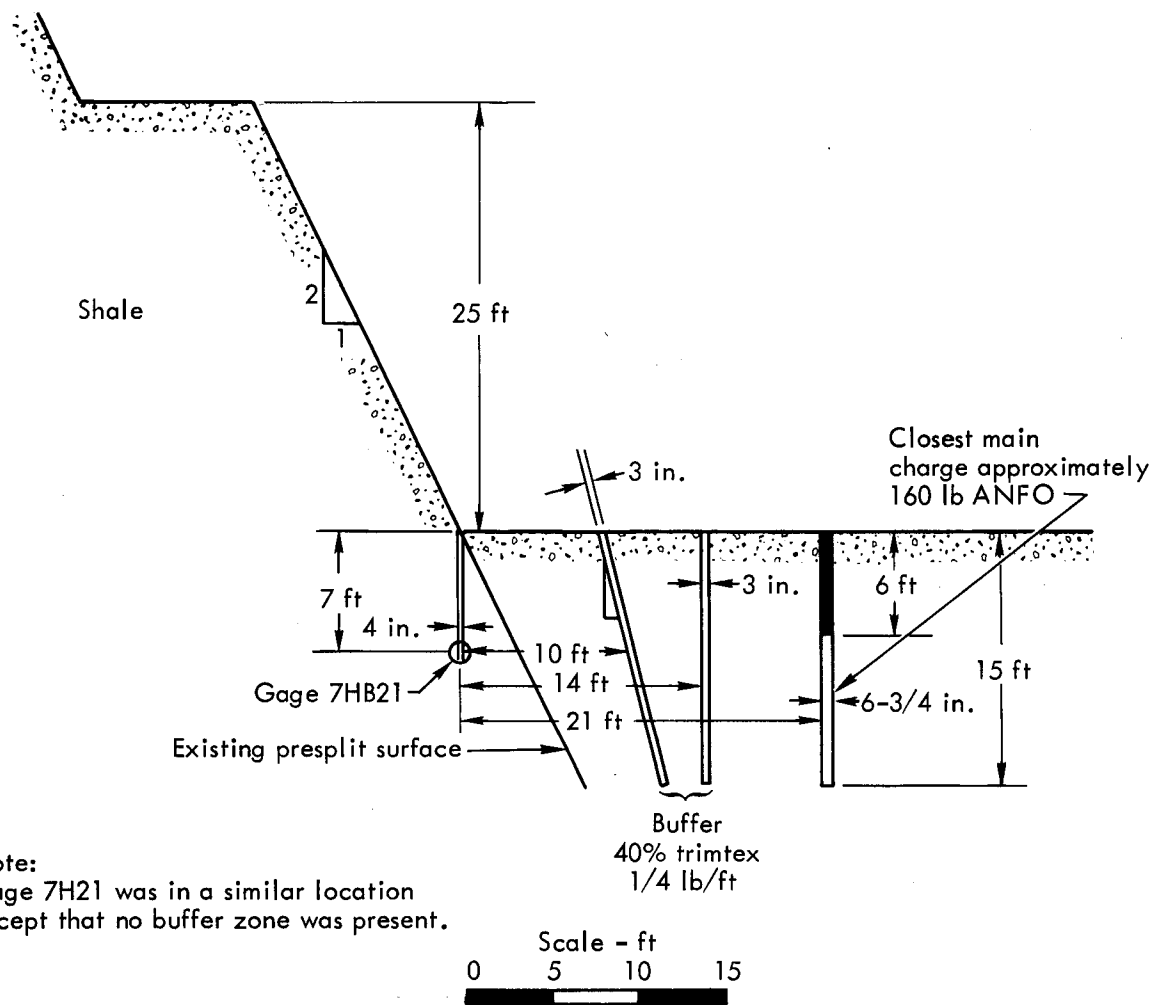


Fig. 60. Velocity gage configuration for PB-3.

Comparison of Dynamic Response Characteristics for Shale and Sandstone

Some comparisons of the dynamic response characteristics of the shale and sandstone can be made from the collected data. Particle velocity records from blasts in sandstone exhibited shorter rise times than in shale, and they also had less rounded shape than those in shale (see Appendix B). Sonic velocities in the shale were measured with a single channel refraction seismograph at eight different locations, with measured values ranging from 3000 to 9000 ft/sec. The

sonic velocity of the Upper Gilbert sandstone was computed to be 15,000 ft/sec, based on pulse arrival times at the PB-7 velocity gages.

Particle Velocity Attenuation with Distance in Sandstone

An array of three pairs of horizontal and vertical velocity transducers was installed for PB-7 (see Fig. 64). These gages were located at distances of 18, 25, and 40 ft from a production charge along a radial line. The attenuation of peak particle velocities can be described by an inverse power law; i.e., an equation of the form shown below applies:

$$V_p = CR^{-x}, \quad (1)$$

where:

V_p = peak particle velocity
 C = constant
 R = distance to gage from charge
 x = attenuation exponent.

A least squares fit was used to calculate "C" and "x." The following equations describe the attenuation of peak particle velocity with distance for the PB-7 case:

$$V_{ph} = 9.46 \times 10^4 R^{-2.27}, \quad (2)$$

where:

V_{ph} = horizontal peak particle velocity (in./sec)
 R = range (ft),

and

$$V_{pv} = 2.48 \times 10^4 R^{-1.84}, \quad (3)$$

where:

V_{pv} = vertical peak particle velocity (in./sec).

Figure 67 is a plot of the data and the best-fit lines.

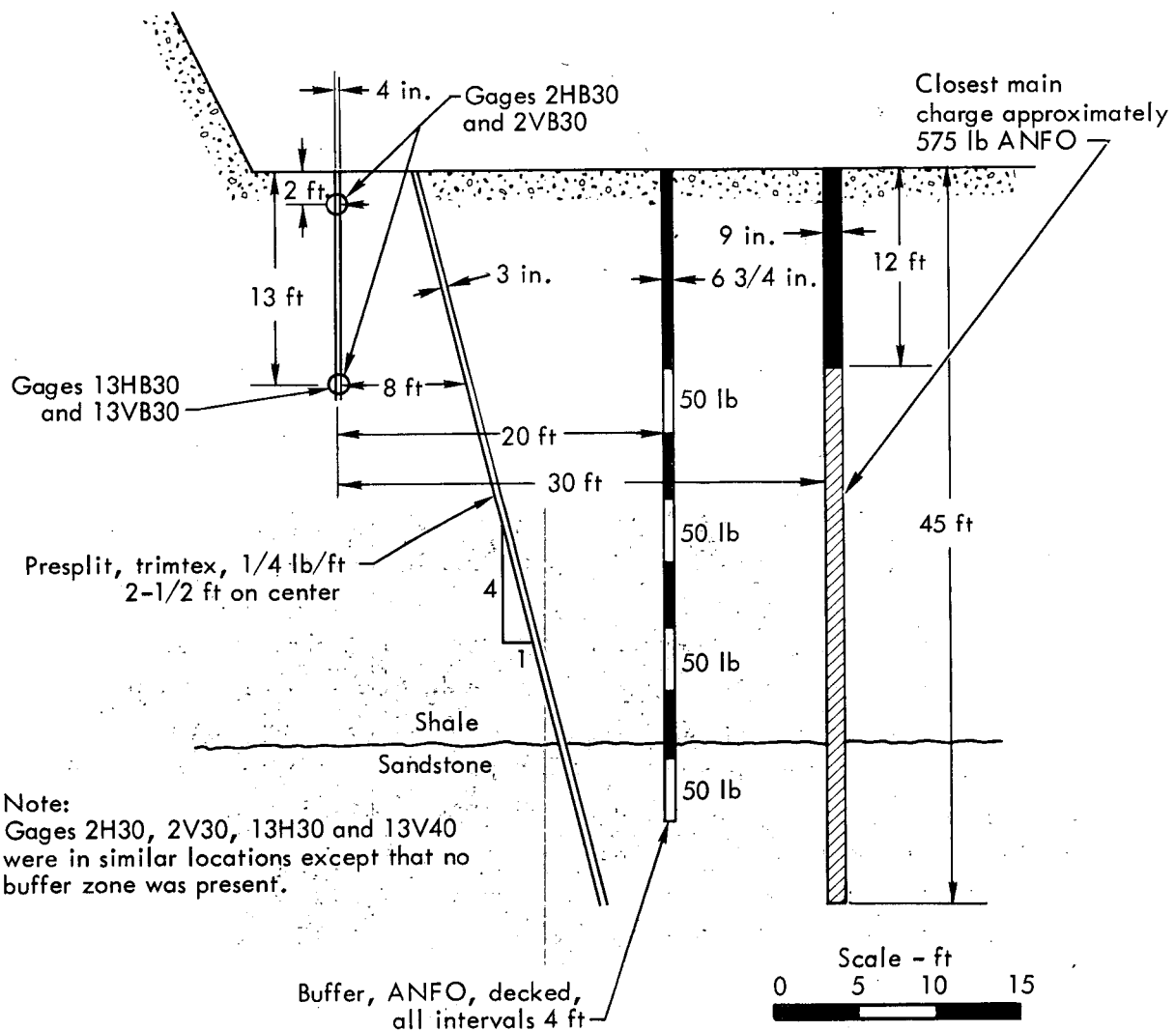


Fig. 61. Velocity gage configuration for PB-4.

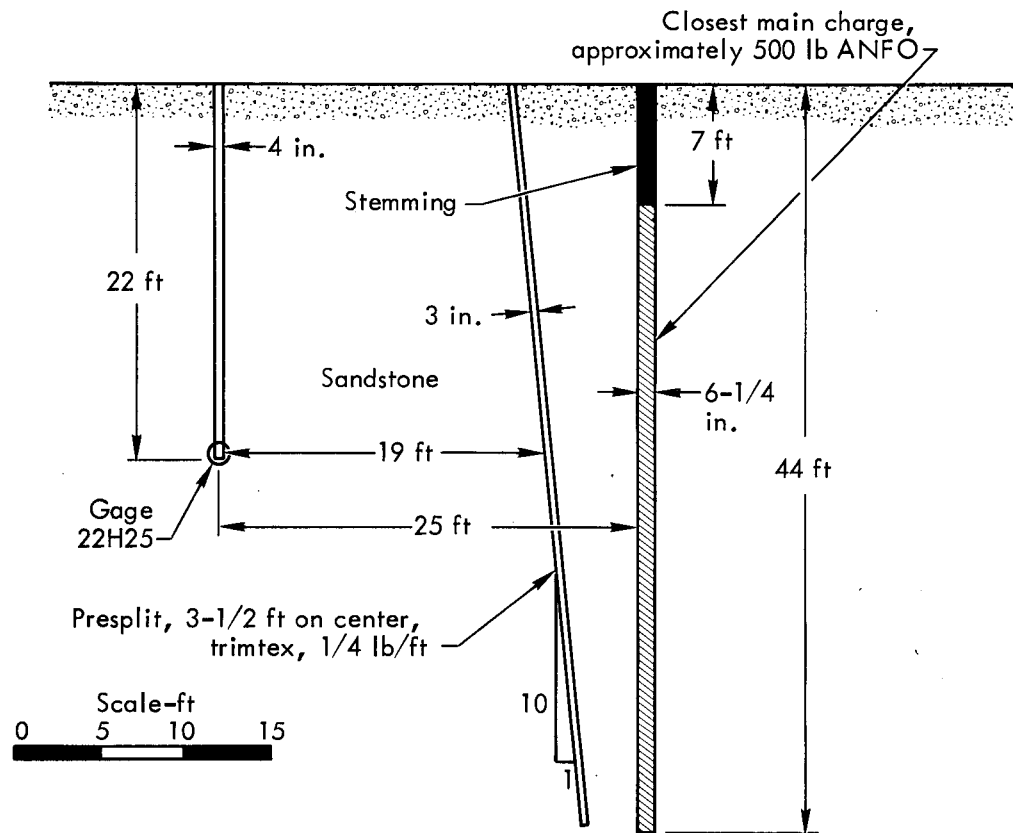


Fig. 62. Velocity gage configuration for PB-6A.

Variation of Peak Particle Velocity with Depth

The variation of peak particle velocity with depth can be observed in the data acquired from test blasts PB-4 and PB-8 (see Table 4) for which gages were placed at two separate depths. In all cases, horizontal peak particle velocities measured near the surface are less than those measured at depth. Near the surface, stress waves traveling from the charge strike the gage at large angles relative to the horizontal plane, resulting in a small horizontal particle velocity component. Also, the gages near the surface were farther away (slant distance) from the charge than those at depth, allowing additional distance for attenuation of the stress wave.

The only data available on the variation of vertical peak particle velocity with depth are for PB-4. In the nonbuffered case the vertical peak particle velocity increased with depth, and in the buffered case it decreased with depth.

It is not known whether or not the vertical and horizontal peak particle velocities occurred simultaneously; therefore, it cannot be assumed that the vector sum of the two is the resultant peak particle velocity.

CONCLUSIONS

It was the objective of the subsurface velocity and blast-induced fracturing program to observe two effects: (1) the effect that buffer zones have on shock

propagation in rock, and (2) the relationship between peak particle velocities with depth below the ground surface in the vicinity of a production blast charge. The subsurface velocity measurement program was generally successful, but the permeability testing program to measure blast-induced fracturing was not. The results of the subsurface velocity measurement program were used to establish safe separation distances between production charges and finished surfaces, presented in Chapter 9.

Effectiveness of Buffer Zones

The data collected were inconclusive regarding the effectiveness of buffer

zones in attenuating particle velocities near production blasts, although the trend of the data suggests that the buffer zones tested were not effective. Scatter in the data and discontinuities in the rock may have been sufficient to mask the effect of the buffer zones. Also, it may be that particle velocity is not the proper parameter to measure as an indicator of stress wave intensity. Although it seems plausible that a zone of crushed rock, such as intended in the buffer zones, would attenuate stress wave propagation, the buffer zone designs tested may not have produced the desired zone of crushed material.

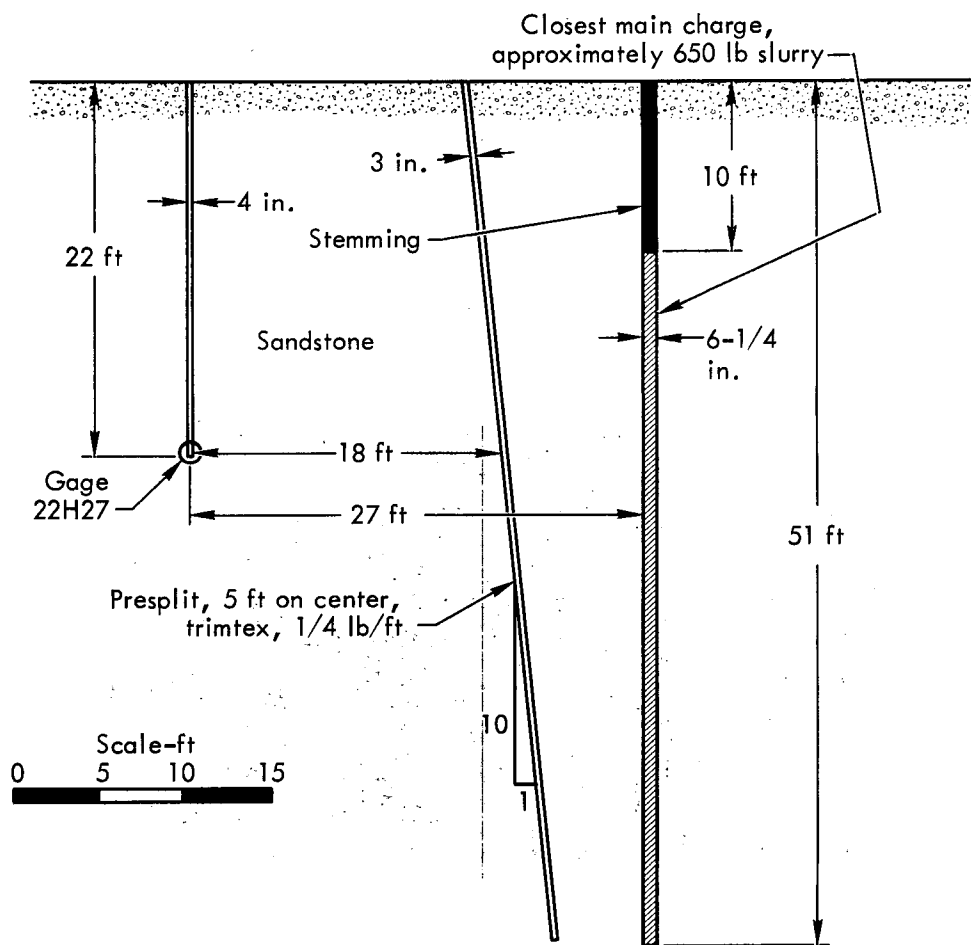


Fig. 63. Velocity gage configuration for PB-6B.

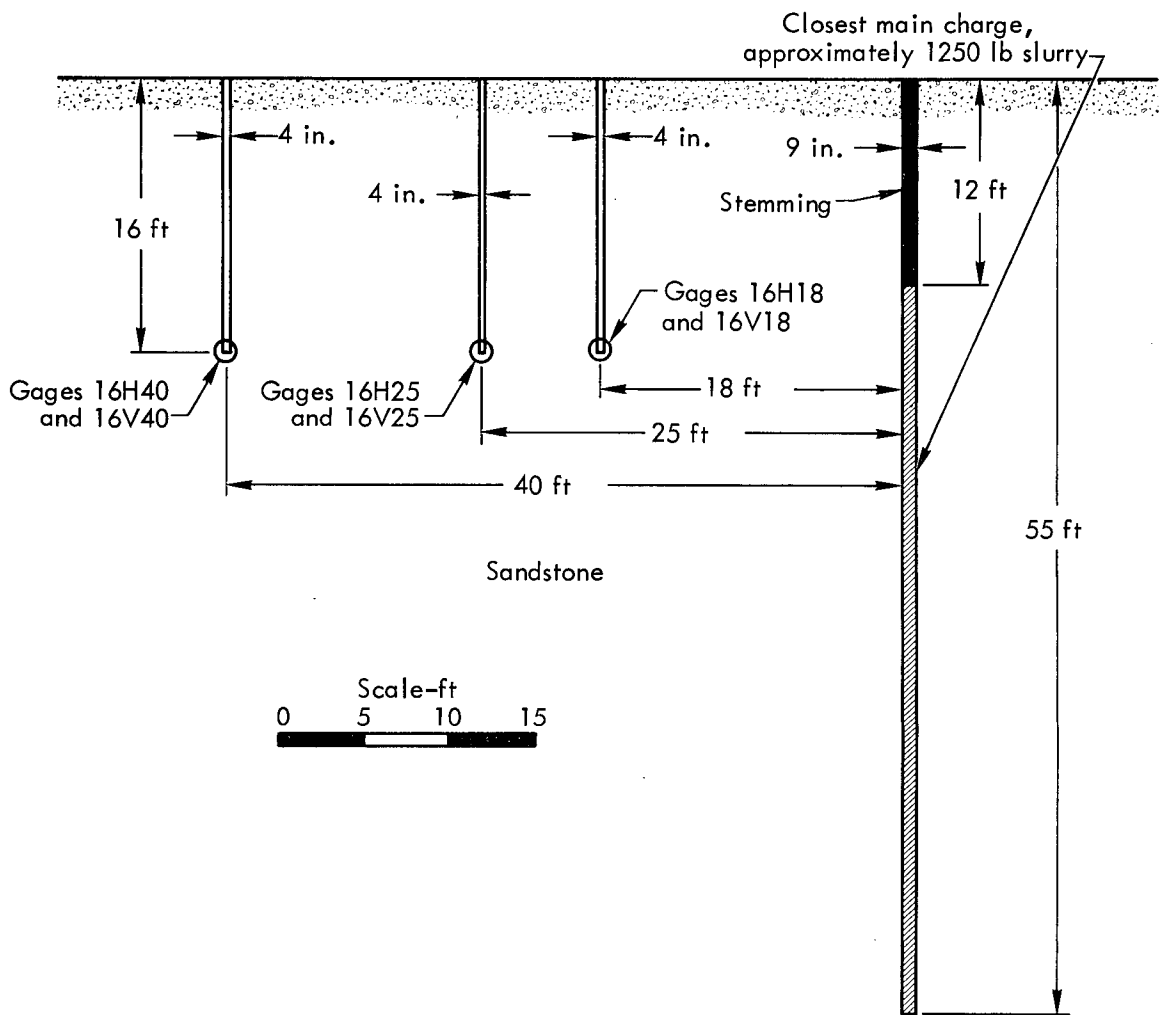


Fig. 64. Velocity gage configuration for PB-7.

Relationship Between Particle Velocity and Blast-Induced Fracturing

The attempt to obtain information on blast-induced fracturing by permeability tests was generally unsuccessful; however, some conclusions can be drawn from the PB-7 particle velocity measurements. Postshot inspection of the perimeter of the blast revealed that the gages emplaced 18 ft from one of the main charges (see Fig. 64) fell very near the boundary of a large conchoidal fracture surface in an area of massive, fresh Upper Gilbert sandstone (Fig. 68). The rock beyond this surface appeared to be unfractured,

thus the peak particle velocities recorded by the gages at a range of 18 ft must be near the threshold required for rock fracturing by a stress wave. The horizontal peak particle velocity at this gage had an amplitude of about 135 in./sec, and the vertical peak particle velocity was 115 in./sec.

Variation of Peak Particle Velocity with Depth

The horizontal peak particle velocities measured were greater at depths (opposite the charges) than near the surface. The results of the vertical peak particle velocity measurements were inconclusive.

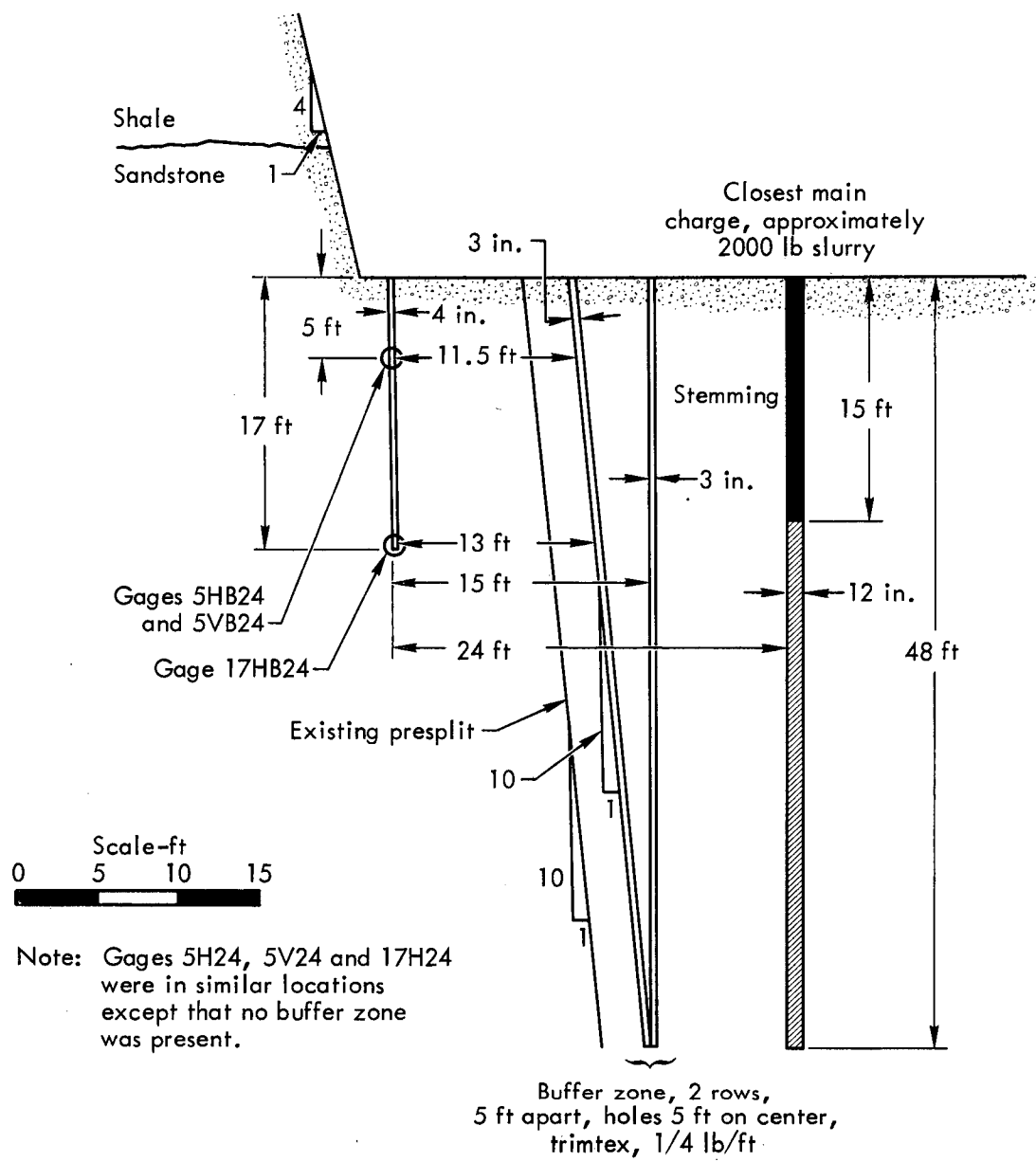


Fig. 65. Velocity gage configuration for PB-8.

Table 2. Summary of peak particle velocity measurements.

Test blast	Gage	Peak origin	Peak particle velocity (in./sec)	Risetime to peak (msec)	Peak acceleration (g)
PB-1	11.5H15	Presplit	65.4	3.0	57
		Main	7.1	4.0	5
	11.5V15	Presplit	24.0	2.0	31
		Main	6.6	4.5	4
PB-3	7HB21	Buffer	15.1	10.0	4
		Main	35.9	8.0	12
	7H21	Main	53.8	10.5	28
PB-4	2HB30	Presplit	19.2	3.0	25
		Buffer	Small	—	—
		Main	3.5	5.0	2
	2VB30	Presplit	47.8	6.5	19
		Buffer	47.2	10.0	21
		Main	27.9	18.0	4
	2H30	Presplit	28.5	3.5	45
		Main	2.5	14.0	Small
	2V30	Presplit	48.7	6.0	32
		Main	8.5 ^a	12.0	2
		Presplit	— ^a	—	—
	13HB30	Buffer	48.0	12.0 ^b	21
		Main	30.1	— ^b	—
		Presplit	26.9	— ^b	—
	13VB30	Buffer	34.4 ^c	8.0	20
		Main	— ^a	—	—
Presplit		—	—	—	
13H30	Main	25.7	7.0	9	
	Presplit	83.6	15.0 ^b	50	
13V30	Main	57.4	—	—	
	Presplit	—	—	—	
PB-6A	22H25	Presplit	33.6	3.5	35
		Main	57.5	2.0	75
PB-6B	22H27	Uncert.	71.4	5.0	93
PB-7	16H18	Main	135	0.5	706
	16V18	Main	115	0.5	601
	16H25	Main	61.3	0.6	266
	16V25	Main	60.3	0.6	262
	16H40	Main	23.4	0.7	87
	16V40	Main	27.3	0.7	101
PB-8	17HB24	Buffer	69.8	3.5	52
		Main	192	1.0	500
	5HB24	Buffer	36.1	4.5	21
		Main	31.9	2.0	42
	5VB24	Buffer	14.5	4.5	14
		Main	47.8	2.5	50
	17H24	Main	99.1	0.7	344
	5H24	Alternate ^d	30.9	1.5	54
		Main	18.0	1.5	31
	5V24	Alternate ^d	75.4	2.0	98
Main		52.0	6.5	47	

^aNot monitored due to instrument failure.

^bPeak shape poorly defined.

^cNo peak observed.

^dAlternate charge was at the center of the rear row (see Fig. 43).

Table 3. Summary of permeability test data.

Test blast	Test	Hole depth (ft)	Pretest water level (ft below collar)	Water column height (ft above top of test interval)	Test interval (ft below collar)	Flow rate (ml/min)
PB-1	Preshot	16.5	15.0	8.0	3.0 to 9.0	66
					9.0 to 15.0	16
	Postshot	15.0	12.0	8.0	4.5 to 10.5	130
					7.0 to 13.0	8
PB-3	Shot area had been ripped down approximately 25 ft; the blast was to remove the remaining 15 ft of material; therefore, there was no bench from which to make a water test.					
PB-4	The packer assembly failed to work properly (air escaped from the packer into the water system); repair was not possible in the time available before the blast.					
PB-6A	A test was attempted, but the packer assembly became stuck in the hole; all efforts to remove it failed.					
PB-6B	No packer test equipment was available due to the loss of the system in PB-6A.					
PB-7	A new packer arrived and tests were completed in one hole, near the gages which were 40 ft from the charge; it was impossible to complete the test because of numerous pinholes in the packer bladders due to abrasion, and efforts to patch the bladders were unsuccessful.					
	Preshot	30.0	Dry hole	28.0	29.0 to 25.0	No flow in 5 min
	(40-ft gages)			28.0	25.0 to 21.0	No flow in 5 min
				22.0	21.0 to 17.0	No flow in 5 min
				17.5	17.0 to 13.0	No flow in 5 min
				13.0	13.0 to 9.0	No flow in 5 min
				13.0	9.0 to 5.0	No flow in 10 min
PB-8	With the water quantity and flow rate available on site, efforts failed to fill the interpacker space; the top 10 ft of the bench was destroyed during the blast, making postshot testing impossible.					

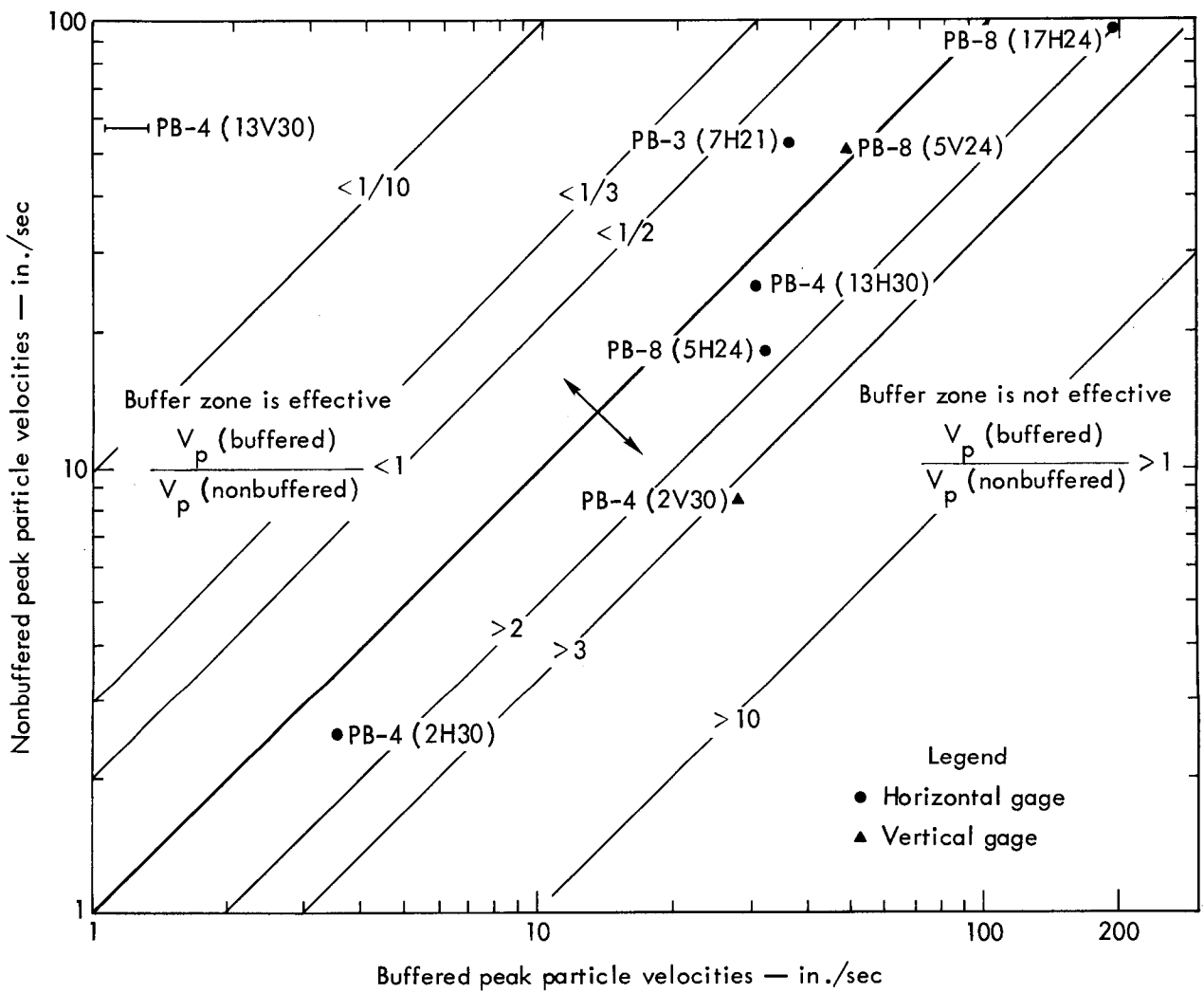


Fig. 66. Plot of effects of presence of buffer zone on peak particle velocities.

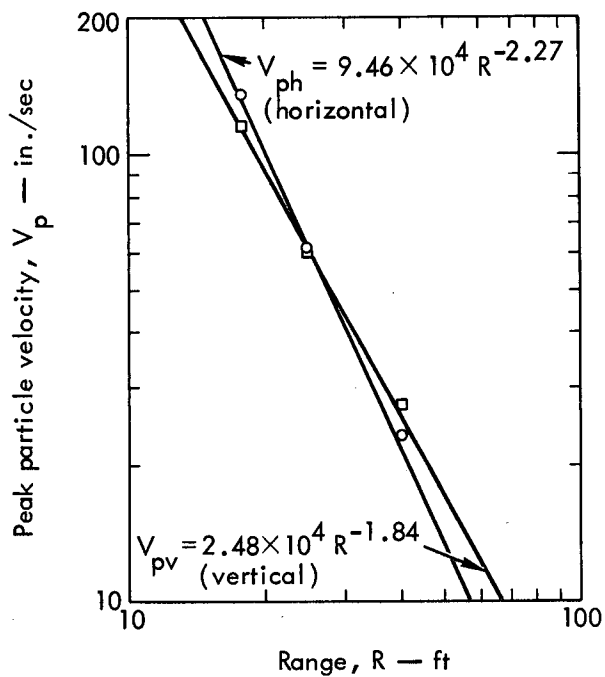


Fig. 67. Peak particle velocity vs distance for both horizontal and vertical gage orientations, PB-7.



Fig. 68. Rear of PB-7 showing approximate location of velocity gage holes, 18 and 25 ft from main charge (PB-7 blast area is to left of dashed line).

Table 4. Variation of peak particle velocities with depth.

Blast	Gage no.	Gage depth (ft)	Gage orientation	State	Peak particle velocity (in./sec)
PB-4	2HB30	2	Horizontal	Buffered	3.5
	13HB30	13	Horizontal	Buffered	30.1
	2VB30	2	Vertical	Buffered	27.9
	13VB30	13	Vertical	Buffered	Small
	2HNB30	2	Horizontal	Nonbuffered	2.5
	13HNB30	13	Horizontal	Nonbuffered	25.7
	2VNB30	2	Vertical	Nonbuffered	8.5
	13VNB30	13	Vertical	Nonbuffered	57.4
PB-8	5HB24	5	Horizontal	Buffered	31.9
	17HB24	17	Horizontal	Buffered	192
	5HNB24	5	Horizontal	Nonbuffered	18.0
	17HNB24	17	Horizontal	Nonbuffered	99.1

Chapter 6. Seismic Motion Program

BACKGROUND

This chapter describes the blast-induced seismic motion measurement program, its objectives, execution, and results. The results were used to evaluate the effects on nearby structures of blasting operations in the spillway of the R. D. BAILEY project.

The close proximity of the town of Justice, West Virginia, to the R. D. BAILEY Lake Project means that precautions must be taken to insure that damage will not occur to buildings in Justice because of blasting operations in the spillway. In addition, a concrete water intake structure, 300 ft high, will be under construction and subjected to seismic motion from spillway blasts. Experimental information was needed to calculate levels of seismic motion at this structure and to establish the maximum weight of explosive that can be detonated in the spillway without exceeding safe seismic motion levels in the town of Justice.

OBJECTIVES AND APPROACH

The objectives of the seismic motion program were:

1. To measure at selected points of interest seismic motion amplitudes as a function of time for all the experimental blasts and to provide documentation in the unlikely event that claims for seismic-motion-induced damage were received.

2. To develop a reliable method, based on experimental data, for predicting seismic motion amplitudes generated by production blasts in the spillway area.

The reliable prediction of peak particle velocity as a function of the weight of explosive and the distance from the blast was necessary to establish the maximum weight of explosive that can be simultaneously detonated in the spillway. Predicted peak particle velocities, when compared to established damage criteria, allow the engineer to assess the effects of a particular designed blast on residential structures and engineered structures, such as the water intake tower.

The approach for the field portion of the seismic motion program was to measure the particle velocities of the ground surface at four points of interest. By having four seismic stations at various distances from the blasts, the attenuation of seismic motion amplitudes with distance from the blasts could be determined.

Peak particle velocities (PPV) were measured for the test blasts and used to establish a relationship between seismic motion amplitudes, charge weights, and distances. The relationship¹⁶⁻¹⁸ is given by:

$$PPV = \kappa w^{\beta} r^{\alpha}, \quad (4)$$

where:

PPV = peak particle velocity (in./sec)

w = weight of the largest amount of explosive detonated per time delay (lb)

r = horizontal distance from the blast to the point of interest (ft)

κ = constant that depends on the medium surrounding the explosive, the foundation conditions at the point of

interest, and the units of the variables

β = explosive weight scaling exponent

α = attenuation exponent.

The parameters κ , α , and β can vary considerably from one project site to another. By using measured values of the variables PPV, w , and r , however, it was possible to calculate κ , α , and β for the R. D. BAILEY spillway site.

EQUIPMENT

Each seismic station consisted of a triaxial array of geophones to measure particle velocity at the ground surface. These geophones were oriented vertically, radially, and transversely with respect to each blast so that the seismic motion was completely defined in three dimensions. The voltage output of each geophone was recorded directly on chart recorders.

PROCEDURE

Four seismic stations were usually monitored during each blast. These were located at the right dam abutment (SS1), at the base of the dam embankment (SS2), at the intake tower (SS3), and at the town of Justice (SS4) - Fig. 69. Because blasting operations were in progress near the intake structure site at the time the first pilot excavation blasts started, it was necessary to move the station location (SS3, SS3A, SS3B) in that area several times. After completion of the intake structure foundation excavation, a seismic station (SS3C) at the northeast corner of the foundation was in operation for the final three test blasts (see Fig. 69).

The radial geophone at each seismic station was oriented toward the blast by line-of-sight or by use of a compass; the other geophones were oriented with respect to the radial geophone to measure orthogonal velocities.

DATA

All PPV data obtained during the pilot excavation blasts are tabulated in Table 5. The PPV's are measured from zero-to-peak and are considered accurate to $\pm 15\%$ unless otherwise noted. Table 5 also provides the horizontal distances from the center of the test blast to the indicated seismic station. These distances were obtained from surveyed blast coordinates and seismic station coordinates and are considered accurate to $\pm 1\%$. The largest simultaneous charge weight (i.e., the largest amount of explosive detonated during one delay) is listed for each blast.

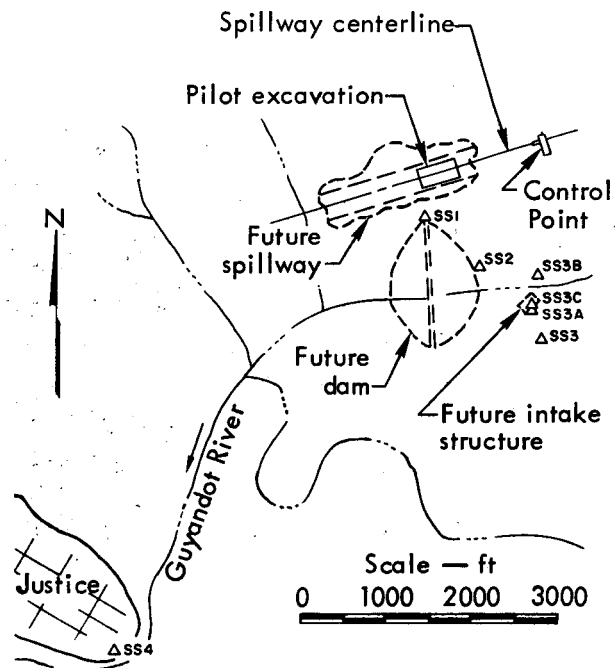


Fig. 69. Seismic station locations.

Table 5. Summary of peak particle velocity (PPV) measurements.

Test blast	Predominant rock type	Explosive type	Largest simultaneous charge weight (lb)	Seismic station	Range (ft)	Peak particle velocity		
						Vertical (cm/sec)	Radial (cm/sec)	Transverse (cm/sec)
PB-1	Shale	ANFO	260	SS1	451	0.66	0.52	0.44
				SS2	1180	0.090	0.11	0.14
				SS3	2231	0.013 ^a	0.019 ^a	0.029 ^a
				SS4	6640	0.0048	0.0089	0.0061
PB-3	Shale	ANFO	3380	SS1	497	4.7	4.9	2.0
				SS2	1180	0.56	1.1	0.40
				SS3	2225	0.087	0.13	0.074
				SS4	6703	0.024	0.046	0.035
PB-3 Buffer Zone	Shale	ANFO	66	SS1	460	0.25	0.36	0.14
				SS2	1168	0.024	0.050	0.020
				SS3	2217	0.0051	0.0084	0.084
				SS4	6661	0.0016	0.0030	0.0032
PB-4	Shale	ANFO	4000	SS1	539	4.4	4.5	2.5
				SS2	1157	0.68	1.5	0.61
				SS3	2191	0.13	0.21	0.062 _b
				SS4	6763	0.053	0.12	
PB-4A PB-4B	Shale	ANFO	250	SS1	584	0.60	0.68	0.54
				SS2	1177	0.060	0.15	0.09
				SS3	2204	0.015	0.020	0.0085
				SS4	6810	0.0042	0.0081	0.010
PB-4C	Shale	ANFO	2500	SS1	531	1.3	1.16	1.12
				SS2	1171	0.36	0.51	0.25
				SS3	2208	0.042	0.055 ^c	0.030
				SS4	6749	0.015	0.122 ^c	0.020 ^c
PB-4 Single Charge	Shale	ANFO	20	SS3	2120	0.00041 _d	0.0012 _d	0.00035
				SS4	6777			0.00044
PB-4D	Shale	ANFO	266	SS1	534	0.36	0.34	0.20
				SS2	1175	0.050	0.10	0.052
				SS3	2213	0.0068	0.0068	0.0052
				SS4	6751	0.0016	0.0027	0.0033
PB-4E	Sandstone	Slurry	290	SS1	546	0.35	0.62	0.32
				SS2	1231	0.055	0.12	0.065
				SS3	2274	0.0077	0.0097	0.0035
				SS3B	1958	0.020	0.019	0.018
PB-5	Sandstone	ANFO	258	SS1	648	0.27	0.22	0.24
				SS2	1134	0.083	0.13	0.071
				SS3	2140	0.0083	0.013	0.0095
				SS4	6880	0.0020	0.0046	0.0074
PB-6A Presplit	Sandstone	70% Dynamite	1250	SS1	584	3.60	2.01	1.54
				SS2	1120	1.07	0.99	0.55
				SS3	2140	0.12	0.16	0.081
				SS3A	1818	0.21 ^c	0.12 ^c	0.10 ^c
PB-6A	Sandstone	ANFO	2868	SS1	591	2.40	2.20	2.10
				SS2	1120	0.80	0.70	0.48
				SS3	2138	0.12	0.21	0.049
				SS3A	1816	0.19	0.085	0.044
PB-6B	Sandstone	Slurry	6000	SS1	532	8.20	6.80	5.20
				SS2	1126	2.10	3.60	1.20
				SS3A	1839	0.52	0.40	0.27
				SS3	2158	0.36	0.51	0.21
PB-6C	Sandstone	Slurry	781	SS1	524	1.10	0.62	0.72
				SS2	1117	0.26	0.33	0.2 _b
				SS3C	1814	0.066	0.028	0.043
				SS3A	1831	0.036	0.025	0.017
PB-7	Sandstone	Slurry	3700	SS1	609	3.6	5.0	3.2
				SS2	1200	0.86	1.16	0.76
				SS3C	1887	0.20	0.16	0.19
				SS4	6833	0.027	0.090	0.081
PB-8	Sandstone	Slurry	11,750	SS1	514	11.6	8.0	5.0
				SS2	1173	1.4	1.9	0.95
				SS3C	1882	0.36	0.39	0.26
				SS4	6727	0.082	0.14	0.16

^a Measurement underranged; precision $\pm 25\%$.

^b No measurement; malfunctioning cable or cable connector.

^c Measurement overranged; table value is an extrapolation and its precision is about $\pm 50\%$.

^d PPV smaller than seismograph sensitivity.

Table 5 shows that 186 data channels were fielded. Two channels of data were lost due to cable trouble; two were lost because the motion from test blast PB-4E was below the sensitivity of the seismograph. An additional eight channels were recorded with less precision than desired. Actual data recovery was about 98%.

The data in Table 5 are graphically illustrated in Appendix C.

ANALYSES

The effects of charge weight and range on seismic motion amplitudes were analyzed using statistical techniques. The effects of other variables (i.e., explosive type, the type of rock that was blasted, and local conditions at different seismic stations) were also studied. An equation to predict PPV's for future blasts in the spillway was developed, and the largest charge weights that can be safely detonated were established.

Effect of Charge Weight and Distance

Equation (4) is an empirical expression relating PPV to charge weight and range. Multiple linear regression analyses^{19,20} were performed to estimate the parameters

(κ, α, β) in Eq. (4) for the various sets of data given in Table 5. Four sets of PPV data were analyzed by a computer code²¹ that performed the regression analyses. The PPV's were separated into vertical, radial, and transverse components of motion so that future predictions of PPV could be made by component, if desired. For safety analyses of residential-type structures, however, it is the peak particle velocity, regardless of the component of motion, that has been related to architectural damage. The PPV's, regardless of the component of motion, were therefore analyzed to provide the parameters for Eq. (4), which was used as a basis for the prediction of PPV's from future blasts in the spillway.

The charge weights used in the regression analyses refer to the largest simultaneous charge weight, or the largest amount of explosive detonated on a single time delay. It is this quantity, rather than the total charge weight, that determines the maximum particle velocities.^{17,22}

Table 6 provides the estimated values of the parameters (κ, α, β) from the regression analyses along with two important statistics. The first is the coefficient of multiple determination, R^2 ,

Table 6. Parameters obtained from regression analyses of PPV as a function of charge weight and distance.

Component of motion	Number of data points	Estimated parameters			Statistics	
		κ	α	β	R^2	s
Vertical	62	964	-2.06	0.90	0.939	1.78
Radial	61	286	-1.81	0.84	0.904	1.97
Transverse	60	133	-1.72	0.79	0.882	2.16
Maximum PPV, regardless of component	62	291	-1.81	0.85	0.923	1.89

which is a statistic that measures the goodness of the fit of the data sets to Eq. (4). (If R^2 equals 1, a perfect fit of the data to the regression equation results; if R^2 equals 0, a total lack of fit results.) The other statistic, s , the standard error of the estimate, is a measure of the dispersal of the data points about the regression equation. The smaller the value of s , the closer the measured PPV's are to the regression equation. The best fit to the data is one that has the largest R^2 and the smallest s .

The estimated parameters in Table 6 when substituted into Eq. (4), should provide reasonable estimates of the PPV's for future detonations in the spillway.

Effect of Rock Type and Explosive Type

During the pilot excavation experiments, some blasts were detonated in a predominantly shale medium and others in a predominantly sandstone medium using two types of explosives, aluminized ammonium nitrate slurry and ANFO. PB-1 through PB-4D were predominantly shale, while PB-4E through PB-8 were mostly sandstone. The type of material in which a blast occurs can affect the resulting PPV magnitudes.^{17,18,23} For example, blasts in hard rock produce larger seismic

amplitudes than blasts in soil or a weak rock. To estimate the effect of the sandstone and shale media on seismic amplitudes, the measured PPV's were separated into two data sets according to the rock type. Regression analyses of these two data sets produced the parameters and statistics given in Table 7. Also shown in Table 7 are the regression analysis results for the combined sandstone and shale data sets. Note that the quality of the regression fits is comparable for the three sets of data. No significant improvements of the fitted data have resulted by separation of PPV's according to rock type.

Before discussing the differences between the two media, it should be noted that the separation of PPV's by media also separates them by explosive type. All of the slurry blasts occurred in sandstone, while all but two of the ANFO blasts took place in the shale media. Therefore, the separate effects of media and explosive type cannot be isolated; the results in Table 7 can only be used to compare PPV's from detonations of ANFO in shale with PPV's from slurry blasts in sandstone.

Two observations can be made from the results in Table 7. The attenuation

Table 7. Parameters obtained from regression analyses of maximum PPV, regardless of component, as a function of charge weight and distance for sandstone and shale.

Detonation medium	Number of data points	Estimated parameters			Statistics	
		κ	α	β	R^2	s
Shale	30	364	-1.76	0.82	0.925	1.97
Sandstone	32	340	-1.89	0.91	0.902	1.85
Shale and sandstone combined	62	291	-1.81	0.85	0.923	1.89

exponent (α) for the slurry-sandstone data is slightly greater than that for the ANFO-shale data, indicating the PPV decreases faster with distance for blasts in sandstone. Blasts in sandstone produce seismic motion with a higher frequency content than blasts in shale, and the PPV's decrease more rapidly with distance from the blast because attenuation in the earth is directly proportional to frequency.²³ The second observation is that the yield scaling exponent (β) is slightly greater for the slurry-sandstone data, suggesting that more of the total blast energy is radiated as seismic motion, and/or that more energy is produced by the slurry for equal charge weights of the two explosives, as already known. In any case, the slurry-sandstone seismic source should produce slightly larger PPV's with a frequency spectrum weighted toward the higher frequencies so that this seismic motion would attenuate with distance more rapidly than the motion from the ANFO-shale seismic source. It is evident from the results shown in Table 7 that the effects of medium and explosive type are of secondary importance compared to the effects of the largest simultaneous charge weight and the range. This is indicated by the fact that there are no dramatic changes in the magnitude of the estimated parameters nor in the statistics that indicate the quality of the resulting fit.

The geometrical arrangement of the explosive into presplit or main charges may have had some effect on the magnitude of the resulting PPV's. There is some evidence from a comparison of the PPV's of the PB-6A presplit, the PB-6A, and the PB-6C blasts that the presplit charge configuration produced unexpectedly large

PPV's. This observation has been made at other locations,²⁴ and has been attributed to the relatively greater confinement of presplitting charges compared to bench-blasting charges.

Effect of Local Geology

Differences in PPV amplitudes can be expected if measurements are obtained at two locations (equidistant from a blast) where the underlying local geology is different.^{18,24} According to Eq. (4), PPV's from a blast should lie on a straight line if the PPV is plotted vs the range on log-log paper. However, actual plots of measured PPV points, shown in Appendix C, indicate that these points usually lie either above or below the predicted straight line. The influence of local geology at the seismic station is often termed the "station factor," and is used to bring about a better fit of the measured PPV's to the regression line. Since the station factors for the R. D. BAILEY experiments were small, it was not necessary to include them in the regression analyses.

Comparisons of PPV's generated by the PB-6C blast and measured at Seismic Stations SS3A and SS3C (approximately the same distance from the blast) show that differences in station factors do indeed exist. These two seismic stations were at the base of a cliff comprised of thinly bedded sandstone (see Fig. 70). Table 8 presents the velocity measurements for PB-6C obtained at these two stations. The PPV's at SS3A were 40 to 90% less than those at SS3C. Not only were there differences in the amplitudes but also in the frequency content of the recorded seismic wave. There was

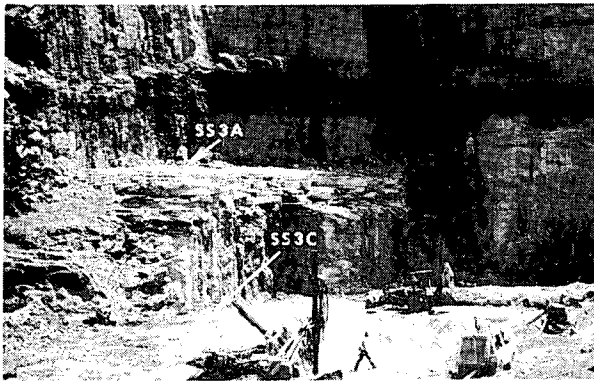


Fig. 70. Location of Seismic Stations SS3A and SS3C at intake structure foundation.

higher frequency motion contained on the SS3C seismogram that was apparently filtered out by the media under SS3A. Both seismograms had the same general shape, however. It appears that the seismic motion was slightly altered between SS3C and SS3A because of the influence of the local geology.

Predicted Peak Particle Velocities for Future Blasts

The main objective of the seismic motion program was to determine the largest simultaneous charge weight that could be detonated in the spillway without damaging residences in Justice or the intake structure being built as part of the R. D. BAILEY project. This objective was accomplished by developing an

equation to predict seismic motion amplitudes, and by solving this equation for the largest simultaneous yield for a given safe PPV.

The results of the regression analyses (see Table 6) when substituted into Eq. (4) indicate that the PPV can be predicted by the following equation:

$$PPV = 291 r^{-1.81} w^{0.85}, \quad (5)$$

where:

PPV = peak particle velocity
(in./sec)

r = horizontal distance from the
blast to the point of interest
(ft)

w = weight of the largest amount
of explosive detonated per
time delay (lb).

Equation (5) should provide good estimates for future blasts in the spillway area, but if conservative estimates of PPV are desired, Eq. (5) may be multiplied by one and a half times the estimated standard error, s. This multiplication results in the following prediction equation:

$$PPV = 825 r^{-1.81} w^{0.85}. \quad (6)$$

This equation provides estimates of PPV with approximately a 90% probability of not being exceeded. Figure 71 is a graph of this equation for several weights of

Table 8. Comparison of PPV's at Seismic Stations SS3A and SS3C from the PB-6C blast.

Component of motion	PPV (cm/sec)		Ratio of PPV's, $\frac{SS3A}{SS3C}$
	SS3A ^a	SS3C ^a	
Vertical	0.036	0.066	0.55
Radial	0.025	0.028	0.89
Transverse	0.017	0.043	0.40

^aSS3A was 1831 ft from the blast; SS3C was 1814 ft.

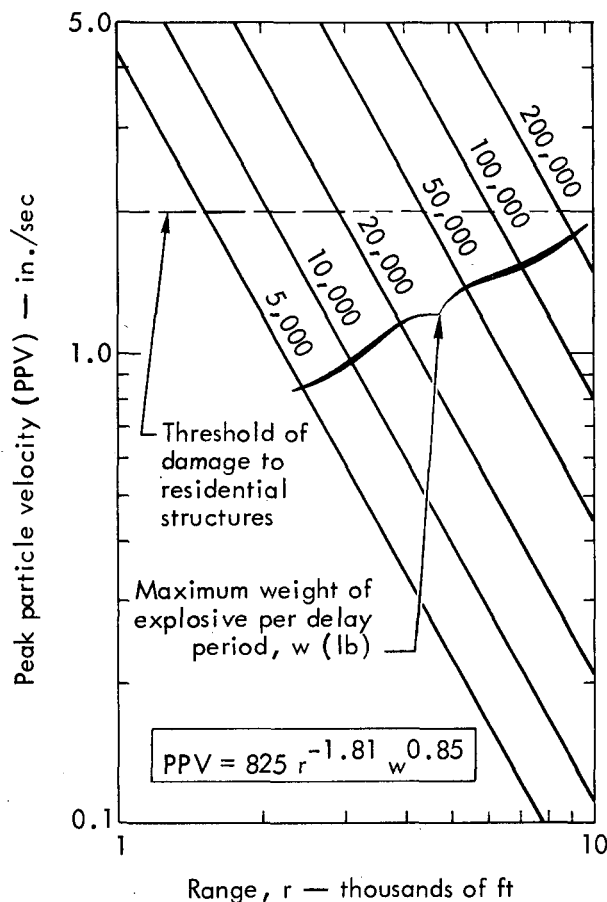


Fig. 71. PPV's with high probability of not being exceeded at various distances from various weights of explosive.

explosive. The figure also shows a line at the 2-in./sec-PPV level. This is the value generally considered to be the threshold of damage to residential structures.

To obtain an estimate of the largest simultaneous yield that can be detonated in the spillway area without exceeding a

specified PPV, Eq. (6) may be rearranged into the form:

$$w = 3.62 \times 10^{-4} \text{PPV}^{1.18} r^{2.13} \quad (7)$$

CONCLUSIONS

From a statistical analysis of measured peak particle velocities, it was determined that charge weight and distance from the blast are the primary variables affecting peak particle velocity amplitudes. At R. D. BAILEY the local geology at the point where seismic motion was measured is of secondary importance. The effects of the rock type and explosive type on particle velocity amplitudes appear to be minor.

The seismic motion technical program measured, analyzed, and evaluated the seismic data that were required to accomplish the program's objectives. Documentation of seismic motion produced by the pilot excavation blasts showed that peak particle velocities were below levels that could cause damage at places where structures were located. In fact, no claims from seismic-motion-induced damage nor complaints of this motion were received from the local populace. The prediction equations of peak particle velocity that were developed allow the engineer to safely design blasts for spillway excavation.

Chapter 7. Airblast Overpressure Program

INTRODUCTION

One of the areas of investigation during the experimental excavation program was

the measurement of airblast overpressures generated by the test blasts. The principal objective of the program was to develop an airblast prediction capability

for quarry-type production blasts. Eight airblast gages, located up to 6000 ft from the excavation, were used to gather data. The data were then analyzed to determine peak overpressures, impulses, and suppression factors due to topographic features.

BACKGROUND

Airblast is a blast effect capable of damaging objects at distances far beyond the immediate vicinity of the blast. Predictions of this effect are useful for determining the probability of damage occurring at various distances from a blast, and they may in turn be used to establish a maximum weight of explosive that can be detonated simultaneously without causing airblast damage.

A subsurface explosion produces airblast pressure waves (also called airblast pulses or airblast overpressures) by two mechanisms.²⁵ First, the initial upward spalling of the ground surface compresses the air above it, much like a piston, producing a region of high pressure, which then disperses in a wavelike manner. Second, when the gases from the blast vent through the fragmenting rock they will generally be at a pressure higher than atmospheric and thus will produce another pressure wave, which travels outwards. Figure 72 illustrates a typical overpressure record resulting from these two mechanisms.

If there is more than one charge in a detonation, airblast waves from different charges combine to produce a resultant wave with an amplitude and shape that are

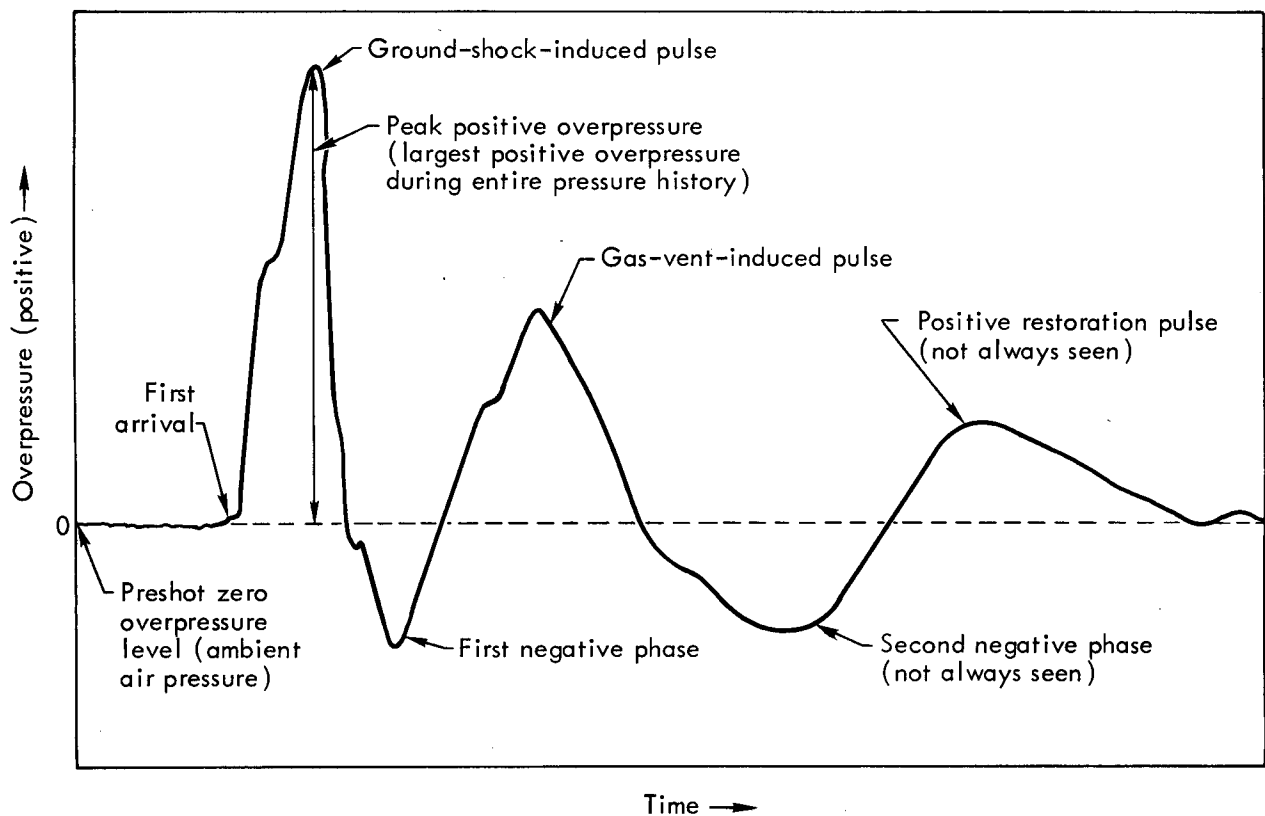


Fig. 72. Typical airblast overpressure vs time record.

different from the single-charge case. In addition, if there are millisecond delays between charges, the combination of measured airblast pulses will depend on delay times, distances between charges and the direction from the blast to the gage.

Previous airblast overpressure data have been collected primarily from single-charge detonations and a few single row and array detonations. Most of these blasts were experiments designed to provide explosive effects data, and therefore produced quite well defined airblast pulses with peak overpressures that were predictable with a fair degree of accuracy. Quarry excavations, on the other hand, usually contain a variety of charge sizes, delays, initiation devices, explosive types, and geologic and topographic features. All of these variables had to be considered when the overpressure measurements from the R. D. BAILEY test blasts were analyzed and when predictions were made for future blasts.

OBJECTIVES AND APPROACH

The objectives of the airblast overpressure measurement program were (1) to determine the shape and the amplitude of airblast overpressure waves produced by the test blasts, and (2) to develop a prediction procedure whereby airblast overpressures at various locations around the spillway could be determined for blasts similar to the test blasts.

The approach used for obtaining airblast measurements was to establish three lines of gages radiating from the test blast area. Two lines were approxi-

mately on the spillway centerline (east and west), and one was perpendicular to the centerline (south). Gage locations will be described in more detail later in this chapter. It was necessary to have several lines of gages to measure the effect of terrain features that modified airblast pulses, and also to determine the effect on airblast signals of millisecond delays in a blast pattern.

EQUIPMENT

The airblast gages used for this project were variable reluctance differential pressure transducers. One side of the differential gage was open to the atmosphere, while the other was equipped with a damping tube designed to allow only low-frequency changes in the ambient atmospheric pressure to be equalized on both sides of the gage (see Fig. 73).

Eight gages were deployed as shown in Fig. 74. Topographic profiles in Fig. 75 show terrain features between the blast area and the gages.

Six of the gages were connected by cable to an oscillograph and a tape recorder. The records included zero-time marks for each millisecond delay fired.

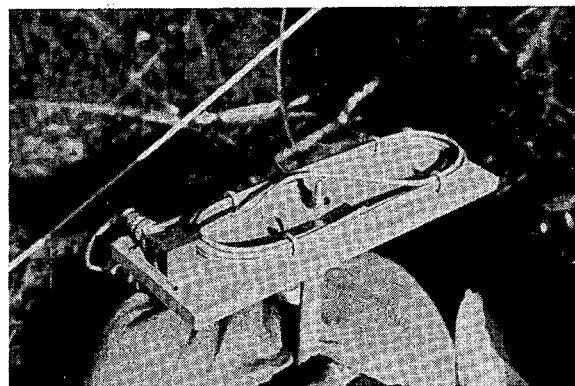


Fig. 73. Airblast gage.

These marks were produced by break-wires attached directly to the delay caps or detonating cord. The use of both an oscillograph and tape recorder provided a means of using different sensitivities in recording a data channel and also giving backup recording protection. A paper record provided the initial field-reduced data, and the tape record was digitized and analyzed by computer. The two remaining gages were remote units. Data from these gages were not recorded on magnetic tape, but paper records were produced by an oscillograph and a pen recorder. No zero-time marks were available for these two stations. The air-

blast gages were originally located so that they would have a clear view of the blast area. As the experimental excavation progressed, however, it became necessary to relocate some of the gages. Airblast gage locations are described in Table 9.

DATA

The results of the airblast data collection program are listed in Table 10. The data recovery rate for the airblast program was 97% (132 successfully recorded data channels out of 136 total). Records from airblast gage E-2 are in Appendix D.

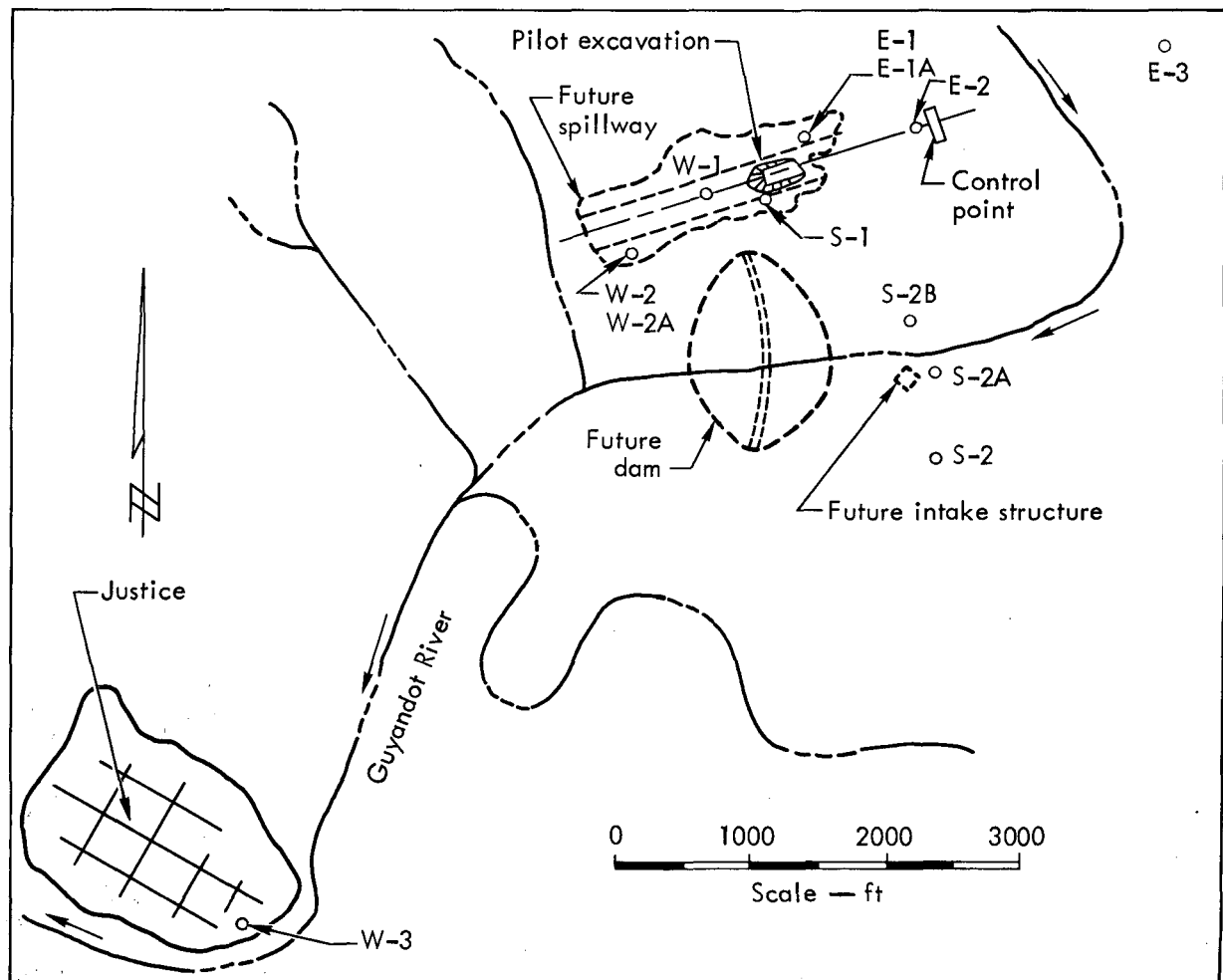
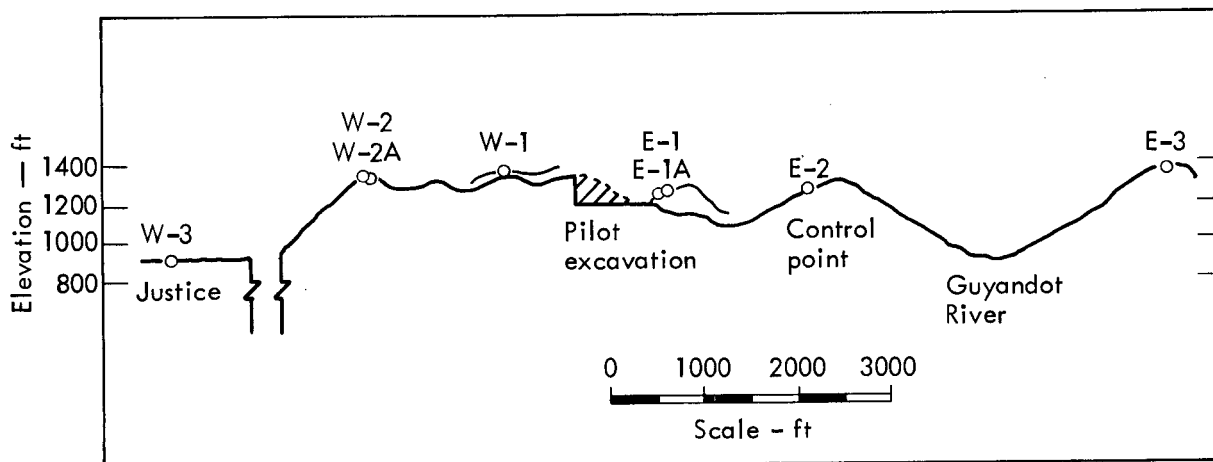
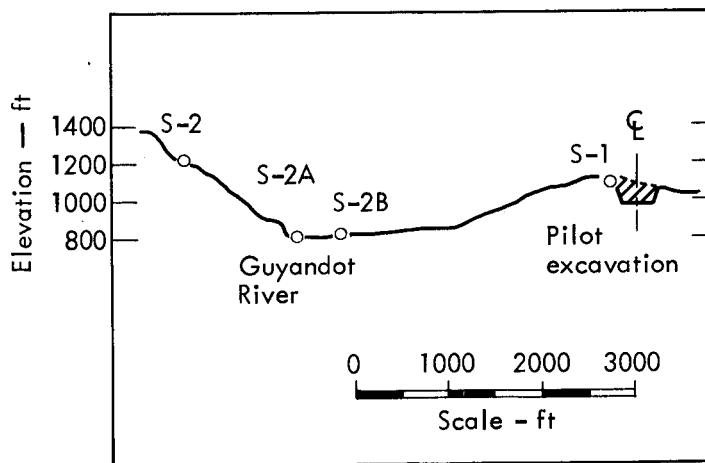


Fig. 74. Plan view of airblast gage locations.



(a) E-W section approximately parallel to spillway center line (looking north).



(b) N-S section approximately perpendicular to spillway center line (looking west).

Fig. 75. Topographic profiles through airblast gage locations.

Table 9. Airblast gage locations.

Gage	Coordinates		Elevation (ft)	Referenced to spillway center line	
	North (ft)	East (ft)		Station	Offset (ft)
W-1	220,506	1,761,196	1373	12 + 29	2 left
W-2	220,080	1,760,613	1338	19 + 13	233 left
W-2A	220,079	1,760,608	1343	19 + 18	232 left
W-3	215,122	1,757,719	890	61 + 65	4090 left
E-1	220,915	1,761,915	1255	4 + 20	172 right
E-1A	220,912	1,761,908	1243	4 + 28	171 right
E-2	220,982	1,762,737	1269	-3 + 84	12 left
E-3	221,625	1,764,586	1349	-23 + 41	45 right
S-1	220,467	1,761,602	1304	8 + 53	161 left
S-2	218,525	1,762,859	1413	2 + 39	2392 left
S-2A	219,164	1,762,884	910	0 + 23	1790 left
S-2B	219,555	1,762,700	920	0 + 81	1361 left

Table 10. Summary of peak positive overpressure measurement and time of arrival.

Test blast	Gage	Horizontal distance from blast (ft)	Time of first pulse arrival (TOA) (sec)	Peak positive overpressure (psi)	Test blast	Gage	Horizontal distance from blast (ft)	Time of first pulse arrival (TOA) (sec)	Peak positive overpressure
PB-1	W-1	300	0.273	0.187	PB-4E	W-1	440	0.401	0.00434
	W-2	1050	0.905	0.0038		W-2A	1200	1.032	0.00590
	W-3 ^a	6000	-	0.0013		S-1	220	0.216	0.096
	S-1	160	0.113	0.0668		S-2B ^a	1700	-	0.0086
	S-2 ^a	1500	-	0.0026		S-2 ^a	2500	-	0.0070
	E-1	500	0.433	0.0386		E-1A	370	0.306	0.0887
	E-2	1350	1.124	0.0368		E-2	1180	1.019	0.0279
	E-3	3300	2.878	0.0200		E-3	3000	2.736	0.00688
	PB-2 Presplit	W-1	300	0.298		0.138	PB-5	W-1	655
W-2		1100	0.930	0.0155	W-2A	1400		1.251	0.00346
W-3 ^a		5940	-	-	W-3 ^a	6000		-	0.000891
S-1		100	0.086	0.152	S-1	300		0.316	0.0324
S-2 ^a		2000	-	0.0035	S-2 ^a	2300		-	0.00572
E-1		500	0.444	0.0316	E-1	260		0.206	0.2205
E-2		1300	1.165	0.0616	E-2	960		0.795	0.0386
E-3		3300	2.928	0.0182	E-3	3000		2.522	0.00649
PB-3 Buffer Zone	W-1	368	0.342	0.0247	PB-6A Presplit	W-1	620	0.499	0.0382
	W-2A	1087	0.970	0.00236		W-2A	1360	1.110	0.00596
	W-3 ^a	6000	-	0.00063		W-3 ^a	6000	-	-
	S-1	150	0.115	0.0315		S-1	260	0.167	0.0448
	S-2 ^a	2300	-	0.00107		S-2 ^a	2300	-	0.00285
	E-1	465	0.407	0.0190		E-1	300	0.230	0.0855
	E-2	1244	1.090	0.0184		E-2	1000	0.856	0.0299
	E-3	3300	2.812	0.0042		E-3	2800	2.578	0.00451
PB-3	W-1	408	0.388	0.0428	PB-6A	W-1	600	0.521	0.059
	W-2A	1127	1.042	0.0116		W-2A	1330	1.135	0.0102
	W-3 ^a	6000	-	0.0026		S-1	250	0.217	0.161
	S-1	160	0.158	0.0995		S-2A ^a	1800	-	0.0067
	S-2 ^a	2300	-	0.0061		S-2 ^a	2400	-	0.0153
	E-1	425	0.377	0.0845		E-1	300	0.224	0.37
	E-2	1204	1.066	0.0220		E-2	1020	0.827	0.058
	E-3	3200	2.781	0.00755		E-3	3000	2.553	0.0121
PB-4 Presplit	W-1	480	0.360	0.0443	PB-6B	W-1	520	0.400	0.0662
	W-2A	1200	0.981	0.00406		W-2A	1270	1.016	0.0125
	W-3 ^a	6000	-	0.00036		S-1	200	0.050	0.104
	S-1	150	0.085	0.110		S-2A ^a	1800	-	0.0231
	S-2 ^a	2300	-	0.0069		S-2 ^a	2400	-	0.0279
	E-1	370	0.317	0.061		E-1A	340	0.188	0.182
	E-2	1200	0.941	0.0571		E-2	1100	0.853	0.0738
	E-3	3220	2.687	0.0168		E-3	3000	2.576	0.0154
PB-4	W-1	480	0.459	0.059	PB-6C	W-1	520	0.443	0.0271
	W-2A	1200	1.075	0.0107		W-2A	1270	1.057	0.00123
	W-3 ^a	6000	-	0.00108		S-1	200	0.172	0.0410
	S-1	150	0.180	0.0935		S-2A ^a	1800	-	0.00734
	S-2 ^a	2300	-	0.0087		S-2 ^a	2400	-	0.00378
	E-1	370	0.263	0.121		E-1A	340	0.245	0.128
	E-2	1200	0.862	0.0302		E-2	1100	0.909	0.0196
	E-3	3220	2.588	0.0060		E-3	3000	2.635	0.00304
PB-4A	W-1	540	0.577	0.0266	PB-7	W-1	530	0.467	0.0402
	W-2A	1290	1.107	0.0094		W-2A	1290	1.101	0.0123
	W-3 ^a	6000	-	0.00217		W-3 ^a	6000	-	0.00187
	S-1	240	0.196	0.238		S-1	250	0.207	0.0959
	S-2 ^a	2300	-	0.0070		S-2 ^a	2480	-	0.0114
	E-1	325	0.245	0.145		E-1A	300	0.170	0.171
	E-2	1090	-	-		E-2	1080	0.858	0.0615
	E-3	2750	2.622	0.00388		E-3	3000	2.583	0.0133
PB-4B, C	W-1	480	0.397	0.102	PB-8	W-1	450	0.403	0.0107
	W-2A	1240	1.005	0.032		W-2A	1200	1.024	0.00905
	W-3 ^a	6000	-	0.0024		W-3 ^a	6000	-	0.00512
	S-1	200	0.125	0.179		S-1	180	0.130	0.306
	S-2 ^a	2300	-	0.0149		S-2 ^a	2450	-	0.0188
	E-1	380	0.249	0.165		E-1A	390	0.300	0.336
	E-2	1134	0.867	0.0175		E-2	1160	1.004	0.113
	E-3	2800	-	-		E-3	3110	2.743	0.0222
PB-4D	W-1	480	0.403	0.0252					
	W-2A	1240	1.034	0.00477					
	W-3 ^a	6000	-	0.00123					
	S-1	200	0.176	0.0915					
	S-2 ^a	2300	-	0.00695					
	E-1	380	0.288	0.113					
	E-2	1134	0.964	0.0220					
	E-3	2800	2.683	0.00431					

^aRemote

ANALYSES

Several types of analyses were performed on the airblast data in an effort to identify the origin of recorded airblast waveforms and peaks. To assist in these analyses airblast measurements from several additional tests were recorded, including a single-charge blast and a blast of detonating cord alone. Airblast records from gage E-2 for PB-1, PB-3, and PB-6A are presented as examples. Gage E-2 was selected because it had a clear "line-of-sight" for all blasts. Other investigations included a study of the variation in peak overpressures and impulses as a function of explosive weight as well as the influence of topography on airblast pulses (see Figs. 76 through 80).

Waveform Analysis

If each charge in a blasting pattern were to produce a classical waveform as shown in Fig. 72, one would expect the peak overpressure to be due to a combination of pulses from individual charges. The record from PB-3, shown in Fig. 76, is a good example. This, however, was not the case for the majority of the test blasts. Usually the peak overpressure was found to be due to surface detonating cord or early venting through weak stemming. These peaks were of higher frequency than the combination of pulses seen in Fig. 76.

As an example, consider the airblast record from PB-1, shown in Fig. 77. Knowing the relative arrival times of discrete airblast pulses, the distances

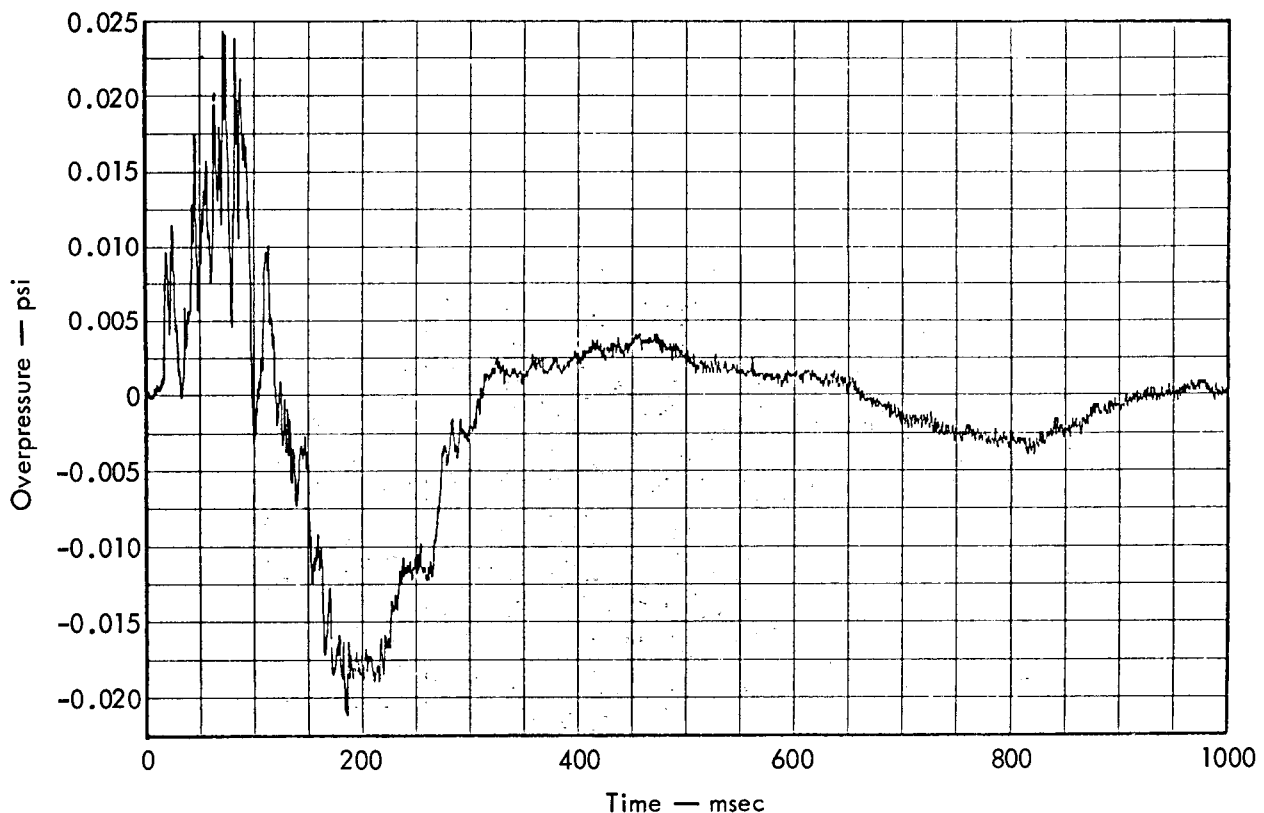


Fig. 76. Overpressure at Gage E-2 from Test Blast PB-3.

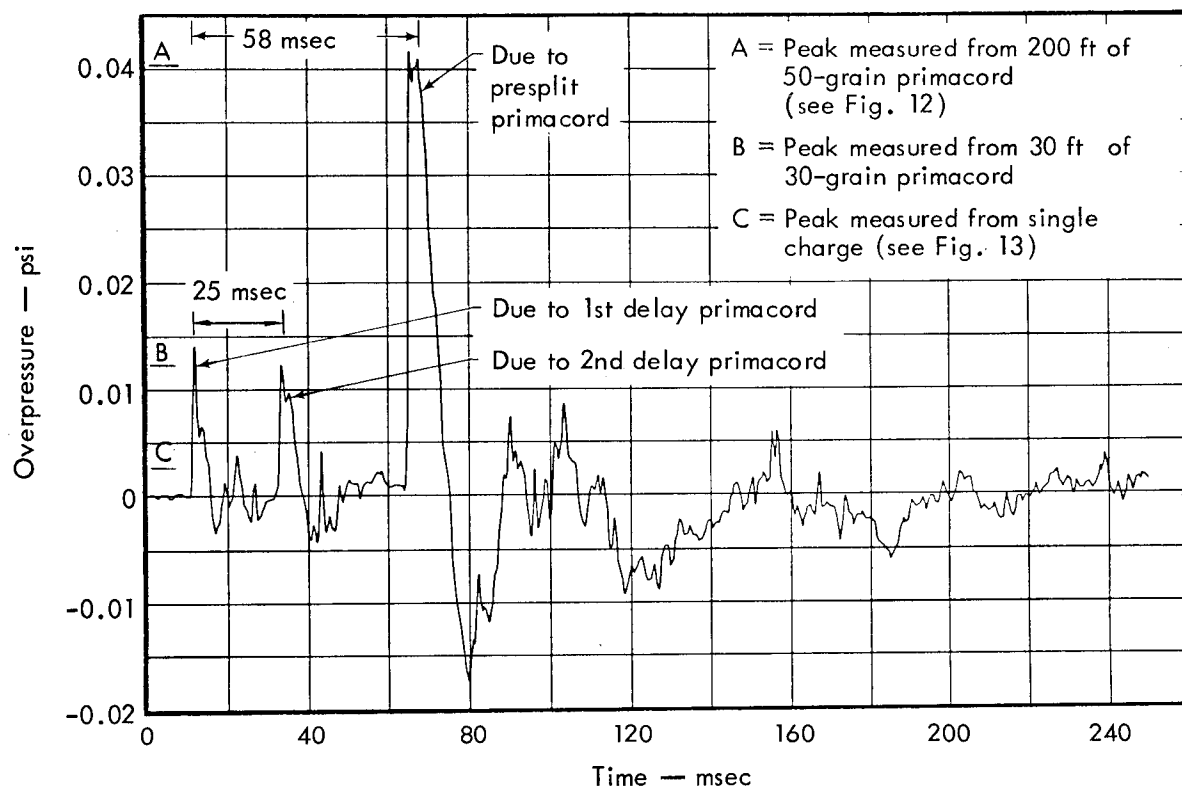


Fig. 77. Overpressure at Gage E-2 from Test Blast PB-1.

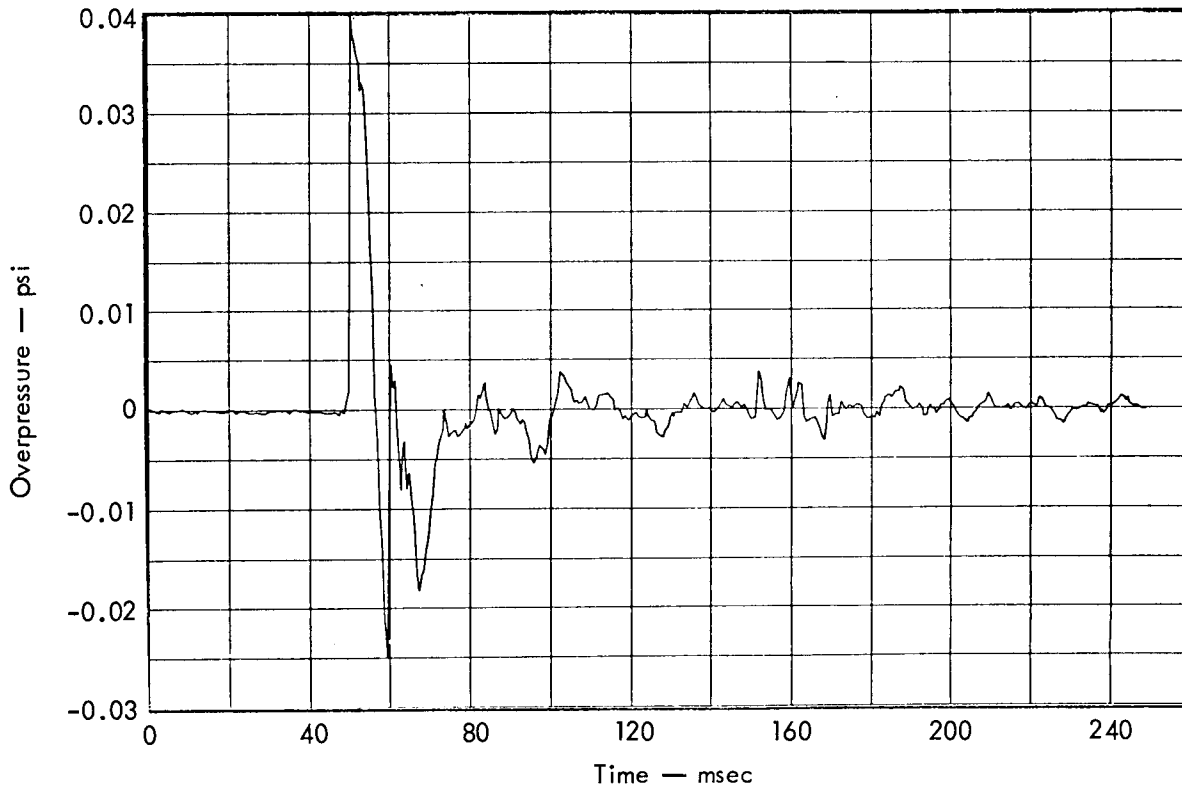


Fig. 78. Overpressure at Gage E-2 from 200 ft of detonating cord lying perpendicular to spillway centerline.

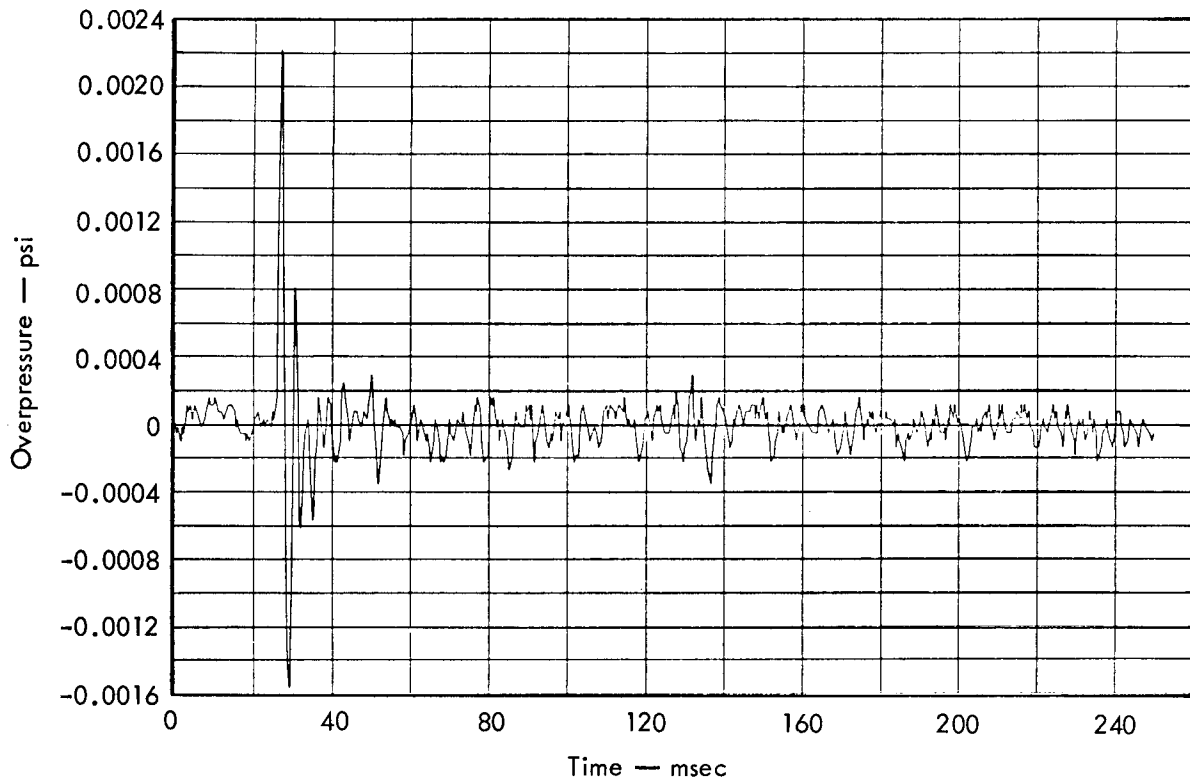


Fig. 79. Overpressure at Gage E-2 from typical single charge.

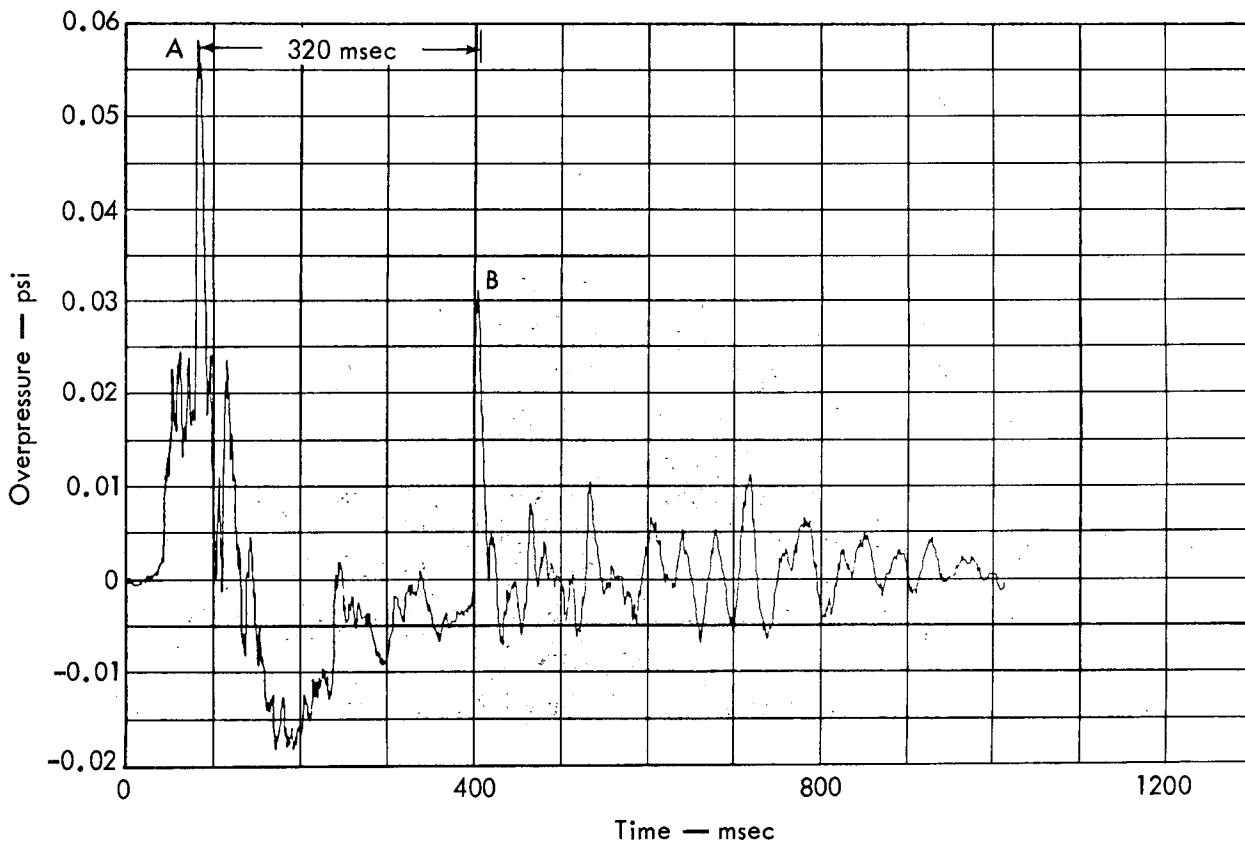


Fig. 80. Overpressure at Gage E-2 from Test Blast PB-6A.

between charges (or the distance between lengths of surface detonating cord), and the delays used in the blasting pattern, it is possible to deduce the origin of some of the prominent spikes in the record. Referring to the PB-1 charge layout in Fig. 8 and the airblast record at gage E-2 (Fig. 77), the first three prominent spikes can be attributed to surface detonating cord connecting charges on the "0" delay, the detonating cord for the "1" delay, and the detonating cord for the presplit line, which was fired on the "0" delay but was farther from the gage. Figures 78 and 79 show records for two additional tests, one of a 200-ft length of 50-grain detonating cord lying perpendicular to the centerline, and the other of a single charge that happened to misfire during the test blast and was later detonated separately. This single charge may be considered typical of the production charges in PB-1. The peaks recorded during these two tests are marked in Fig. 77 for comparison.

The record from gage E-2 for test blast PB-6A (shown in Fig. 80) is an example of two spikes (A and B) attributed to the venting at relatively early time of high-pressure gases through stemming material. At first it was suspected that the peaks were due to surface detonating cord, but after viewing high-speed movies of the blast and comparing the records from gages E-2 and W-1 it was confirmed that the spikes were due to the early venting of two charges. One of the charges that vented was on the left end of the second row from the front of the pattern, and the other was on the right end of the rear row (see Fig. 30).

Peak Overpressure and Peak Impulse as a Function of Explosive Weight

In order to compare the airblast data from various test blasts it was necessary to establish an equivalent basis for the data. This was accomplished (1) by plotting the peak overpressures and the peak impulses at gages E-1, E-2, and E-3 as a function of distance from each blast, and then (2) by interpolating the values of peak overpressure and peak impulse at a distance of 1000 ft from the blast. These interpolated values were designated $\Delta P-E_{1000}$ (for peak overpressure) and $I-E_{1000}$ (for peak impulse). Impulses were calculated by a computer program that integrated the overpressure data with respect to time. Table 11 summarizes this information along with attenuation exponents and explosive weights.

The attenuation exponents, b , in an easterly direction were determined by measuring the slope of the lines connecting data points on plots of peak overpressure vs range, r , and peak impulse vs range. Therefore, $\Delta P-E_{1000}$ and $I-E_{1000} \propto r^{-b}$. These exponents varied from 0.7 to 1.7, but most were about 1.5. This rapid decay rate is typical of small charges that produce short-duration pulses. Airblast overpressure records for gage E-2 are included in Appendix D.

The $\Delta P-E_{1000}$ and $I-E_{1000}$ values for each blast, listed in Table 11, were plotted against the total weight of explosive and the largest simultaneous weight of explosive on log-log paper. Although $\Delta P-E_{1000}$ and $I-E_{1000}$ tended to increase with increasing weight of explosive, the points were scattered enough so that no definite conclusions could be drawn for use

Table 11. Peak overpressure and impulse data.

Test blast	Total weight of explosive (lb)	Largest simultaneous weight of explosive (lb)	Overpressure		Impulse	
			Attenuation exponent, b^a	$\Delta P-E_{1000}$ (psi)	Attenuation exponent, b^a	$I-E_{1000}$ (psi-sec)
PB-1	1,150	260	0.7	0.044	0.718	0.00035
PB-3	3,380	3,380	1.1	0.027	1.29	0.0017
PB-4 Presplit			1.3	0.075		
PB-4	20,000	4,000	1.5	0.036		
PB-4A	803	803	1.6	0.021		
PB-4B&C	4,811		1.7	0.023		
PB-4D	1,581		1.6	0.026		
PB-4E	550		1.4	0.032		
PB-5	1,188	258	1.5	0.037	1.35	0.00019
PB-6A Presplit			1.5	0.030		
PB-6A	15,350	2,868	1.5	0.050	1.26	0.0016
PB-6B	8,600	3,993	1.5	0.082	1.06	0.0024
PB-7	19,950	3,700	1.2	0.067	0.907	0.0025
PB-8	32,100	10,990	1.4	0.14	1.56	0.0070

$^a \Delta P-E_{1000} \propto \text{range}^{-b}$, $I-E_{1000} \propto \text{range}^{-b}$.

in developing an airblast prediction system on the basis of explosive weight. The scatter may be explained by the fact that airblast is produced by several different mechanisms, as discussed earlier in this chapter, any one of which may be predominant in any particular blast. The plot that exhibited the most linearity was that of $I-E_{1000}$ vs the largest simultaneous weight of explosive, shown in Fig. 81.

The improved linearity of the impulse plot compared to the overpressure plot may be attributed to the fact that short-duration airblast spikes contribute less to the peak value of impulse than to the peak value of overpressure.

Suppression Factors

For the purpose of this analysis, suppression factors are defined as dimensionless numbers that are ratios of the airblast overpressure (or impulse) from gages in a westerly and southerly direction to the signal from gages in an easterly direction. The easterly gages were used as a datum because each had an unobstructed line-of-sight to the blast area (see Fig. 75). The suppression factors listed in Table 12 were calculated by determining the ratio of the peak overpressure at any gage to the peak overpressure in the easterly direction at a comparable distance.

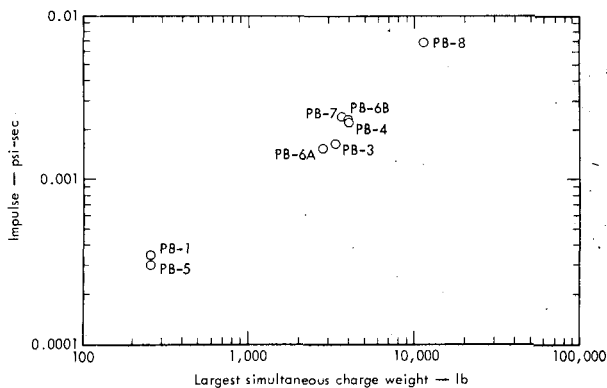


Fig. 81. Impulse at 100 ft east vs largest simultaneous weight of explosive.

Several observations may be made based on the suppression factors in Table 12. Note that airblast suppression in the westerly and southerly directions generally increased (indicated by a decrease in suppression factor) as the blasting progressed deeper into the excavation, and high, steep walls were developed on the westerly and southerly sides of the cut. Notice also, that for blasts near the west wall, such as PB-4E and PB-8, the airblast was significantly more suppressed at the near gage, W-1, than at the far gage, W-2. This suggests that the west wall directed the airblast upwards to the top of the wall where it was refracted to points horizontally distant, so that points farther from the wall experienced a higher proportion of refracted airblast than did the close-in points.

Another interesting observation is that the impulse suppression factors are gen-

erally higher than comparable peak overpressure suppression factors. Topographic features, therefore, were less effective in reducing peak impulse than in reducing peak overpressure.

Predictions

Peak airblast overpressures were predicted at the E-2 gage (unobstructed line-of-sight) using the technique described in Ref. 26 (see Table 13).

The details of the prediction method used are beyond the scope of this report; however, the technique essentially predicts ground-shock-induced airblast overpressures due to a "typical" single charge in the blasting pattern. Appropriate reinforcement factors are then applied to account for the multiple-charge configurations. This technique was developed for large cratering charges, so that a certain number of assumptions had

Table 12. Airblast suppression factors.

Blast	Overpressure suppression factors				Impulse suppression factors	
	Gage W-1	Gage W-2	Gage W-3	Gage S-2	Gage W-1	Gage W-2
PB-1	2.0	0.75	0.7	0.7	1.15	0.3
PB-3	0.60	0.48	0.7	0.55	0.218	0.357
PB-4 Presplit	0.20	0.07	0.045	0.28	—	—
PB-4	0.67	0.37	0.44	0.85	—	—
PB-4A	—	—	2.0	1.4	—	—
PB-4B&C	—	—	—	—	—	—
PB-4D	0.31	0.26	1.0	1.1	—	—
PB-4E	0.06	0.22	—	0.78	—	—
PB-5	0.39	0.16	0.39	0.6	0.647	—
PB-6A Presplit	0.80	0.33	—	0.44	—	—
PB-6A	0.45	0.26	—	0.9	0.468	0.333
PB-6B	0.51	0.50	—	1.2	0.583	0.421
PB-7	0.36	0.26	0.32	0.75	0.68	0.53
PB-8	0.045	0.11	0.58	0.58	—	0.120

Table 13. Comparison of predicted and measured peak airblast overpressures at Gage E-2.

Test blast	Predicted value (psi)	Probable value due to main charges ^a	Measured value
PB-1	0.00759	0.0080	0.0410
PB-3	0.0438	0.0240	0.0240
PB-4	0.0260	0.0302	0.0302
PB-5	0.0152	0.0120	0.0310
PB-6A	0.0360	0.0240	0.0570
PB-6B	0.0237	0.0260	0.0740
PB-7	0.0523	0.0340	0.0590
PB-8	0.104	0.112	0.112

^aNeglects short-duration spikes due to detonating cord and early-time gas venting.

to be made in order to apply it to the types of blasts detonated at R. D. BAILEY.²⁶ The peak measured value of the overpressure and the probable value of the overpressure due to the main charges (obtained by eliminating the short duration spikes from the detonating cord and early time venting) are also shown in Table 13.

CONCLUSIONS

It is possible to predict within a factor of two the peak airblast overpressure to a point with an unobstructed line-of-sight from the main production charges. However, much work remains to be done to account for the effects of topography and exposed detonating cord.

Chapter 8. Test Fills

INTRODUCTION

A portion of the rock removed during the experimental excavation was used to construct 17 test fills. The purpose of these test fills was to determine the best procedure for placing in the dam embankment the rock excavated from the spillway.

The design of the dam called for stringent limitations on settlement. The test fill program, therefore, experimented with various lift thicknesses and several types of spreading and compacting equip-

ment in order to determine which factors would maximize compaction, and thus minimize later settlement. Table 14 shows pertinent data on each of the test fills.

EQUIPMENT

The rock was spread on the test fills with Caterpillar Models D6, D8, and D9 tractors with dozers. Compaction equipment used consisted of a double-drum tamping roller shown in Fig. 82 and a Buffalo-Bomag 10-ton vibratory roller,

Table 14. Test fill data.

Source	Fill number ^a	Material	Fill size (ft)	Test pit size Diam Depth (ft) (in.)	Lift thickness (in.)	Type roller ^a	Number of passes	Dry density (lb/ft ³)	Spreading equipment ^b
PB-3	1	Ripped shale	- ^c	0.92 × 12	8	Modified SFR	6	121.7	-
PB-4	2	Ripped shale	- ^d	0.96 × 35	8	SFR	6	123.5	-
PB-4	A-VR-4	Shale	20 × 50 × 5	4 × 12	12	10t VR	6	124.3	-
PB-4	B-SFR-4	Shale	20 × 50 × 5	4 × 36	8	SFR	6	116.3	-
PB-4	C-SRTR-4	Shale	20 × 50 × 5	4 × 35	12	SRTR	6	125.6	-
PB-4	D-VR-4	Sandstone	20 × 40 × 10	6 × 39	24	10t VR	4	134.7	D9
PB-6A	E-VR-6A ^e	Sandstone	20 × 40 × 10	6 × 39	24	10t VR	4	125.8	D8 w/r ^f
PB-6B	F-24VR-6B	Sandstone	20 × 40 × 10	6 × 28	24	10t VR	4	137.6	D9
PB-6B	F-36VR-6B	Sandstone	20 × 40 × 10	6 × 39	36	10t VR	4	126.5	D9
PB-7	G-24VR-7 ^e	Sandstone	20 × 40 × 10	6 × 24	24	10t VR	4	127.9	D8 w/r
PB-7	G-36VR-7 ^e	Sandstone	20 × 40 × 10	6 × 33	36	10t VR	4	130.6	D8 w/r
PB-8	H-24VR-8	Sandstone	20 × 40 × 10	6 × 27	24	10t VR	4	129.1	D8
PB-8	H-36VR-8	Sandstone	20 × 40 × 10	6 × 39	36	10t VR	4	131.7	D8
PB-8	I-24D8-8	Sandstone	20 × 40 × 10	6 × 29	24	None	0	129.9	D8
PB-8	I-24D9-8	Sandstone	20 × 40 × 10	6 × 29	24	None	0	132.8	D9
PB-8	J-48VR-8	Sandstone	20 × 40 × 10	6 × 47	48	10t VR	4	122.8	D8
PB-8	J-60VR-8	Sandstone	20 × 40 × 10	6 × 60	60	10t VR	4	108.0	D8

^aSFR = Sheepsfoot roller.
 10t VR = 10-ton vibratory roller.
 SRTR = Simulated rubber-tired roller (loaded Cat 769B end-dump truck).

^bData not available for first five test fills.

^c20 ft × 50 ft × 32 in.

^d20 ft × 50 ft × 32 in.

^eSettlement measurements made.

^fw/r = with ripper.

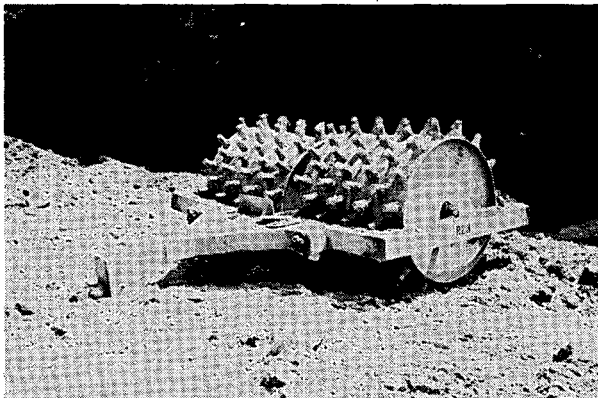


Fig. 82. Double-drum tamping roller.

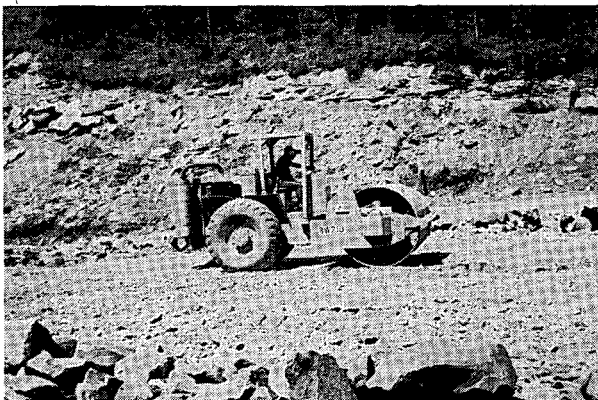


Fig. 83. Buffalo-Bomag 10-ton vibratory roller.

shown in Fig. 83. A "modified" sheepsfoot tamper with rectangular steel pads on the ends of the feet (not shown) was used on the first test fill. A loaded 35-ton haul truck was used to simulate a rubber-tired roller.

PROCEDURE

The test fills were constructed on firm foundations in configurations generally similar to that shown in Fig. 84. Usually two fills were constructed side by side. When rock for the test fills was excavated, an effort was made to select rock that was typical of that produced by each particular blast. Oversize rocks were pushed to the sides of the fills (see Fig. 85). The test fill was compacted at natural moisture content, and a thin layer of lime was spread over the surface of each lift. These lime layers served as markers between lifts when observation trenches were later cut through the fills.

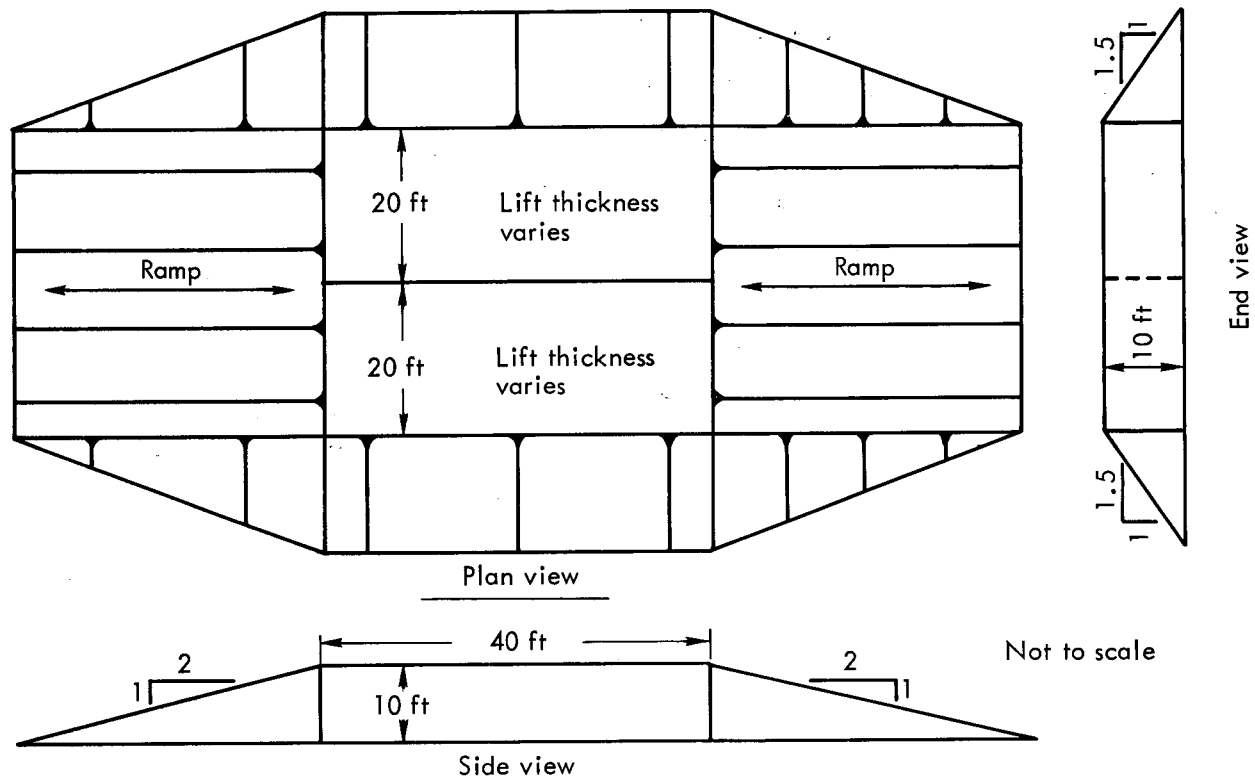


Fig. 84. Two typical test fills.

Three of the test fills were selected for settlement measurements. After the fills had been rolled in the usual manner, a 5-ft-square grid was established on the surface of the fill, and the elevation of each intersection was measured. Two additional passes with the vibratory roller were then made, and elevations on the grid points were remeasured. This procedure was repeated after an additional four and six passes (see Table 15).



Fig. 85. Dumping and spreading test fill material.

Table 15. Summary of test fill settlement data.

Test fill	Density after 4 passes (lb/ft ³)	Average additional settlement after			Total (ft)
		6 passes (ft)	8 passes (ft)	10 passes (ft)	
E-24VR-6A	125.8	0.037	0.024	0.015	0.076
G-24VR-7	127.9	0.025	0.026	0.012	0.063
G-36VR-7	130.6	0.039	0.017	0.017	0.073



Fig. 86. Digging test pit.

Test pits were dug in all of the fills (see Fig. 86). The rock removed was screened, sieved, and weighed in order to establish gradation curves. The volume of the test pit was measured by lining it with plastic and filling it with a measured quantity of water. With this volume and the weight of rock removed, the density was computed for the material in the test pit. Qualitative percolation tests were performed on all test pits by filling them up with water and measuring the rate at which the water level dropped as the water drained through the fill.

RESULTS AND CONCLUSIONS

Several conclusions may be drawn from the results of the test fill program:

1. The use of a Caterpillar D9 tractor to spread rock on the 24-in. fills generally resulted in higher test pit densities than spreading with a D8 model tractor.

2. No significant reduction in test pit densities was observed in the sandstone fills placed in 36-in. lifts compared to those placed in 24-in. lifts. The fills constructed with 48- and 60-in.-thick lifts were significantly less dense, however.

3. Percolation tests indicated that the fills constructed with sandstone were generally free-draining, while those constructed with shale were generally not free-draining.²⁷

4. Most compaction of the sandstone fills occurred during spreading and the first four passes of the vibratory roller. Measured settlement after an additional six passes with the vibratory roller averaged only 0.07 ft.

It should be noted that several of these conclusions are drawn from test pit densities. Only one pit was dug in each fill; therefore, if the pit happened to be in an anomalous area of the fill, the results could be misleading. In order to increase confidence in the test pit findings, it would be necessary to dig several test pits in each fill and average the results.

The specifications developed by Huntington District for embankment construction call for placing most of the material in two zones — a rolled random rock zone, which is the core of the dam, and a rolled rock zone to form the outer shell. All material in these zones is to be spread with a Caterpillar D-9 tractor or equivalent, and no moisture control is required.

The rolled random rock includes weathered and unweathered shale, and severely weathered sandstone taken from the spillway excavation. The material is to be placed in 12-in. lifts, shall be quarry-run, and must pass a 12-in. opening; the thickness of individual pieces shall not be less than one-half the length. The rock will be compacted by two passes with a tamping roller (sheepsfoot) followed by four passes with a rubber-tired roller. Both rollers will be towed by a Caterpillar D-9 tractor or equivalent.

The rolled rock zone will consist of tough, durable, free-draining sandstone from the required spillway excavation. The material is to be placed in 24-in. lifts, shall be quarry-run, and must pass an

18- X 24-in. opening. Compaction will be accomplished by not less than six passes with a 10-ton vibratory roller towed by a Caterpillar D-9 tractor or equivalent.

Chapter 9. Recommendations For Improved Blast Design

GENERAL

The information in this chapter is based on observations and technical data gathered during the experimental excavation program. The approach used to design the experimental blasts and the constraints under which the program was carried out are discussed below. The second part of this presentation describes two blast design techniques, one based on breaking to a vertical face and the other on breaking to the ground surface. The third part of this presentation covers blast design considerations; these considerations include geological conditions, stemming design, fragmentation, flyrock, presplitting, buffer zones, and separation distances between presplit surfaces and main charges. Finally, a critique of the test blasts is presented, and possible design refinements are discussed.

Approach

As mentioned at the beginning of this report, the primary objective of the experimental excavation program was to investigate the feasibility of using larger blastholes than normally used in structural excavations to reduce the cost of drilling and blasting. In order to carry out this investigation, a series of test blasts were planned, starting with a 3-in.-diameter

blasthole pattern and working up to patterns with blast hole diameters of 6-3/4, 9, and 12 in. These blasts were to be conducted in both the Eagle shale and the Upper Gilbert sandstone. Also, two types of explosives were to be tested in the sandstone.

Considering the large number of variables involved in blast design, it is obvious that the scope of the experimental program could not include the optimization of blast designs for each of the four blast hole diameters in two material types. Generally, one blast was planned for each hole size (in each of the two material types) without extreme modification of design procedure so that comparisons could be made of rock fragmentation as a function of blasthole diameter. The next logical step was to select a blasthole diameter, based on the results of the comparative tests, and to optimize a pattern using that hole diameter. The selection of a blasthole diameter would probably depend on the fragmentation required, bench height limitations, the type of drill rigs available, and a complete cost analysis.

Constraints

The principal constraint on blast designs during the test program was the limited amount of space available.

Because the experimental program was budgeted on a specific estimated volume of rock to be excavated, the rock produced by the experimental blasts could not appreciably exceed that volume. The number of test blasts was limited, therefore, as was the area in which to conduct them.

The geometry of the excavation called for a cut into a very steep hillside. For this reason some of the blasts were narrow and were confined on three sides, or had one sloping side. These conditions, which are not optimum for bench blasting, will not exist once benches are established and blasting for the spillway begins on a production basis.

BLAST DESIGN TECHNIQUES

In designing a quarry-type blast the objective is usually to produce rock that falls within specified gradation limits. Sometimes it is desired to produce large size rocks, such as used for armor stone, and at other times it is essential to minimize the amount of fines produced, but usually the problem requires that the number of large rocks produced by a blast be minimized. In order to achieve optimum fragmentation from a particular blast, the rock mass must not be overconfined, and must be allowed to break towards a free surface. Other factors are also important; however, only these two are considered here.

Breaking to Horizontal Free Surface

In 1956, Livingston published his "Crater Theory."²⁸ This theory was developed for the blasting of a constant weight of explosive at various depths

below the rock surface. The depth at which a maximum crater volume is created by a given weight of explosive is called the "optimum depth." The depth at which surface failure first occurs is known as "critical depth." This theory was adapted by Charles Grant for designing blasts in open-pit mines.²⁹

The PB-3 experimental blast was designed to break to the horizontal free surface, as was the lower part of PB-6B. Both did a satisfactory job of fracturing the rock. No delays were used.

Breaking to Vertical Free Surface

The most common way to design quarry blasts is to plan on breaking to a vertical free surface (bench blasting). This technique usually depends on the use of a series of increasing time-delay caps in order to provide for displacement of blasted rock. Ash has established design standards for this technique based on empirical data gathered on many rock excavation projects.³⁰

All of the experimental blasts, except for PB-3 and the lower part of PB-6B, were designed to break to a vertical free surface through the use of various delay patterns.

Comparison of Two Techniques

A limitation on the maximum useful depth of charge is inherent in a blast designed to break to the horizontal free surface. Rigorous experiments have not been conducted to establish a "critical depth" for long columnar charges. Generally, critical depth is determined for a given segment of charge (say 6X the blasthole diameter), and this is used to establish the maximum blasthole depth.

Explosive placed below this depth will not fragment the rock enough for it to be excavated.

A blast designed to break to a vertical free surface, as in bench blasting, theoretically does not have any depth limitation. In practice, however, as a blast with sequential delays proceeds from the row nearest the bench face to the rear of the blast, the depth of excavatable, fragmented rock decreases. This limits the number of practical rows, or delays, in a blasting pattern.

Bench blasting is by far the most commonly used blasting technique. The use of deep blastholes has the economic advantage that a smaller percentage of drill rig time is devoted to moving from hole to hole. Also, the stemming depth is independent of the blast-hole depth, and therefore stemming comprises a smaller percentage of the total footage drilled for deep blastholes than for shallow blastholes. This means that more explosive per foot of drilling is emplaced when deep blastholes are used.

A blast designed to break to the horizontal free surface has the advantage of not relying on delays between rows to prevent overconfinement of the rock to be blasted. This design technique might also be advantageous in certain excavation geometries. Opening up an excavation in which no vertical free face exists is one example. Another is a long, narrow excavation, such as a railroad cut, where bench blasts would have to be very small, but blasts designed to break to the horizontal free surface could extend the full length of the excavation.

BLAST DESIGN CONSIDERATIONS

During the course of the experimental excavation many problems were encountered that required special consideration when the test blasts were being designed. These are discussed in the following paragraphs, and recommendations are made concerning the handling of similar problems in the future.

Geological Conditions

Certain types of geological conditions exist in the spillway area that pose potential problems to efficient blast design. These include the presence of joints, groundwater, variations in rock hardness, and coal layers.

Joints

The joint system, described in detail in Chapter 2, generally consisted of two perpendicular sets of sheet joints spaced from 6 to 30 ft apart. The material in the immediate vicinity of these joints was more weathered than the surrounding rock. When a blast is being designed, it is best to avoid locating blastholes within these joints. Explosive energy from blastholes in joints is wasted in compacting weathered material rather than fracturing fresh rock. Also if a charge is located in a sheet joint near the front of a bench, energy might be lost due to premature venting of high pressure gases along the joint.

Another problem with these joints is that they act like presplit surfaces and tend to inhibit fracturing of rock beyond the joint. This condition was observed in the left-rear (southwest) corner of PB-8, where a roughly cubicle block of rock, bounded by two intersecting joints, was

not sufficiently fractured by the main charges and had to be drilled and blasted later (see Fig. 47). This situation could be improved by locating satellite holes, of a smaller diameter than the main charges, between the peripheral production holes and the presplit surfaces.

Groundwater

The only major problem encountered with groundwater was in PB-4. Water seeped into blastholes from a coal layer at about the middle of the PB-4 lift, filling blastholes with up to 18 ft of water. Immediately prior to loading the blastholes, the water was bailed out and plastic sleeves were inserted to protect the ANFO from moisture (ANFO will not detonate if it gets wet).

The PB-4 presplit holes also contained 18 to 20 ft of water. No attempt was made to remove this water, and no degradation of the presplit surface was evident when it was compared to the surface created by presplitting in the dry. Other cases have been reported, however, where damage to finished surfaces has been attributed to presplitting in saturated rock.

Variation in Rock Hardness

Another problem encountered in PB-4 was the variation of rock hardness with depth. Approximately the top half of the lift consisted of weathered shale below which came the water-bearing coal layer followed by hard, predominantly unweathered shale and sandstone. Because the blast was designed for the weathered shale, the blastholes were consequently too far apart to satisfactorily fracture the hard shale and sandstone. The bottom of PB-4 remained 6 to 12 ft above the

planned grade after all the loose rock had been excavated (see Fig. 21). Generally the area between the main charges and the presplit was left about 12 ft above grade while the interior portion, where interaction between charges occurred, was only 6 ft above grade.

Common practice, when a gross mismatch in rock hardness is discovered as in PB-4, is to adjust the blast design to break to the contact instead of attempting to blast through the contact. If it is necessary to blast through the contact, it may be possible to use a more powerful explosive in the harder rock. Variations in the hardness of rock strata can often be detected by watching the drilling operation and by measuring penetration rates.

Coal Layers

Prior to the detonation of PB-4 there was some speculation that there might be a problem in blasting through coal layers with large diameter charges. It was believed that the coal layers might present an avenue for high-pressure gases to force their way behind the presplit surface and cause damage to the structural face. Examination of the PB-4 walls revealed no evidence of this type of damage.

A coal layer might influence blast design in another way if the layer were sufficiently thick to contaminate rock that is necessary for the dam embankment construction. The best design procedure in this case would be to excavate down to the top of the coal layer, and then to remove the coal layer mechanically before the continuation of blasting operations.

Fragmentation

The program for determining rock fragmentation was discussed in Chapter 4, and the economic implications of fragmentation control are discussed in Chapter 10. This section is concerned primarily with the effect that various patterns, delays, and charge configurations have on fragmentation.

Patterns and Delays

All of the patterns used for the test blasts were basically square, with the delay system establishing the effective burden and the effective spacing. The effective spacing was generally twice the burden. For example, PB-6A and PB-6B were delayed to produce a "staggered row" effect. PB-7 was delayed diagonally, while PB-1, PB-4, and PB-8 were delayed in a vee pattern. Because of the variation in blasthole diameters, material types, and explosive types, it is difficult to conclude that one delay pattern did a better job of fragmenting the rock than an other pattern. It is apparent, however, that rock fragments produced by PB-4C, in which no delays were used, were coarser than those produced by similar patterns with delays (see Fig. 52).

It was noted that, when the rock fractured by the staggered row pattern of PB-6A was excavated, humps were left between the main charges around the perimeter of the pattern. Because of the better distribution of explosive around the perimeter of the blast area, these humps did not occur when the pattern was oriented as in PB-7 or PB-8. It was believed that the block of rock blasted by PB-6A was too long and narrow for a vee pattern to be effective; therefore a staggered row pattern was selected.

The pattern used for PB-7 (delayed diagonally) worked quite well in this situation where the rock prism to be blasted was confined on only two sides. Several large blocks (10 to 15 ft across) remained, however, in the lower left side of the blast area between the first row of production charges and the free surface. This area was not subject to shock wave interaction between charges, and it appeared that many of the blocks were bounded by joints.

In general, the vee delay used for PB-8 pulled the rock away from the side walls and piled it in the middle of the blast area. Even though the top portion of a 10-ft wide bench planned for the rear of PB-8 was completely destroyed, about 3 ft of rock adhered to most of the remaining presplit surface and was difficult to dislodge with the front-end loader. This may have been due to the fact that rock adjacent to the rear wall below a depth of 10 or 15 ft remained confined at both ends during the blast. This rock was subjected primarily to compressional forces during the blast, and it was constrained from moving horizontally. The rock adjacent to the side walls, however, fell away from the presplit surface with no difficulty. This material was free to move towards the front of the blast area as the delays progressed sequentially towards the rear.

Charge Configurations

As mentioned in this chapter, the test blast design criteria were not drastically modified as blasthole diameters were increased so that a relationship could be determined for fragmentation as a function of charge spacing and blasthole diameter.

In Chapter 4 it was concluded that the degree of rock fragmentation generally decreases with the greater charge separation associated with larger blasthole diameters. It may, however, be possible to counteract this trend by the use of modified charge configurations.

The rock in the collar region (that zone between the ground surface and the top of the explosive column) contained no explosive in the designs tested at R. D. BAILEY. When closely spaced 3-in.-diameter blastholes are being used, the fact that there is no explosive in the collar region is of little consequence with respect to the production of oversized blocks because only 3 or 4 ft of stemming are used. When 12-1/4-in.-diameter blastholes are being used, however, say in a 30- by 32-ft pattern with 15 ft of stemming (as in PB-8), the collar region comprises a large volume of rock containing no explosive. Therefore, one relies almost entirely on displacement (tearing and wrenching) as a fracturing mechanism. Surface spalling due to shock wave reflection is generally believed to be of minor importance to surface rock breakage in normal blast designs.

One way to reduce the number of oversize rocks produced in the collar region is to reduce the stemming in the main charge holes. Less stemming, however, tends to increase the amount of flyrock. Another requirement of the stemming is to contain the high-pressure gases long enough so that most of the energy is used to fracture the rock mass, and not vented into the atmosphere. This requirement prevents an excessive reduction of stemming depth.

Another way to improve the distribution of explosive in the collar region is by the use of decking charges and satellite charges. A decking charge is a quantity of explosive located in the stemming column of the main blastholes. Satellite charges are contained in holes that are usually of a smaller diameter than the main charge holes. The satellite holes are generally located midway between main charge holes, and are drilled to approximately the same depth as the stemming in the main charge holes.

Flyrock

Flyrock may or may not be a constraint on blast design, depending on the location of the excavation. It is possible to control the flyrock almost completely by keeping the size of the blast small and using blasting mats. However, this procedure is very expensive, and is usually used only when blasting in urban areas. At remote construction sites the usual procedure is to move all personnel well out of the range of possible flyrock.

The amount of flyrock produced by a blast depends on the geological structure of the rock, the stemming depth, and the burden. A brittle rock that has many incipient planes of weakness (joints, fractures, bedding planes) usually requires a small powder factor to achieve acceptable fragmentation, and flyrock can be kept at a minimum without too much difficulty. In a massive tough rock, such as the Upper Gilbert sandstone, however, a higher powder factor is required to achieve satisfactory fragmentation, and a larger amount of flyrock is to be expected. There is a tradeoff between fragmentation and flyrock in this situation.

Flyrock can be reduced by increasing the stemming depth and burden, but if this is done the percentage of oversize rock requiring secondary blasting is also increased. The problem then becomes one of economics, weighing the cost of dealing with the hazards of flyrock against the cost of additional secondary blasting.

Presplitting

During the course of the experimental excavation several different presplitting designs were tested in both the shale and the sandstone. Spacings, loadings, and stemming depths were varied.

Good results were consistently obtained in the shale using "70% Trimtex" (1/4 lb/ft) in 3-in.- diameter holes spaced 30 in. apart and stemmed to a depth of 4 ft. The maximum hole depth was about 50 ft. Good results were also obtained in the sandstone at spacings of 3-1/2 and 4 ft. Maximum hole depth in the sandstone was about 50 ft.

The experience at R. D. BAILEY also pointed out the risk of damage to production blastholes if they have been drilled prior to detonation of the presplit charges. This occurred on PB-6A, and prevented loading of the main charge holes to full depth. The recommended procedure is to fire the presplit charges prior to drilling the production holes, or to fire them on a millisecond delay just before detonation of the production charges.

Trimming

Details of the trimming procedure used in PB-2 and PB-3 are presented in Chapter 3. The technique worked well and allowed considerable flexibility in scheduling of excavation operations. The technique was tested only in the weathered shale, however.

Buffer Zones

The term "buffer zone" has several meanings in the blasting vernacular. In one case, a buffer zone is defined as the zone of rock between the presplit surface (or neat line) and the first row of production charges. This zone is made sufficiently wide such that the production charges do not damage the presplit surface. The buffer zone may contain small-diameter charges that are detonated along with the production charges, or it might be drilled and blasted with small-diameter charges subsequent to detonation of the production charges.

The term "buffer zone," as used in this report, refers to a zone of relatively crushed or fractured rock between the presplit plane and the production charges that attenuates stress and provides an escape vent for gases produced by the blast. It is hypothesized that the shock wave would be attenuated by the buffer zone because of its decreased density and shear strength relative to the intact rock, thus limiting fracturing beyond that zone.

As discussed in Chapter 5, techniques for creating buffer zones with small diameter charges are still under investigation. No conclusions could be drawn from the R. D. BAILEY data regarding the effectiveness of buffer zones in protecting presplit planes from overbreak.

Separation Distances Between Presplit Surfaces and Production Charges

When a structural excavation is being blasted, it is imperative that blast damage to the walls of the excavation be minimized. A smooth, intact wall is more resistant to weathering than one that has been fractured by overbreak during

production blasting; moreover, a smooth, intact wall costs less to maintain, and is safer.

The blast designer should not be overly conservative, however, in establishing separation distances between production holes and the presplit surface, because the result may be that the production blast does not fracture all the way to the presplit surface. Common practice is to use smaller diameter blastholes around the blast perimeter; i.e., between the production holes and the presplit surface. This, however, can become very costly if the separation distance is excessive, and care must be taken to assure that the bottoms of the smaller diameter charges do not encroach upon or penetrate presplit surfaces.

After completing the experimental excavation, EERL furnished the Huntington District's resident engineer on the R. D. BAILEY project a set of blasting guidelines to assist him in evaluating blasting procedures proposed by the contractor. The following procedure for determining safe separation distances between presplit surfaces and main charges has been extracted from those guidelines.

A sketch of the typical geometry of the problem is shown in Fig. 87. The parameter of primary concern is the critical distance, x , necessary to preserve the bench shown in the figure. It should be noted that if no bench is required (dashed line) the overlying rock buttresses the rock opposite the blast so that " x " can be decreased. Notice also that the separation distance at the bottom of hole, b , is less than at the top for sloping presplit surfaces. This is usually acceptable because the rock at depth is well confined. Re-

sults of the experimental excavation were inconclusive with respect to determining a safe b distance, but the critical distance, x , is usually controlling for steep presplit surfaces.

Figures 88 through 90 are a set of graphs for determining the separation distances between main production charges and presplit surfaces based on data collected during the experimental program. Separation distances were tabulated for each of the experimental blasts (PB-1 through PB-8), and the postshot condition of the presplit surface was noted for each. In those cases in which overbreak occurred,

Definitions:

- x = Critical distance (ft)
- h = Stemming depth (ft)
- b = Distance from bottom of blasthole to presplit plane (ft)
- l = Charge length

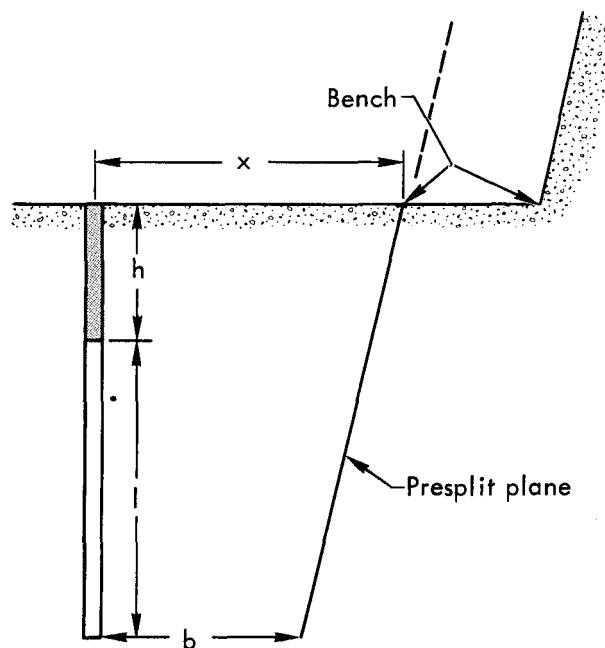


Fig. 87. Typical geometrical relationships and notations for blastholes and presplit planes.

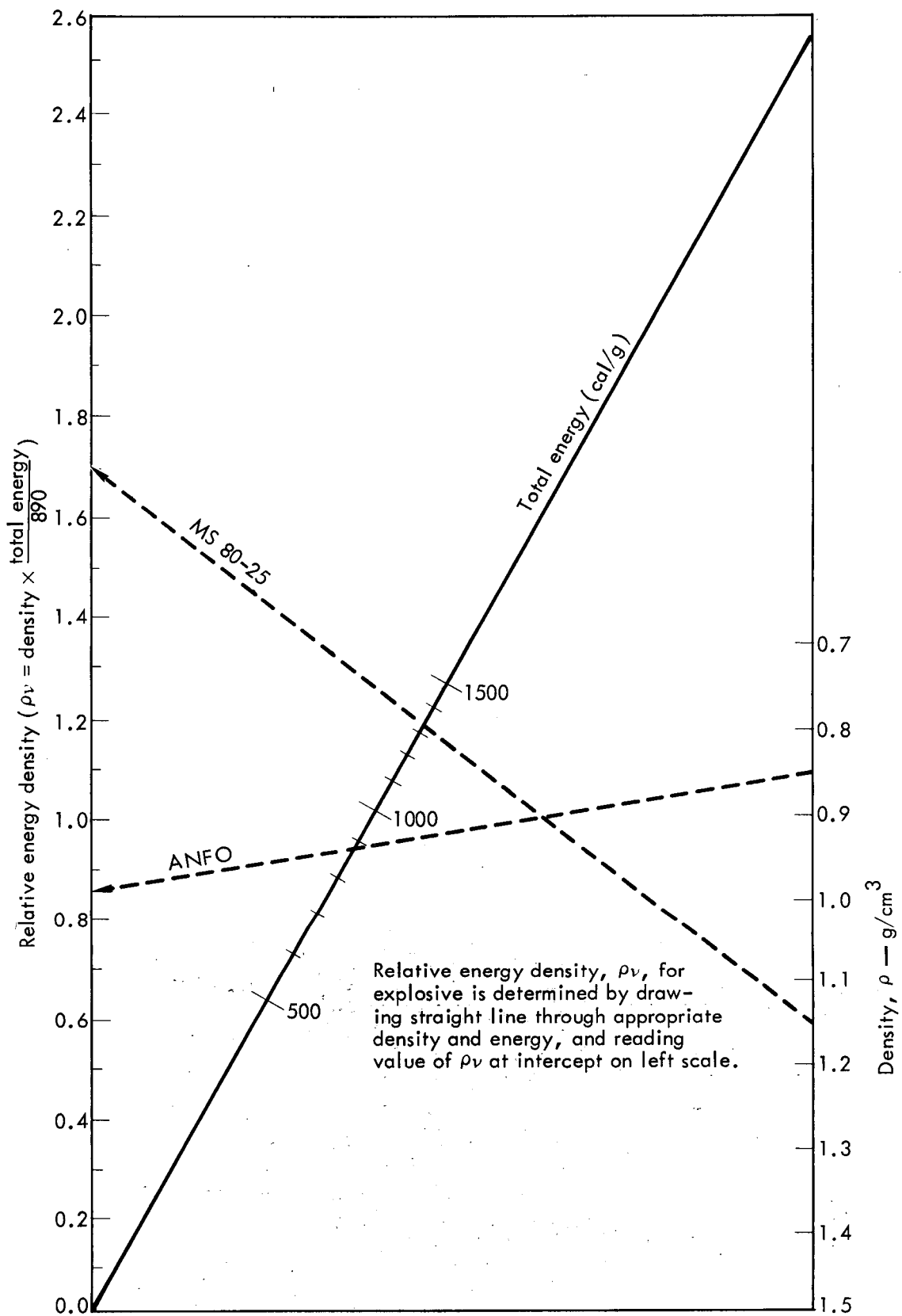


Fig. 88. Nomograph for computing relative energy density.

the separation distances were revised to a greater value, which seemed reasonable based on visual observation of the damage. A generalized prediction equation for the critical distance was then developed and used to plot the families of curves shown in Figs. 89 and 90.

The explosives used for the experimental excavation were ANFO and MS 80-25 aluminized ammonium nitrate slurry. The physical properties of interest are listed in Table 16. The term

"average loading density" refers to the average density of the explosive in the blasthole as determined by actual loading records during the R. D. BAILEY test program. The total energy of the explosive can usually be obtained from the manufacturer.

The relative energy density may be determined for any explosive by using the nomograph in Fig. 88. This value may then be used in Figs. 89 and 90 to determine critical distances for charge

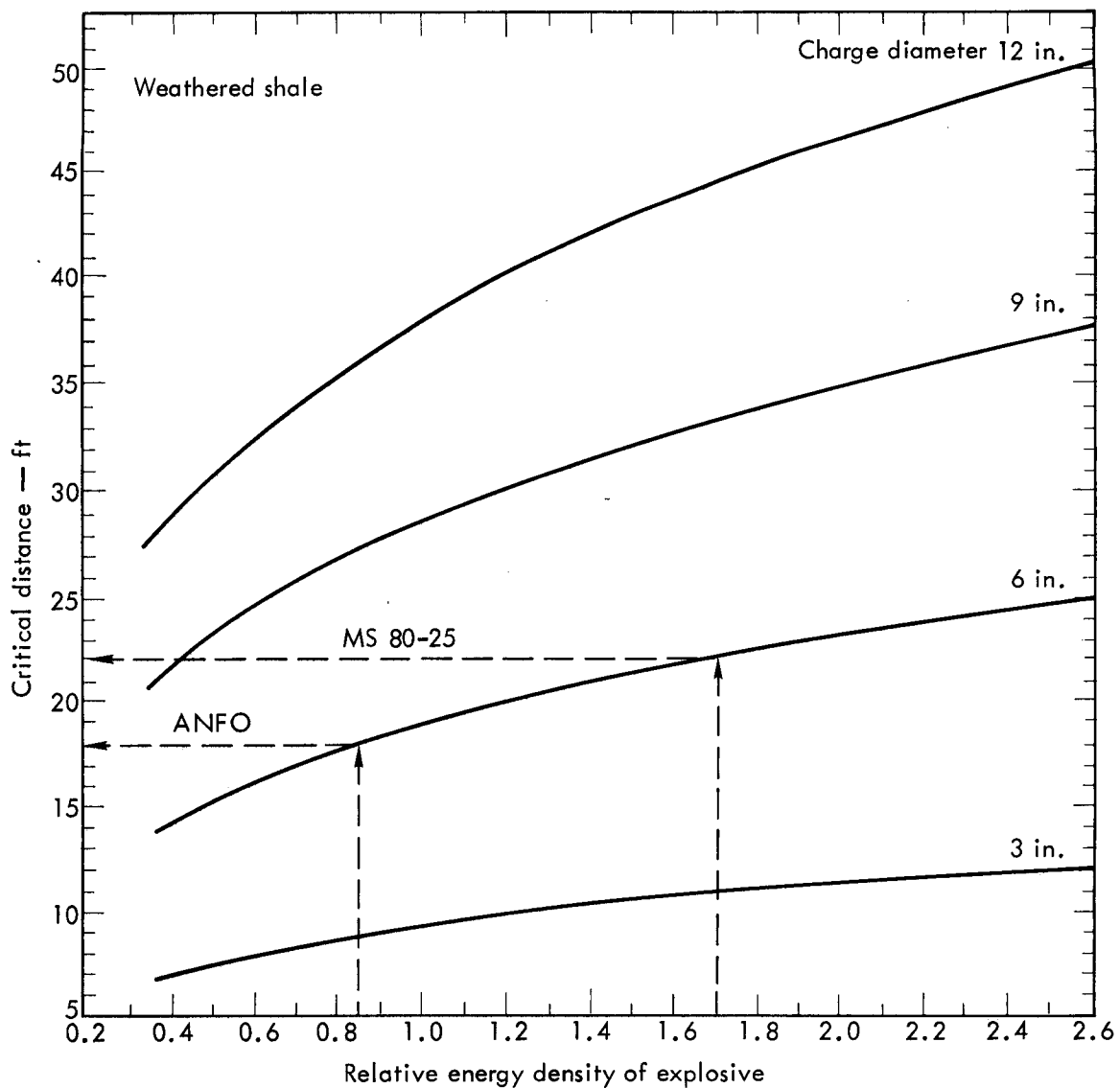


Fig. 89. Critical distance as a function of relative energy density and charge diameter for weathered shale.

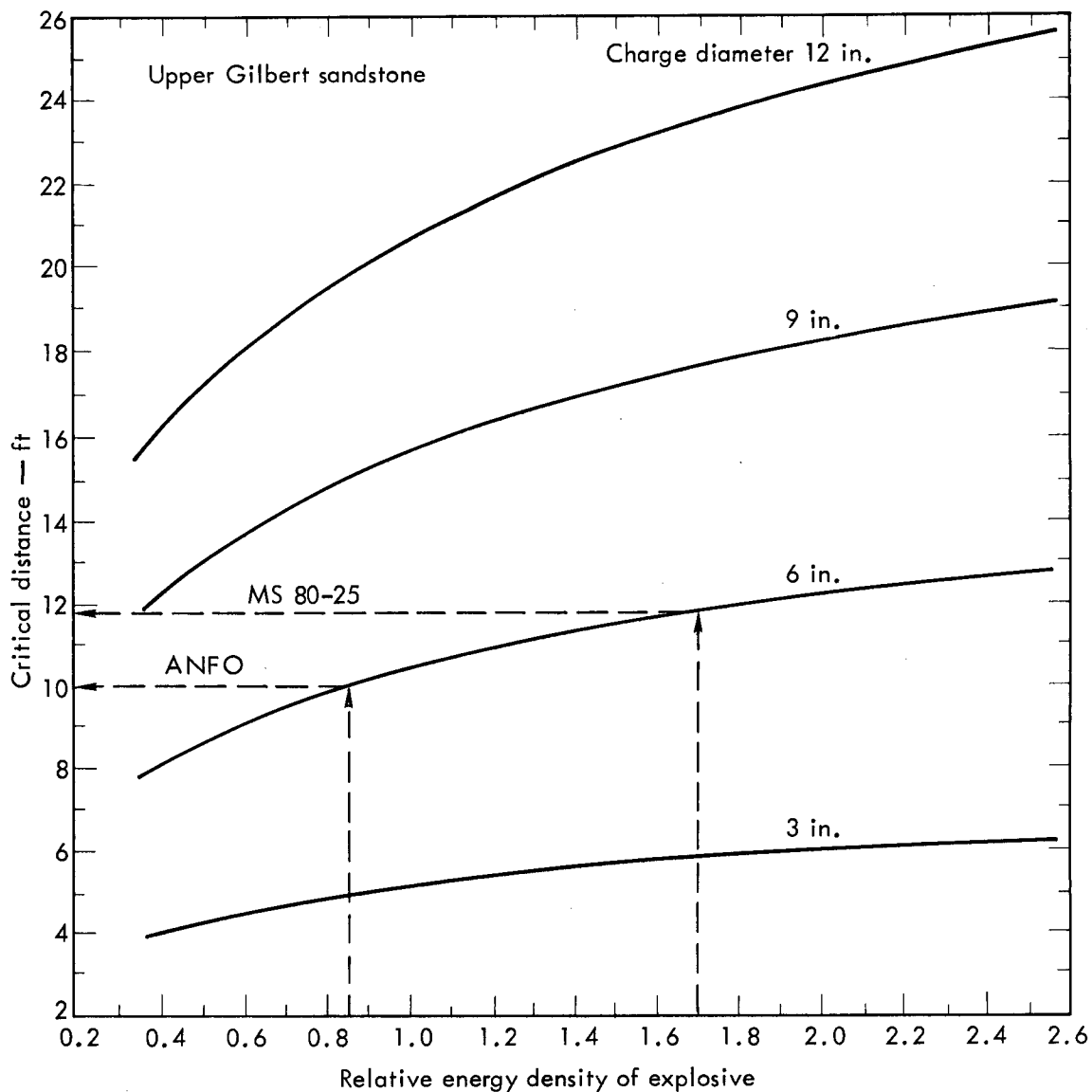


Fig. 90. Critical distance as a function of relative energy density and charge diameter for Upper Gilbert sandstone.

Table 16. Physical properties of explosives.

Explosive	Average loading density, ρ^a (g/cm ³)	Total energy ^b (cal/g)
ANFO	0.85	890
MS 80-25	1.15	1330

^aBased on R. D. BAILEY experimental blasts.

^bBased on manufacturers' tests.

diameters of 3, 6, 9 or 12 in. The curves in Fig. 89 are based on the shale observed in test blasts PB-1, PB-3, and PB-4. The curves in Fig. 90 are based on the Upper Gilbert sandstone observed in PB-5 through PB-8 test blasts. The dashed lines show how to determine critical distances for ANFO and MS 80-25 in 6-in.-diameter charges.

Stemming Design

A new procedure for designing stemming depths has been proposed by J. Lattery of EERL.³¹ Although the procedure was not used for all of the test blasts, the stemming depths that it predicts are consistent with observations of stemming performance made during the test blast series.

The approach is based on the concept of a depth of burial, DOB, which is the distance from the horizontal ground surface to the center of mass of the buried charge. The DOB can be divided by the cube root of the weight of the explosive and is then termed the scaled depth of burial, dob. It has been noted that a plot of dob vs the charge length has a definite minimum value for a fixed depth of stemming. It is assumed that a charge length having the minimum scaled depth of burial should be used for predicting surface effects of that charge (i.e., no permanent effect, some fracturing or mounding, or cratering).

The scaled depth of burial is computed by:

$$\text{dob} = \frac{h + \frac{1}{2}}{w^{1/3} l^{1/3}}, \quad (8)$$

where:

h and l are defined in Fig. 87

w is the charge weight per unit length of the explosive column.

Plots of dob vs the blasthole depth (h + 1) are shown in Fig. 91. The minimum of the function, for a fixed h and w, is computed by setting the derivative of dob with respect to l equal to zero and solving for l. This value of the charge length substituted in Eq. (8) gives the minimum dob:

$$\frac{d}{dl} (\text{dob}) = \frac{1}{w^{1/3}} \left[\frac{1}{2l^{1/3}} - \frac{h + \frac{1}{2}}{3l^{4/3}} \right] = 0.$$

Solving for l gives:

$$l = h$$

It is evident, therefore, that the minimum dob occurs for a column of explosive equal in length to the depth of stemming. This relationship is substituted into Eq. (8) to give:

$$\text{dob} = \frac{3 h^{2/3}}{2 w^{1/3}}. \quad (9)$$

Equation (9) can now be solved for the stemming depth, h,

$$h = \left[\frac{2}{3} \text{dob} w^{1/3} \right]^{3/2},$$

or

$$h = 0.544 (\text{dob})^{3/2} w^{1/2}. \quad (10)$$

Equation (10) is the basic equation for computing stemming depth.

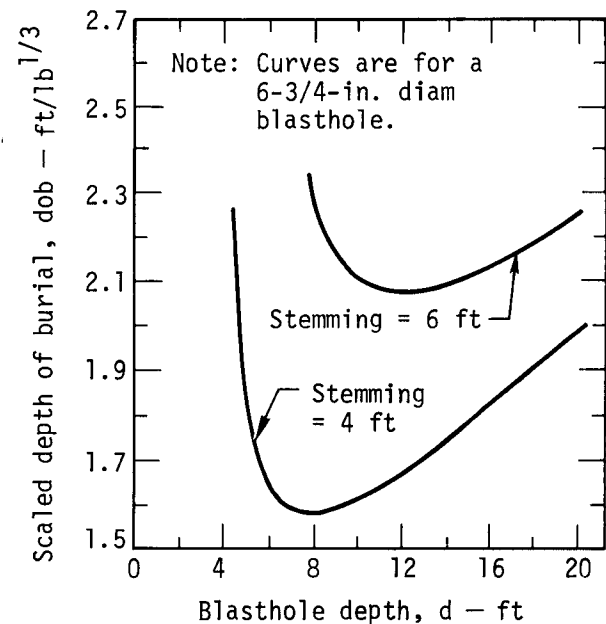


Fig. 91. Scaled depth of burial vs blasthole depth for stemming depths of 4 and 6 ft.

The best way to determine what value of w_{eq} to use in Eq. (10) is to develop a "cratering curve" for the particular explosive in the particular rock to be blasted.^{18,28} This cratering curve may be developed by detonating explosive charges of identical weight at various depths below the ground surface and observing the surface effect. If the charge is too shallow, excessive cratering and flyrock will result, and if the charge is too deep, poor surface breakage will occur. Previous experience with ANFO in sandstone has shown that the best w_{eq} for mounding ranges from 2.4 to 2.7 ft/lb^{1/3} (Ref. 29). If experimental data are not available for the rock of interest, a w_{eq} in this range can be used as a first approximation for stemming design. If an explosive other than ANFO is to be used, an equivalent w term, w_{eq} , must be substituted for w . The w_{eq} term can be computed by:

$$w_{eq} = 0.34\rho\nu k^2, \quad (11)$$

where

w_{eq} = equivalent weight of explosive per foot of blasthole (lb/ft)

ρ = average loading density of explosive (g/cm³)

ν = total energy of the explosive divided by the total energy of ANFO

k = blasthole diameter (in.)

The product $\rho\nu$ may be obtained from the nomograph in Fig. 88. Note that the equivalent weight of explosive calculated by this expression is not the actual weight of an explosive other than ANFO.

As an example, consider using this technique to calculate a stemming depth for the PB-8 test blast given the following information:

Rock type: Upper Gilbert sandstone
 Explosive type: Dow MS 80-25 aluminized ammonium nitrate slurry
 Average loading density: 1.15 g/cm³
 Total energy: 1330 cal/g
 w_{eq} : 2.5 ft/lb^{1/3} ANFO (assumed)
 Blasthole diameter: 12-1/4 in.
 Solving Eq. (11) for w_{eq} we get:

$$w_{eq} = 0.34 \times 1.15 \text{ g/cm}^3 \times \frac{1330 \text{ cal/g}}{890 \text{ cal/g}} \times (12-1/4 \text{ in.})^2$$

$$w_{eq} = 87.7 \text{ lb/ft.}$$

Substitute this into Eq. (10) to solve for the stemming depth, h :

$$h = 0.544 (2.5 \text{ ft/lb}^{1/3})^{3/2} (87.7 \text{ lb/ft})^{1/2}$$

$$\underline{h = 20.1 \text{ ft.}}$$

The stemming depth actually used on PB-8 was 15 ft, and a considerable amount of flyrock resulted. Had the 20 ft of stemming calculated above been used for PB-8, the amount of flyrock may well have been substantially reduced.

Figure 92 shows recommended stemming depths vs blasthole diameters for the four combinations of explosive and material types encountered at the site of the R. D. BAILEY experimental excavation. Equation (10) was used to develop these curves for assumed w_{eq} 's of 2.5 ft/lb^{1/3} (ANFO) in the Upper Gilbert sandstone and 3.0 ft/lb^{1/3} (ANFO) in the weathered shale.

CRITIQUE OF TEST BLASTS

This section discusses each of the test blasts, some of the problems encountered,

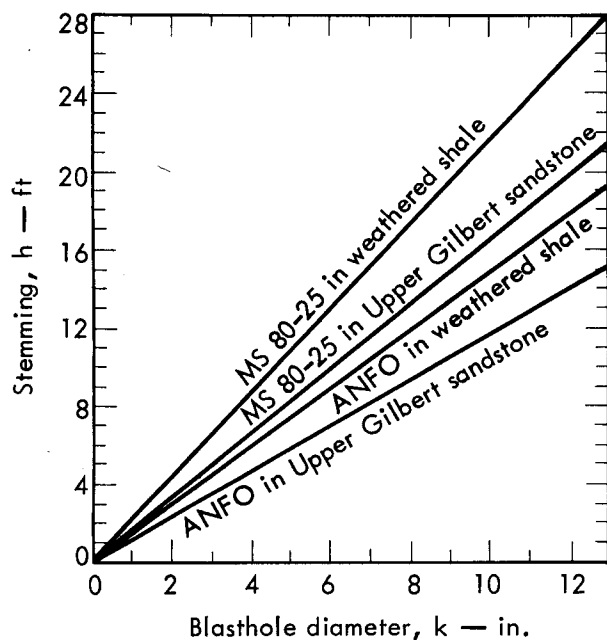


Fig. 92. Recommended stemming depths for ANFO and Dow MS 80-25 slurry in weathered shale and Upper Gilbert sandstone for various blasthole diameters.

and possible ways to avoid these problems in the future. Detailed information on the design of each blast is presented in Chapter 3. Improved designs are suggested for several of the test blasts.

One indicator of the blasting characteristics of a particular rock type is the weight of explosive required to fragment a given volume of the rock. This is often known as the "powder factor." The powder factors referred to in the following paragraphs were determined by using the average loading density and computing the number of theoretical cubic yards fractured per production blasthole. The explosives used for presplitting and other blasting around the perimeter of the test blasts were not included in the powder factors. Powder factors for different explosives cannot be compared directly because of differences in density and total energy.

PB-1 Test Blast

Although the material in PB-1 could not be efficiently excavated with a D-8 bulldozer blade, it could have been readily ripped. This is true for the material in PB-2, PB-3, and the top half of PB-4. The ANFO powder factor for PB-1 was relatively low, 0.55 lb/yd³. It was sufficient, however, to break up the material enough to be excavated with the front-end loader, and no change in this quantity is recommended. It should be noted that ANFO does not develop full detonation velocity in blastholes less than about 11 in. in diameter. The efficiency of ANFO, therefore, increases with increasing blasthole diameter, up to about 11 in., because more energy per unit weight is delivered as the detonation velocity increases. Figure 93 depicts the influence of charge diameter on the detonation velocity of ANFO.

PB-2 Test Blast

The blast that trimmed the walls of PB-2 was very successful. Trimming

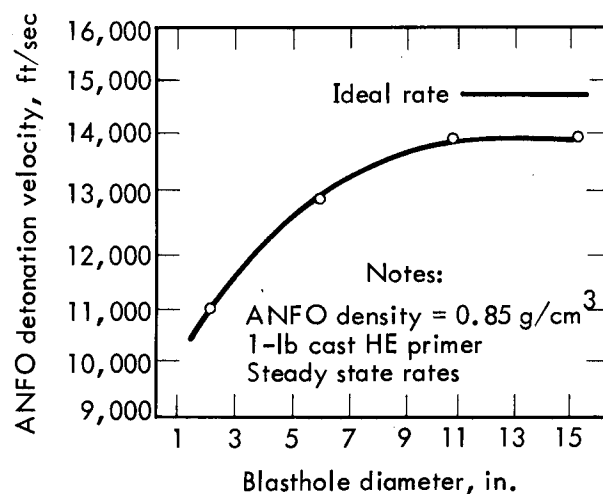


Fig. 93. Change in detonation velocity of ANFO as a function of blasthole diameter.³²

was desirable in lieu of presplitting because it allowed ripping and drilling to proceed concurrently and avoided possible damage to the finished surface from the ripping operation. There is no apparent need to change the design used for the trimming blast.

PB-3 Test Blast

All of the production charges in the PB-3 blasts were designed to break to the horizontal ground surface instead of breaking to a vertical free face as in conventional bench blasting design. Therefore, delays were not required between blastholes. The powder factor was 0.79 lb/yd³. Postshot observations showed evidence of excessive cratering in the vicinity of some of the charges. This excess could be remedied by increasing the stemming depth from 6 to 10 ft. The rationale for stemming adjustments recommended here has been discussed earlier in the chapter (see Fig. 92). If the stemming depth were increased to 10 ft, the powder factor would be reduced to 0.52 lb/yd³. Based upon the observed results of the PB-1 blast, this powder factor would be satisfactory.

With a stemming depth of 10 ft there might be some large fragments produced in the collar region (the region between the top of the explosive charge and the ground surface). Experience in the weathered shale, however, demonstrated that almost any large block could be mechanically broken down without much difficulty. It is doubtful that decking charges or satellite holes would be warranted for any blast in the weathered shale.

PB-4 Test Blast

The powder factor (ANFO) for the PB-4 blast was 0.82 lb/yd³. This value was excessive for the weathered shale, but inadequate for the hard shale in the bottom half of the 43-ft bench. The stemming depth was adequate for weathered shale. To improve the design of this blast, assuming that it is desired to blast the full depth, the pattern could be closed up to increase the powder factor to 1.16 lb/yd³ (similar to PB-6A in sandstone), which would call for a 20-ft² pattern instead of one 24-ft². A second option would be to use a more powerful explosive, such as MS 80-25 slurry, in a 23-ft² pattern with 19 ft of stemming. This would give a powder factor of 1.05, similar to that used for PB-7. A third approach would be to use slurry explosive in the bottoms of the emplacement holes and ANFO for the upper sections. This option might permit a wider hole spacing than would be possible with ANFO alone, resulting in a lower drilling and blasting cost.

PB-4A Through PB-4E Test Blasts

This series consisted of several blasts using 3-in.-diameter blastholes, and various patterns and delay sequences to remove material left in the bottom by the PB-4 blast. The powder factors were as follows: PB-4A, 1.12 lb/yd³ (ANFO); PB-4B, 0.90 lb/yd³ (ANFO); PB-4C, 2.03 lb/yd³ (ANFO); PB-4D, 1.12 lb/yd³ (ANFO); and PB-4E, 2.30 lb/yd³ (slurry). All of these blasts, with the exception of PB-4C, produced similar results. PB-4C, the only blast that did not contain any delays, produced large blocks and did not break to the depth intended. The rock

that remained intact in the bottom-rear corner of PB-4C was hard sandstone with a joint on one side and shale-sandstone contact on the top. This ledge of rock was redesignated PB-4E and blasted again (see Fig. 27). There was also artesian water flowing in this area. These conditions obviously present difficult blasting problems. There was evidence that some of the ANFO in PB-4C had become damp and did not detonate. If the original design of PB-4C had called for slurry explosive (for its high water-resistance) and the use of delays to improve fragmentation, the results would probably have been greatly improved.

PB-5 Test Blast

PB-5 was another difficult blasting situation. The blast area was located on the edge of the haul road, and the rock had been fractured by blasting for road construction. This caused difficulty in drilling and loading the holes. Blastholes were often blocked due to rock shifting while adjacent holes were being drilled. Some holes intersected open fractures, and ANFO poured into the fractures during loading. One way to alleviate this would have been to presplit behind the earlier haul road blasts to prevent damage to rock that must be blasted later.

PB-6A Test Blast

In an attempt to accelerate the test excavation construction schedule, some of the production holes for the PB-6A test blast were drilled prior to detonation of the presplit charges that encompassed the blast area on three sides. It was also desired to accomplish the presplitting before the test blast so that particle

velocities could be recorded separately for each. During the presplit detonation, a mass shifting of the rock in the blast area blocked most of the production holes at a bedding plane about 42 ft below the surface. This procedure is not recommended unless one is willing to accept a high risk of damage to predrilled production holes by the presplit detonation.

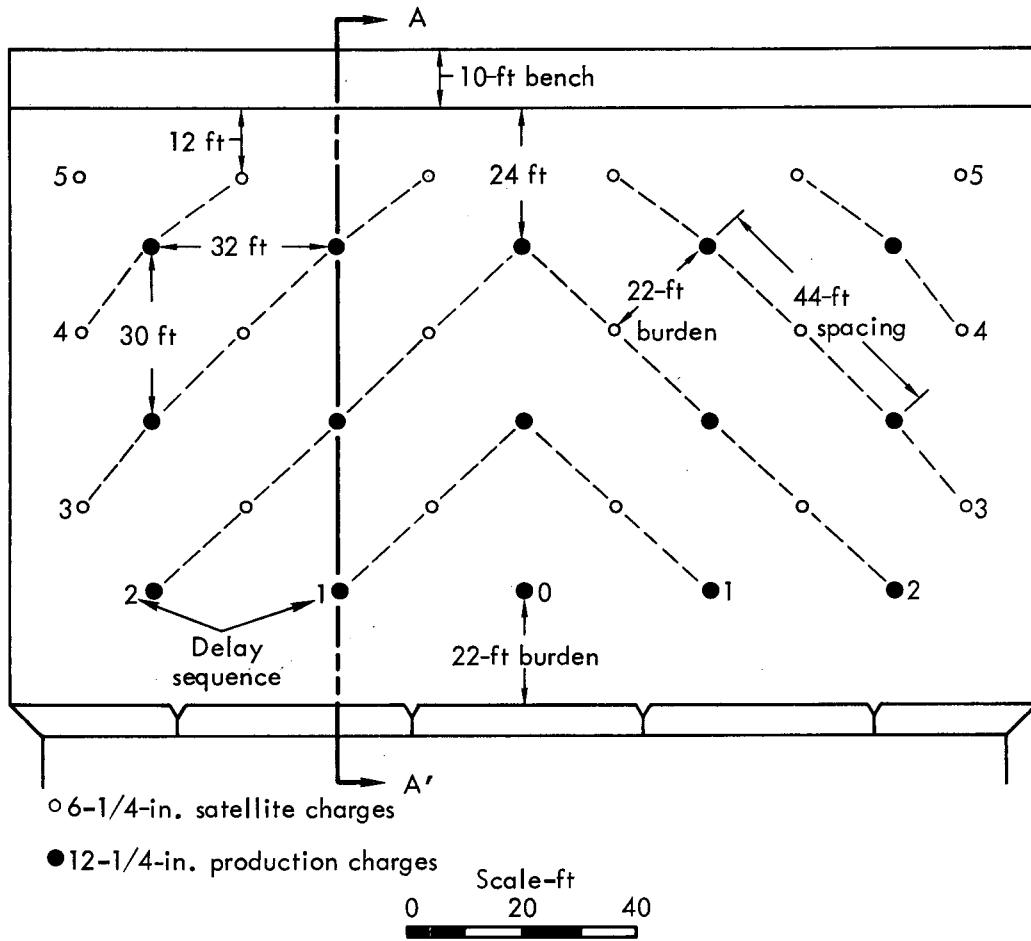
The powder factor for PB-6A (ANFO) was 1.16 lb/yd³. The shape of the rock prism to be blasted seemed to lend itself best to a staggered row pattern. This led to a poor distribution of explosive around the perimeter of the blast, however, which left humps between the production charges at the toes of the side walls after blasting. Although these were removed by the loading equipment they were difficult to excavate. A possible solution to the problem would be to locate small diameter charges between the production charges and the walls of the excavation.

PB-6B Test Blast

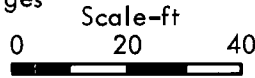
Difficulties were encountered in loading packaged slurry explosive into the blastholes. The problems were due primarily to improper packaging of the slurry for the size of blasthole being loaded. The slurry that was packaged in 4-in.-diameter sausages loaded well into the 6-1/4-in.-diameter blastholes. Slurry in larger diameter bags (8-in.-diameter) had to be sliced with a knife and dropped in piece-by-piece, a very time-consuming process. Slurry loaded in this manner also had a tendency to bridge the hole before reaching the bottom, sometimes causing blockages that could not be dislodged. The air gaps thus created were

obviously very detrimental to blasting efficiency. Two blastholes in the front row of the pattern were blocked in this

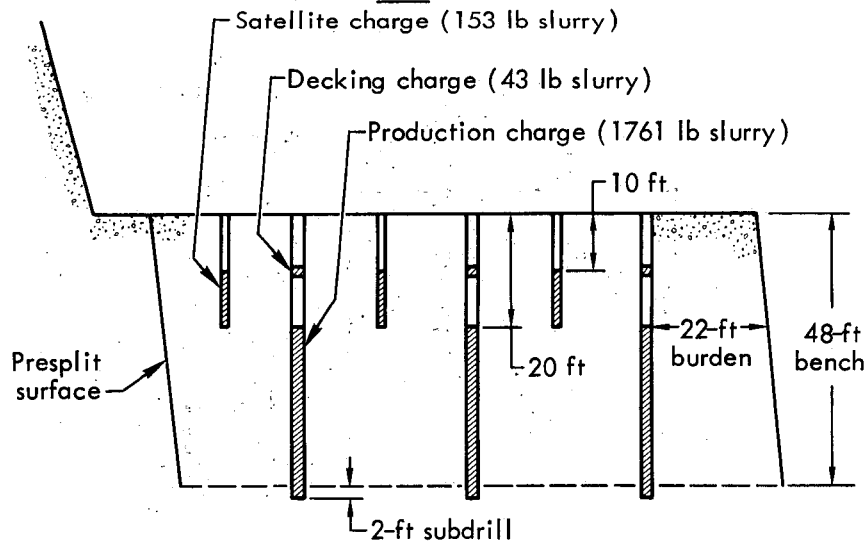
manner. The pattern called for row-by-row delays, so when the first row did not adequately fracture and move the rock at



○ 6-1/4-in. satellite charges
● 12-1/4-in. production charges



Plan



Section A-A'

Fig. 94. Improved design for PB-8 test blast - slurry.

the front of the pattern, the following rows were overconfined, and poor breakage resulted. The rock could not be excavated below about half the bench height. The

blasted rock from the top half of the bench seemed to be as well broken up as that in PB-6A, so it was decided to use slurry explosive on the remainder of the blasts.

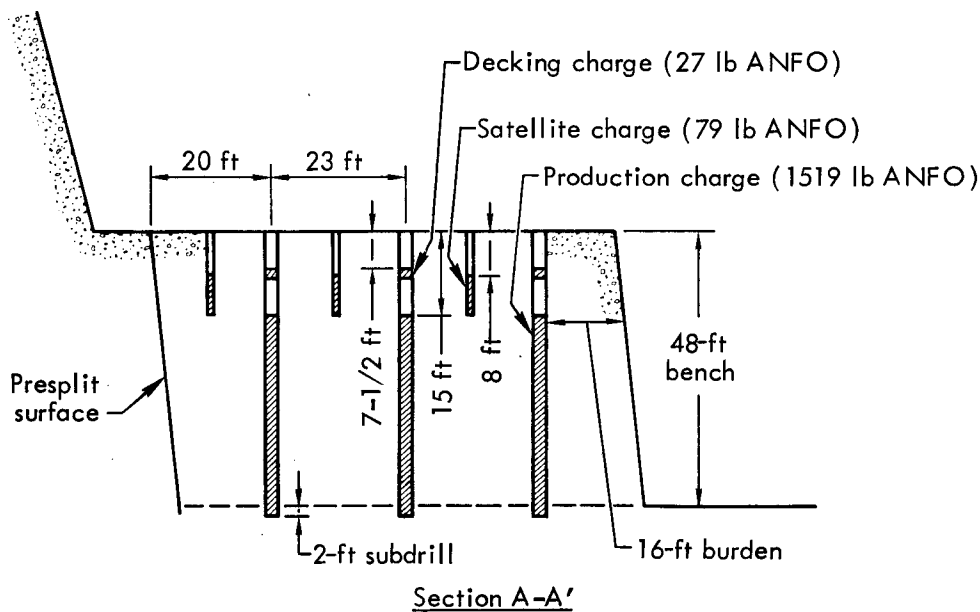
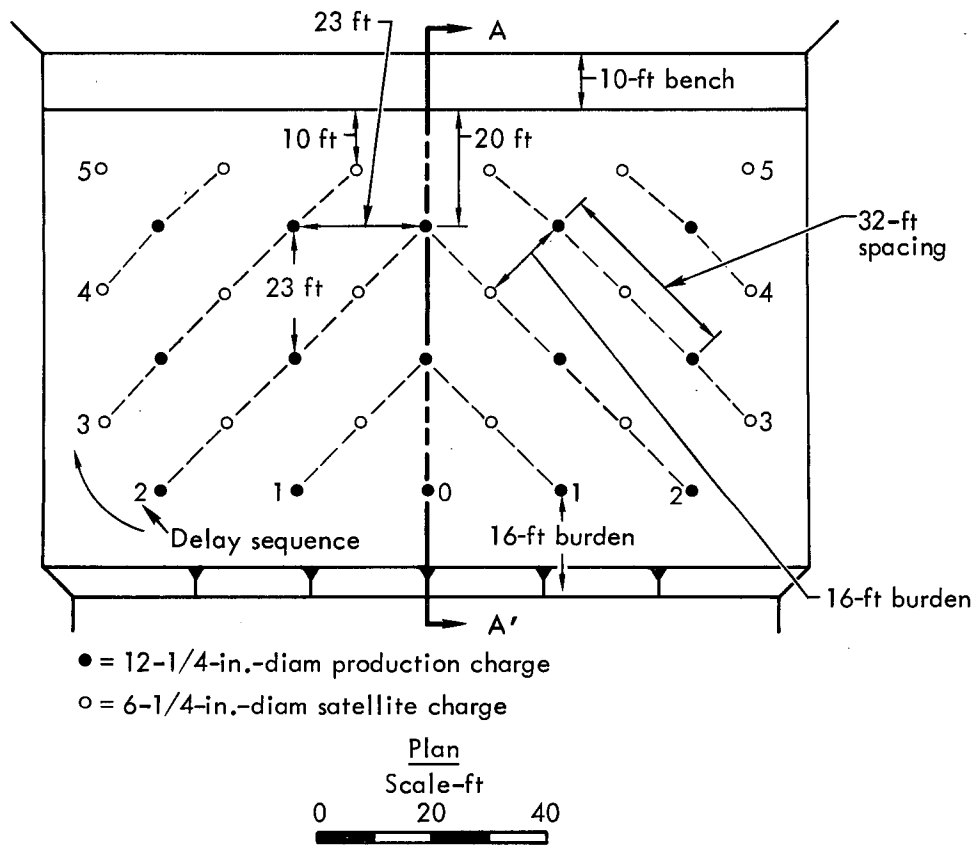


Fig. 95. Improved design for PB-8 test blast - ANFO.

PB-6C Test Blast

This blast was designed to remove the rock that remained after excavation of the broken material from the PB-6B test blast. Because the rock in the vicinity of the blastholes was shattered, new 6-3/4-in.-diameter holes were drilled between the old hole locations. The powder factor was 0.78 lb/yd³.

PB-7 Test Blast

The powder factor for PB-7 was 1.05 lb/yd³. The stemming in this design could probably have been increased from 12 to 15 ft to help reduce flyrock. Decking charges and satellite holes could also have been used to improve fragmentation in the collar region.

PB-8 Test Blast

In order to fit a sufficient number of 12-1/4-in.-diameter blastholes to observe the interaction between charges in the pattern, it was necessary to use smaller

separation distances between the production charges and presplit surfaces than would normally be desired. These smaller distances resulted in damage to the bench at the rear of the blast and possible damage to the side walls. The burden on the first row of production charges was also less than desirable, which probably was the cause of the large amount of flyrock seen in PB-8. The powder factor for this blast (slurry) was 1.20 lb/yd³.

An improved design for PB-8, using MS 80-25 slurry, is shown in Fig. 94. The design includes satellite holes and decking charges and has a slurry powder factor of 1.15 lb/yd³. Another improved PB-8 design using ANFO instead of slurry is presented in Fig. 95. This design results in an ANFO powder factor of 1.73 lb/yd³. It may be possible to eliminate the decking charges and add their explosive to the main charge holes. This option should be considered as well.

Chapter 10. Cost Analyses

Cost Savings for the R. D. BAILEY Project

After completion of the field work at the R. D. DAILEY site, EERL and the Huntington District made an evaluation of the impact the test excavation had on the R. D. BAILEY Lake Project. Although it is not possible to identify in a quantitative manner those aspects of the experimental excavation program that led to the cost savings, the following qualitative benefits of the program undoubtedly contributed:

1. The test excavation provided potential bidders with a visual inspection capability for rock to be excavated in the spillway. Ninety-two percent (11 out of 12) of the bidders surveyed (including Guy F. Atkinson, Morrison-Knudsen, S. J. Groves and Sons, Dravo, and Nello L. Teer) said that observation of the materials in the pilot excavation helped them to make a better evaluation of appropriate excavation techniques than could have been done by observing core boring results alone.

Table 17. Estimated reduction in project cost attributable to test excavation.

Estimated cost of spillway excavation prior to test excavation	\$8,155,495
As-bid cost	-5,844,305
	2,311,190
Useful work accomplished	+ 252,363
	2,563,553
Test excavation contract cost	- 353,895
Net reduction in project cost	<u>\$2,209,658</u>

2. The Data Report furnished to potential bidders provided contractors with information on methods of performing the excavation, and also information that might eliminate from the contractor's consideration some potentially unworkable methods.

The qualitative benefits mentioned above, an extension of information over that normally furnished bidders, probably led to reduced bid contingency costs. In addition there were the following tangential benefits to the government:

1. It is believed that because of information obtained during performance of the test excavation, the plans and specifications were better contract documents.

2. Material was provided for use in test fills from which placement techniques were developed.

3. Government construction personnel were provided valuable background information on materials and appropriate excavation techniques.

A government estimate of spillway excavation cost made before the test excavation (December 1972) was updated and compared to the successful bidder's price. The value of useful work accomplished during the test excavation, and the cost of the test excavation itself, were also considered in arriving at an estimated

reduction in project cost of about \$2.2 million (see Table 17).

One of the most likely items for a significant additional cost savings at the R. D. BAILEY Lake Project is in the drilling and blasting of the 882,000 yd³ of Upper Gilbert sandstone in the spillway. In order to estimate these possible savings, a comparison has been made between the government estimate for drilling and blasting the Upper Gilbert sandstone, and an estimate based upon a blast design developed and tested during the experimental excavation program.

The government estimate was based on using 3-in. diameter blastholes 10 ft deep in an 8- by 8-ft pattern. The explosive was assumed to be gelatin dynamite with a powder factor of 1 lb/yd³. The unit cost of drilling and blasting with this design is \$1.00/yd³ + 6% profit, or \$1.06/yd³.

The estimate resulting from experience gained during the experimental excavation is based on using 9-in. diameter charges 50 ft deep in a 19- by 19-ft pattern. The explosive is assumed to be ANFO with a powder factor of 1.4 lb/yd³. The unit cost of drilling and blasting with this design is \$0.37/yd³, including 6% profit. This estimate also includes secondary blasting for 15% oversize rocks.

By comparing these two unit costs it may be seen that there is a possible savings of $\$1.06/\text{yd}^3 - \$0.37/\text{yd}^3 = \$0.69/\text{yd}^3$. When this figure is applied to the 882,000 yd^3 of Upper Gilbert sandstone, the total possible additional savings is \$608,580. Although these estimated additional savings may not be realized on the R. D. BAILEY Lake Project, the $\$0.69/\text{yd}^3$ savings possible from the use of larger charges should be considered in the planning and design of future projects with large excavations requiring drilling and blasting.

Effect of Charge Diameter and Bench Height on Blasting Costs

Another analysis was made to determine the effect of charge diameter and bench height on the unit cost of drilling

and blasting in the Upper Gilbert sandstone. Calculations were made for using ANFO and slurry as bulk explosives. The results are shown in Figs. 96 and 97. The curve for each charge diameter extends for its maximum useful range for blast patterns with more than two or three rows of holes. It is apparent from the graphs that there is a definite trend towards lower unit costs as the bench height is increased. This is primarily due to more efficient use of the blast holes — that is, the stemming being constant regardless of bench height, occupies a smaller percentage of a hole drilled on a higher bench than a hole drilled on a low bench. It should be noted that these curves do not include secondary blasting costs. As shown in Fig. 53, there is a slight decrease in fragmentation for the larger charge

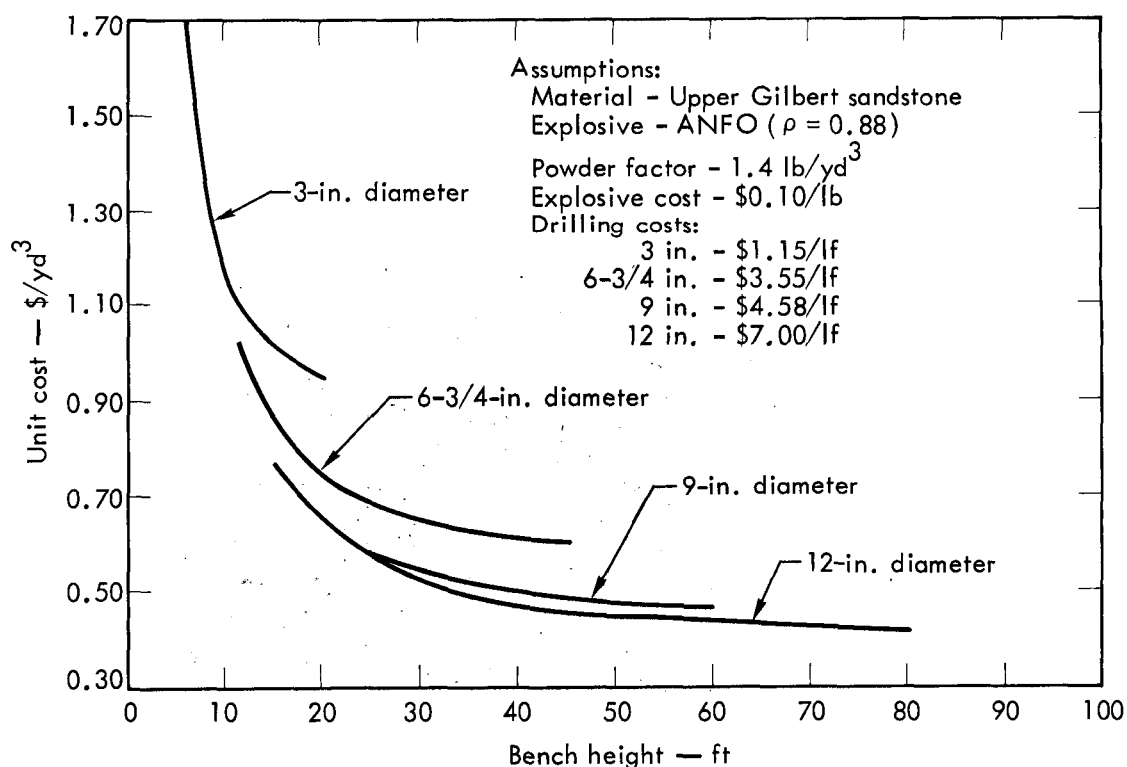


Fig. 96. Unit cost for drilling and blasting vs bench height for various blast hole diameters — ANFO.

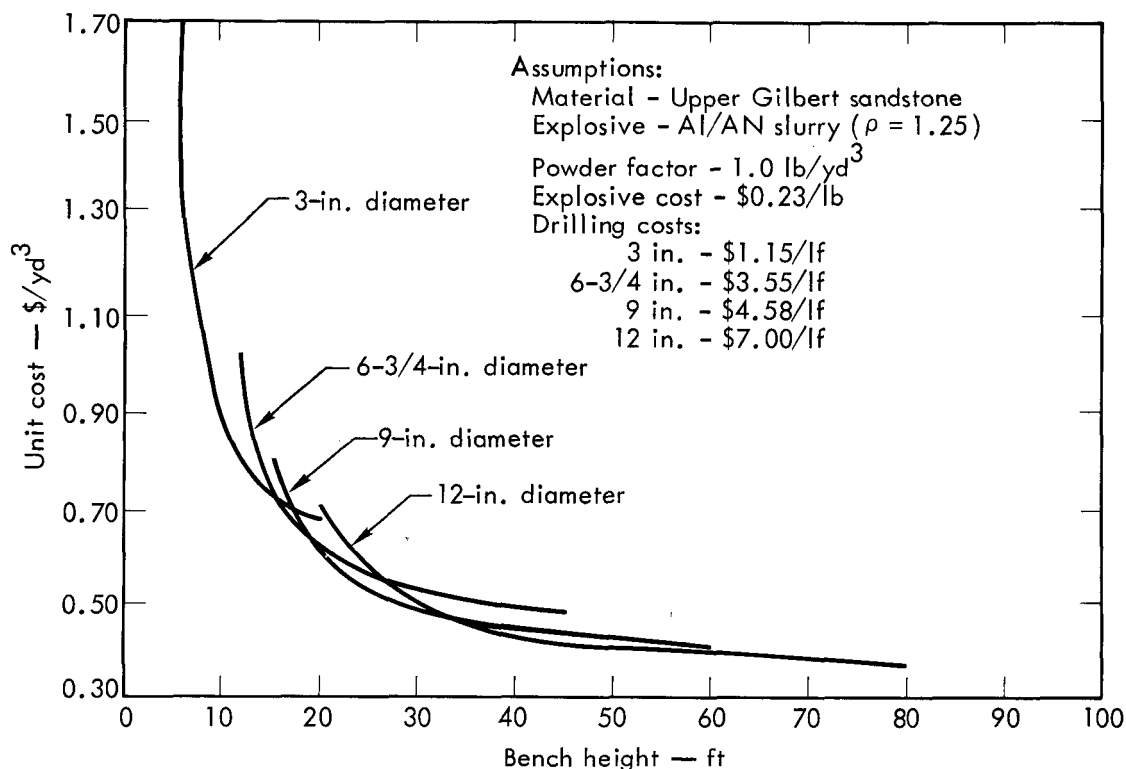


Fig. 97. Unit cost for drilling and blasting vs bench height for various blast hole diameters - slurry.

diameters. The cost of additional secondary blasting for large diameter charges must therefore be taken into

account on projects where there is an upper limit specified for the size of blasted rock.

Chapter 11. Summary and Conclusions

Much valuable information was obtained during the course of the experimental excavation program. Some of this information was of a basic scientific nature, and some was of immediate practical engineering interest.

The R. D. BAILEY experimental excavation included a program for collecting data on rock fragmentation, using the point counting technique. This was the first time that the technique has been used on a large scale in an attempt to make quantitative estimates of fragmentation resulting from various pro-

duction blasting patterns. The point count data were also used to quantify the general shape of the blasted rocks according to the Zingg Classification System.

The close-in subsurface ground shock was successfully measured using piezoelectric crystal velocity transducers grouted into drill holes. The effort to relate peak particle velocity to blast-induced fracturing, however, was not entirely successful due to the failure of the permeability test apparatus designed to detect increases in fracturing. The

double-packer system does not appear to be a very promising approach to this problem because of the difficulty of post-shot reentry into drill holes in the immediate blast vicinity. An attempt was made to determine the effect of buffer zones on peak particle velocities in rock masses to be protected from production blasting, but the results were inconclusive. The buffer zone concept, therefore, should still be considered experimental.

Seismic motion measurements made during the test blasts were used to develop a seismic motion prediction equation for the spillway site. This equation was used to establish the maximum weight of explosive that can be detonated in the spillway without endangering a 300-ft-high water intake structure under construction nearby.

Extensive airblast measurements were made in an attempt to develop an airblast prediction technique applicable to quarry-type blasts. Previous prediction techniques developed for cratering charges were used as a basis for predictions, but due to the many differences in the two blasting techniques, it was necessary to make many simplifying assumptions in order to apply the prediction technique for cratering to quarry blasting. It was demonstrated, however, that airblast overpressures can be predicted within a factor of two if the effects of surface detonating cord and venting through weak stemming material are eliminated. The airblast from these two factors can be greatly reduced by burying the detonating cord and by taking particular care with stemming design and procedure.

Seventeen test fills were constructed by Huntington District with shale and sandstone from the experimental excavation.

The fills were placed in lifts of various thicknesses with several different types of spreading and compacting equipment. A test pit was dug in each fill to measure density, gradation, and percolation characteristics. The information gained from this program was useful for verifying the accuracy of design assumptions, and aided in the preparation of specifications for construction of the dam embankment.

The scope of the experimental excavation program did not allow for optimization of a blasting pattern for any particular size of blasthole, rock type, or explosive type. It did, however, provide a starting point for further development of blasting patterns, and recommendations are made on how to improve upon the blasts in the experimental series.

After completion of the experimental excavation program, EERL and Huntington District made an evaluation of the economic impact the program had on construction costs for the R. D. BAILEY Lake Project. It was estimated that the resulting reduction in project cost was about \$2.2 million.

An independent analysis of drilling and blasting costs, as a function of blasthole diameter, was made using data from the experimental excavation program. There appears to be a substantial reduction in drilling and blasting costs with increasing blasthole diameter.

Another product of the experimental excavation was a Data Report, which contained information of a noninterpretive nature on the experience gained during the test program. This was made available to potential bidders on the dam contract to allow them to make a more informed bid for the unclassified excavation contract item than would normally be

possible if only core borings were available.

Also, a set of blasting guidelines, based on the experience gained during the experimental excavation program, was furnished to Huntington District personnel for use in the review and monitoring of

blasting operations in the spillway of the R. D. BAILEY Lake Project.

In the light of the above accomplishments, it may be concluded that the experimental excavation was very successful, and provided much useful scientific and engineering data.

Appendix A

Gradation Curves

The gradation curves in this appendix are based on point count data obtained during the course of the experimental excavation program. Take, for example, the data from PB-3. Measured rock dimensions were tabulated as shown in Table A1. The measured breadths of the rock fragments were separated into size groups as shown in Table A2. The 95% confidence interval was determined for each size group by use of the following relationship.

$$\bar{X} - 1.96 \sqrt{\frac{P_0 (1 - P_0)}{N}} < P < \bar{X} + 1.96 \sqrt{\frac{P_0 (1 - P_0)}{N}}$$

where:

\bar{X} = the proportion of rocks in the sample that are less than the maximum size of the specified interval

P_0 = the percentage of rocks in a sample within a specified size interval

N = the total number of rocks in the sample

P = the population proportion.

The computations of the 95% confidence band for PB-3 are shown in Table A3. The upper and lower limits of the band were then plotted for each size group and the points connected with smooth curves. There is a 95% probability that the actual gradation curve will fall within the indicated band.

Table A1. PB-3 fragmentation data.

No.	Length Breadth Width			b/a	c/b	No.	Length Breadth Width			b/a	c/b
	a (in.)	b (in.)	c (in.)				a (in.)	b (in.)	c (in.)		
1	2	1-1/2	1	0.75	0.70	60	2	1	1/2	0.50	0.50
2	5	3-1/2	1	0.70	0.30	61	2-1/2	1-3/4	1-1/2	0.70	0.86
3	6	4	3	0.70	0.70	62	2-3/4	2	1-1/2	0.73	0.75
4	12	9-1/2	5	0.79	0.53	63	13	12	6	0.92	0.50
5	2	1	1	0.50	1.00	64	20	11	6	0.55	0.55
6	6-1/2	3-1/2	2-1/2	0.54	0.71	65	2	1-1/4	3/4	0.63	0.60
7	5	4	3	0.80	0.75	66	10	7	7	0.70	1.00
8	2-1/2	2-1/2	2-1/2	1.00	1.00	67	7	3-1/2	2	0.50	0.57
9	20	14	6	0.70	0.43	68	3	1-1/2	1	0.50	0.67
10	4-1/2	2	2	0.44	1.00	69	5	4	2-1/2	0.80	0.63
11	1-1/2	1	1	0.67	1.00	70	4-1/2	4	2-1/4	0.89	0.56
12	2	1	1/2	0.50	0.50	71	6	3	2-1/2	0.50	0.83
13	2-1/2	1-1/2	1-1/2	0.60	1.00	72	4	3	1-1/4	0.75	0.42
14	10-1/2	5-1/2	4-1/2	0.52	0.82	73	3-1/4	1-1/4	1	0.38	0.80
15	1	1	1/2	1.00	0.50	74	3	2-1/2	1-1/2	0.83	0.60
16	5-1/2	2-1/2	1	0.45	0.40	75	2	1-1/4	1-1/4	0.63	1.00
17	10	8	5	0.80	0.63	76	4	2	1-1/2	0.50	0.75
18	6	4-1/2	1-1/2	0.75	0.33	77	20	18	6	0.90	0.33
19	7	3-1/2	3	0.50	0.86	78	12	8	4	0.67	0.50
20	1-1/2	1	1/2	0.67	0.50	79	8	5-1/2	2	0.69	0.36
21	2	1-1/2	1	0.75	0.67	80	5	5	2	1.00	0.40
22	3	2-1/2	2	0.83	0.80	81	7-1/2	4	2-1/2	0.53	0.63
23	5-1/2	3	1-1/2	0.55	0.50	82	3	2-1/2	1	0.83	0.40
24	2	1	1	0.50	1.00	83	5-1/2	4	2-1/4	0.73	0.56
25	2-1/2	1-1/2	1/2	0.60	0.33	84	3-1/2	1-3/4	1	0.50	0.57
26	10-1/2	8	3-1/2	0.76	0.44	85	5	3	2	0.60	0.67
27	3	1-1/2	1	0.50	0.67	86	6	4	2-1/2	0.67	0.63
28	30	20	16	0.67	0.80	87	5	2-1/2	2-1/4	0.50	0.90
29	4-1/2	2-1/2	1-1/2	0.56	0.60	88	6	5-1/2	2	0.92	0.36
30	5	4	3	0.80	0.75	89	2-1/2	1-1/2	3/4	0.60	0.50
31	15	10	5	0.67	0.50	90	12	11	2-1/2	0.92	0.23
32	6-1/2	4-1/2	2	0.69	0.44	91	11	4	3-1/2	0.36	0.88
33	4	3	2	0.75	0.67	92	9	3-1/2	2	0.39	0.57
34	3	1-1/2	1/2	0.50	0.33	93	12	8	4	0.67	0.50
35	3	2	1-1/2	0.67	0.75	94	14	11	4-1/2	0.79	0.41
36	5	3	2-1/2	0.60	0.83	95	24	22	9	0.92	0.41
37	3	2	1	0.67	0.50	96	12	8	4	0.67	0.50
38	11	8	4	0.73	0.50	97	6-1/2	5	2-1/2	0.77	0.50
39	5	4	2	0.80	0.50	98	3	2	2	0.67	1.00
40	2-1/2	1-1/2	1	0.60	0.67	99	2-1/2	2	3/4	0.80	0.38
41	5	4	3	0.80	0.75	100	2-1/2	1-1/2	1-1/4	0.60	0.83
42	3	1-1/2	1	0.50	0.67	101	6	3	2	0.50	0.67
43	6	2-1/2	2-1/2	0.42	1.00	102	3	2	2	0.67	1.00
44	3	2	1	0.67	0.50	103	3-1/2	2-1/2	1-1/4	0.71	0.50
45	3	1-1/2	1-1/2	0.50	1.00	104	2	1-1/2	3/4	0.75	0.50
46	1-1/2	1/2	1/4	0.33	0.50	105	5	2	1	0.40	0.50
47	3	2-1/4	2-1/4	0.75	1.00	106	13	11	4	0.85	0.36
48	4-1/2	1-1/4	3/4	0.28	0.60	107	3	1-1/2	3/4	0.50	0.50
49	2-1/2	1-1/2	1-1/2	0.60	1.00	108	3	1-3/4	1	0.58	0.57
50	12	12	9	1.00	0.75	109	1-1/2	1-1/4	1	0.83	0.80
51	24	18	11	0.75	0.61	110	2	2	1-1/2	1.00	0.75
52	22	13	7	0.59	0.54	111	2-1/2	2	1	0.80	0.50
53	8	5	4	0.63	0.80	112	6	2-1/2	2	0.42	0.80
54	6	3	2	0.50	0.67	113	11	2-1/2	2-1/2	0.23	1.00
55	2-1/2	1-1/2	1/2	0.60	0.33	114	1-1/2	1	1	0.67	1.00
56	3	3	2	1.00	0.67	115	3	1-1/2	1	0.50	0.67
57	2-1/4	1-3/4	3/4	0.78	0.43	116	3-1/2	3-1/2	2	1.00	0.57
58	5	2-1/2	1-1/2	0.50	0.60	117	12	10	8	0.83	0.80
59	24	14	12	0.58	0.86						

Table A2. Breadths from PB-3 fragmentation data.

Breadth (in.)	Frequency	Relative frequency, P_0 (%)	Cumulative frequency (%)
0-1	9	7.69	7.69
1-2	38	32.48	40.17
2-4	39	33.33	73.50
4-8	15	12.82	86.32
8-16	12	10.26	96.58
16-32	4	3.42	100.00
Totals	117	100.00	

Table A3. Computations for PB-3 95% confidence band.

Breadth (in.)	P_0 (%)	$1.96 \sqrt{\frac{P_0(1-P_0)}{N}}$	Cumulative P_0 (%)	Lower limit (%)	Upper limit (%)
0-1	7.69	0.0482	7.69	2.87	12.51
1-2	32.48	0.0849	40.17	31.68	48.66
2-4	33.33	0.0854	73.50	64.96	82.04
4-8	12.82	0.0606	86.32	80.26	92.38
8-16	10.26	0.0550	96.58	91.08	102.08
16-32	3.42	0.0329	100.00	96.71	103.29

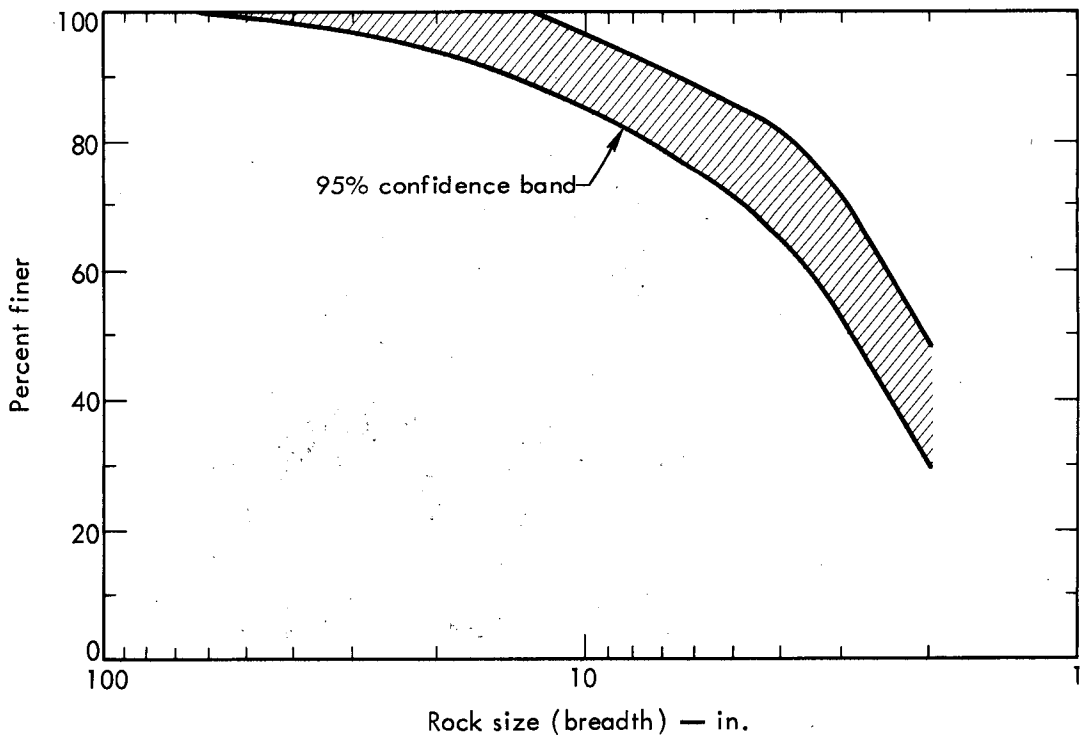


Fig. A1. Particle size distribution curve for PB-3 (based on point count of 117 particles).

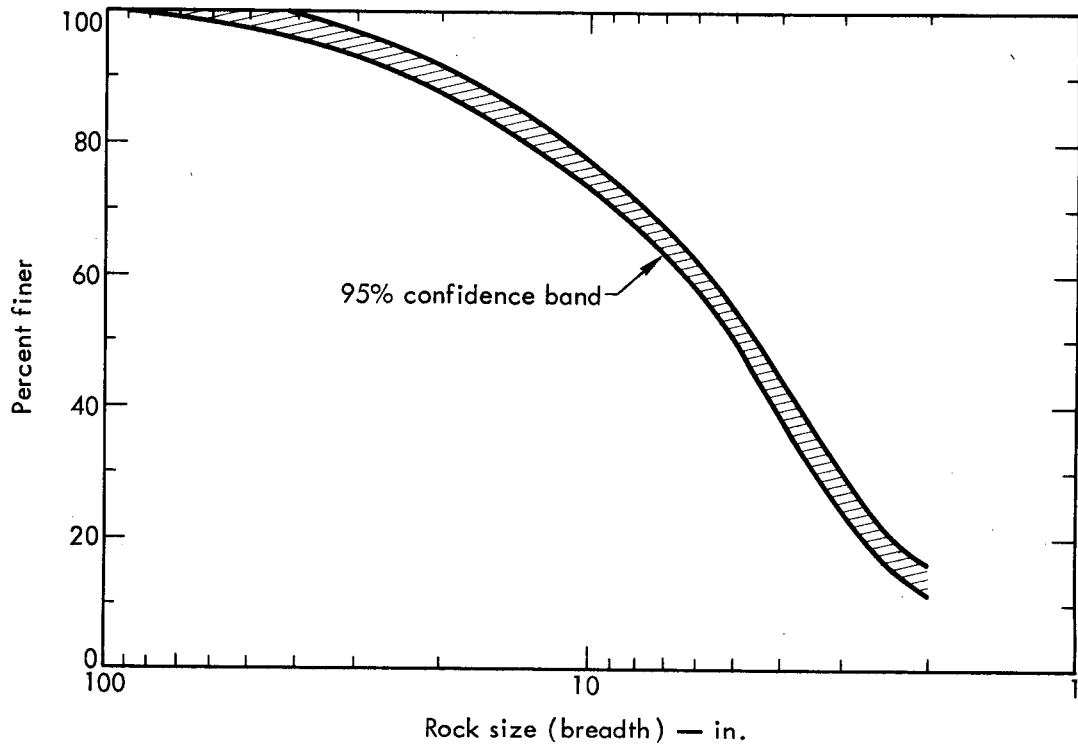


Fig. A2. Particle size distribution curve for PB-4 (based on point count of 1064 particles).

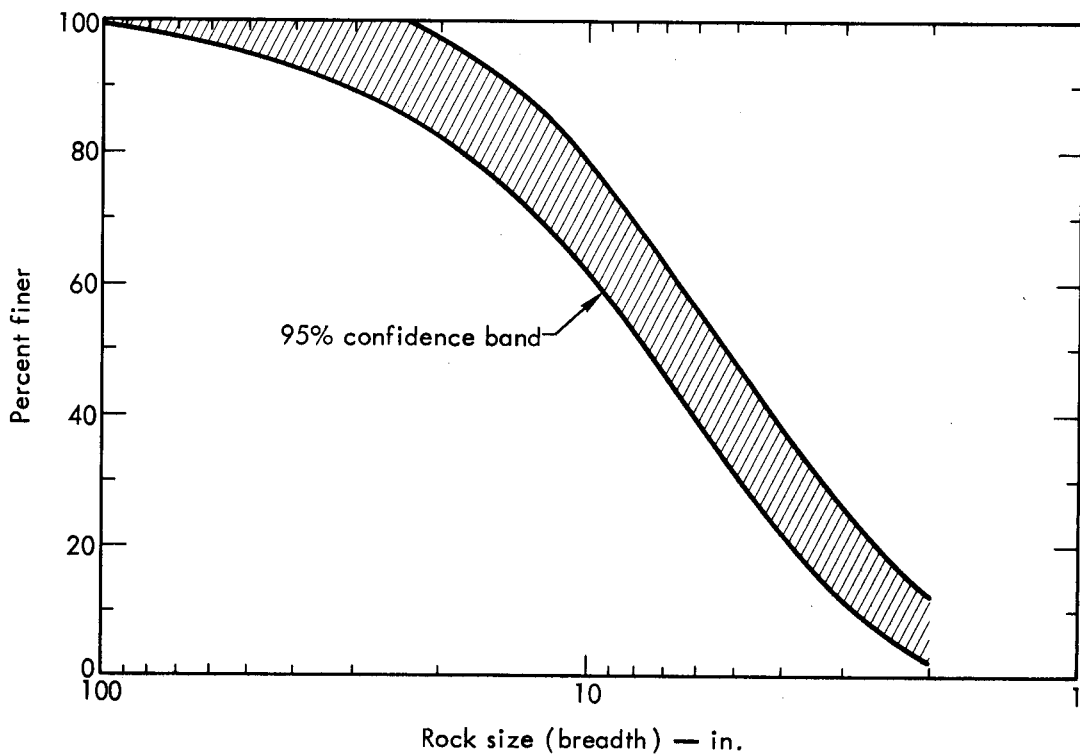


Fig. A3. Particle size distribution curve for PB-4A (based on point count of 100 particles).

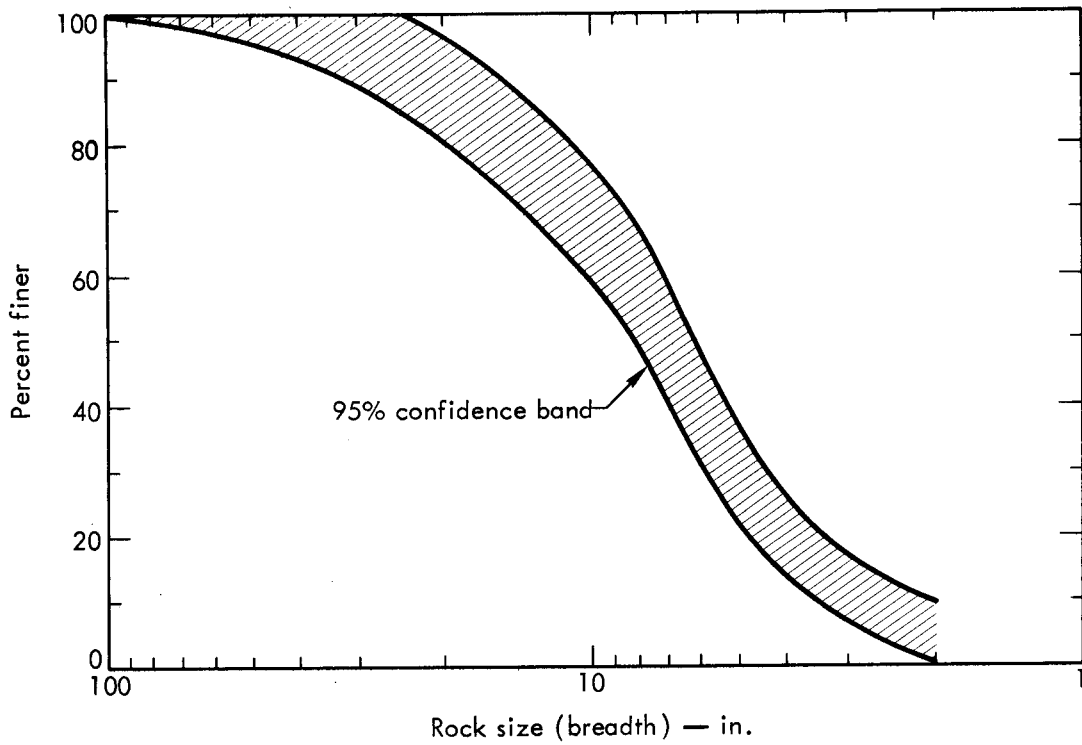


Fig. A4. Particle size distribution curve for PB-4B (based on point count of 98 particles).

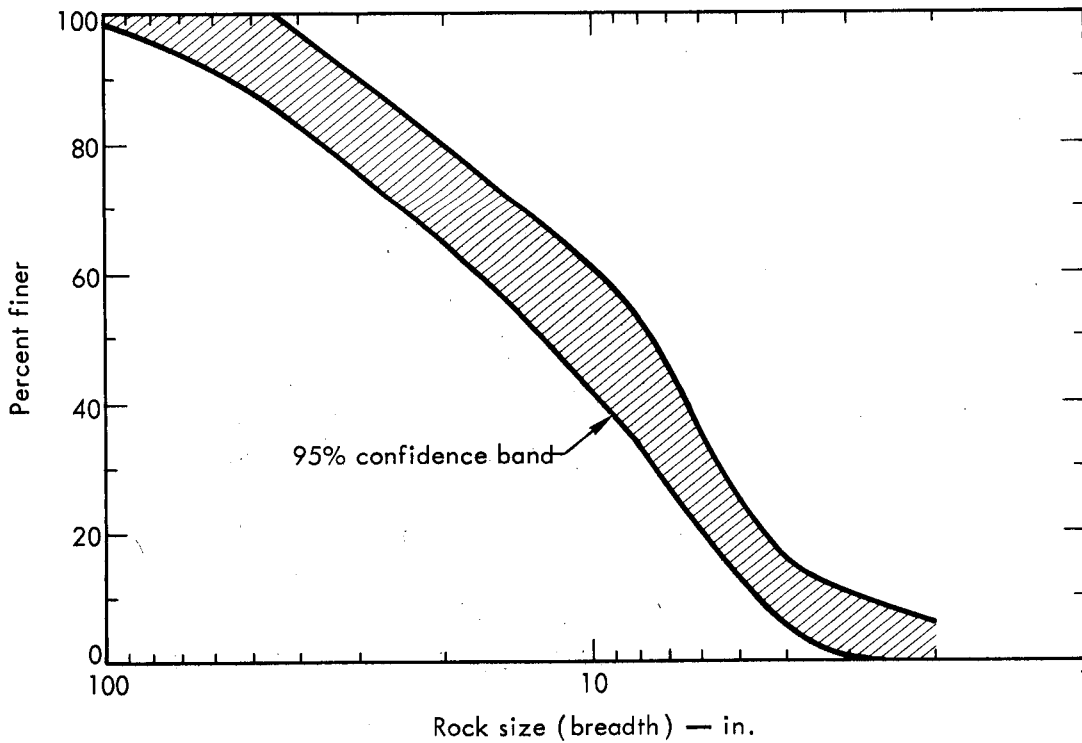


Fig. A5. Particle size distribution curve for PB-4C (based on point count of 126 particles).

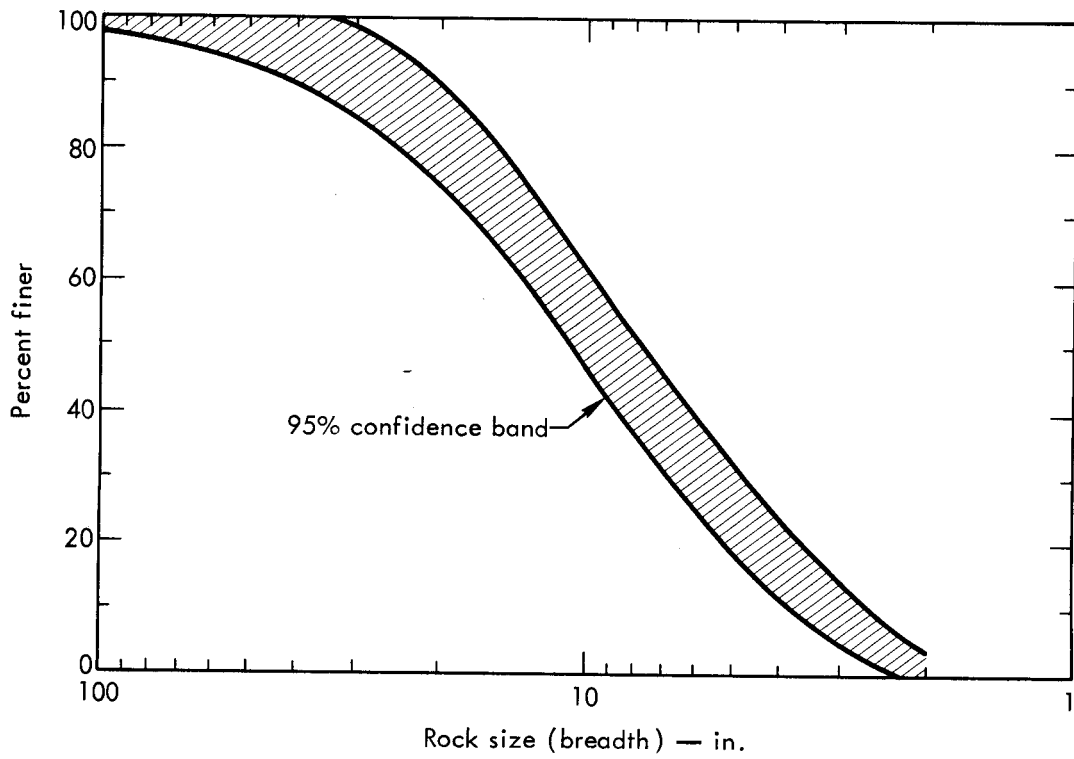


Fig. A6. Particle size distribution curve for PB-4D (based on point count of 126 particles).

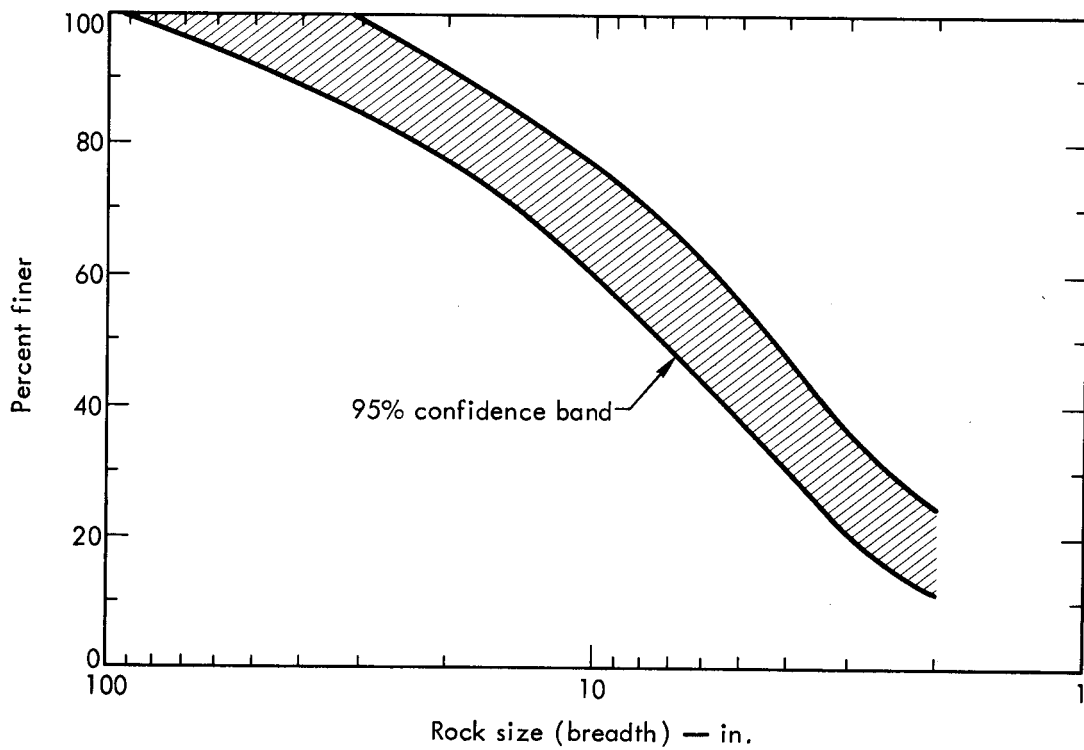


Fig. A7. Particle size distribution curve for PB4E (based on point count of 80 particles).

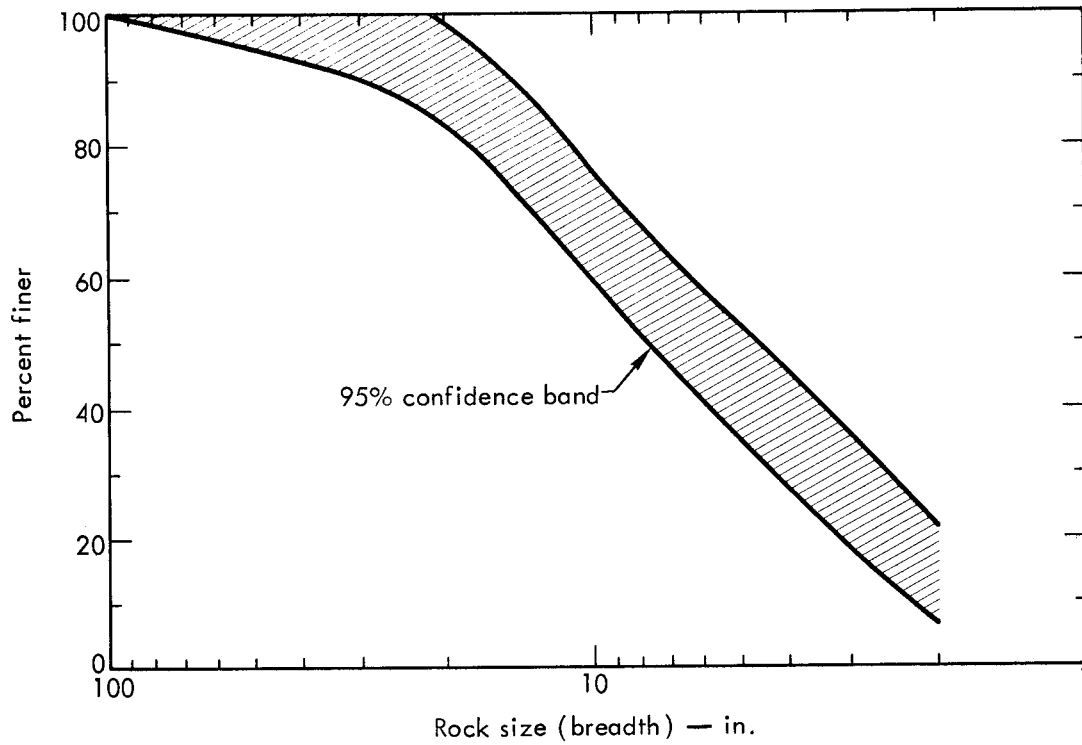


Fig. A8. Particle size distribution curve for PB-5 (based on point count of 87 particles).

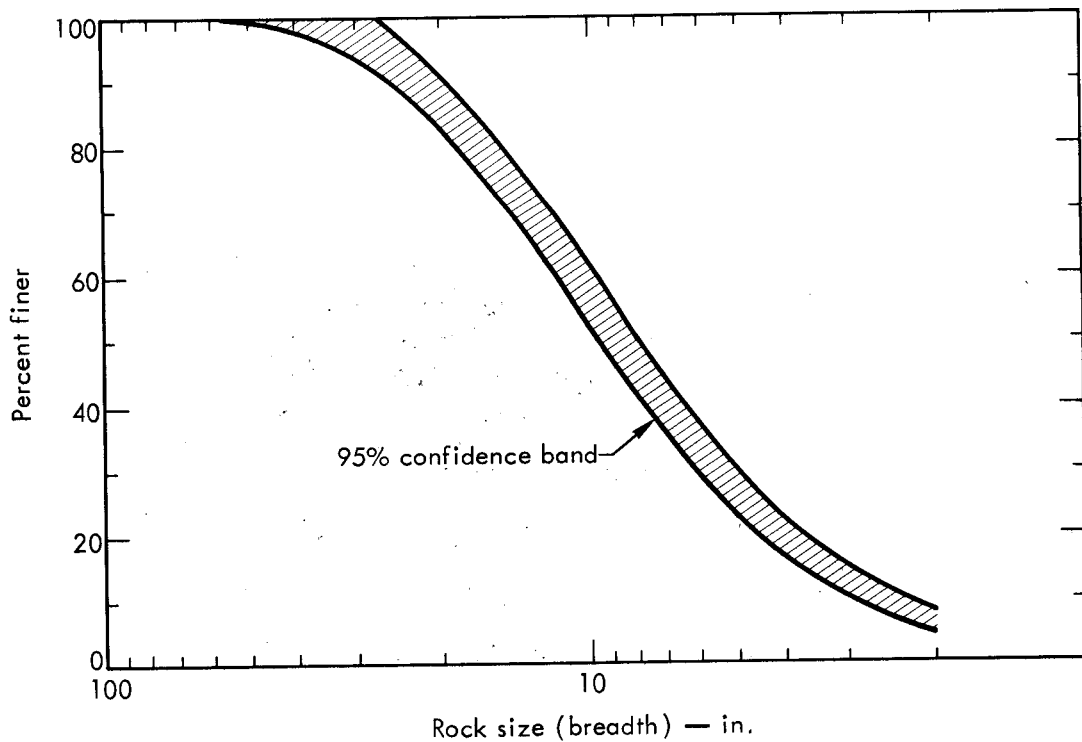


Fig. A9. Particle size distribution curve for PB-6A (based on point count of 341 particles).

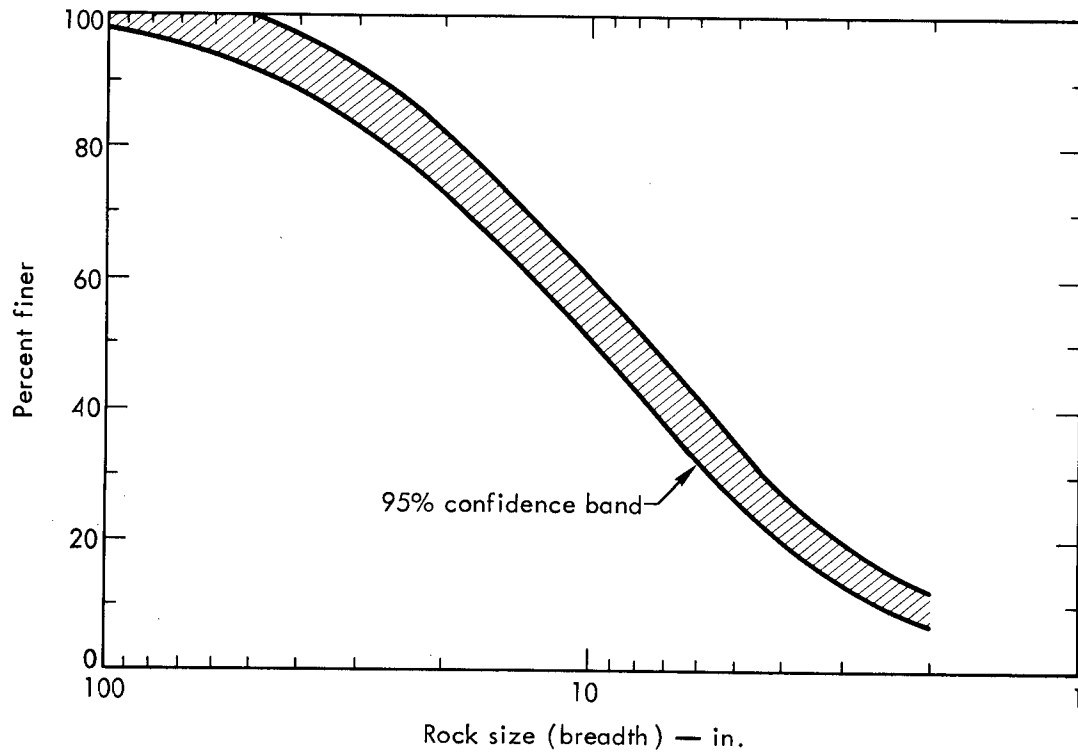


Fig. A10. Particle size distribution curve for PB-6B (based on point count of 262 particles).

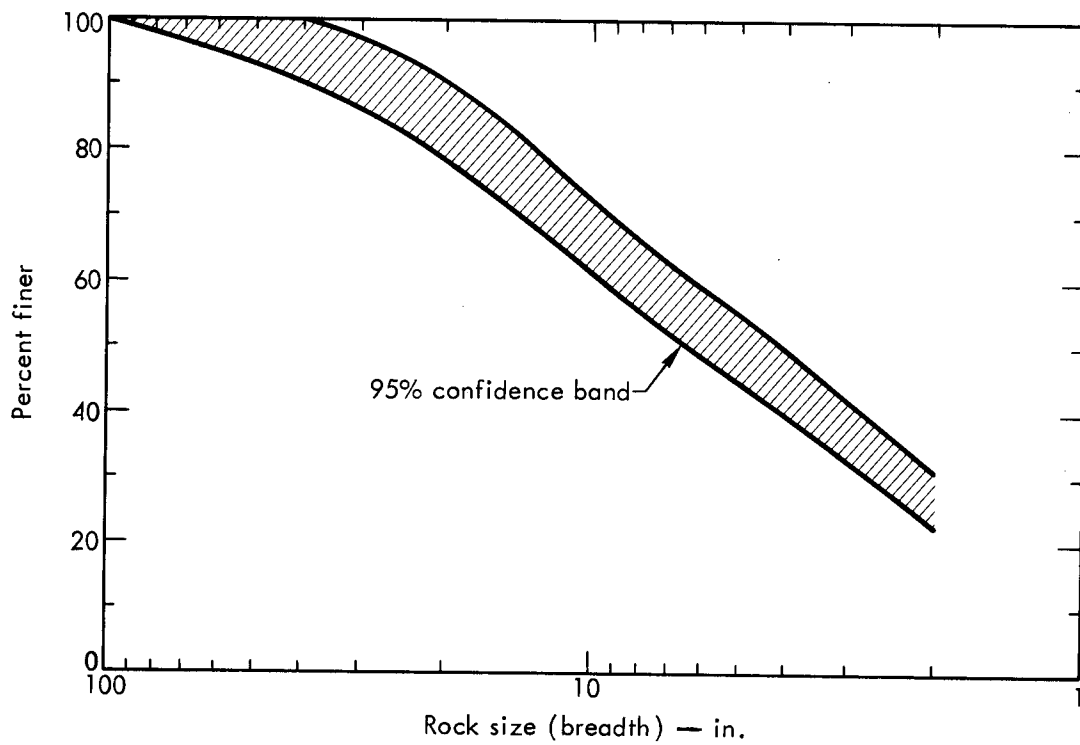


Fig. A11. Particle size distribution curve for PB-6C (based on point count of 174 particles).

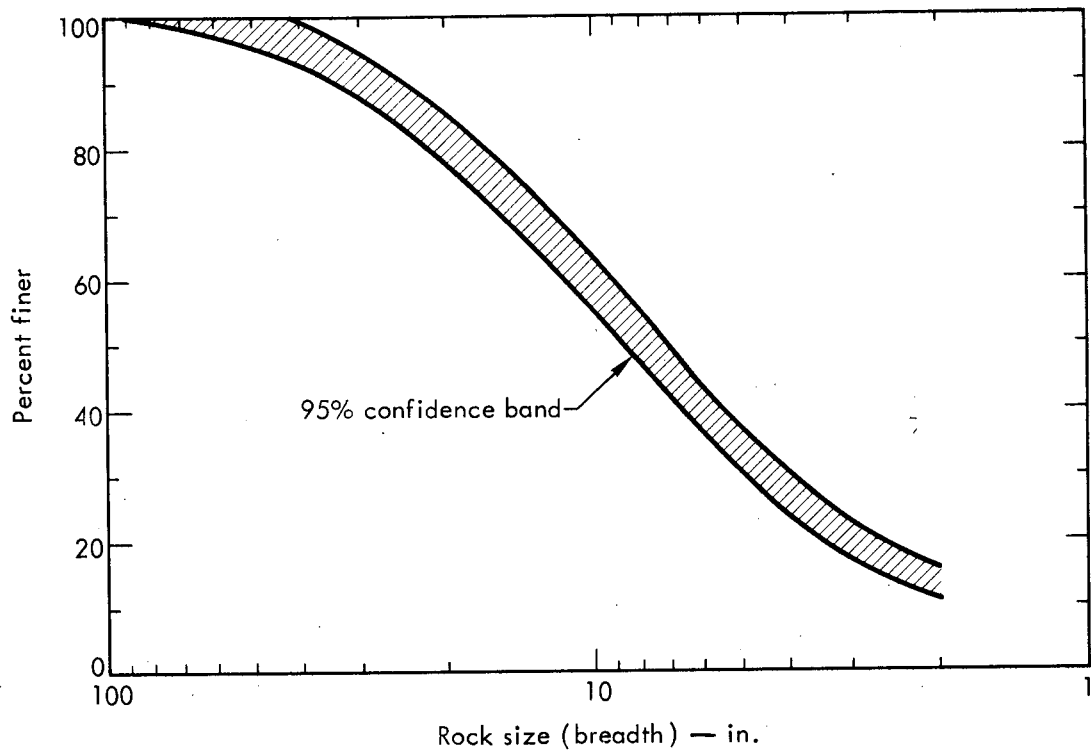


Fig. A12. Particle size distribution curve for PB-7 (based on point count of 391 particles).

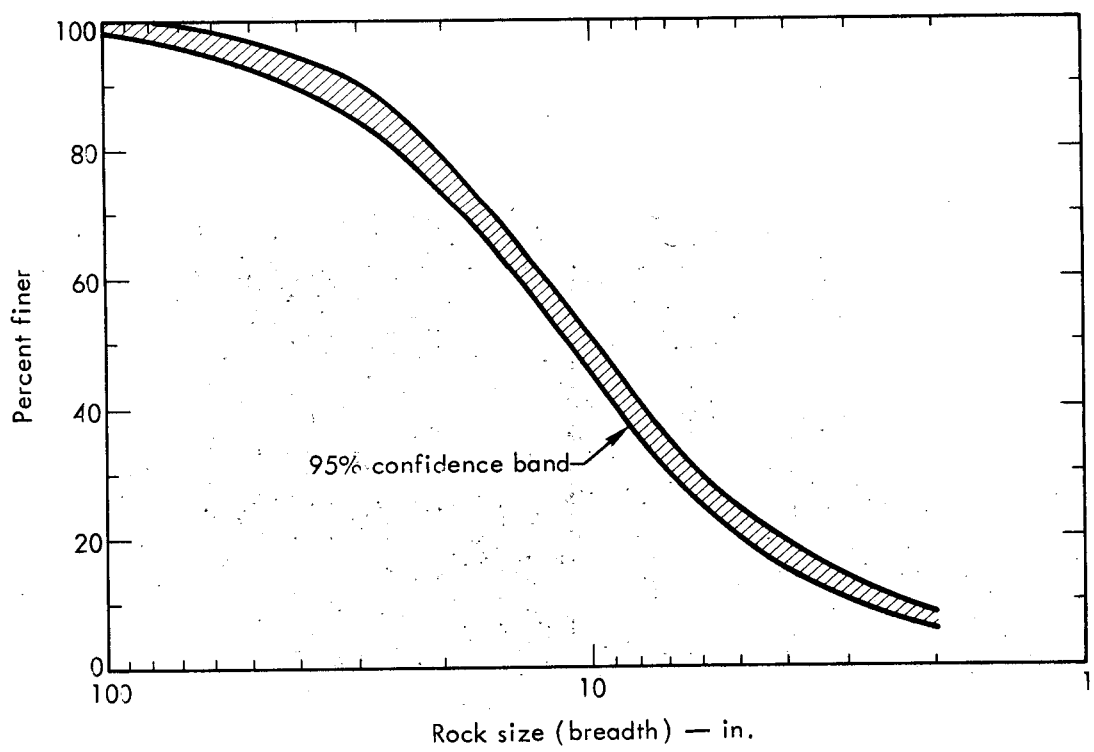


Fig. A13. Particle size distribution curve for PB-8 (based on point count of 879 particles).

Appendix B

Subsurface Particle Velocity Records

The following pages contain facsimiles of the original velocity recordings taken during the blasting of the pilot excavation of the R. D. BAILEY spillway. However, before the reader begins to look over the traces, he should read the notes below. These notations explain various codes and symbols used in the traces as well as help to clarify the scales presented.

1. The letters PV used in identifying the vertical scales refer to particle velocity.

2. The vertical scales presented in each case should be used in a manner analogous to that of a map scale. This is due to the fact that the zero line drifts somewhat after a pulse comes through. Subsequently, later pulses should be measured from their point of initiation to their peak rather than from the original zero line of the gage.

3. The traces are identified by a series of letters and numbers as in the example, PB-5 presplit 15 HNB 22.

a. PB-5 refers to the blast designation.

b. Presplit differentiates between the records taken during a separate firing of the presplit line as opposed to the main production blast. This term is omitted in the main blast cases.

c. 15 refers to the depth of gage emplacement in feet.

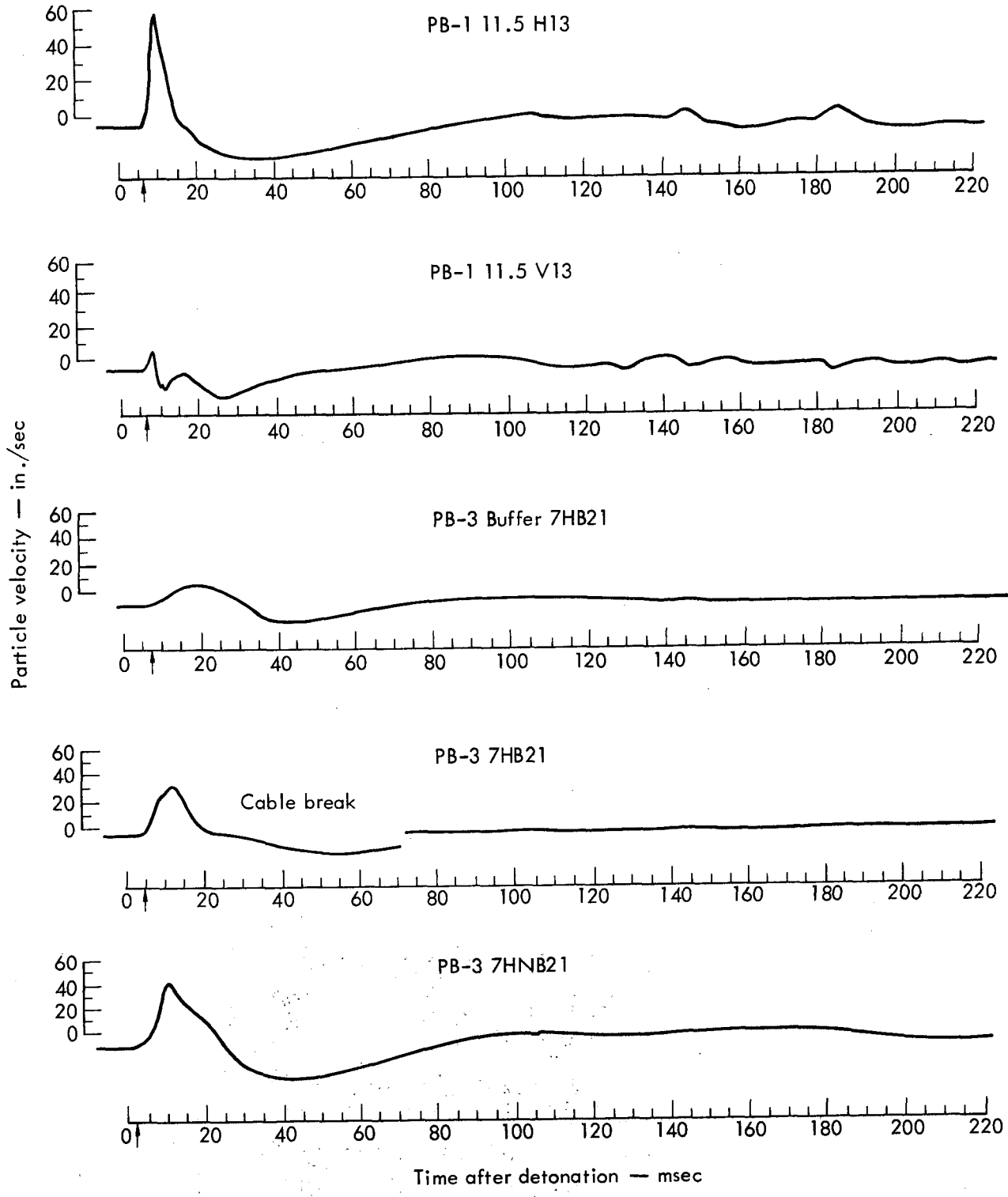
d. H refers to the gage orientation; H signifies a radially horizontal orientation while V is vertical.

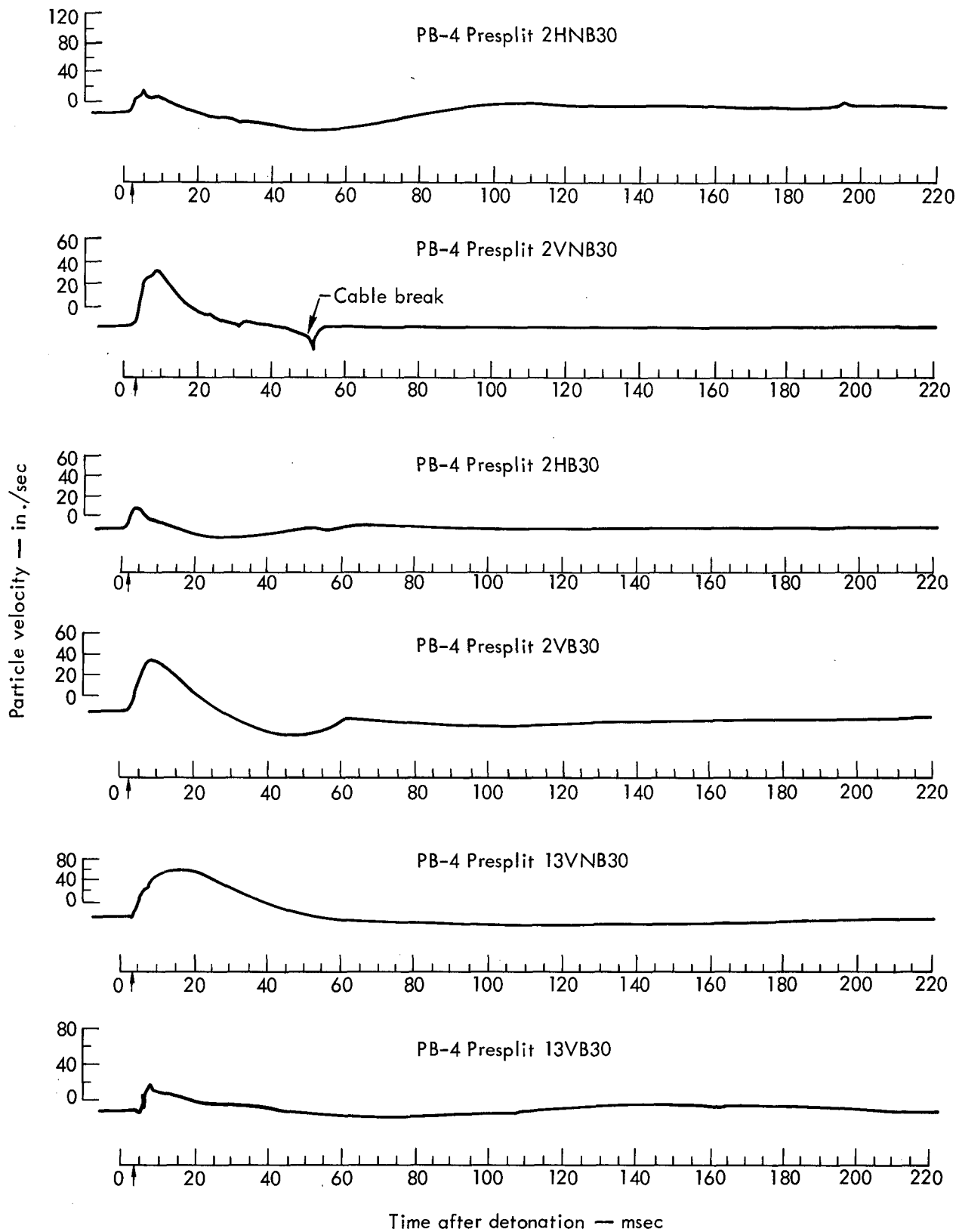
e. NB refers to a gage unprotected by an intervening buffer zone; B refers to the opposite condition where a buffer zone is present. This term is omitted in blasts in which buffer zones were not used.

f. 22 refers to the horizontal separation between the gage and the nearest main charge hole.

4. The arrow pointing to the time scale indicates the time of initial signal arrival.

5. In cases in which the horizontal scale is labeled "time scale" rather than "time after detonation," zero time was not successfully recorded. The time scale, however, can be used to calculate relative time between two events on the trace.





60
40
20
0

PB-4 2HB30

0 20 40 60 80 100

Particle velocity — in./sec

60
40
20
0

PB-4 2VB30

0 20 40 60 80 100

40
20
0

PB-4 2HNB30

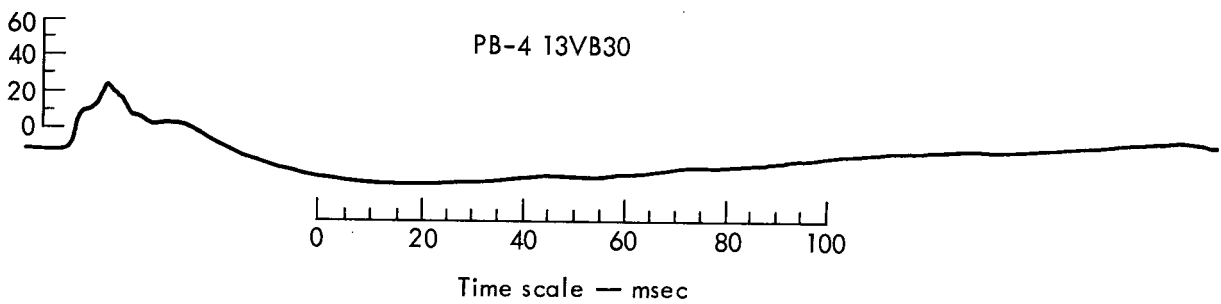
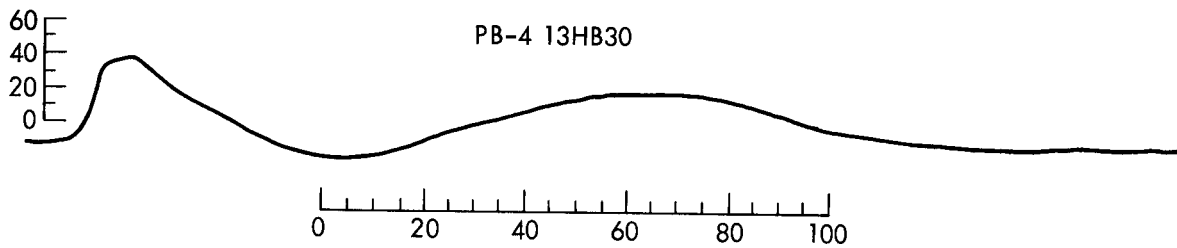
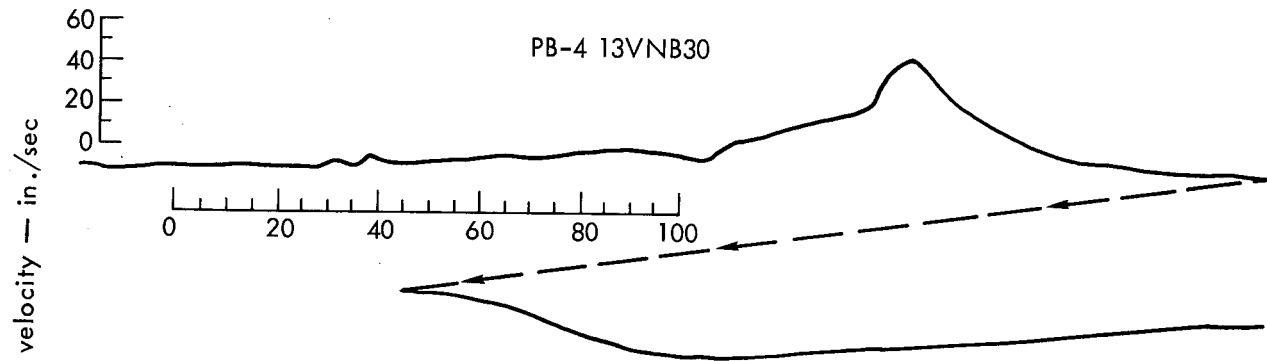
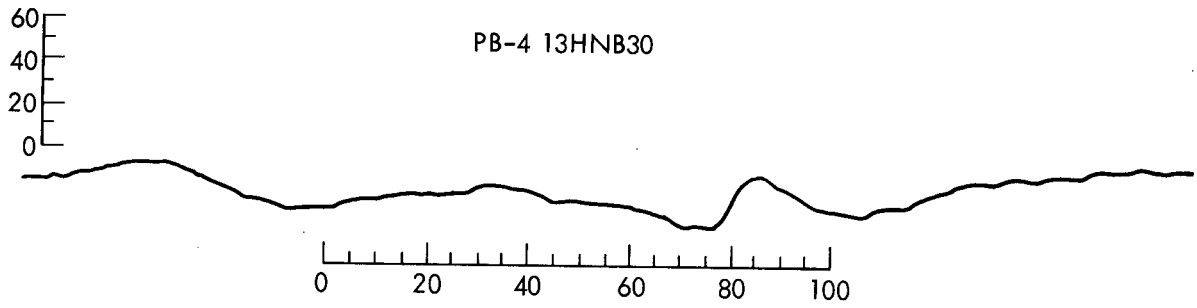
0 20 40 60 80 100

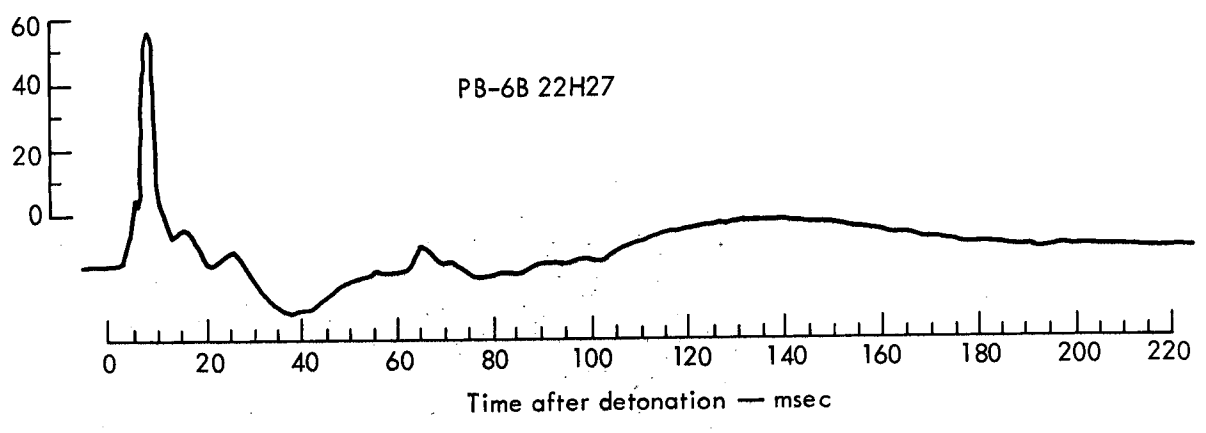
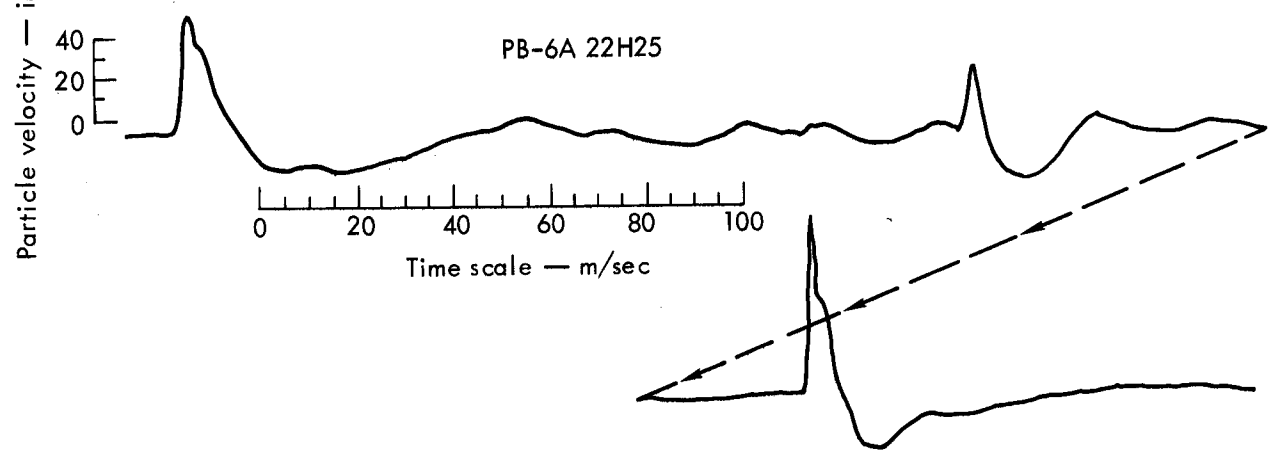
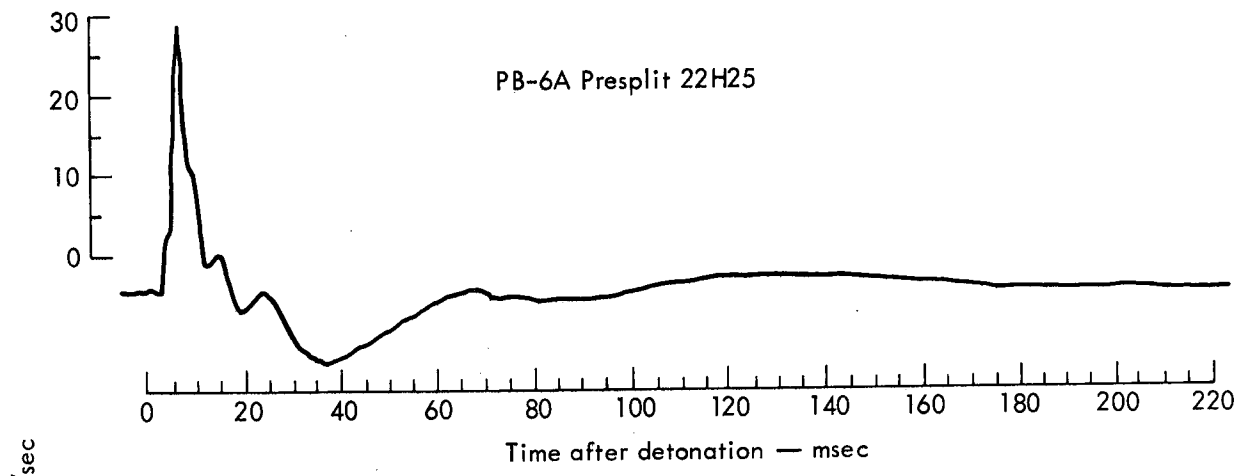
60
40
20
0

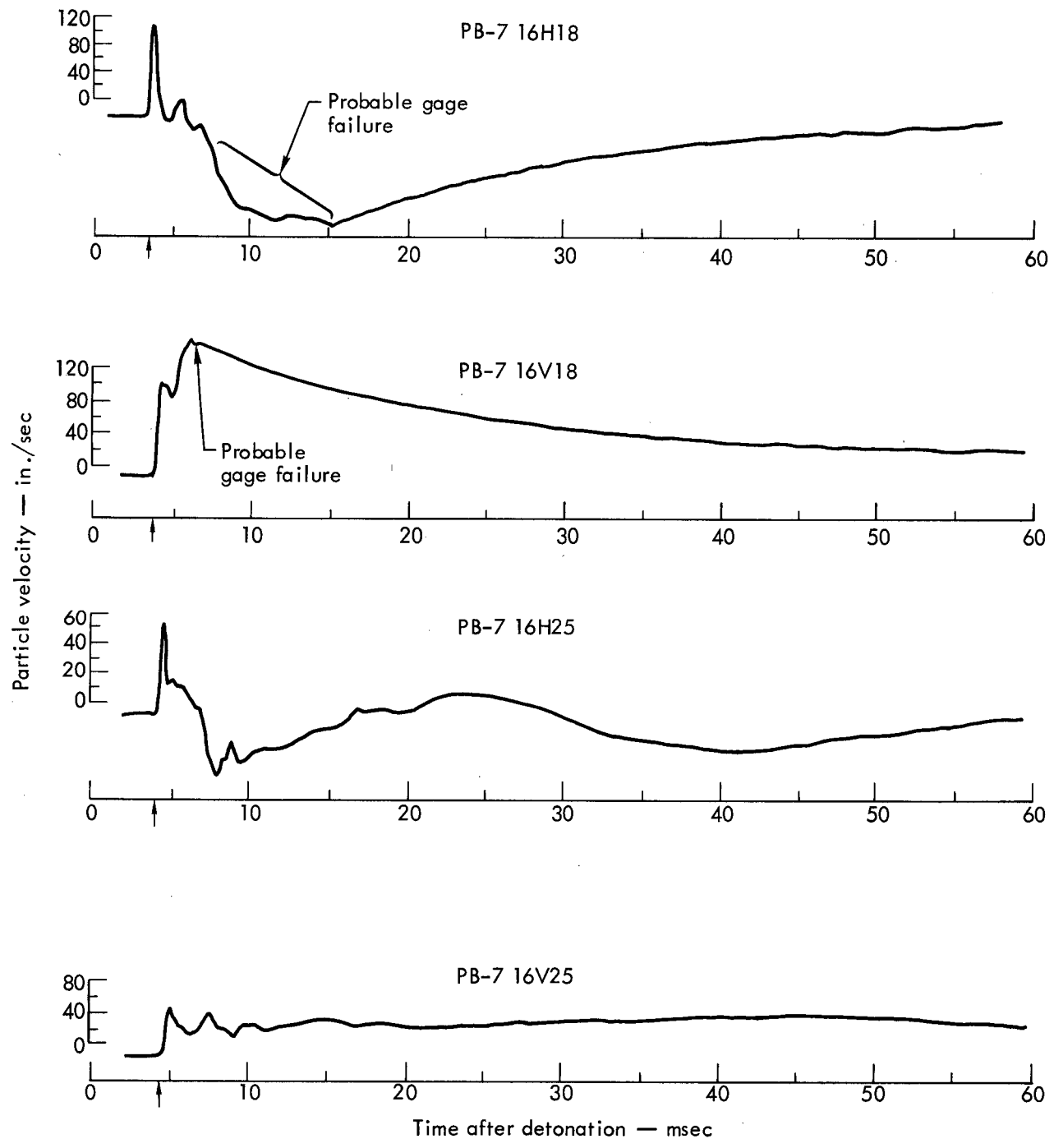
PB-4 2VNB30

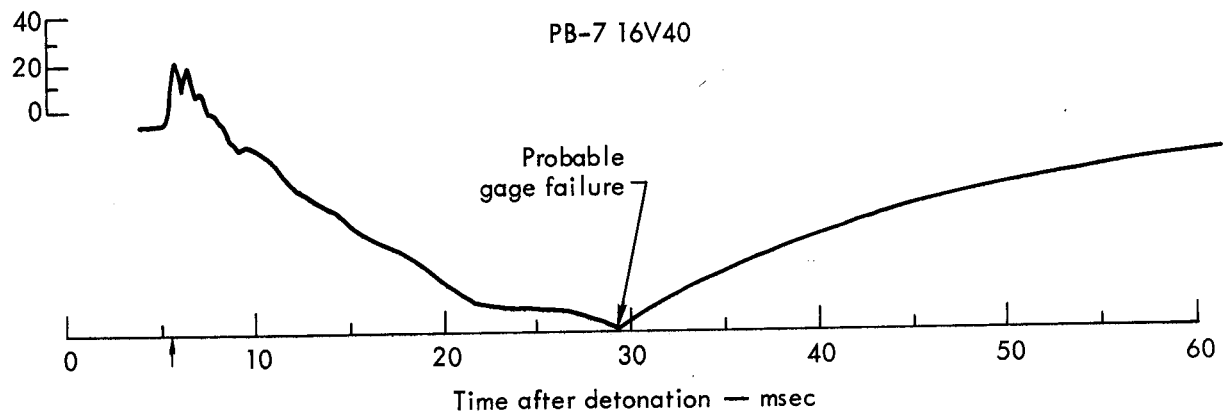
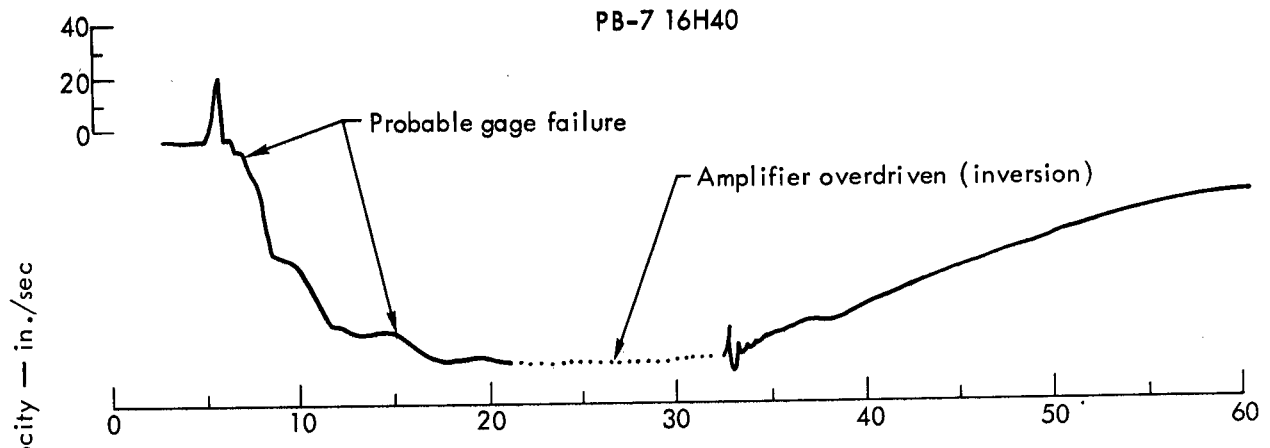
0 20 40 60 80 100

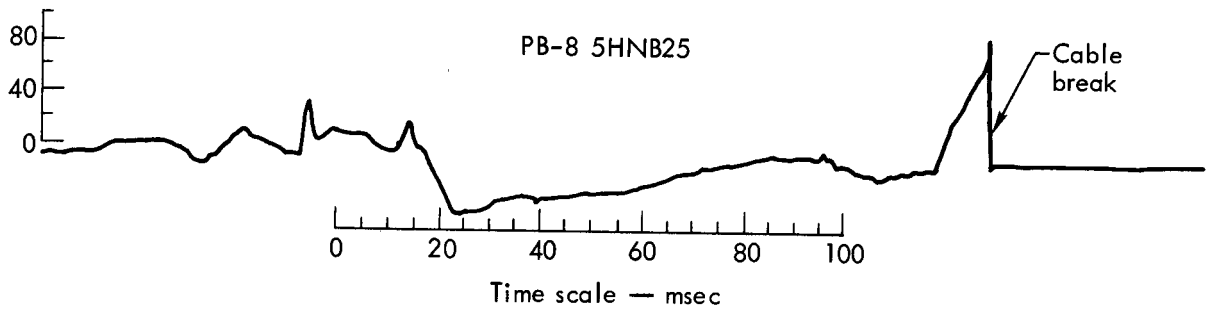
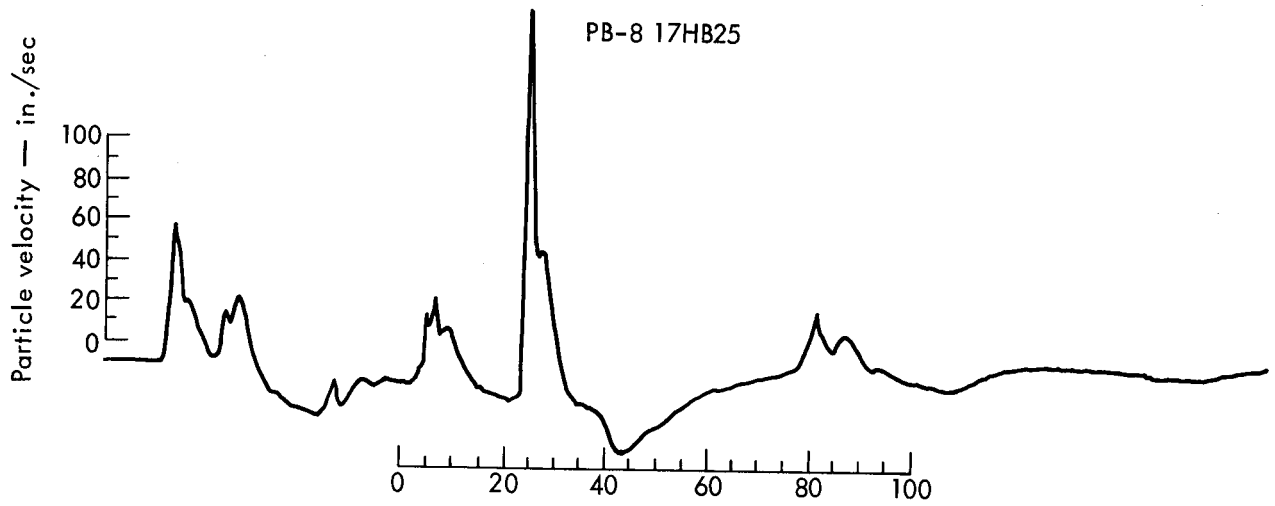
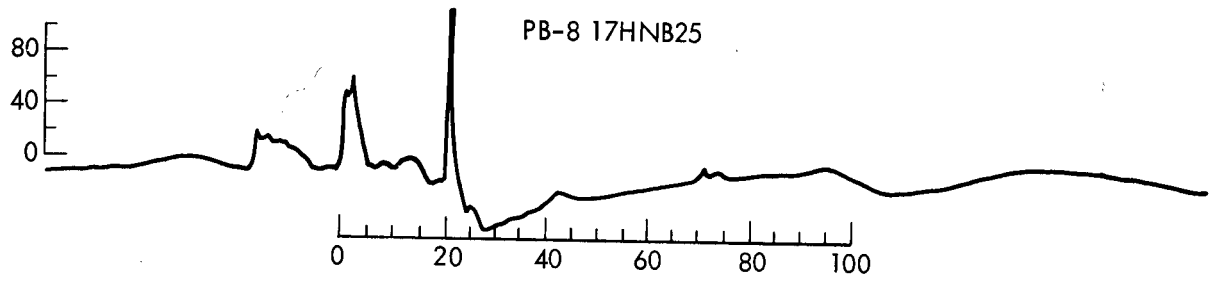
Time scale — msec

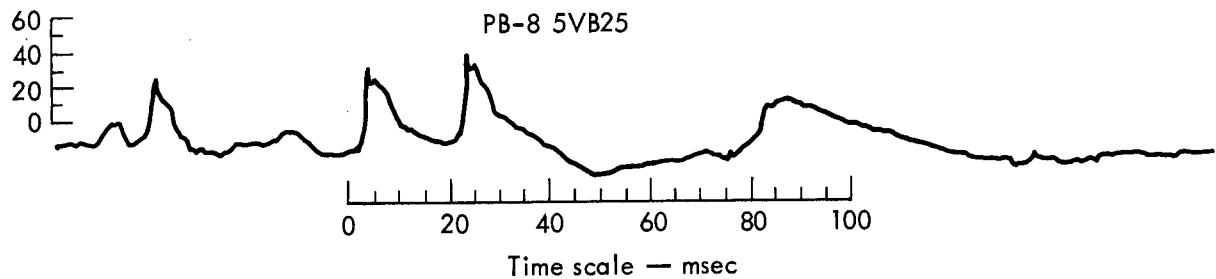
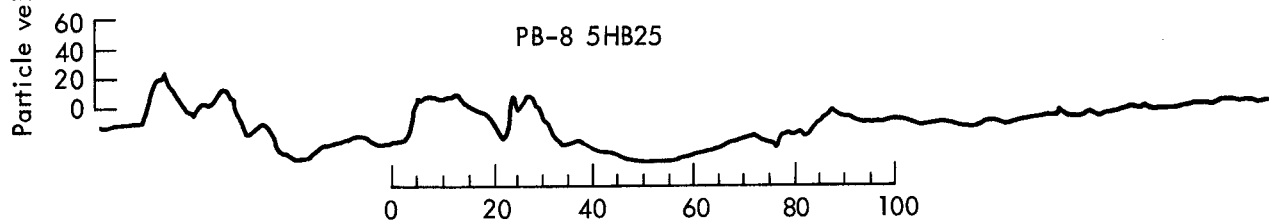
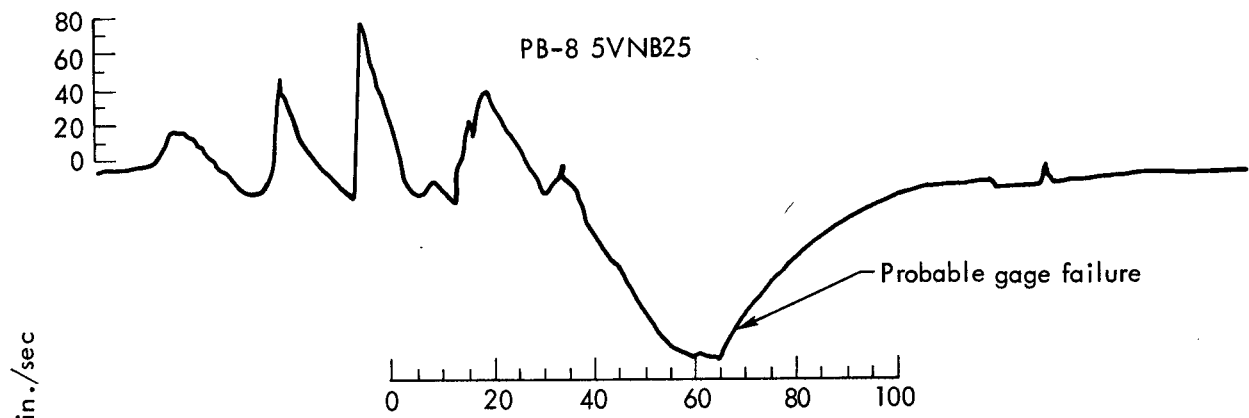














Appendix C
Seismic Data

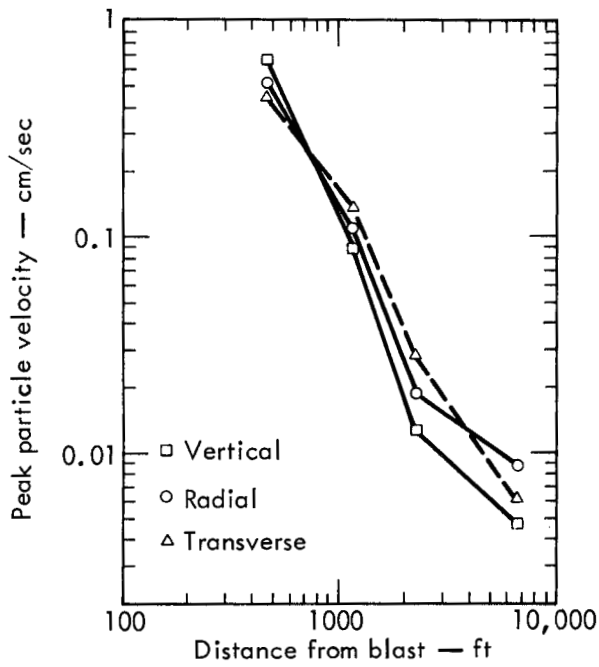


Fig. C1. Peak particle velocity vs distance from blast, PB-1.

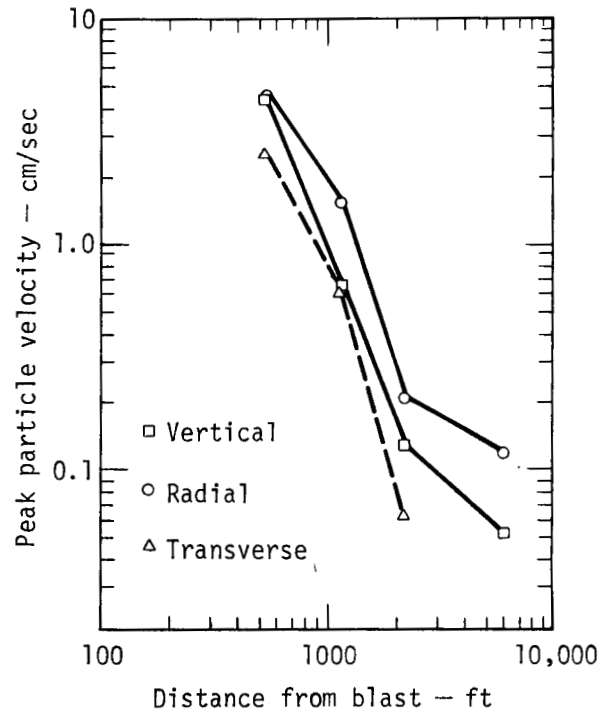


Fig. C3. Peak particle velocity vs distance from blast, PB-4.

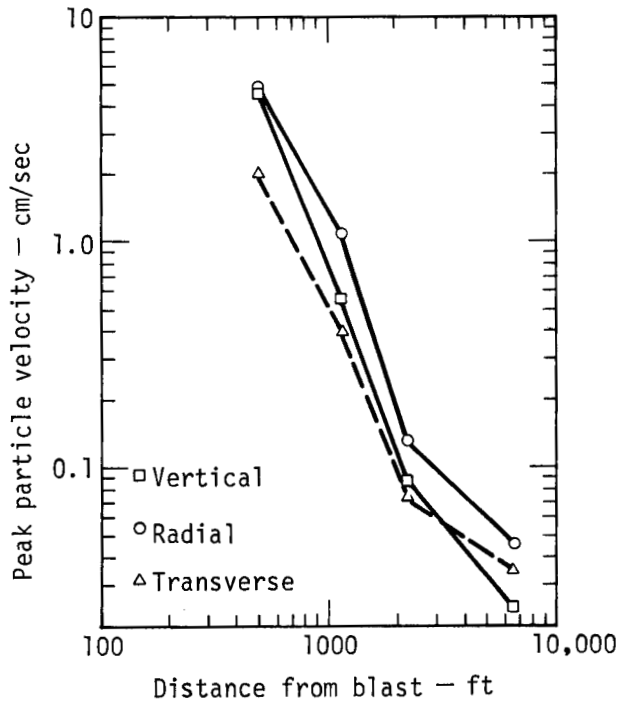


Fig. C2. Peak particle velocity vs distance from blast, PB-3.

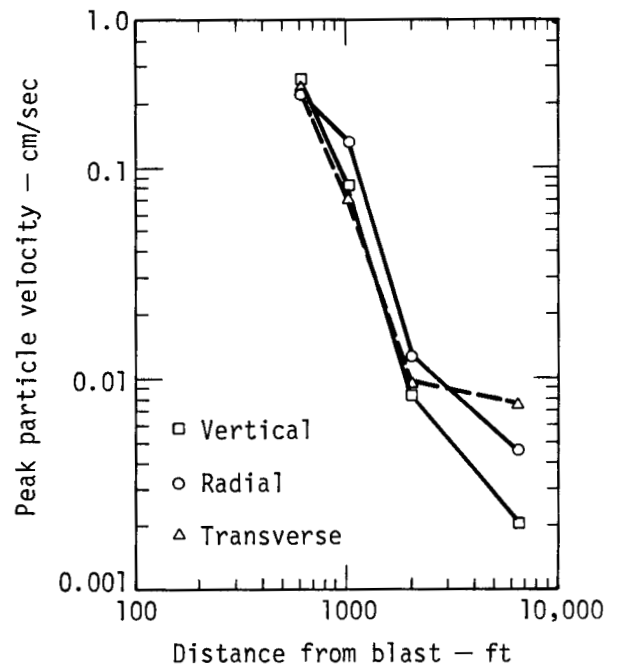


Fig. C4. Peak particle velocity vs distance from blast, PB-5.

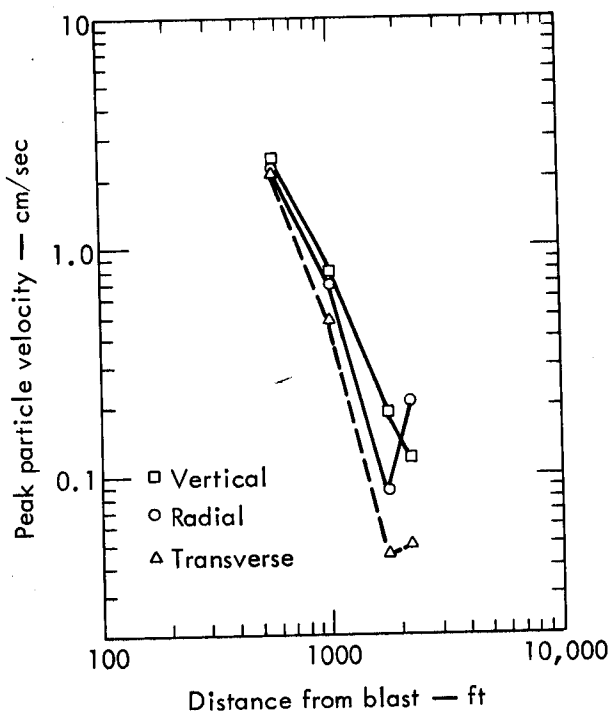


Fig. C5. Peak particle velocity vs distance from blast, PB-6A.

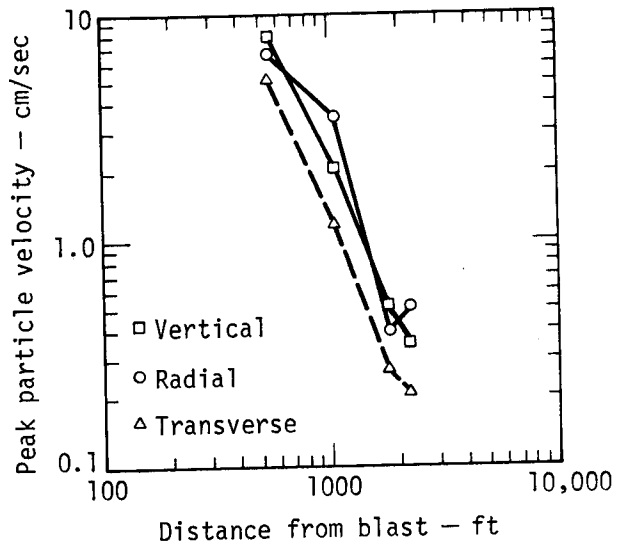


Fig. C6. Peak particle velocity vs distance from blast, PB-6B.

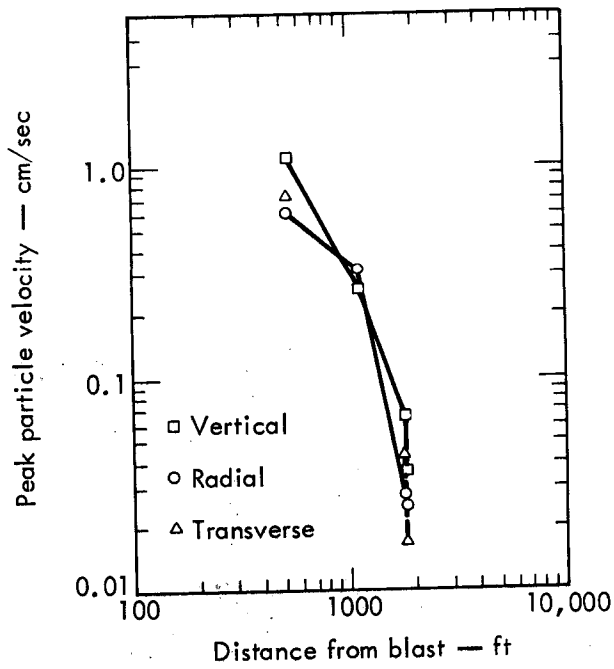


Fig. C7. Peak particle velocity vs distance from blast, PB-6C.

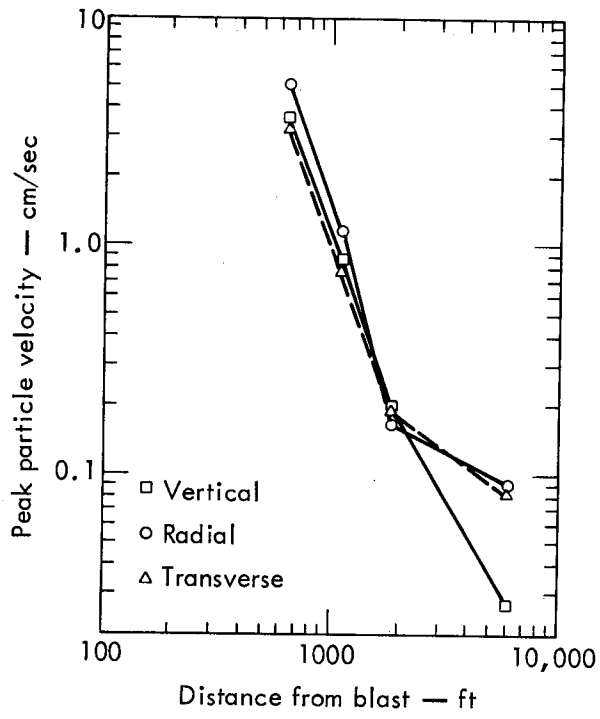


Fig. C8. Peak particle velocity vs distance from blast, PB-7.

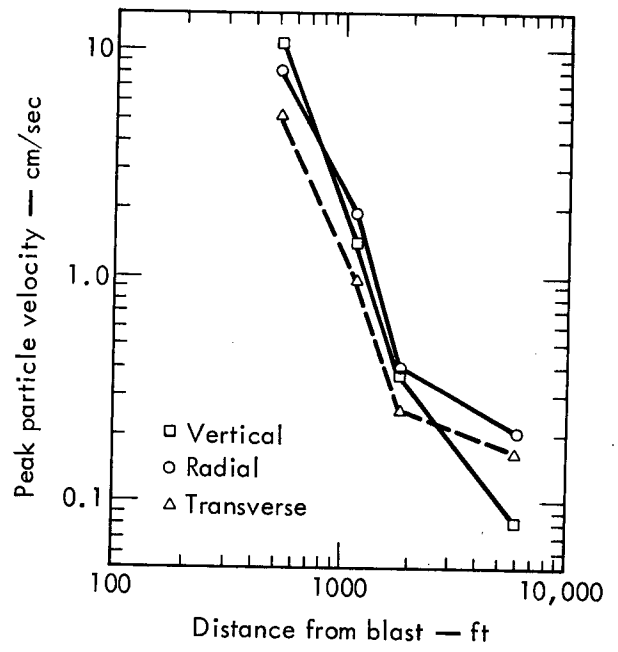


Fig. C9. Peak particle velocity vs distance from blast, PB-8.

Appendix D
Airblast Data

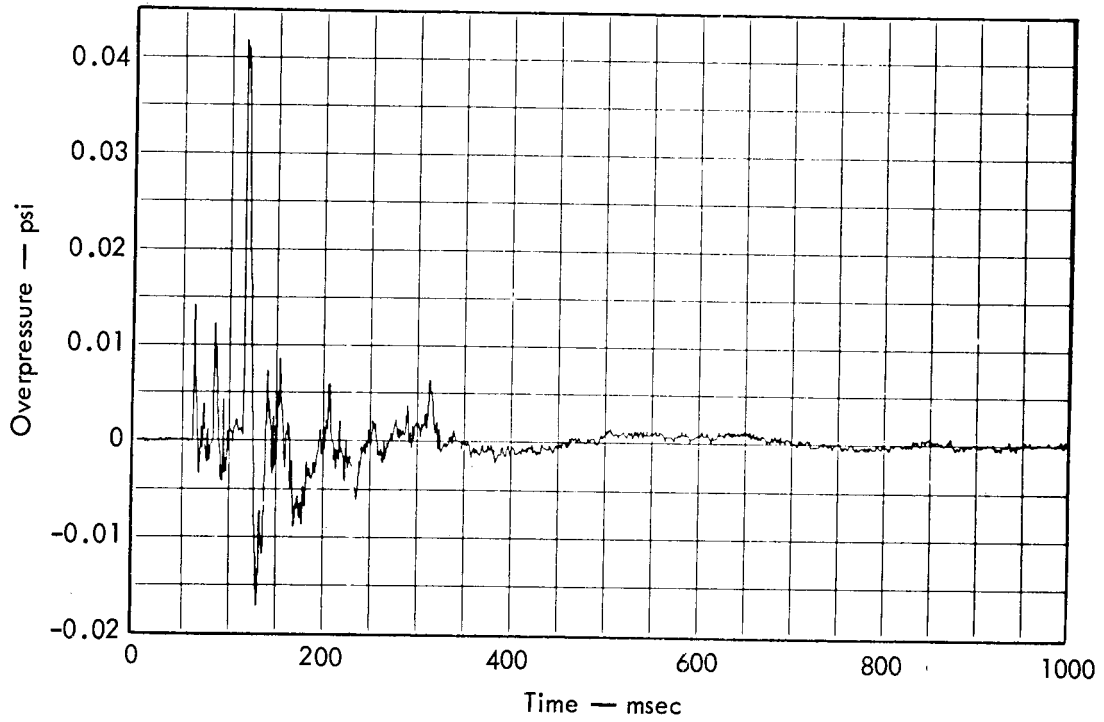


Fig. D1. Overpressure at Gage E-2 from Test Blast PB-1.

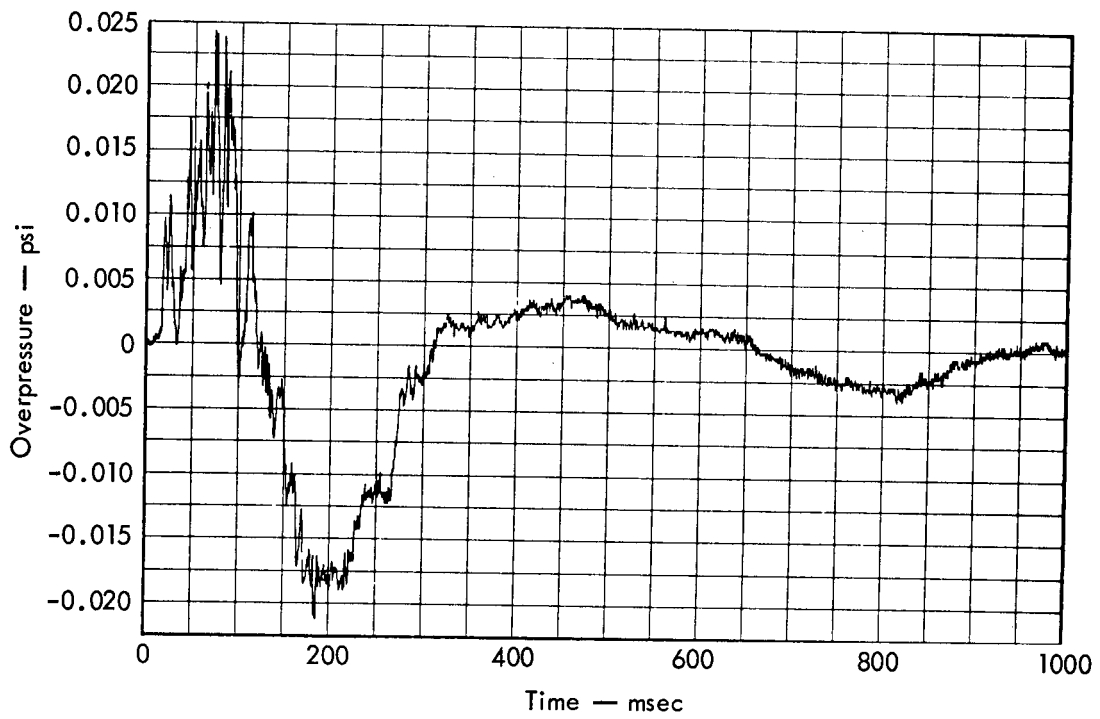


Fig. D2. Overpressure at Gage E-2 from Test Blast PB-3.

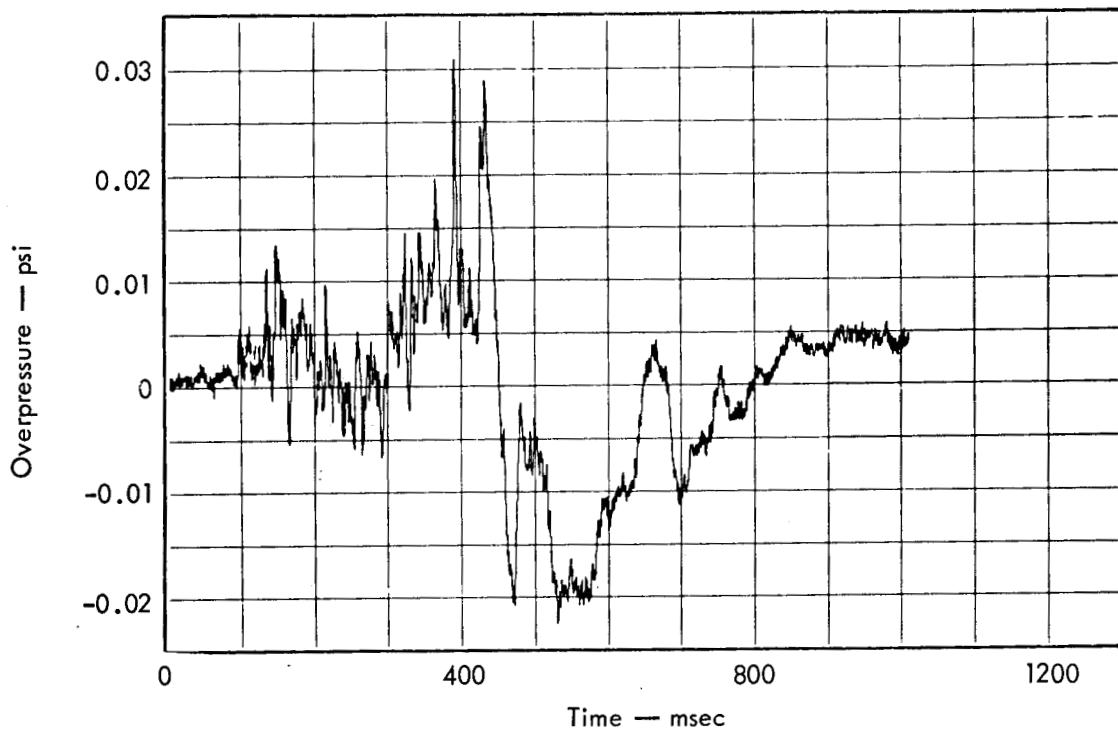


Fig. D3. Overpressure at Gage E-2 from Test Blast PB-4.

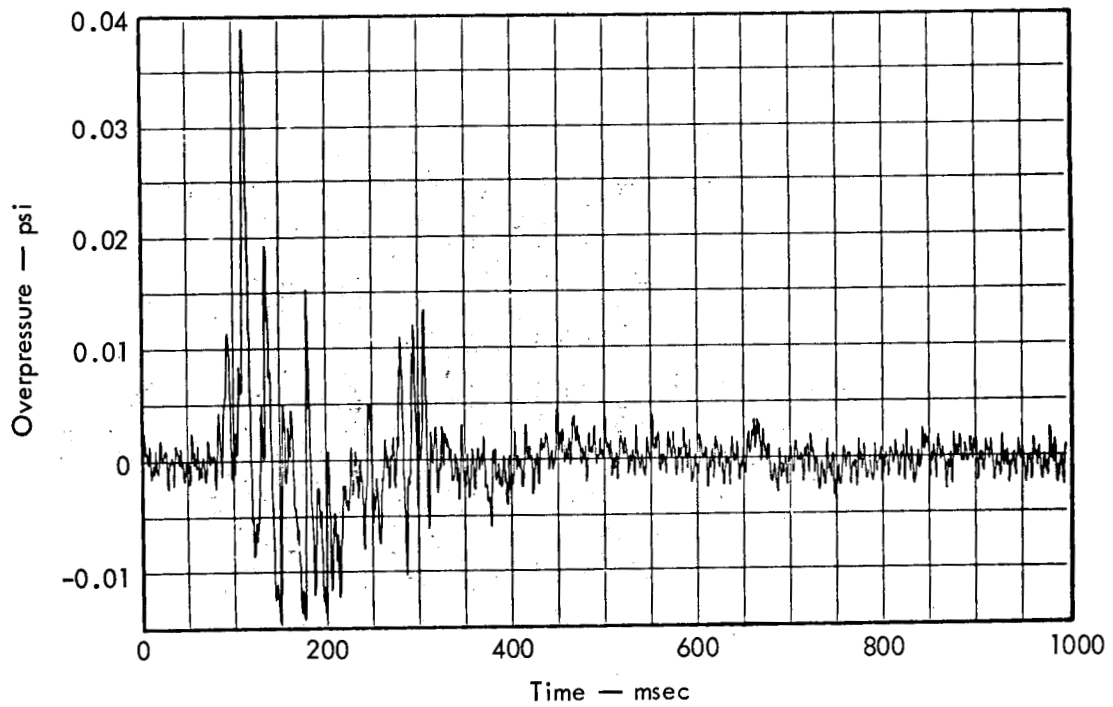


Fig. D4. Overpressure at Gage E-2 from Test Blast PB-5.

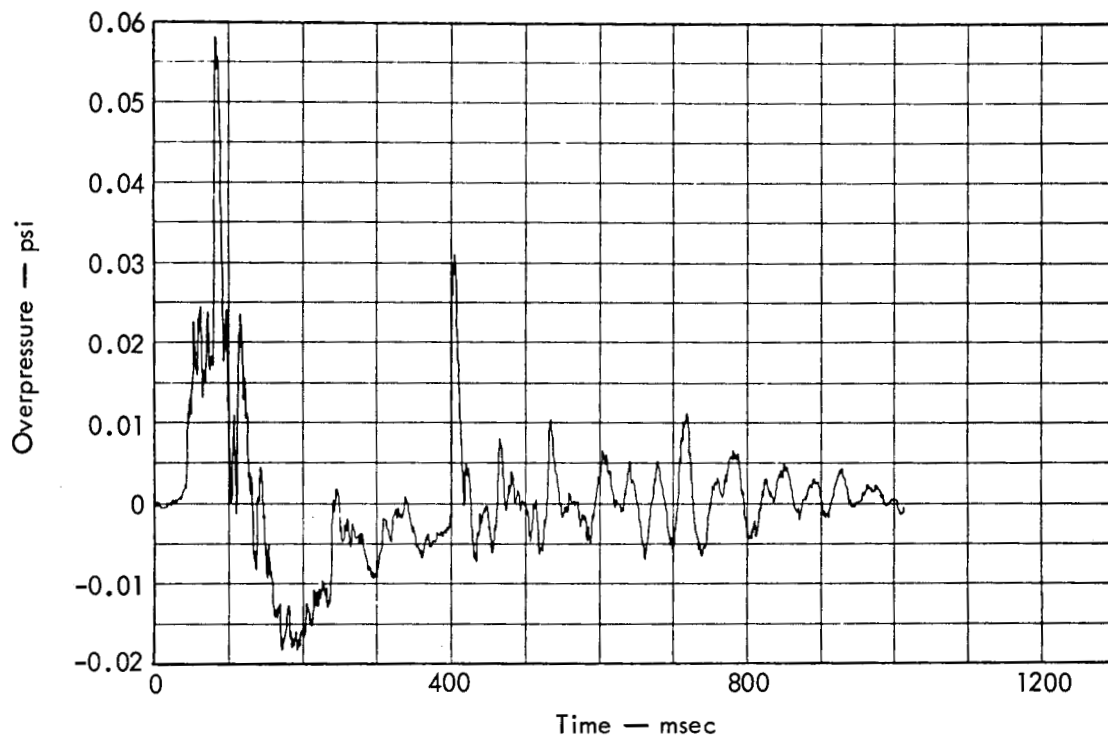


Fig. D5. Overpressure at Gage E-2 from Test Blast PB-6A.

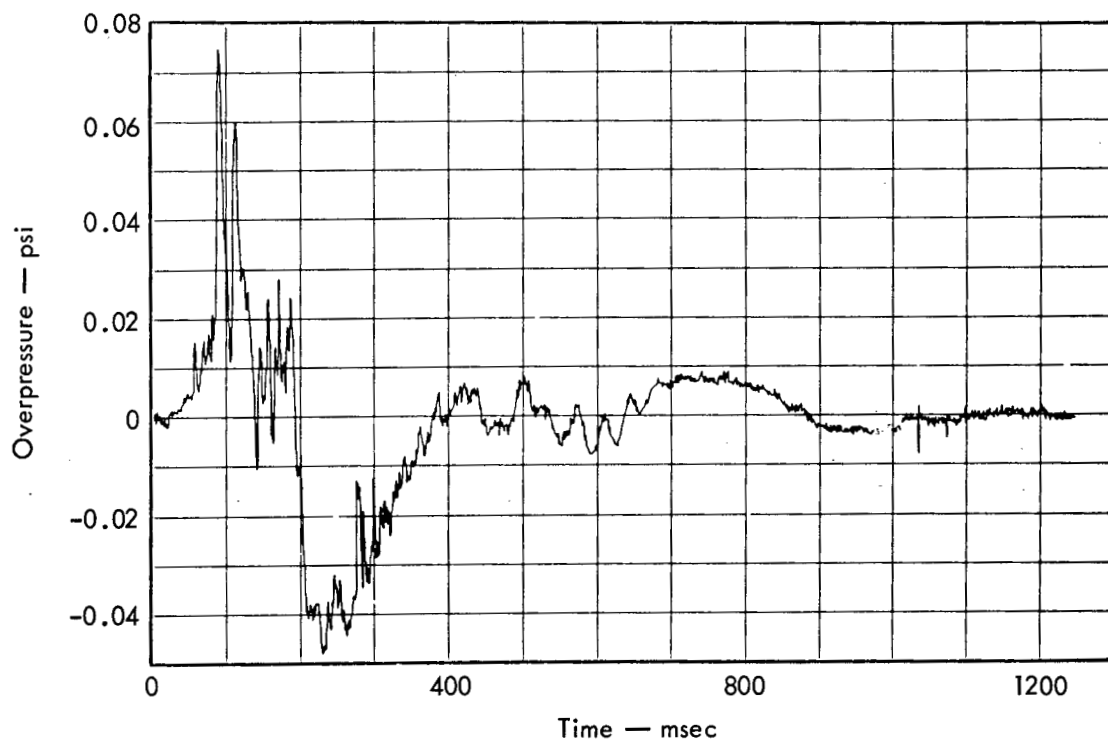


Fig. D6. Overpressure at Gage E-2 from Test Blast PB-6B.

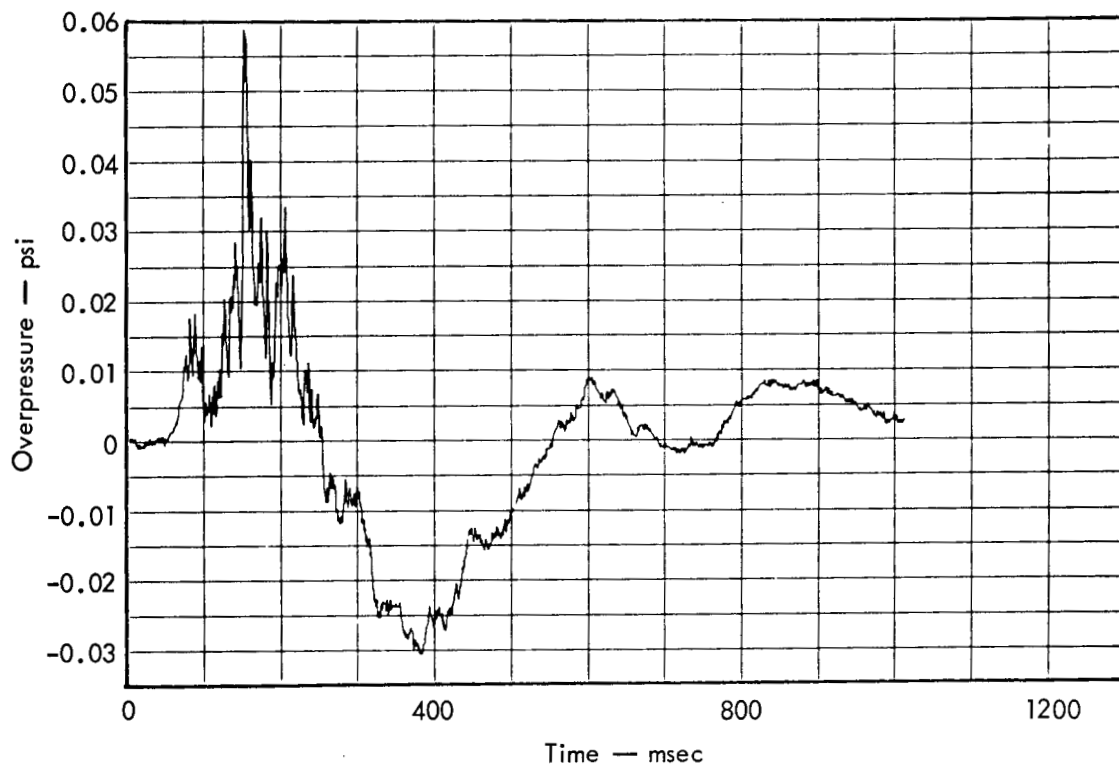


Fig. D7. Overpressure at Gage E-2 from Test Blast PB-7.

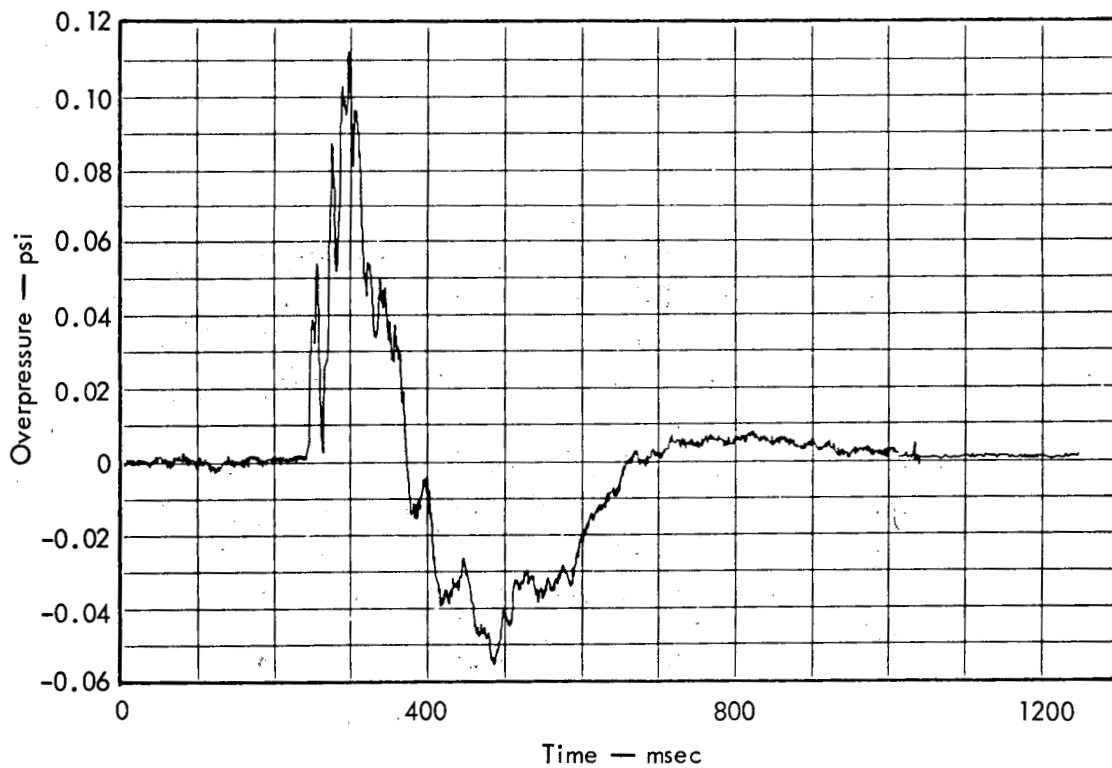


Fig. D8. Overpressure at Gage E-2 from Test Blast PB-8.

References

1. Technical Concept, R. D. BAILEY Lake Project Experimental Excavation Program, U.S. Army Engineer Waterways Experiment Station Explosive Excavation Research Laboratory, Livermore, Calif., (1972).
2. Operations Plan, R. D. BAILEY Lake Project Experimental Excavation Plan, U.S. Army Engineer Waterways Experiment Station Explosive Excavation Research Laboratory, Livermore, Calif., (1973).
3. R. D. BAILEY Lake Project Experimental Excavation Program Data, U.S. Army Engineer Waterways Experiment Station Explosive Excavation Research Laboratory, Livermore, Calif., and Huntington District, U.S. Army Corps of Engineers, Huntington, West Va., (1973).
4. W. R. Bechtell, Blasting Guidelines for the Spillway Excavation at R. D. BAILEY Lake, West Va., U.S. Army Engineer Waterways Experiment Station Explosive Excavation Research Laboratory, Livermore, Calif., Rept. EERL PR E-74-2, (1974).
5. R. D. BAILEY Design Memorandum 7B, Dam and Spillway, Huntington District, U.S. Army Corps of Engineers, Huntington, West Va., (1970).
6. M. G. Wolman, "A Method of Sampling Coarse River-Bed Materials," Trans. American Geophys. Union, 35, 951 (1954).
7. B. D. Anderson, A Simple Technique to Determine the Size Distribution of Crater Fallback and Ejecta, U.S. Army Engineer Waterways Experiment Station Explosive Excavation Research Laboratory, Livermore, Calif., Rept. TR-18 (1970).
8. C. C. McAneny, Project Lost Creek: Field Tests of Mounding and Controlled Blasting, U.S. Army Engineer Waterways Experiment Station Explosive Excavation Research Laboratory, Livermore, Calif., Rept. TR-E-75-1 (1975).
9. F. J. Pettijohn, Sedimentary Rocks, (Harper & Brothers, New York, 1957), 2nd ed.
10. B. B. Redpath, Project Trinidad: Explosive Excavation Tests in Sandstone and Shale, U.S. Army Engineer Waterways Experiment Station Explosive Excavation Research Laboratory, Livermore, Calif., Rept. TR E-73-1, (1972), pp. 39, 40, 79.
11. W. J. Dixon and F. J. Massey, Introduction to Statistical Analysis, (McGraw-Hill, N.Y., 1969), 3rd ed., pp. 100, 247.
12. W. R. Bechtell, "Discussion of Controlled Blasting Techniques and the Results of the Site 300 Experimental Program for Investigating the Buffer Zone Concept," in Project Minimound, T. J. Shackelford, U.S. Army Engineer Waterways Experiment Station Explosive Excavation Research Laboratory, Livermore, Calif., Rept. TM 71-10 (1972).
13. T. J. Shackelford, Project Minimound, U.S. Army Engineer Waterways Experiment Station Explosive Excavation Research Laboratory, Livermore, Calif., Rept. TM 71-10 (1972).

14. B. B. Redpath, An Investigation of a Concept of Limiting the Effects of Cratering Detonations, U.S. Army Engineer Waterways Experiment Station Explosive Excavation Research Laboratory, Livermore, Calif., Rept. MP E-74-3, (1974).
15. J. C. Jaeger and N. G. W. Cook, Fundamental of Rock Mechanics (Chapman and Hall Limited and Science Paperbacks, London, 1969).
16. H. C. Rodean, "Explosion-Produced Ground Motion: Technical Summary with Respect to Seismic Hazards," in Proc. Symposium on Engineering with Nuclear Explosives, January 14-16, 1970 (American Nuclear Society, Las Vegas, Nev., May 1970).
17. H. R. Nicholls, C. F. Johnson, and W. I. Duvall, Blasting Vibrations and Their Effect on Structures, U.S. Dept. of Interior, Bureau of Mines, Washington, D. C., Bulletin 656 (1971).
18. S. M. Johnson, Explosive Excavation Technology, U.S. Army Engineer Waterways Experiment Station Explosives Excavation Research Laboratory, Livermore, Calif., Rept. NCG-TR-21, (1972).
19. B. Ostle, Statistics in Research (Iowa State University Press, Ames, Iowa, 1969), 2nd ed.
20. N. R. Draper and H. Smith, Applied Regression Analysis (John Wiley & Sons, Inc., New York, 1966).
21. IBM Application Program, System/360 Scientific Subroutine Package, (360A-CM-03x) Version II, Programmer's Manual, International Business Machines Corp., White Plains, New York, Rept. H20-0205-1 (1967).
22. T. M. Tami, Analysis of Ground-Motion Peak Particle Velocities from Cratering Experiments at Trinidad, Colorado, U.S. Army Engineer Waterways Experiment Station Explosive Excavation Research Laboratory, Livermore, Calif., Rept. MP E-73-3 (1973).
23. B. B. Redpath and M. K. Kurtz, Project Pre-Gondola: Seismic Site Calibrations, U.S. Army Engineer Waterways Experiment Station Explosive Excavation Research Laboratory, Livermore, Calif., Rept. PNE-1100 (1968).
24. L. L. Oriard, "Dynamic Effects on Rock Masses from Blasting Operations," Slope Stability Seminar, University of Nevada, 1 May 1970.
25. C. M. Snell and D. L. Oltmans, A Revised Empirical Approach to Airblast Prediction, U.S. Army Engineer Waterways Experiment Station Explosive Excavation Research Laboratory, Livermore, Calif., Rept. TR-39 (1971).
26. C. M. Snell, D. L. Oltmans, and E. J. Leahy, Prediction of Airblast Overpressures from Underground Explosions, U.S. Army Engineer Waterways Experiment Station Explosive Excavation Research Laboratory, Livermore, Calif., Rept. TR-7 (1971).
27. J. Coffman, Chief, Soils Section, Huntington District, private communication (1973).
28. C. W. Livingston, "Fundamental Concepts of Rock Failure," Quarterly, Colorado School of Mines, 51, (3) (1956).

29. C. H. Grant and V. N. Cox, "A Comparison of Metalized Explosives," Trans. Soc. of Mining Eng. AIME, 226 (1963).
30. R. L. Ash, "The Mechanics of Rock Breakage," Pit and Quarry, 56, Nos. 2, 3, 4, 5 (1963).
31. J. E. Lattery, WES Explosive Excavation Research Laboratory, Livermore, Calif., private communication (November 1974).
32. J. J. Yancik, "Monsanto Blasting Products: AN-FO Manual - Its Explosive Properties and Field Performance Characteristics," The Monsanto Company, St. Louis, Mo. (1972).

Distribution

LLL Internal Distribution

Roger E. Batzel, L-1
J. S. Kahn, L-41
H. L. Reynolds, L-21
J. Toman, L-47
J. B. Bryan, L-51
D. Burton, L-51
C. M. Snell, L-51
B. Crowley, L-51
L. Schwarz, L-47
A. Lewis, L-47
J. Hannon, L-42
D. Larson, L-42
R. Terhune, L-51
L. Ramspott, L-44
R. Austin, L-505
A. Lundberg, L-505
TID File, L-3

External Distribution

HQDA (DAEN-FEZ-A)
Washington, D.C. 20314

HQDA (DAEN-CWZ-A)
Washington, D.C. 20314

HQDA (DAEN-CWE-G)
Washington, D.C. 20314

HQDA (DAEN-RDZ-A)
Washington, D.C. 20314

HQDA (DAEN-MCZ-A)
Washington, D.C. 20314

HQDA (DAMA-AR)
Pentagon
Washington, D.C. 20314

US Army Engr Div, Lower
Mississippi Valley
P.O. Box 80
Vicksburg, MS 39180

US Army Engr Div, Huntsville
P.O. Box 1600 West Station
Huntsville, AL 35807

US Army Engr Dist, Memphis
668 Clifford Davis Fed Bldg
Memphis, TN 38103

US Army Engr Dist, New Orleans
P.O. Box 60267
New Orleans, LA 70160

US Army Engr Dist, St. Louis
210 North 12th Street
St. Louis, MO 63101

US Army Engr Dist, Vicksburg
P.O. Box 60
Vicksburg, MS 39180

US Army Engr Div, Missouri River
P.O. Box 103, Downtown Station
Omaha, NE 68101

US Army Engr Dist, Kansas City
700 Federal Office Building
601 East 12th Street
Kansas City, MO 64106

(5)

US Army Engr Dist, Omaha
6014 USPO & Court House
215 North 17th Street
Omaha, NE 68102

US Army Engr Div, New England
424 Trapelo Road
Waltham, MA 02154

US Army Engr Div, North Atlantic
90 Church Street
New York, NY 10007

US Army Engr Dist, Baltimore
P.O. Box 1715
Baltimore, MD 21203

US Army Engr Dist, New York
26 Federal Plaza
New York, NY 10007

US Army Engr Dist, Norfolk
803 Front Street
Norfolk, VA 23510

US Army Engr Dist, Philadelphia
US Custom House
2nd & Chestnut Street
Philadelphia, PA 19106

US Army Engr Div, North Central
536 South Clark Street
Chicago, IL 60605

US Army Engr Dist, Buffalo
1776 Niagara Street
Buffalo, NY 14207

US Army Engr Dist, Chicago
219 South Dearborn Street
Chicago, IL 60604

US Army Engr Dist, Detroit
P.O. Box 1027
Detroit, MI 48231

US Army Engr Dist, Rock Island
Clock Tower Building
Rock Island, IL 61201

US Army Engr Dist, St. Paul
1210 US Post Office & Custom House
St. Paul, MI 55101

US Army Engr Div, North Pacific
210 Custom House
Portland, OR 97209

US Army Engr Dist, Alaska
P.O. Box 7002
Anchorage, AK 99501

US Army Engr Dist, Portland (2)
ATTN: Library
Maj. R. Gates
P.O. Box 2946
Portland, OR 97208

US Army Engr Dist, Seattle
1519 Alaskan Way, South
Seattle, WA 98134

US Army Engr Dist, Walla Walla
Bldg 602, City-County Airport
Walla Walla, WA 99362

US Army Engr Div, Ohio River
P.O. Box 1159
Cincinnati, OH 45201

US Army Engr Dist, Huntington (6)
P.O. Box 2127
Huntington, WV 25721

US Army Engr Dist, Louisville
P.O. Box 59
Louisville, KY 40201

US Army Engr Dist, Nashville
P.O. Box 1070
Nashville, TN 37202

US Army Engr Dist, Pittsburgh
Federal Bldg, 1000 Liberty Avenue
Pittsburgh, PA 15222

US Army Engr Div, Pacific Ocean
Bldg 96, Ft. Armstrong
Honolulu, HI 96813

US Army Engr Div, South Atlantic
510 Title Building
30 Pryor Street, SW
Atlanta, GA 30303

US Army Engr Dist, Charleston
P.O. Box 919
Charleston, SC 29402

US Army Engr Dist, Jacksonville
P.O. Box 4970
Jacksonville, FL 32201

US Army Engr Dist, Mobile
P.O. Box 2288
Mobile, AL 36628

US Army Engr Dist, Savannah
P.O. Box 889
Savannah, GA 31402

US Army Engr Dist, Wilmington
P.O. Box 1890
Wilmington, NC 28401

US Army Engr Div, South Pacific (2)
ATTN: Library
R. L. Fraser
630 Sansome Street, Room 1216
San Francisco, CA 94111

US Army Engr Dist, Los Angeles (2)
ATTN: Library
P. Davis
P.O. Box 2711
Los Angeles, CA 90053

US Army Engr Dist, Sacramento
650 Capitol Mall
Sacramento, CA 95814

US Army Engr Dist, San Francisco
100 McAllister Street
San Francisco, CA 94102

US Army Engr Div, Southwestern
1114 Commerce Street
Dallas, TX 75202

US Army Engr Dist, Albuquerque
P.O. Box 1580
Albuquerque, NM 87103

US Army Engr Dist, Fort Worth
P.O. Box 17300
Fort Worth, TX 76102

US Army Engr Dist, Galveston
P.O. Box 1229
Galveston, TX 77550

US Army Engr Dist, Tulsa
P.O. Box 61
Tulsa, OK 74102

US Army Engineer Center
Fort Belvoir, VA 22060

Commandant
US Army Engineer School
ATTN: ATSEN-DD
Fort Belvoir, VA 22060

Engineering Societies Library
345 East 47th Street
New York, NY 10017

US Army Cold Regions Research &
Engineering Laboratories
P.O. Box 282
Hanover, NH 03755

US Army Construction Engineering
Research Laboratory
P.O. Box 4005
Champaign, IL 61820

US Army Engr Dist, Little Rock
P.O. Box 867
Little Rock, AR 72203

Physics International Co.
ATTN: F. Sauer
2700 Merced Street
San Leandro, CA 94577

S. J. Groves & Sons, Co.
ATTN: H. Nelson
Route 1, Box 184A
Elkview, WV 25071

University of California
ATTN: T. Brekke
R. Goodman
472 Davis Hall
Berkeley, CA 94720

Dow Chemical Co.
ATTN: C. Grant
R. Moen
2030 Dow Center
Midland, MI 48640

Monsanto Industrial Chemicals Co.
ATTN: G. Aland
P.O. Box 816
Soda Springs, ID 83276

U.S. Bureau of Mines (4)
ATTN: B. Larsen
J. Olson
R. Dick
L. Fletcher
P.O. Box 1660
Twin Cities, MN 55111

USAE Waterways Experiment Station (5)
ATTN: Library
R. Lutton (S&PL)
J. Ballard (WEL)
L. Watson (ISD)
J. Tarver (ISD)
P.O. Box 631
Vicksburg, MS 39180

Stanford University
Civil Engineering Department
ATTN: A. Hunsbedt
Stanford, CA 94305

U.S. Army Corps of Engineers (3)
R. D. Bailey Lake Project
ATTN: G. Robinette, Resident Engineer
Route US 52
Justice, WV 24851

LTC Robert R. Mills, Jr., CE
84th Engr Bn (Const)
APO San Francisco, CA 96225

MAJ G. Matt Miller
P.O. Box 383
Platte City, MO 64079

Michael J. Hoeft
910 Lincoln Ave.
Waukesha, WI 53186

Mathew Zahn
213 NW First Street or P.O. Box 123
Linton, ND 58552

(2) Kenneth A. Crichton
1110 Saylor Drive, Apt. 2C
Columbus, IN 47201

William R. McCloud
1828 Anza Street, #2
San Francisco, CA 94118

Ing° Fernando Paz Castillo
Instituto Nacional de Canalizaciones
Edificio Atlantic 5° y 6° Piso
Av. Andres Bello - Los Palos Grandes
Apartado de Correos del Este 61959
Caracas, Venezuela

Hudson A. Washburn
Physics Dept.
Colorado State University
Fort Collins, Colorado 80521

W. R. Bechtell (12)
West NAVFAC, Code 411
Box 727
San Bruno, CA 94066

Defense Documentation Center (12)
Cameron Station
Alexandria, VA 22314

USAE Waterways Experiment (55)
Station Explosive Excavation
Research Laboratory
Livermore, CA 94550

Distribution Category, UC-35 (207)

